UNIVERSITY OF SOUTHAMPTON

FACULTY OF MEDICINE

Clinical and Experimental Sciences

Development of Multi-layered Models of the Airway Mucosa

by

Angela Tait

Thesis for the degree of Doctor of Philosophy

April 2014

UNIVERSITY OF SOUTHAMPTON

ABSTRACT

FACULTY OF MEDICINE

Thesis for the degree of Doctor of Philosophy

DEVELOPMENT OF MULTI-LAYERED MODELS OF THE HUMAN AIRWAY MUCOSA

By Angela Tait

Introduction: Asthma is a global burden, leading to around 180,000 deaths worldwide annually. Translation of therapies from animal models is limited, suggesting these models do not recapitulate adequately genetic and environmental aspects of asthma. Existing human cell culture models are usually simplistic and do not mimic the *in vivo* tissue architecture; therefore there is a need to improve three-dimensional human tissue culture models. We hypothesised that use of cell sheet engineering would help overcome this problem.

Aims: Thermoresponsive polymers or ultrasound standing waves (Sonotweezers) will be tested for their compatibility for the formation of cell sheets which can be used for tissue engineering.

Methods: Poly (2-alkyl-2-oxazolines) are polymers with thermoresponsive properties and were tested for biocompatibility using cell motility and adhesion assays, immunofluorescent staining, and measurement of p38 phosphorylation. Multiple cell types were seeded onto thermoresponsive polymers (either NiPAAm, poly(2-alkyl-2-oxazolines) or thermo-gels of poly(2-isopropyl-2-oxazoline)-carboxymethylcellulose)) and cell sheet release assessed after incubation at 20ºC. Cell sheets were also created using ultrasound standing waves (Sonotweezers) or incubation on a thermo-gel. Adhesion junctions in cell sheets were assessed by staining for E-cadherin, ZO-1 and the actin cytoskeleton; cell viability was monitored using 7-Aminoactinomycin D. Subsequently, epithelial cell sheets were used to created co-cultures with fibroblasts. Cytokine release (IL-6 and IP-10) following Poly (I:C) stimulation from cell-sheet co-cultures was compared to conventional models by ELISA.

Results: Using conventional cell culture techniques a multi-layered cell structure by the addition of epithelial cells onto a confluent fibroblast layer was not possible as it resulted in redistribution of the cells to form a single layer comprising islands of epithelial cells surrounded by fibroblasts. Consequently alternative methods were explored using thermoresponsive polymers or Sonotweezers. Cells could be lifted from a commercial NiPAAm coated dish (UpCell) after attachment to a membrane, but during the release process cells either rounded up and lost contact (fibroblasts, HeLa cells) or epithelial cell sheets were damaged and incompletely released. Sonotweezers also could not generate sufficient force to release and levitate the cells. As alternatives, cell sheets were created by levitation in the Sonotweezers device or overlaying the cells on a thermo-gel to allow cell sheet formation followed by sedimentation onto an underlying layer of fibroblasts. Levitation of single cells resulted in the formation of a cell sheet within 2 hours, which gradually contracted becoming three-dimensional by 24 hours. Contraction could be inhibited by removal of Ca^{2+} to prevent adherens junction formation or by adding cytochalasin D to prevent actin filaments or an E-cadherin neutralising antibody to prevent adherens junction formation. After 2 hours of levitation, the cell sheet could be placed onto confluent MRC5 fibroblasts and epithelial cells used plithotaxis to spread across the fibroblasts to create two distinct layers. Oxazoline polymers with a range of hydrophobicities covalently attached to glass were biocompatible, but not thermoresponsive. A gel of poly(2-isopropyl-2-oxazoline-co-2-butyl-2-oxazoline)-carboxymethylcellulose was thermoresponsive, enabling formation of epithelial cell sheets which were used to form cell-sheet co-cultures. The cell-sheet co-cultures achieved an electrically tight barrier and when challenged with the viral mimic Poly(I:C), showed increased IL-6 and IP-10 release. IL-6 release was predominantly apical, whereas IP-10 was basolateral, suggesting polarised mediator release**.**

Conclusions: Multi-layered cell culture models can be created using either the Sonotweezers device or gelling polymers. The latter offers potential for formation of multi-layered structures in a high through-put manner.

Contents

List of figures

DECLARATION OF AUTHORSHIP

I, Angela Tait declare that this thesis and the work presented in it are my own and has been generated by me as the result of my own original research.

Development of Multi-layered Models of the Airway Mucosa

I confirm that:

1. This work was done wholly or mainly while in candidature for a research degree at this University;

2. Where any part of this thesis has previously been submitted for a degree or any other qualification at this University or any other institution, this has been clearly stated;

3. Where I have consulted the published work of others, this is always clearly attributed;

4. Where I have quoted from the work of others, the source is always given. With the exception of such quotations, this thesis is entirely my own work;

5. I have acknowledged all main sources of help;

6. Where the thesis is based on work done by myself jointly with others, I have made clear exactly what was done by others and what I have contributed myself;

7. None of this work has been published before submission

Signed: Date: 25th April 2014

Acknowledgements

This thesis would not have been possible without the continued support of my friends, family and colleges. It is not possible to list all those who have help me, but I would like to acknowledge those who have been fundamental in my progress throughout my PhD.

Firstly I would like to thank my supervisors Professor Donna Davies and Professor Martyn Hill, without their guidance and knowledge, I would have been lost.

As this was a multidisciplinary project there were many people I worked closely with, I am grateful to the production of NiPAAm polymers by Dr Andrew Treherne and oxazoline polymers by Adam Fisher. I would also like to mention Tom Hartland who attached the oxazoline polymers to approximately 500 glass coverslips during his summer internship. I am extremely appreciative of Adam Fisher who spent many meetings explaining the polymer chemistry to me, as well as his supervisor Dr Martin Grossel for his contribution to group meetings and enthusiasm for the project. All the Sonotweezers devices used within this project were created by Dr Peter Glynne-Jones who was also always available to explain the physics behind the ultrasonic levitation and to overcome any issues that arose with the devices, as well as his encouragement during times when nothing was working.

I would also like to thank Richard Jewel for calling the engineers every time the time-lapse microscope had an issue and for showing me how to use the FACsAria.

I would also like to thank David Johnston for his help with confocal imaging which can be seen in some of the impressive images we gained from this project.

I am grateful to all those who work within the Brooke lab for all the guidance and support provided during my time here and for providing a cup of tea and a chat during stressful times. I would like to pick out Dr Emily Swindle who was instrumental in the initial setting up of this project and has been a constant go to person for any questions no matter how big or small and Dr Cornelia Blume who was always available to discuss any queries regarding cell culture and for showing me how to carryout ELISAs. I would also like to thank Lizzie Davies, Jess Donaldson and Matthew Loxham for allowing me to hide in their office with a cup of tea when I needed a break.

I would also like to say a big thank you to all the people working as Dyslexia practitioners within student services especially Jane Warren, without their support this thesis would not have got written.

From a non-academic standpoint I would like to thank my boyfriend Colin Standen for standing by my decision to start a PhD 3 hours from our then home, and making him homeless. He has been my rock during all the stressful periods of this PhD and now thinks he knows as much about this project as I do, due to his constant questions helping me to formulate answers for my viva. Lastly I would like to thank my family who have always supported me in every venture I undertake.

Abbreviations

ADAM33	a disintegrin and metalloprotease 33
AFM	Atomic force microscopy
AHR	Airway hyperresponsiveness
AIBN	Azobisobutyronitrile
ALI	Air liquid interface
APS	Ammonium persulphate
BALF	Bronchial alveolar lavage fluid
BAEC	Bovine aorta endothelial cells
BHR	Bronchial Hyperresponsiveness
Bis*i*PrOx	2-isopropyl-2-oxazoline-2-Bisoxazoline
BSA	Bovine Serum Albumin
CD	Cytochalasin D
DC	Dendritic cells
DMEM	Dulbecco's Modified Eagles Medium
DMSO	Dimethyl Sulphoxide
EC	Extracellular cadherin
ECL	Enhanced Chemiluminescence
ECM	Extracellular Matrix
EDTA	Ethylenediaminetetraacetic Acid
EGTA	Ethylene glycol tetraacetic acid
ELISA	Enzyme Linked ImmunoSorbant Assay
EMTU	Epithelial Mesenchymal Trophic Unit
EtOx	2-ethyl-2-oxazoline
FACs	Fluorescence-activated cell sorting
FBS	Foetal Bovine Serum
FEV_1	forced expiratory volume in 1 second
FLG	Filaggrin
G418	Geneticin
GFP	Green fluorescent protein
GPCR-3s	G protein coupled receptor 3
HAEC	human aortic endothelial cells
HBSS	Hank's Balanced Salt Solution
HCL	Hydrochloric Acid

HRP	Horseradish Peroxidase
HUVEC	human umbilical vein endothelial cells
Ig	Immunoglobulin
IL	Interleukin
IPA	Isopropyl alcohol
IP-10	Interferon gamma induced protein 10
*i*PrOx	p(2-isopropyl-2-oxazoline)
JAM	junctional adhesion molecule
LABA	Long acting β2-adrenoceptor agonist
LCST	lower critical solution temperature
MAGUK	membrane–associated guanylate kinase
MAPK	Mitogen-activated protein kinase
MDCK	Madin Darby canine kidney
MeOx	Methyl oxazoline
MMA	methyl methacrylate
MMP	metalloproteases
$\boldsymbol{M_n}$	number average molecular weight
$\boldsymbol{M_w}$	weight average molecular weight
*n*BuOx	n-2-butyl-2-oxazoline
NiPAAm	N-isopropylacrylamide
NMR	nuclear magnetic resonance
NO	Nitric oxide
ORMDL3	orosomucoid1-like3
OVA	ovalbumin
p38	p38 mitogen activated protein kinase
PBECs	Primary Bronchial Epithelial Cells
PBS	Phosphate Buffered Saline
PDI	Polydispersity index
PDMS	polydimethylsiloxane
PEGM	polyethylene glycol
P*i*PrOx-co-*n*BuOx-CMC	poly(2-isopropyl-2-oxazoline-co-2-butyl-2-oxazoline)-carboxymethylcellulose
PRRs	pattern recognition receptors
PVDF	polyvinyl idene fluoride
PZT	Piezoelectric transducer

ROS	Reactive oxygen species
SABA	short acting β2-adrenoceptor agonist
SDS	Sodium Dodecyl Sulphate
SDS-PAGE	Sodium Dodecyl Sulphate Polyacrylamide Gel Electrophoresis
SFM	Serum Free Medium
SNP	single nucleotide polymorphism
SRS-A	slow releasing substance of anaphylaxis
TBS	Tris Buffered Saline
TER	Tran's epithelial electrical resistance
TEMED	N',N',N',N'-tetramethylenediamine
TGF-β	transforming growth factor-β
Th1	T helper cell type 1
Th2	T helper cell type 2
TLR	toll like receptor
TNFα	Tumour Necrosis Factor α
VEGF	Vascular endothelial growth factor
XPS	X-ray photoelectron spectroscopy
ZO	zonula occludens
ZONAB	ZO-1 associated nucleic acid-binding protein
70:10:20	NiPAAm -co-MMA-co-PEGM
7AAD	7-aminoactinomycin D

1. Introduction

1.1 Asthma

Asthma causes a large burden on society; in Europe alone it affects approximately 30 million children and adults below the age of 45. The annual cost of treating these patients is estimated to be €19.5 billion with a further €14.4 billion lost on indirect costs, such as absences from work (Gibson et al., 2013).

Asthma is a complex disorder characterised by variable airway obstruction (bronchoconstriction), inflammation and hyper responsiveness. The narrowing of the airways gives rise to symptoms including shortness of breath, wheezing, chest tightening and coughing. These can range from mild with occasional symptoms, to severe with persistent symptoms impacting on quality of life. It is associated with a variety of environmental factors, for example, allergens such as animal dander which can bring on an exacerbation. An exacerbation is the rapid decrease in lung function despite regular treatment. One of the main clinical signs of asthma exacerbation is a rapid decrease in FEV_1 (forced expiratory volume in 1 second). This is a measure of lung function that can be used to investigate reversibility of airway obstruction before and after the use of a bronchodilator (Bateman et al., 2008 8843).

1.2 The structure of the airways

The airways come into contact with over 10,000 litres of air every day (Van der Schans, 2007) bringing with it particles, allergens, pathogens and pollutants. The airways have evolved various mechanisms to cope with this continuous assault. The air initially enters the sinuses where large particles >10μM (PM10) (Gerritsen (J, 2000) are trapped due to the rapid change in air flow. Unable to change direction, they hit the epithelium, becoming trapped in the mucus layer. As the air flows down the airways the particle sizes are gradually filtered out, with mainly fine particles < 2.5μm (PM2.5) accumulating in the airways (Valavanidis et al., 2008). Ultrafine particles <0.1μm (PM0.1) can travel down the whole airway reaching the alveoli (Valavanidis et al., 2008).

The bronchial epithelium is pseudostratified, meaning that it looks like multiple layers but all cells are in contact with the basement membrane (Figure 1).

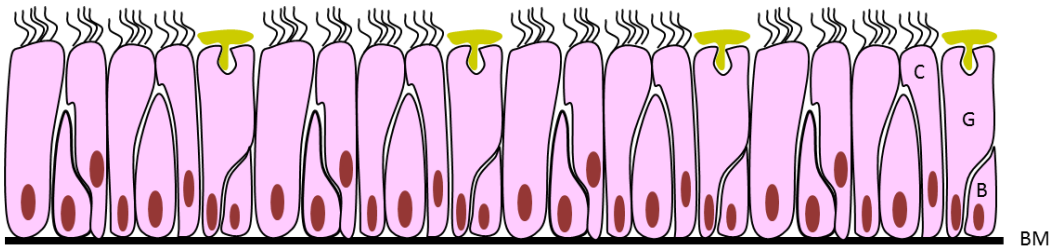

Figure 1 schematic of a pseudostratified epithelium.
Where C shows ciliated columnar epithelium, G shows goblet cell, B shows basal cell and BM shows the basement membrane.

The three main cell types are ciliated columnar epithelium, mucus producing goblet cells and basal cells which act as progenitors (Hong et al., 2004). There are also neuroendocrine cells and intermediate cells. Progression through the airways leads to the epithelium becoming simpler and goblet cells being replaced by surfactant releasing Clara cells before reaching the alveoli. The alveoli are made up of two epithelial cell types, alveolar type (pneumocyte) one cells which are flat and aid in gas exchange and alveolar type two cells which are rounder and release surfactant. The surfactant aids in gas exchange and reduces the surface tension, preventing the alveoli from collapsing.

The bronchial epithelium is formed of a polarised cohesive sheet of cells. The individual cells are held together by a series of junctional complexes; tight junctions, adherens junctions, desmosomes and gap junctions; the epithelial sheet binds to the basement membrane using hemidesmosomes and focal adhesions (Figure 2).

The bronchial epithelium is coated in a mucus layer made up of hydrated mucins, mainly MUC5AC and MUC5B. MUC5AC is produced in goblet cells (Hovenberg et al., 1996) and MUC5B is secreted from mucous glands in the submucosa (Wickstrom et al., 1998). Mucins are glycoproteins that tangle together forming a viscoelastic gel. Any particles that hit the side of the airway become trapped in the mucus; this can then be removed via the mucociliary escalator and swallowed (Swindle et al., 2009). Mucus also contains a number of defence molecules including defensins, lactoferrin, lactoperoxidase and lysozyme. Lactoferrin acts in multiple ways it is a glycoprotein which binds iron and it has both bactericidal and virus-blocking properties. It kills bacteria by binding to the lipopolysaccharide of the cell wall; oxidizing the bacteria via formation of peroxides that affect the cell permeability resulting in cell lysis. Some viruses enter cells by binding to lipoproteins on the epithelial cell surface enabling penetration of the cell membrane (Yamauchi et al., 1993). Lactoferrin can also bind to these lipoproteins blocking access of

the virus (van der Strate et al., 2001). Defensins form a pore in a bacterial cell wall (Lehrer et al., 1993). Lactoperoxidase is a peroxidase enzyme with antibacterial activity, it catalyses the oxidation of various substrates by hydrogen peroxide. These oxidised products cause damage to the cell membrane of the bacterium (Nicod, 1999). Lysozyme is an enzyme that attacks the peptidoglycans found on bacterial cell walls resulting in hydrolysis (Jacquot et al., 1987). IgA can opsonise a pathogen for destruction by an immune cell (Underdown and Schiff, 1986). The main immune cell found in the mucus is the macrophage, which phagocytose pathogens and necrotic cell debris (Lehnert, 1992).

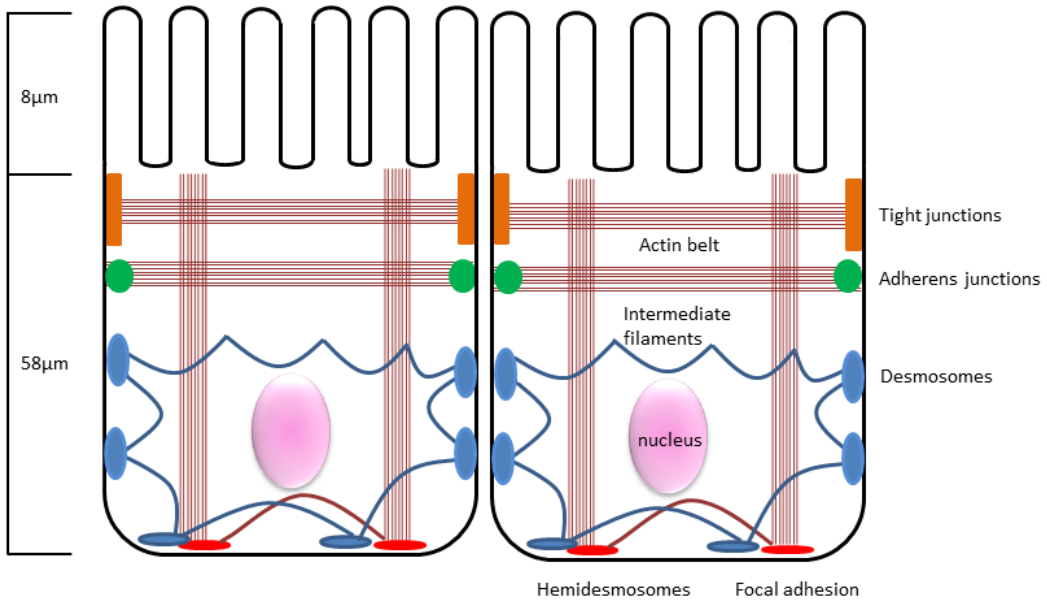

Figure 2 Schematic of the configuration of the cell to cell contacts within the bronchial epithelium. The tight junctions are located at the apical surface of the cell; they interact with the actin cytoskeleton. They are closely associated with adherens junctions which also interact with the actin cytoskeleton. The most basal components, the desmosomes interact with the intermediate filaments of the cytoskeleton. All these interactions keep the cell sheet strong. The Hemidesmosomes bind to the basement membrane and the intermediate filaments. The focal adhesions also bind to the basement membrane and actin filaments.(Patton and Byron, 2007)

The adherens junctions are an intercellular junction that aids in the adhesion of the epithelial cell sheet. They are the first junction to form at areas of cell-cell contact and bind to the actin cytoskeleton aiding in the strength of the epithelial cell sheet (Gumbiner et al., 1988). They are a complex of transmembrane and intracellular proteins (Figure 3). E-cadherin (epithelial cadherin) is a classical single-pass transmembrane glycoprotein that homophilically dimerises with adjacent cells (Gumbiner et al., 1988). The extracellular domain is made up of 5 extracellular cadherin (EC) repeats, Ca^{2+} ions are required to stabilise the extracellular domain and aid the formation of the homophilic interactions (Chappuis-Flament et al., 2001). The intracellular domain contains binding sites for the catenins p120 (Niessen and Gumbiner, 1998) and β-catenin (Aberle et al., 1994). The

catenin p120 binds to the microtubules (Franz and Ridley, 2004) and its loss has been linked to tumour progression and invasion in lung cancer (Liu et al., 2009). β-catenin binds to the C-terminal domain of E-cadherin and contains binding sites for α-catenin. α-catenin can bind to both β-catenin (as a monomer) and F-actin (as a dimer). It was initially thought to bind to both β-catenin and F-actin at the same time linking the actin cytoskeleton to the adherens junction. However it cannot bind to both at the same time, the exact link has yet to be determined. However it has been suggested that there is a pool of α-catenin near the adherens junctions where part is bound to β-catenin and part is bound to the F-actin (Drees et al., 2005). It has been noted that there is redistribution of E-cadherin in bronchial biopsies from severe asthmatic airways (Hardyman et al., 2013).

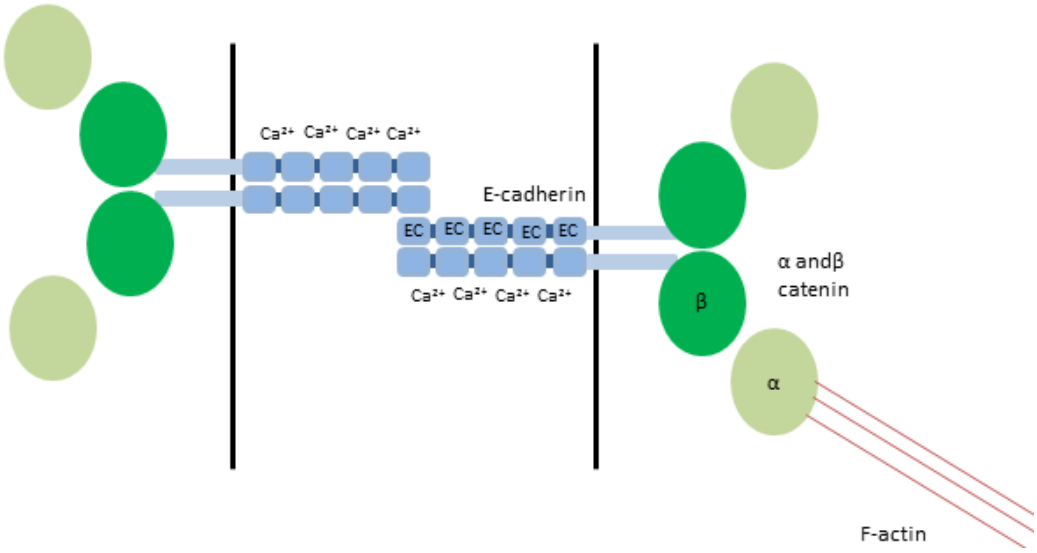

Figure 3 Schematic of the adherens junction.
The adherens junctions are made up of intercellular homophilic calcium dependent binding of E-cadherin. The intracellular domain binds to β catenin, which in turn binds to α catenin. α catenin links the adherens junction to the actin cytoskeleton.

The formation of the adherens junction then promotes the formation of the tight junctions, for example ZO-1 by its interaction with α-catenin providing the first scaffolding for the tight junctions (Itoh et al., 1997).

The tight junctions are the most apical of the junctions; they regulate the paracellular transport of macromolecules and ions between the apical and basal domains. They also maintain the polarity of the cells ensuring membrane located molecules maintain their relative positions in the apical or basolateral compartments. They are a complex of transmembrane and peripheral membrane proteins (Figure 4). The transmembrane proteins are occludin, claudin and junctional adhesion molecule (JAM). Occludin has four

transmembrane domains with two extracellular loops and two intracellular domains (Feldman et al., 2005). Claudins are also made up of four transmembrane domains and two intracellular domains; however there is no sequence similarity between Claudin and Occludin. The Claudins regulate the paracellular selectivity by forming ion selective pores. Some claudins form cationic pores (2, 10b and 15) while some form anionic pores (10a and 17) (Günzel and Alan, 2013). The Claudins found in the proximal airway are 1, 3, 4, 5, 7, 1 and 18 (splice variant 1)(Günzel and Alan, 2013). JAM's are part of the immunoglobulin superfamily. They contain one transmembrane domain and an extracellular domain, which in turn contains two Ig-like motifs and a cytoplasmic tail (Kostrewa et al., 2001). These transmembrane proteins interact with numerous peripheral membrane proteins. The most studied of which are zonula occludens (ZO) proteins they are part of the membrane–associated guanylate kinase (MAGUK) family, with a basic structure of at least one PDZ (PSD-95/DISCS-large/ZO-1) domain, a Src homology 3 (SH3) domain and a guanylate kinase (GUK) domain (Gonzalez-Mariscal et al., 2000). These proteins act as scaffolding binding to both transmembrane proteins and the cytoskeleton. There are three ZO proteins, ZO-1, ZO-2 and ZO-3 which can interact with each other using their PDZ domain. The tight junctional components associate with those on opposing cells forming paired strands. The ZO's bind to the actin cytoskeleton forming a cohesive belt around the cells (Itoh et al., 1997). The tight junctions appear to be disrupted within asthma patients (Xiao et al., 2011) suggesting that they have a defective barrier function, potentially permitting pathogens or allergens across the epithelium activating the immune response.

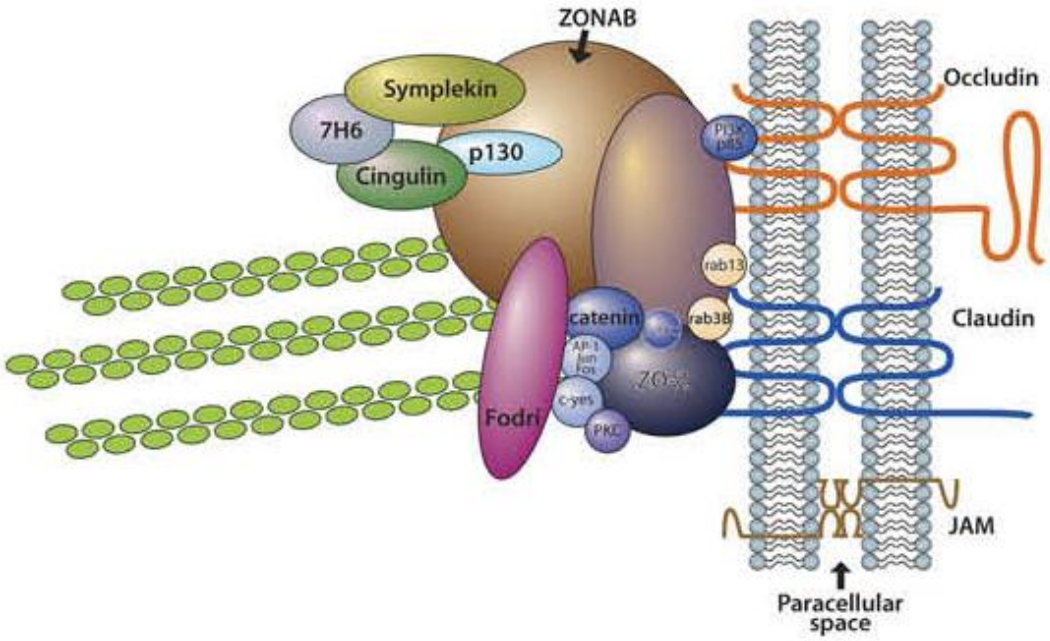

Figure 4 Schematic showing the tight junctional complex.
There are three transmembrane proteins that make up the tight junction, occludin, claudin and JAM. These interact with many cytosolic proteins and eventually the actin cytoskeleton. (Swindle et al., 2009)

The tight junctions and adherens junctions both bind to the actin cytoskeleton (Hartsock and Nelson, 2008). By anchoring to these junctions the actin filaments form a network under the plasma membrane that provides mechanical support, helps maintain cell shape and is involved in cell motility. There is constant turn over between G- actin (globular) and filamentous F-actin. The actin monomer is a 42kDa protein (Holmes et al., 1990), which forms polar polymers that have a right-handed helical twist and a barbed end and a pointed end. The majority of the polymerisation occurs at the barbed end (Pollard, 1986). The filaments that bind to cell-cell and cell-matrix junctions are stably cross-linked antiparallel bundles which contain myosin II molecular motor protein which can induce contraction (Blanchoin et al., 2014). Modification of the actin cytoskeleton can change the morphology of the cell and is used in cell motility (Pollard and Borisy, 2003).

Desmosomes are another adhesional junctional complex (Figure 5). They are discoid junctions composed of desmoplakin plaques which bind intracellularly to the intermediate filaments and 2 single transmembrane cadherin proteins desmogleins and desmocollins (Green and Jones, 1996) which bind homophilically with the plaque of adjacent cells. They provide mechanical stability in epithelia.

Gap junctions also occur between epithelial cells, allowing communication between neighbouring cells (Kumar and Gilula, 1996).

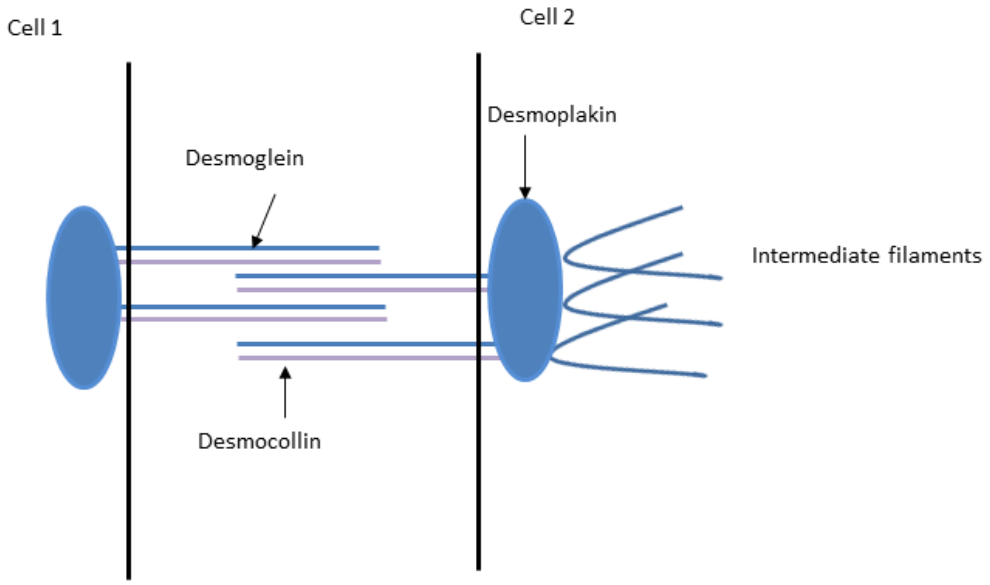

Figure 5 Schematic of the Desmosomes.

The Focal adhesion and hemidesmosomes are located on the basal side of the cells and bind to the ECM. Focal adhesions consist of the transmembrane glycoproteins integrin α and β dimers which span the membrane interacting with the ECM, they then bind to F-actin. The integrin dimers allows for the formation of different combinations allowing for binding to different ECM components (Burridge and Chrzanowska-Wodnicka, 1996). There are 18 α subunits and 8 β subunits in humans that can form 24 different combinations (Arnaout et al., 2005), with 8 dimers found in the lung, α2β1, α3β1, α6β4, α9β1, α5β1, αvβ5, αvβ6, αvβ8 (Cambier et al., 2000). These 8 can recognise a wide range of ECM proteins including collagen I, tenascin C, laminins 5,10,11, osteopontin, fibronectin and vitronectin (SHEPPARD, 2003). The integrins α3β1 and α6β4 bind to laminin 5, 10 and 11 in the ECM found in the basement membrane (Carter et al., 1991). α5β1 which binds to fibronectin is not found in healthy lung but is expressed in lung epithelial cells when they are healing a wound (Pilewski et al., 1997). Bronchial epithelial cells polarise and the signals for this are derived from the integrins binding to the ECM, for example binding of the α6 subunit to laminin is essential for the polarisation of epithelium in developing kidney tubules (Sorokin et al., 1990). Hemidesmosomes contribute to the resistance to mechanical stress on the epithelial cells. They consist of the transmembrane proteins integrin α6β4 which bind to laminin extracellularly. Plectin and BPAG1 make up

the intracellular plaque (de Pereda et al., 2009). The intermediate filaments bind to the plaque.

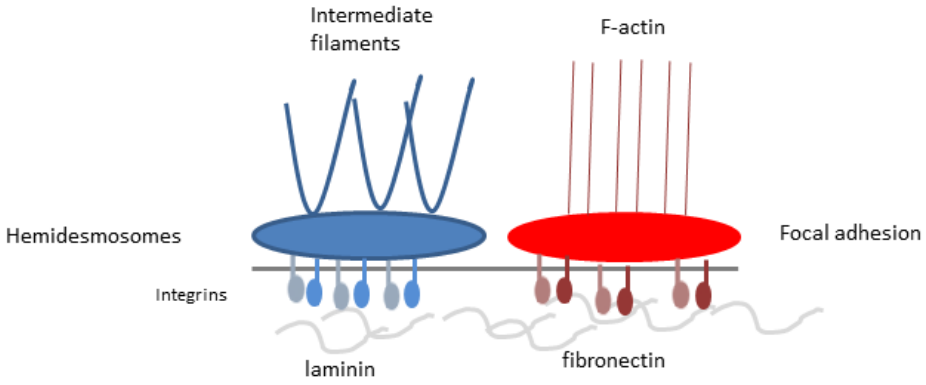

Figure 6 Schematic showing the Hemidesmosomes and focal adhesion binding to the basement membrane.

The intermediate filaments in epithelial cells are made up of keratin fibres which attach to the nuclear envelope and to desmosome and hemidesmosomes (Goldman et al., 2011). They provide the mechanical support to the cell membrane, are dynamic and constantly being recycled. Due to the homophilic binding of the desmosomes they provide the strength and rigidity of the epithelial cells sheet.

The interaction between all these components forms a strong cell layer that can act as a barrier to the external environment.

Underneath the epithelium is the basement membrane. This is comprised of the lamina reticularis, and the lamina densa, these are made up of collagen and fibronectin respectively (Figure 6). Beneath this membrane layer is the lamina propria, consisting of fibroblasts, capillaries and immune cells, such as mast cells. Fibroblasts are mesenchyme derived cells, which produce and degrade the extracellular matrix (ECM) proteins maintaining the structural integrity of the ECM. They degrade the ECM by producing matrix degrading proteases, such as metalloproteases (MMPs) (O'Connor and FitzGerald, 1994) and are involved in wound healing. They also secrete cytokines that are important in defence mechanisms, as they recruit and activate leukocytes (Sabatini et al., 2002). If fibroblasts are stimulated with TGF-β (transforming growth factor-β) they can differentiate into myofibroblasts, these are contractile cells that are involved in wound healing and also secrete cytokines (Wicks et al., 2006 8967). Below the lamina propria is the smooth muscle layer. This is the defining point between the mucosa and the submucosa. Beneath the

smooth muscle layer is the submucosa, this contains the mucous and serous glands. Figure 7 shows a schematic of the composition of healthy airways.

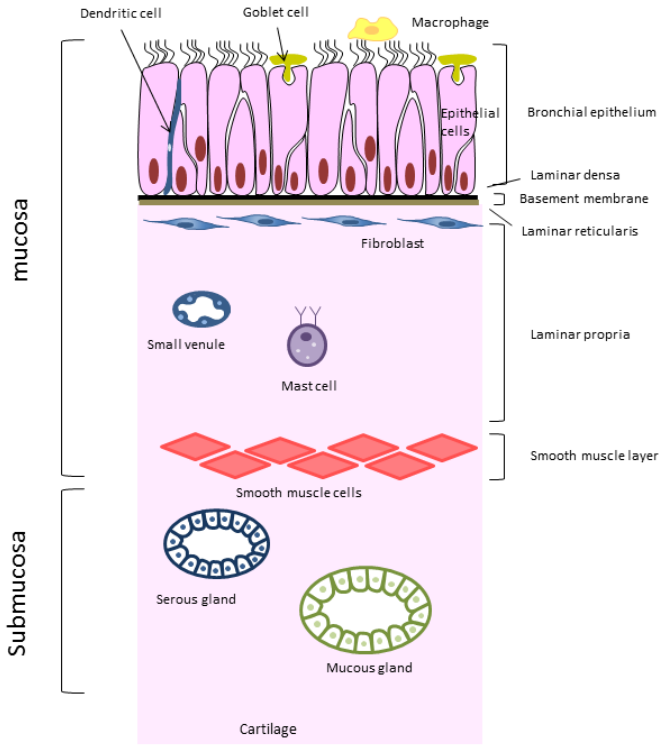

Figure 7 Schematic showing the composition of a healthy airway.

1.3 Pathophysiology of asthma

Asthma is a heterogeneous disease, not all patients have the same phenotype. The severity of the disease is broken down into 5 steps based on the medication used (Turner et al., 2011) (Figure 8). Step 1 contains mild asthmatics that only use inhaled short acting β2 agonists. Step 2 contains those who need to regularly use inhaled corticosteroids. Step 3 contains those who need additional therapy on top of inhaled corticosteroids. Step 4 contains those with persistent symptoms with poor control and step 5 contains those who need continuous use of oral steroids with poor control. This causes problems when trying to find adequate drugs, there will not be a single treatment. Stratified medicine will be the way to progress asthma drug discovery. Even with this every asthmatic will undergo some degree of airway inflammation and remodelling.

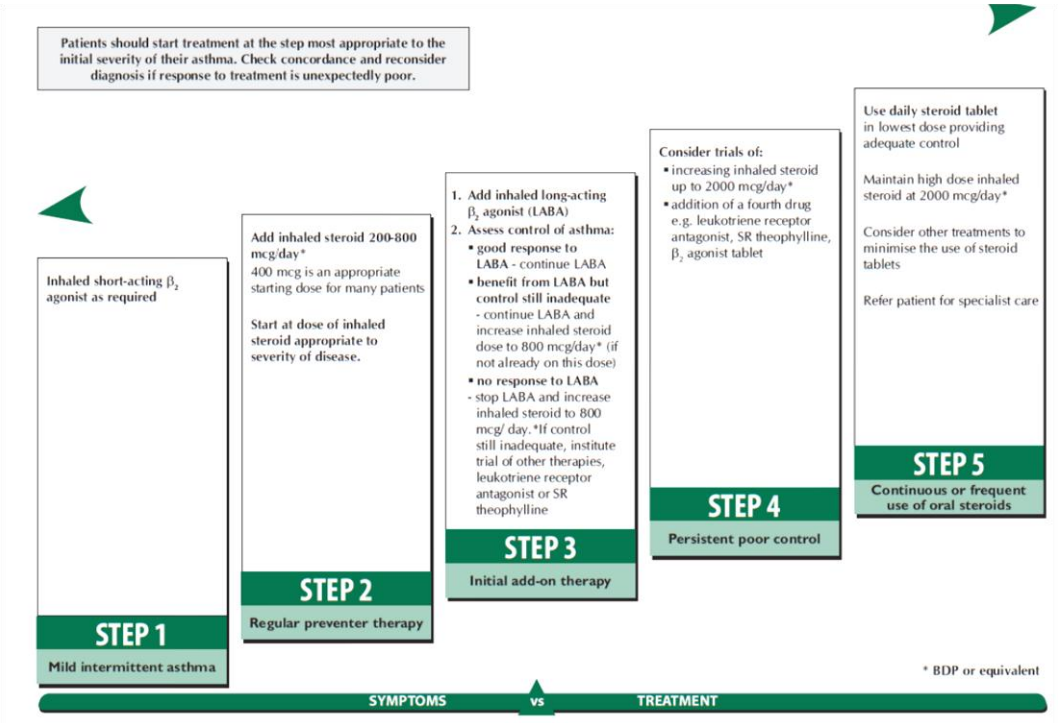

Figure 8 BTS guidelines.
(Network, 2008)

1.3.1 Airway inflammation

Asthma is a chronic inflammatory condition; there are degrees of asthma ranging from mild, to moderate, to severe. Due to this there are variations in the cells that infiltrate the airways. Allergic asthma is the most common phenotype (Mukherjee and Zhang, 2011) characterised by a T-helper-2 (Th2) response associated with eosinophilia. However other asthmatics have airway neutrophilia (especially those with severe steroid refractory disease) whereas others are characterised by a paucicellular response.

Allergic asthma is skewed to a Th2 response to innocuous allergens, leading to bronchoconstriction upon allergen inhalation. Th2 cells secrete cytokines mostly interleukins IL-4, IL-5 and IL-13, which stimulate mast cell degranulation, leading to

eosinophilia, leucocytosis and enhanced B cell IgE production, along with more Th2 cell formation (Murphy and O'Byrne, 2010). Allergic inflammation can be classified into categories, allergic sensitisation, early phase, late phase and chronic inflammation.

In individuals susceptible to asthma, such as those with atopy, the initial sensitisation arises from an allergen being detected by a dendritic cell (DC). The DC takes up the antigen, transport it to the lymph nodes and present it to naïve T cells. In the presence of IL-4 the T cells mature into Th2 cells; these leave the lymph nodes and travel to the detection site. Th2 cells secrete cytokines IL-4, IL-5 and IL-13 which maintain the Th2 promoting environment. They interact with B cells via a CD40 ligand on their surface, which interacts with the CD40 receptor on the surface of B cells. This interaction along with an environment containing IL-4 or IL-13 causes the B cell to convert to producing IgE rather than IgG or IgM (Galli et al., 2008). The IgE then binds to the surface of a mast cell or basophil via interaction with the high affinity receptor FcεR1 on their surface. Once a sensitised person inhales and comes into contact with the same allergen, the allergen binds to the IgE on the cell surface activating it, causing degranulation (Larche et al., 2006). This releases histamine, cytokines, chemokine's and lipid mediators, causing smooth muscle contraction, increased mucus production (Akdis and Akdis, 2011) and increased vasodilation and permeability (Galli et al., 2008), known as the early phase response. The mediators produced also attract eosinophils, basophils and Th2 cells.

The late phase reaction involves the recruitment of immune cells such as eosinophils and basophils. Typically the late phase reaction occurs 2-6 hours after exposure (Galli et al., 2008). Eosinophils are innate immune granulocytes that release cationic proteins which cause damage to parasitic pathogens and in chronic allergic diseases they can damage host tissues (Shamri et al., 2011). Under normal situations they are situated within mucosal tissue which forms an interface with the environment (Shamri et al., 2011). This location allows them to identify and respond to pathogens (Shamri et al., 2011). Basophils are granulocytes, which respond to various stimuli and are involved in the Th2 immune response (Schneider et al., 2010). They promote the development of IgE-mediated chronic allergic inflammation in mice; however this has been hard to prove in humans (Schneider et al., 2010).

Chronic inflammation causes damage to the epithelium, allowing more allergen or damaging agents through, forming a chronic wound scenario, which can lead to airway remodelling (Holgate et al., 2000).

1.3.2 Airway remodelling

1.3.2.1 Pathology

In asthma there are significant structural changes that occur, known as airway remodelling. The epithelium appears to be fragile; as creola bodies (Beasley et al., 1989) (small clumps of epithelial cells that still have beating cilia) can be seen in Bronchial alveolar lavage fluid (BALF) of asthmatic patients, suggesting that it is more easily damaged than that of a healthy subject. It has also been shown that the ZO-1 is not located as regularly in the tight junctions, suggesting that the tight junctions are leaky (de Boer et al., 2008). Bronchial brushings from asthmatic patients, when grown at ALI, show lower TER (Trans epithelial electrical resistance) and greater transport of FITC dextran (a fluorescently labelled sugar) across the barrier than those taken from healthy volunteers (Xiao et al., 2011). This suggests that both the ion and macromolecular transport is poorly regulated in asthmatics, due to these leaky tight junctions. The epithelium has also been shown to have increased goblet cells (goblet cell metaplasia), creating more mucus (ORDOÑEZ et al., 2001). This reduces the number of ciliated cells, therefore reducing the clearance of mucus. It is thought that the epithelium in an asthmatic patient is undergoing a chronic wound healing response. In asthmatics the fibroblasts become activated and gain a myofibroblastic phenotype. Myofibroblasts contain α-smooth muscle actin microfilaments, and have greater cell numbers in asthmatic airways (Brewster et al., 1990). It has been shown that the basal lamina secreted by the epithelial cells remains the same thickness, whereas the lamina reticularis composed of fibroblast secreted ECM thickens (Brewster et al., 1990).

There is increased vascularisation in the lamina propria (LI and WILSON, 1997), allowing increased entry to circulatory immune cells and extra nutrients for the activated cells within the asthma phenotype. Beneath the lamina propria is the smooth muscle layer, which becomes thicker, due to hypertrophy and hyperplasia (Jeffery, 2004). This increase only occurs in the mucosa layer not below into the submucosa. Within the submucosa there is an increase in the mucus and serous glands, increasing the mucus within the airways. Figure 9 shows the changes that occur during airway remodelling.

Studying the early stages of asthma has shown that these structural changes occur in the absence of inflammation (Saglani et al., 2007). This suggests that in asthmatic patients airway remodelling may occur independently of inflammation.

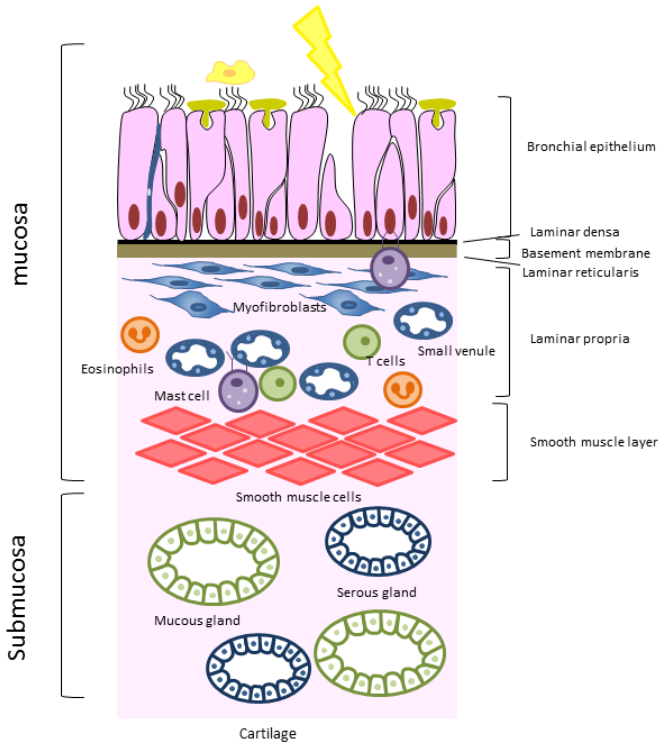

Figure 9 Schematic of an asthmatic airway.
The epithelium in the asthmatic airway is damaged, and has increased goblet cells. Underneath the epithelium the lamina reticularis is thickened, there is an increase in fibroblasts which have a myofibrotic phenotype. There is an influx of immune cells and increased vascularisation of the lamina propria. The smooth muscle has increased into the lamina propria. There are increased serous and mucous glands in the submucosa. Adapted from (Swindle and Davies, 2011).

1.3.2.2 Mechanisms

Epithelial repair in a normal subject starts with de-differentiation, flattening and migration from the wound edge, followed by proliferation of new epithelial cells (Knight, 2001). The wound healing is carried out with the help of the fibroblast layer below the basement membrane, in asthmatics the fibroblasts become activated and gain a myofibroblastic phenotype. Myofibroblasts contain α-smooth muscle actin microfilaments, and are found in greater numbers in asthmatic airways (Brewster et al., 1990). They can release inflammatory and fibrotic mediators that perpetuate the airway remodelling (Evans et al., 1999). There is a layer of fibroblasts with a close proximity to the epithelium, neural tissue and ECM known as the attenuated fibroblast sheath (Evans et al., 1999). The interactions between the sheath and the other tissues make up the EMTU (epithelial mesenchymal

trophic unit). The EMTU is first seen in branching morphogenesis in the developing foetal lung (Plopper and Hyde, 2008); it appears to be reactivated by the chronic wound response. By activating the EMTU the tissue environment may become skewed towards the Th2 inflammation in asthma (Holgate, 2008). The damaged epithelium releases TGF-β which can modify the phenotypes of fibroblasts in to myofibroblasts.

There is an increased angiogenesis in the airways in asthmatic subjects which brings in an increased number of immune cells. This is due to the pro-angiogenic action of inflammatory mediators for example VEGF which is secreted by epithelial cells, fibroblast and myofibroblasts (Meyer and Akdis, 2013).

1.3.3 Genetics

The majority of asthma is associated with atopy (the inherited predisposition to generate IgE against common environmental allergens) which affects up to half the adult population. However the majority of those who are atopic do not develop asthma (Holgate et al., 2009), suggesting that there are more mechanisms causing asthma than the Th2 story.

Asthma is a complex genetic disease that results from the effects of multiple genetic and environmental factors (Holloway et al., 2010). Many genes have been linked to asthma and their effects may influence disease susceptibility, severity and the response or lack of response to treatment. These genes have been discovered in several different ways; initially candidate genes were located based on evidence linking them to the asthma phenotype. Positional cloning was the next tool used in the investigation of genes. This is hypothesis independent; it searches through random markers within a family's genome looking for linkages to the phenotype in question. The latest method is genome-wide association studies, these are also hypothesis-independent, and can provide larger statistical power when investigating the same number of subjects (Holloway et al., 2010).

There are four main genetic components that have been linked to asthma susceptibility, sensing the environment, the immune response, barrier function and tissue responses (Holloway et al., 2010).

Genes associated with sensing the external environment, are involved in the triggering of the immune system. The induction of allergic inflammation and regulation of IgE are

influenced by polymorphisms in genes coding pattern recognition receptors (PRRs) and extracellular receptors, such as TLR2 (toll like receptor 2) (Eder et al., 2004). A SNP (single nucleotide polymorphism) in TLR2 has been strongly associated with asthma susceptibility. TLR2 transmembrane protein which recognises lipopolysaccharides found in the membrane of gram-negative bacteria (Lien et al., 1999). This SNP can alter the risk of immune responses to innocuous allergens.

The regulation of inflammation includes genes that regulate the differentiation of naïve CD4+Th cells into the Th2 cell phenotype, a key process in allergic asthma. There are many asthma susceptibility genes located within the IL-4 gene cluster on chromosome 5q31. IL-4 is a cytokine involved in the up-regulation of IgE. An SNP in the promoter region has been shown to influence serum IgE levels and airway hyperesponsiveness (Kabesch et al., 2003). This increases IL-4 production, which is linked to total IgE levels (Rosenwasser et al., 1995). This SNP has been shown to reduce FEV_1 (forced exhaled volume in 1 minute) in asthmatics (BURCHARD et al., 1999) and to be a risk factor for severe near fatal or fatal asthma (Sandford et al., 2000). Also linking atopy to allergic asthma is a SNP in the β-chain of FcεR1, this is one of the most replicated asthma susceptibility genes (Shirakawa et al., 1994). FcεR1 forms either a tetramer ($\alpha\beta\gamma_2$) or a trimer ($\alpha\gamma_2$), the inclusion of the β subunit amplifies the surface expression and signalling of the receptor (Donnadieu et al., 2003). This may affect the IgE dependant release of inflammatory mediators by mast cells and Th2 cytokine release from non-T cells and IgE-dependant antigen presentation by DC's. (Vercelli, 2008)

The epithelial barrier is vitally important in the fight against the inhaled environment; it secretes protective molecules. A large proportion of the novel genes located during genome-wide linkage studies are expressed in the epithelium. *ORMDL3* (orosomucoid1-like3) (Moffatt et al., 2007) is thought to be implicated in endoplasmic reticulum-mediated inflammation (Cantero-Recasens et al., 2010) and in sphingolipid dysregulation that may contribute to the development of asthma (Breslow et al., 2010). SNPs in ORMDL3 are linked to an increased risk of childhood asthma (Ober and Yao, 2011) that is not associated with atopy (Bisgaard et al., 2009).

The tissue response group consists of genes that control the effects of chronic inflammation and airway remodelling such as *ADAM33* (a disintegrin and metalloprotease 33) (Van Eerdewegh et al., 2002). Polymorphisms in this gene are associated with a rapid decline in

lung function and can predict reduced lung function in young children (Simpson et al., 2005). It has also been located in mesenchymal progenitor cells in developing lungs (Haitchi et al., 2005) suggesting that it has an influence in early life. In adults it is detected in the smooth muscle of the conducting airways (Haitchi et al., 2005) linking it to AHR. There is a soluble 55-kD form of the protein (sADAM33) which has been found in BALF from asthmatics, but not from healthy subjects. Increasing levels of sADAM33 in BALF correlate with decreased lung function, providing an insight into a disease-related effect (Lee et al., 2006). TGF-β enhances the release of sADAM33 suggesting that factors which cause epithelial damage may also be linked to *ADAM 33* and asthma pathogenesis, (Puxeddu et al., 2008) supporting the concept of the importance of the EMTU (Davies, 2009). sADAM33 has also been shown to be angiogenic (Puxeddu et al., 2008); angiogenesis is increased in both adults and children with asthma and correlates with reduced lung function (Vrugt et al., 2000). It is possible that this may contribute to inflammation in the lung by allowing the influx of immune cells and provide a source of nutrients for the developing smooth muscle. *ADAM33* is not linked to allergic asthma and atopy.

1.4 Treatments

Current treatment guidelines for asthma recommend a stepwise approach to increase the number, frequency and dose of medications based on increasing severity until the disease is under control (Figure 8).

The mildest form of asthma is treated with a short acting β2-adrenoceptor agonist (SABA), such as salbutamol (Cullum et al., 1969). The β2-adrenoceptor located in bronchial smooth muscle, causes bronchodilation when stimulated. Salbutamol has been used since the 1960's and is still the most common reliever. For all other forms of asthma inhaled corticosteroids are the standard treatment, with increasing doses dependent on the severity. Corticosteroids are currently the most effective anti-inflammatory drugs used in asthma treatment, improving lung function, decreasing AHR, reducing symptoms, and reducing the frequency and severity of exacerbations (Mcfadden, 1988). Dexamethasone was the first steroid to be shown to have an anti-asthma action through inhalation; however it had poor lung selectivity (Brown et al., 1972). There have been various improvements in corticosteroids over the years. Beclomethasone was the next created; its effects were confined to the airways. Fluticasone developed in 1996, has decreased absorption from mucosa (maintaining its action within the lung), while budesonide has a large first-pass metabolism and ciclesonide, is administered as a prodrug that can be activated locally by esterase's in the lung (Kevin, 2011). These drugs do not eradicate the disease, and studies have shown that some people never gain control of their asthma which is why we need to understand the disease better.

In moderate and severe asthma, a long acting β2-adrenoceptor agonist (LABA), salmeterol or formoterol can also be used to reduce symptoms. These are co–administered with inhaled corticosteroids as their use alone led to an increase in asthma mortality (Taylor, 2009). These have a longer duration of action that SABA approximately 12 hours or above. Formoterol has a quicker response time, making it better at relieving symptoms, as well as symptom prevention (Kevin, 2011).

Methylxanthines such as theophylline, have been used since the 1860's, where it was observed that a strong cup of black coffee could relieve symptoms in asthmatics (Persson, 1985). Theophylline is taken orally and has a short half-life; it has weak bronchodilatory effects giving greater benefits when used in conjunction with corticosteroids. It is a non-

specific phosphodiesterase inhibitor; use of specific phosphodiesterases inhibitors has given poor results for asthma treatment.

Cromones, such as cromoglycate were initially shown to act by inhibiting mast cell degranulation by blocking calcium entry. As sodium cromoglycate has a short half-life, a large amount of research has been carried out to create a more specific molecule, several got to clinical trial but none made it any further. One molecule nedocromil was found to be more efficient than cromoglycate. It has recently been shown that these molecules have an effect on other cells and are GPCR-3s (G protein coupled receptor 3) agonists (Edwards and Howell, 2000). The lipid mediators released by degranulation of the mast cell are eicosanoids formed via 5-lipoxygenase enzyme (Samuelsson, 2000). Another search for antagonists for mast cell degraulation found the cromone FPL55712 (Augstein et al., 1973). The first drug to enter the market was pranlukast in 1995, this incorporated components of FPL55712 which was a cystLt1 antagonist (Kevin, 2011). The second drug zafirlukast is composed of structural elements of FLP55712 and leukotrienes. Montelukast is a quinolone modified with Leukotriene structural elements (1998). These have a small/variable bronchodilatory effect, but can reduce symptoms such as cough, improve lung function and reduce airway inflammation. These are used in conjunction with inhaled corticosteroids.

Omalizumab is a humanized monoclonal anti-human IgE antibody. It binds to free IgE with a greater affinity that the FcεR1 high affinity receptor. This reduces the amount of free IgE within 1-2 hours after administration. It recognises the same epitope that binds to FcεR1, so only binds to free IgE, meaning that it cannot cause cross linkage or cell degranulation. There is a close correlation between free serum IgE and the amount of FcεR1 expressed on basophils. This causes a feedback loop which down regulates the receptors expressed, bringing down the levels of free IgE (Presta et al., 1993).

1.5 Models used in airway research

Over the past 30 years only 4 new asthma drugs have come on to the market. This may be due to the focus on the immune system for research, and the models used to investigate new molecules. As discussed earlier in this chapter asthma is not just a disease of Th2 driven allergic responses with more research needed into the structural aspects of the disease and also the different endotypes of asthma. Asthma is a disease where susceptibility genes and the interaction with environmental stimuli drive the disease, this needs to be recapitulated within the models used to study it. Animal models for example the mouse are not well suited to asthma research as they do not spontaneously develop asthma like symptoms

1.5.1 Animal Models

Animal models have been used to gain insight into the *in vivo* environment associated with asthma, although they should be thought of more as a model of allergic airway inflammation than asthma. The most common models used are rodents, due to their ease of handling and cost effectiveness compared to larger models. With the exception of the cat and horse, animals do not appear to spontaneously develop asthma-like diseases (Robin J, 2011). There are many ways to induce asthma like symptoms, the most common being sensitisation of the immune system to a previously unrecognised antigen, then challenging the airways with the allergen so that the allergic responses can be studied (Zosky and Sly, 2007). The most commonly used model is murine sensitisation to ovalbumin (OVA) (Tang et al., 2006). This protein is readily available and is easy to restrict from the animal. The sensitization is carried out via intraperitoneal injection with OVA and an adjuvant often aluminium hydroxide. The animal is subsequently challenged with an aerosol of OVA after an initial incubation period, giving rise to an immunological response similar to that of asthma (Zosky and Sly, 2007). The adjuvant has been shown to promote the Th2 phenotype (Brewer et al., 1999). There are some models that do not use an adjuvant, where sensitisation is carried out by exposing the immune system to the allergen or by transferring primed cells into a naïve animal. Hogan *et al* investigated adding antigen-primed $CD4^+$ T cells from the spleen of sensitised mice to non-sensitised mice (Hogan et al., 1998).

One of the main problems with most animal models is the lack of chronicity. The majority represent an acute inflammatory event. It has been shown that small animals that have been

sensitised to an allergen will initially respond, but if repeatedly challenged become tollerant (Kumar and Foster, 2002). A model with a more chronic presentation of the disease has been created by sensitising the animal, then exposing it to low doses of the aerosolised allergen following the initial sensitisation event (Temelkovski et al., 1998). As OVA is not an allergen that actually affects asthmatic patients, models using more relevant allergens have been developed; these natural substances also contain non immunogenic substances that act as adjuvants such as proteases (Goplen et al., 2009). Cates *et al* created a murine model sensitised to purified house dust mite extract (Cates et al., 2004). This can be administered through the airway mucosa and results in Th2 sensitization and airway eosinophilic inflammation. Goplen *et al* investigated a model sensitised against 3 natural antigens, dust mite, ragweed and aspergillus and compared it to the OVA model (Goplen et al., 2009). They showed that by using the combination of natural allergens they removed the tolerance (Schramm et al., 2004) that animals gained when chronically challenged with OVA. There is also a canine model that appears to have a chronic phenotype (Redman et al., 2001). This has been selectively bred using individual animals that have high IgE levels and eosinophilia. The puppies are sensitised to ragweed, then exposed to the aerosol at 13 day intervals and a third time 45 days later. After the third exposure the airway response to histamine was elevated and remained so for at least 5 months (Redman et al., 2001). However the cost effectiveness and labour involved in a canine model make it an unattractive choice. As well as determining the underlying mechanisms to allergic sensitisation, these models have been used to investigate remodelling (Reinhardt et al., 2005), viral infections in adult models (Tourdot et al., 2008) and weanlings (Becnel et al., 2005). Laboratory mice are usually genetically pure inbred strains of mice therefore lacking the heterogeneity seen in the human population; each breed has been bred to produce a specific phenotype. BalB/C mice are often used because they have a Th2 response (Watanabe et al., 2004). The Th2 response provided by these animal models is steroid sensitive, so does not model the uncontrolled asthma that does not respond to corticosteroid treatment.

Although an allergic response can be induced within mice there are several differences between the mouse and human lungs. Murine lungs have one lobe on the left and 3 lobes on the right, whereas humans have 2 lobes on the left and 3 on the right. There will also be a different pattern of deposition of particulates between the mouse and human lung due to the mouse being quadrupedal. There are further morphological differences within the structure of the airways. Humans have dichotomous branching whereas mice have

monopodial branching (Hyde et al., 2006). Humans have extensive submucosal glands beneath the epithelium whereas mice have them only in the trachea (Wenzel and Holgate, 2006). In the human proximal airways the mucus producing cells are goblet cells which decrease in number upon progression through the airway with more Clara cells in the distal airways. In contrast mice have clara cells throughout the whole airways (Pack et al., 1981). Basal cells in mice are only found in the trachea whereas in humans they are present throughout the airways (Rock et al., 2009).

Mouse models have identified IL-5 as a key mediator in allergic airway inflammation and highlighted its potential as a therapeutic target. However the use of a monoclonal antibody blocking IL-5 (mepolizumab) failed to provide a reduction in the late asthmatic response or airway hyper-responsiveness in clinic trails (Leckie et al., 2000). The mepolizumab was subsequently investigated using a subset of asthmatics with sputum eosinophilia and symptoms that persist with prednisone treatment. This provided a significant decrease in sputum and blood eosinophils leading to improved asthma control and FEV1(Nair et al., 2009). This highlights the need for models showing the various endotypes of asthma seen.

1.5.2 Cell culture models

Cell culture models are important in dissecting the fundamental processes and mechanisms controlling normal cellular physiology as well as variations in disease, allowing the identification of important pathways which may not always be present in animal models. The cells can be transformed virally, for example 16HBE14o- (16HBE) an SV40 large T antigen transformed bronchial epithelial cell line (Cozens et al., 1994) or be cancer derived cell lines for example A549. These can be used as submerged monolayers, on either tissue culture plastic or on transwells for biphasic conditions. Monolayers on tissue culture plastic enable investigation of the effects of cytokines on the cells when the orientation of release is not needed. The use of monolayers on transwells allows for the detection of released mediators either apically or basolaterally from the cells. In airway epithelium, this is the difference between the lumen and the tissue. Cell lines are transformed cells and are not the same as primary cells. Also they are undifferentiated, taking on a more basal cell phenotype. The cell lines are always submerged further removing them from the environment that is being modelled.

Primary bronchial epithelial cell (PBEC) cultures using cells from bronchial brushes obtained during bronchoscopy can be grown either as submerged monocultures or at an air

liquid interface (ALI) (Whitcutt et al., 1988). When grown at ALI with retinoic acid the PBECs differentiate into basal cells, ciliated columnar epithelium and mucus producing goblet cells, modelling the psuedostratified epithelium seen in the airways (de Jong et al., 1994). The use of these ALI cultures using cells from asthmatics or healthy volunteers has shown that in asthma the tight junctions are leaky, as shown by a decrease in TER and greater passage of FITC dextran across the cell sheet. These models are more representative of the human airways and can show the variation between healthy and diseased tissue.

Other methods for creating three dimensional models involve the use of aggregates. For example Carterson *et al* grew the A549 lung epithelial cell line in a rotating-wall bioreactor to produce aggregates, which were used to study infection with *Pseudomonas aerugunosa*. The outcome was that the cytokine response to infection was closer to the *in vivo* model than a cell monolayer (Carterson et al., 2005). However these studies are limited, as they contain only one cell type and are not in the same configuration as within the tissue of origin.

Numerous co-cultures have been used to investigate different aspects of airway disease, as these allow for the investigation of cross talk between cells. The two most popular methods are to grow cells separated by a thick layer of extracellular matrix or by the polymer membrane of a transwell. Zani *et al* used matrix-embedded epithelial and endothelial cells to study wound healing, discovering that a full recovery occurred when both cells were present (Zani et al., 2008).

Blank *et al* investigated the defence mechanisms to fine particles, using a three cell co-culture using epithelial cell lines grown on transwells, with macrophages added on top of the cells and dendritic cells added to the media below. They showed that the integrity of the epithelium influence particle uptake by dendritic cells, allowing an understanding of the interplay between the different cell types (Blank et al., 2007). There are also models of the airway blood barrier created by having endothelial cells on the underside of the transwell with epithelial cells on the top (Chowdhury et al., 2010). Chowdhury *et al* showed that the combination of epithelial and endothelial cells in close proximity caused an increase in TER. A similar model has been used to investigate the migration of immune cells; Mul *et al* for example noted an increase in neutrophil migration across the co-culture as well as an increase in cytokine release (Mul et al., 2000).

The use of technology has given rise to more techniques. For example Laser assisted bioprinting uses a modified laser printer to pattern cells onto a surface in the same way that ink would be. This approach can also be used to create multiple layers by printing cells on top of those already patterned. For example skin keratinocytes have been printed for use as skin grafts (Michael et al., 2013). Xu *et al* investigated the printing of Chinese hamster ovary cells and primary embryonic motoneurons from Sprague-Dawley rats. Here the cells were resuspended in Dulbeccos phosphate buffered salt solution and printed onto a hydrogel on a glass coverslip. The hydrogels used were a collagen gel or a soy agar gel. Both cell types had normal morphology after printing (Xu et al., 2005). Koch *et al* printed NIH3T3 fibroblasts, HaCaT keratinocytes and Bone marrow-derived human mesenchymal stem cells. The cells were resuspended in a mixture of blood plasma and alginate hydrogel and printed onto a matrigel layer on a glass slide. There were no viability problems or modifications to the phenotype or genotype of the three printed cell types. in addition the human mesenchymal stem cells didn't undergo any differentiation after printing suggesting that it was not harmful to the cells (Koch et al., 2009).

The addition of novel microfluidic technology into these techniques has allowed for the creation of mechanical forces within a model. This is beneficial for research into the behaviour of alveoli as there is mechanical strain across the cells during inspiration. Huh *et al* set up an air liquid interface with alveoli epithelial cells on one side of a PDMS (polydimethylsiloxane) membrane and endothelial cells on the other within a microfluidics chamber. A vacuum was set up to move the membrane in a manner that mimics inspiration (Huh et al., 2010). In this model it was found that mechanical strain enhanced both epithelial and endothelial cell uptake of the silica nanoparticles and accentuated the inflammatory and toxic responses to the nanoparticles compared to a static model.

Brushings are not the only primary cells that can be obtained from bronchoscopies. Biopsy's can also be taken and used in two different ways; tissue explant out growth models or tissue explant models. The outgrowth models involve placing the biopsy onto a transwell and allowing the fibroblasts to grow out, followed by the epithelial cells. The biopsy is then removed and the cells fill the wound (Lechner et al., 1982). This helps to keep all the cells within the same configuration as they were within the tissue and allows for direct contact between the epithelial cells and fibroblasts. This however is technically challenging and difficult to reproduce even with tissue from the same donor (Swindle and Davies, 2011). Tissue explant models use the whole biopsy which is stimulated to

determine how the whole tissue reacts (Jaffar et al., 1999). However this method does have disadvantages in that it does not have a circulatory supply, so cannot show the true extend of its recruitment of immune cells. It also has limited viability so only short-term experiments can be carried out on the tissue.

1.6 Thermoresponsive polymer surfaces

Cell sheet engineering is a technique whereby sheets of cells are grown to confluence and then used to create multi-layered constructs of different cell types. This technique takes advantage of thermoresponsive surfaces that allow the manipulation of cell sheets for the construction of a multi-layered 3d cell culture model. Conventionally, the cell sheets are lifted using a membrane that ensures the cell sheet does not fold up upon release from the polymer (Figure 10).

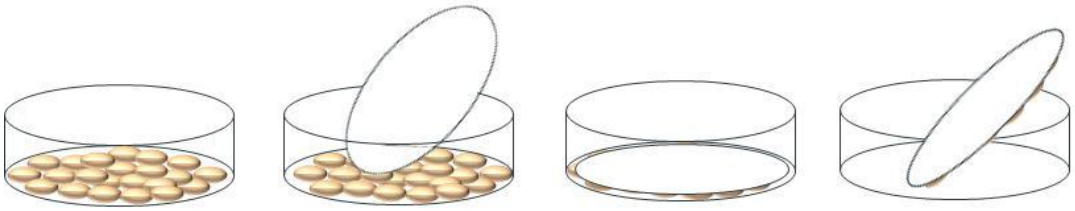

Figure 10 Schematic showing the method used to release cells from the UpCell dish.
Cells are grown to confluence; the provided membrane is placed over the cells and incubated at 20°C for 30 minutes. The membrane is peeled off the dish with the cells attached; it is then placed onto the next cell layer. After incubating for a further 30 minutes at 37°C the membrane is removed leaving behind the intact cell sheet.

The thermo-responsive polymer Poly(N-isopropyl acrylamide) (NiPAAm) has been shown to allow cell attachment to its surface when the temperature is above its lower critical solution temperature (LCST) of 37°C and cell detachment below its LCST of 20°C (Okano et al., 1993). When the temperature is above the LCST the polymer is collapsed, and below the LCST it becomes fully expanded (Figure 11). It is this change in wettability, which causes the release of a whole cell sheet without disrupting cell-cell interactions, for epithelial cells without disrupting the barrier function.

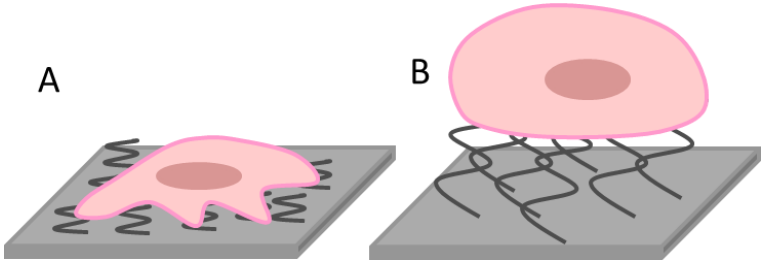

Figure 11 Schematic showing the change in polymer with decreased temperature.
A shows a cell on the compact polymer above its LCST and B shows the polymer fully expanded below its LCST.

There is a commercially available product which uses this thermoresponsive surface technology: “Thermo Scientific Nunc UpCell surface”, where NiPAAm is covalently attached to the surface of tissue culture plastic. The NiPAAm polymer has been used to create various cell culture models and grafts. Shimizu *et al* grew neonatal rat cardiac myocytes on the NiPAAm polymer coated tissue culture surface for 4 days to achieve confluence. The dish was incubated at 20ºC for 1 hour, after which time the cell sheet had spontaneously detached. The released cell sheet was transferred to the next cell layer by gently aspirating it into the tip of a 10ml pipette. Once transferred media was dropped onto the centre of the sheet to reduce folding, after the sheet had spread the medium was removed to allow the two sheets to adhere. After 30 minutes the transferred sheet had attached to the new cell layer. When the sheets of cells were overlaid the cells could be seen to beat presenting an avenue for transplantation of grafts for damaged heart tissue (Shimizu et al., 2002). Damage to the corneal epithelium can cause loss of stem cells leading to poor vision. Nishida *et al* investigated the release of both Human and rabbit limbal stem cells; the multi layered cells were released without damage to the cell sheets. The rabbit cell sheets transplanted into the eye without the need for sutures, which gave successful corneal surface reconstruction (Nishida et al., 2004).

Other polymers that have been shown to have an LCST are based upon poly(2-alkyl-2-oxazolines. These are an interesting group of polymers particularly for biological applications “as a rule of thumb” they have low toxicity (Luxenhofer et al., 2011, Mero et al., 2008) (Goddard et al., 1989) with both methyl and ethyl poly(2-oxazoline)s (MeOx and EtOx respectively) having FDA approval (Caponi et al., 2011). These two polymers also display ‘stealth’ behaviour, meaning they show reduced interactions with immune system proteins (Goddard et al., 1989, Gaertner et al., 2007). It has been shown that MeOx and EtOx polymers added in the medium of lymphoid mouse macrophages P388.D1, does not inhibit the activation of the immune system, and causes no loss of viability as shown by the MTT test (Kronek et al., 2011).

Oxazoline polymers are formed via the living cationic ring-opening polymerization of 2-oxazolines monomers (Seeliger et al., 1966); the polymers have a low polydispersity index due to this monomeric addition. The side chain can be easily modified with amines(Cesana et al., 2006) or carboxylic acids (Zarka et al., 2003) to achieve the different conditions required allowing for further enhancement of the surface via peptide conjugation or other

functionalization, for example adding small side chains such as propyl groups causes the polymer to become more thermoresponsive (Hoogenboom and Schlaad, 2011).

There are several biological applications already being researched using these polymers (Sedlacek et al., 2012), including drug delivery using micelles (Luxenhofer et al., 2010) or conjugation to a drug or protein (Tong et al., 2012). Co-polymers have been investigated for the creation of antimicrobial surfaces (Kelly et al., 2013), to block protein and cell adhesion for coating implant surfaces (Zhang et al., 2012) and a hydrogel for tissue engineering (Wang et al., 2011).

For cell adhesive surfaces it has been shown that Poly(2-ethyl-2-oxazoline) (PEtOx) attached to glass, allows the growth of HUVECs (human umbilical vein endothelial cells), and primary rat and sheep fibrocytes (Chang et al., 2002), HUVECs can adhere and spread on fibronectin coated PEtOx and PMeOx attached to glass (Zhang et al., 2012)and primary human dermal fibroblasts adhere to and proliferated on P*i*PrOx and a co polymer poly[(2-ethyl-2-oxazoline)-co-(2-nonyl-2-oazoline)] (Dworak et al., 2014). Dworak *et al* investigated the genotoxicity of the two polymers P*i*PrOx and a co-polymer poly[(2-ethyl-2-oxazoline)-co-(2-nonyl-2-oazoline)] using the comet assay (single cell gel electrophoresis for the detection of DNA damage) and found that growth on the polymer surfaces caused no DNA damage. Gene expression of the dermal fibroblasts on the co-polymer poly[(2-ethyl-2-oxazoline)-co-(2-nonyl-2-oazoline)] was investigated. Eight genes were upregulated (COL6A1, ICAM1, VCAM1, MMP8, MMP9, MMP10, MMP11 and MMP13). COL6A1 codes for the alpha 1 subunit of collagen IV, ICAM1 and VCAM1 are involved in cell-cell interactions and MMPs are involved in collagen organisation. These genes suggest that the cells are producing and organising ECM. There were 3 genes down regulated ITGA3, ITGA6 and SPP1. ITGA are integrin alpha subunits and SPP1 is involved in the attachment of osteoclasts to bone or bind hydroxyapatite with high affinity. The modified expression of these genes may be because different integrins are used to bind to the polymer surface. They were able to release the primary human dermal fibroblasts from P*i*PrOx and the co-polymer. Very little else is known about the biocompatibility of related polymers, in particular for the growth of cells.

1.7 Sonotweezers

In1874 August Kundt showed fine particles collected at the nodes of a standing wave (Sarvazyan, 2010). Over recent years this knowledge has been used for the manipulation of

cells, for example Petersson *et al* separated red blood cells and platelets (Petersson et al., 2007).

A standing wave is formed when a sound wave is reflected back on itself; it causes interference where the two waves moving in opposite directions come together forming a constant nodal position. This standing wave generates a stationary pressure gradient across the fluidic chamber. A simplistic view is that acoustic manipulation moves particles from areas of high acoustic pressure to areas of low acoustic pressure by means of acoustic radiation pressure. The pressure node of the standing wave is the area where there is no pressure, so particles will accumulate here. However particles move through the pressure gradient dependent upon their density and compressibility when compared to the surrounding fluid. Acoustic radiation forces within a standing wave are generated by the interaction between the acoustic field scattered by the particle and the standing wave itself. The time averaged radiation force on a particle relates to the gradients of the kinetic and potential energy densities. The kinetic energy density gradient is related to the acoustic velocity field within the standing wave. It is dependent on the densities of the particle and the surrounding fluid. The potential energy gradient is related to the acoustic pressure within the standing wave and is related to the compressibility of the particle and the surrounding fluid. Most particles of interest are denser and less compressible than the surrounding fluid. Therefore the force on them tends to move them to the acoustic pressure node and the acoustic velocity antinode. In a planar resonator these are co-located (Glynne-Jones et al., 2012)**.** Modification of the surrounding fluid may be used to reverse the direction of this force; which can be used for particle separation. There will also be a lateral force moving the cells towards the central axis. This is a much weaker force than that in the axial plane but is used within devices to keep particles central against fluid flow (Nilsson et al., 2009). The majority of devices currently used for particle manipulation are half wavelength devices, where the chamber height is half a wavelength. This means that at resonance there is a pressure node and a velocity antinode in the centre of the chamber (Figure 12).

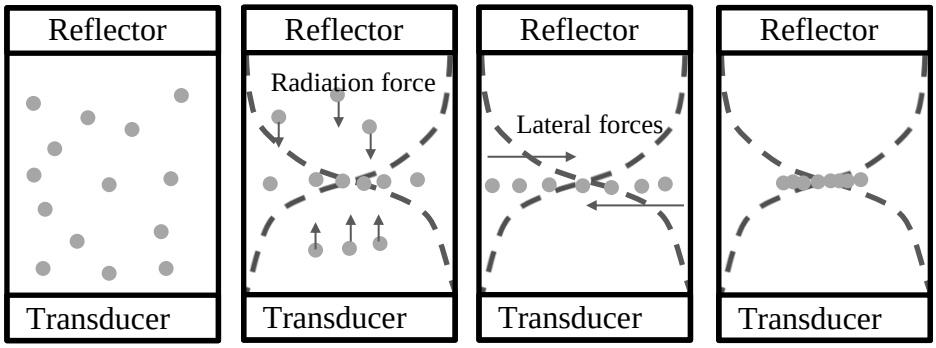

Figure 12 Schematic showing the forces acting on particles within an acoustic tweezers device such as the Sonotweezers. Adapted from (Nilsson et al., 2009).

There are many applications for these devices including particle filtration, washing, separation, sensing and detecting, cell-interaction studies and sonoporation. As this project is interested in cell manipulations these will be reviewed here. The majority of work using similar devices work on cells in suspension, where the cells move to the nodes of the wave (Shi et al., 2009). Both single cells (Wu, 1991) and two dimensional cell aggregates (Bazou et al., 2005b) have been levitated or 'trapped'. Hulstrom *et al* studied the viability of COS-7 cells after the application of ultrasonic forces and found that after thirty minutes of manipulation with ultrasonic standing waves there was no detrimental effect on cell viability (Hultstrom et al., 2007). When looking at two dimensional neural cell aggregates within a half wavelength device Bazou *et al* determined that there was no decrease in cell viability during 1 hour levitation. They added the live cell stain calcein AM, the dead cell stain ethidium homodimer-1 and the apoptosis stain Annexin V into the device during levitation and compared the uptake of the dyes by the cells at 1 minute and after 1 hour. Fluorescence analysis of the captured sheets showed no difference between the time points (Bazou et al., 2005a). The same laboratory has carried out a substantial amount of cell studies; they established that monolayers can be formed within the devices (Coakley et al., 2004). These investigators studied the initial cell-cell interactions in chondrocytes; which form monolayers within the device. They looked at f-actin and gap junctional communication. After 1 hour the F-actin had accumulated at the cell-cell contact interface and the gap junctions had formed. These were removed from the trap for immunofluorescent staining. This showed that this cell type formed cell-cell interactions within the device without interacting with the matrix (Bazou et al., 2006b). They also investigated the differences in prostate epithelial cell line (PZ-HPV-7) and cancerous prostate epithelial cell line (DU-145). They showed that the normal epithelial cell line formed more contacts than the cancer cells during the hour within the device, suggesting that some cell-cell contacts were made within epithelial cells without contact to the matrix

(Bazou et al., 2006a). However these studies did not determine whether the cells became polarised, as this is thought to be dependent upon integrin matrix interactions allowing the cells to determine their apical and basal sides. The current data shows that there is no decrease in viability for cells levitated for 1 hour and that cell-cell junctions have started to form suggesting that there will be no adverse effects from the use of the Sonotweezer device on bronchial epithelial cells.

1.8 Aim

The aim of this project is to create a multi-layered cell culture model of the airways for the study of asthma using cell sheet engineering.

1.9 Hypothesis

A multi-layered three dimensional cell culture model of the airways for the study of asthma can be created; an epithelial cell sheet grown on a thermoresponsive polymer can be released from the surface and levitated using ultrasonic standing waves, once levitated various cell types can be added underneath.

1.10 Objectives

1.10.1 Characterisation cell release from the UpCell dish

I. Demonstrate release of a bronchial epithelial cell sheet from the thermoresponsive UpCell dishes.
II. Immunofluorescently stain for ZO-1 and F-actin within the released sheet. To determine whether the tight junctions or actin cytoskeleton have been disrupted by the manipulations carried out on the sheet.
III. Establish the release of single cells from the cooled UpCell dish within the Sonotweezers device.

1.10.2 Characterisation of the cellular responses on novel polymer surface.

I. Demonstrate release of a bronchial epithelial cell sheet from the NiPAAm based polymer 70:10:20 provided by the University of Southampton School of chemistry department.
II. Determine whether bronchial epithelial cells will form cohesive sheets on Oxazoline based polymer surfaces.
III. To determine the adhesion of the polymer coated surface for bronchial fibroblasts and bronchial epithelial cell lines.
IV. To determine the cell motility on the polymer coated surface.
V. To investigate cell selectivity of the polymer coated surface.
VI. To determine whether there are any stresses on the cells caused by growth on these surfaces.
VII. Investigate release of a bronchial epithelial cell sheet from an oxazoline coated surface.

1.10.3 levitating sheets of bronchial epithelial cells within the Sonotweezers device

I. Establish that bronchial epithelial cells will survive within the Sonotweezers for 5 days.
II. Demonstrate that bronchial epithelia cells will form cell-cell interactions without contact with a surface.
III. Determine the viability of the cells within the Sonotweezers device.
IV. Demonstrate that F-actin is important in to formation of cell-cell interactions.
V. Use the sheets formed with in the device to make a multi-layered cell culture model.

1.10.4 Thermo-gelling polymer

I. Determine cell viability on thermo-gel.
II. Create a multi-layered cell culture model using the thermo-gel.

1.10.5 Ethics

Initial experiments will be carried out using the 16HBE14o- cell line, so no ethical approval is needed. The primary cells used for ALI culture will be obtained as part of the study “Pathophysiology of Airway diseases such as asthma and COPD” which has already been granted approval from the Southampton local research ethics committee. Rec. No 05/Q1702/165, code MRC0268. These cells are obtained from volunteers who have given informed consent, with only those who have received ethical approval present, and all samples are randomised with only a number present when received in the laboratory.

2. Methods

2.1 Cell Culture

Five cell types were used within this study; all were cultured at 37°C, in 5% CO_2 in air. 16HBE14o- (referred to as 16HBE, a gift from Professor D.C. Gruenert, San Fransisco, USA (Cozens et al., 1994) passage 48-60 were cultured in modified Eagle's medium (MEM) plus glutamax (Life technologies, Paisley, UK) supplemented with 10% heat-inactivated foetal bovine serum (FBS)(50 units/ml) (Life technologies) and 1% penicillin (50units/ml)/streptomycin mix (20µg/ml).

HeLa cells passage 80-95 were cultured in Dulbecco's modified Eagle's medium (DMEM) (Life technologies) supplemented with 10% FBS (50 units/ml) and 1% penicillin (50 units/ml)/streptomycin (20µg/ml), 1% L- glutamine (2mM).

MRC5 passage 40-50 were cultured in DMEM supplemented with 10% FBS (50 units/ml) and 1% penicillin (50units/ml)/streptomycin (20µg/ml), 1% L-glutamine (2mM), 1% sodium pyruvate (1mM), and 1 % non-essential amino acids (1mM).

HUVEC (human umbilical vein endothelial cells) passage 1 were cultured in M199 medium (Life technologies) supplemented with 20% Human serum, 1% L-glutamine (2mM) and 1% Penicillin (50 units/ml)/streptomycin (20µg/ml). These cells were isolated from primary tissue by Dr Tim Millar prior to culturing.

Primary bronchial epithelial cells (PBECs) were obtained via bronchial brushings from bronchoscopy. Ethical approval was obtained from the Southampton local research ethics committee under the description 'pathophysiology of airway diseases such as asthma and COPD', rec. No 05/Q1702/165, code MRC0268.All volunteers had provided informed consent. These samples were anonymous-linked; the access to patient information was only available to those with prior ethical approval. These cells were cultured in BEGM (bronchial epithelium growth medium) (BEBM) (Clonetics, San Diego, CA, USA), supplemented with 52µg/ml bovine pituitary extract, 10µg/ml transferrin, 5µg/ml insulin, 1.5µg/ml BSA, 0.5µg/ml hydrocortisone, 0.5µg/ml epinephrine, 6.5ng/ml triiodothyronine, 0.5ng/ml human epidermal growth factor, 50nM retinoic acid and 0.1% GA-1000 solution (singlquots).

All media were pre-warmed to avoid stressing the cells. The passage numbers of the cell lines are those recorded on stocks within the Brooke Laboratory, no record of the passage number of the cell lines when they arrived at the laboratory has been documented. The cell types were cultured separately to ensure that there was no cross contamination, which was confirmed using microscopy due to the varying morphology of the different cell types.

2.1.1 Routine passage and seeding

The cells were washed with HBSS (Hanks buffered salt solution) without calcium or magnesium, to remove any traces of FBS. Proteins in FBS can block the action of trypsin. 1ml of trypsin (0.05% trypsin-EDTA, HBSS) was added and incubated for approximately 7 minutes at 37°C, 5% CO_2 for 16HBE cells, 2 minutes at 37°C, 5% CO_2 for HeLa cells and 2 minutes at room temperature for HUVEC cells. 9ml of complete medium was added to halt the activity of trypsin on the cells. The cells were centrifuged at 300 x g and resuspended in 1ml of complete medium. Cells were quantified using trypan blue exclusion cell count method. 5µl of cell suspension was added to 15µl of HBSS and 5µl trypan blue, 10µl of this was placed in the haemocytometer. The viable cells within the centre $1mm^2$ square were counted; the viable cell count was calculated using the following equation.

Viable cells per ml = Cell count/mm^2 x 10^4 (volume of the chamber) x 5 (dilution factor)

The cell suspension was supplemented with the appropriate amount of medium, dependent upon the cell concentration needed for each experiment. For routine maintenance 3×10^5 cells were added to a collagen coated T75 flask.

2.1.2 Cryogenic storage and revival

To prepare cells for cryogenic storage a flask was passaged as describe in 2.1.1, these are made up to a concentration of $1x10^6$ cells per ml in cold freezing medium (complete medium plus 10% DMSO) and frozen in 1ml aliquots in 2 ml cryopreservation tubes. DMSO (dimethyl sulfoxide) is a cryoprotectant, it reduces the formation of ice crystals when the suspension is frozen; warm it is toxic to the cells as it can permeabilise the cell membranes. The cells were cooled slowly to -80°C before, transferring to liquid nitrogen for long term storage.

A vial containing $1x10^6$ cells was removed from liquid nitrogen storage; 1ml of warm medium was immediately added to thaw the vial rapidly, reducing damage to the cells. 9mls of medium was added, the cells were centrifuged at 300 x g for 5 minutes, and the supernatant was discarded, removing DMSO.

2.1.3 Commercially available Nunc UpCell

Cells were passaged as describe in 2.1.1, and 8 x 10^5 16HBE or 5 x 10^5 HeLa cells seeded on 3.5cm^2 UpCell tissue culture dishes (Nunc, Fisher scientific, Loughborough, UK) and grown to confluence overnight. Images were taken on Leica DMI 6000B microscope, with the heated chamber at 37°C to maintain the polymer in its compressed formation. The majority of the medium was removed and the membrane placed on top of the cell sheet. These were incubated for 45 minutes at room temperature. The membrane was carefully removed and placed onto tissue culture plastic dish and incubated for a further 30 minutes at room temperature. A small amount of room temperature medium was added on top of the membrane, which was gently removed using forceps. The dish was topped up with media and the cells replaced into the incubator (Figure 13).

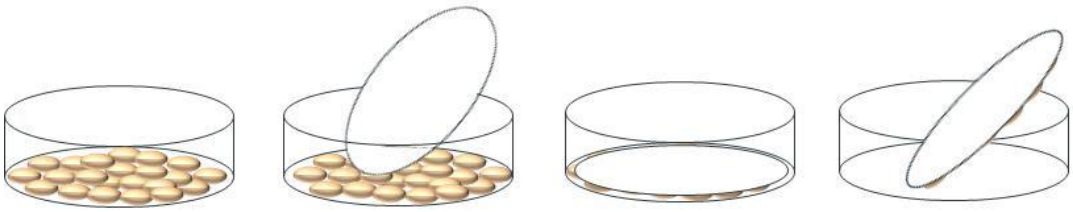

Figure 13 Schematic showing the release of a cell sheet from the UpCell dishes.
Cell are grown to confluence, the provided membrane is placed over the cells and incubated at 20°C for 30 minutes. The membrane is peeled off the dish with the cells attached it is then placed onto the next cell layer. After incubating for a further 30 minutes at 37°C the membrane is removed leaving behind the intact cell sheet.

This method was further modified for the bronchial epithelial cell line within (Figure 33).

2.2 Creation fluorescent cell lines

To aid in the visualisation of the different cell types used for the creation of the co-culture model 16HBE and MRC5 cells were transfected with fluorescent proteins

2.2.1 GFP transfected 16HBE cells

5 $x10^5$ 16HBE cells were seeded into a 6 well plate and left to adhere overnight to reach 60% confluence. Transfection was carried out using TransIT-2020 transfection reagent

(Mirus Bio, Madison, USA). The TransIT-2020 reagent was warmed to room temperature. 250µl of Opti-MEM reduced serum medium was added into a 0.5 ml tube with 2.5µg (2.5µl of 1µg/µl stock) of GFP plasmid (Clontech, California, USA) (Figure 14) and gently mixed. 7.5µl of TransIT-2020 reagent was then added and incubated at room temperature for 30 minutes. While this was occurring the media was changed on the cells. The reagent DNA solution was added drop wise over the well, and gently mixed by moving the plate. After 48 hours selection medium was added containing 600µg/ml G418 (Life technologies) to select for the plasmid containing cells. The selection medium G418 concentration was dropped to 200µg/ml once the majority of cells were green

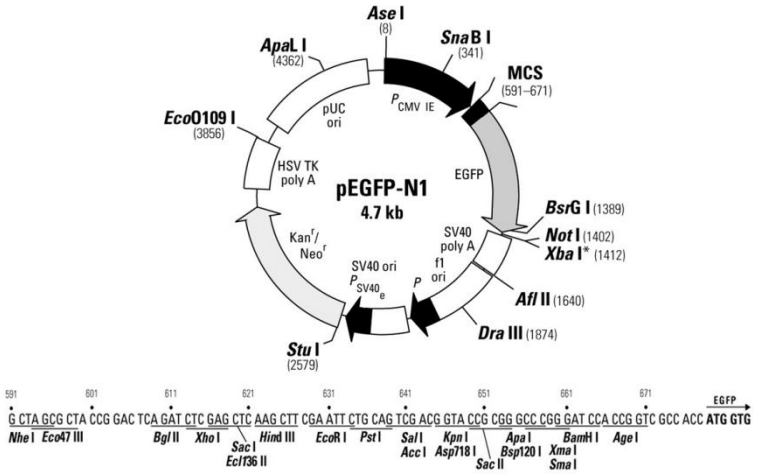

Figure 14 GFP plasmid used to create the 16HBE GFP cell line

The remaining cells were left to achieve confluence before being FACs sorted. A single cell suspension of non-transfected 16HBE cells was used to determine the parameters before the GFP transfected cells were sorted using FACSAria (BD biosciences, New Jersey, USA) (Figure 15).

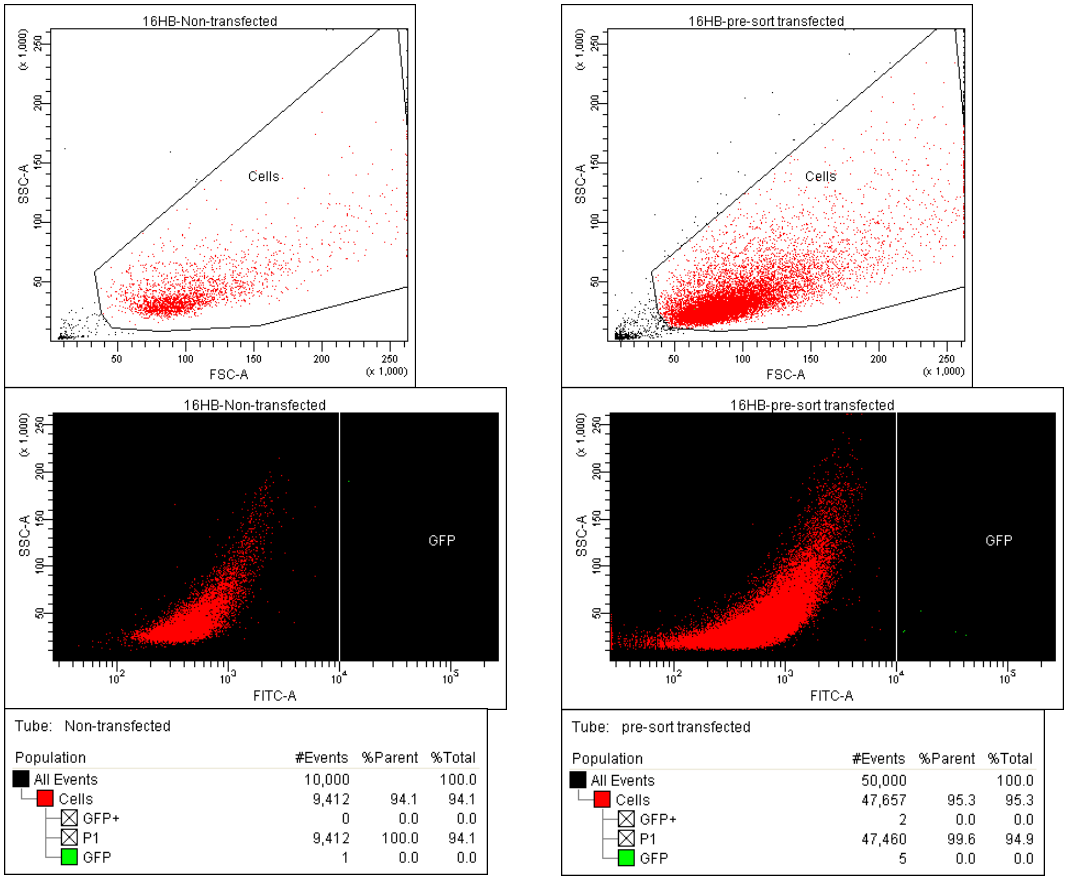

Tube: Non-transfected

Population	#Events	%Parent	%Total
All Events	10,000		100.0
Cells	9,412	94.1	94.1
GFP+	0	0.0	0.0
P1	9,412	100.0	94.1
GFP	1	0.0	0.0

Tube: pre-sort transfected

Population	#Events	%Parent	%Total
All Events	50,000		100.0
Cells	47,657	95.3	95.3
GFP+	2	0.0	0.0
P1	47,460	99.6	94.9
GFP	5	0.0	0.0

Figure 15 Parameters for the FACs sorting GFP 16HBEs

2.2.2 Creation of DsRed transfected MRC5 cells

2 x 10^6 MRC5 cells were resuspended in 300µl of Ingenio Electroporation solution (MirusBio), 250µl of this was added into a 0.4cm cuvette along with 7µl of DsRed plasmid (0.1µg/µl stock) (Clonetech) (Figure 16). The DsRed fluorescence is driven by a CMV promoter. This was then electroporated using the BioRad Gene Pulser (BioRad) at 280 volts, 950µF capacitance for 15ms. The cells were then plated into a T25 with 5 ml DMEM without antibiotics. The media was changed after 24 hours, after 3 days the selection antibiotic G418 was added at a concentration of 400µg/ml until the majority of the cells fluoresced. The G418 concentration was then dropped down to 100µg/ml for maintenance of the transfected population. The cells were then FACs sorted to obtain a pure population (Figure 17).

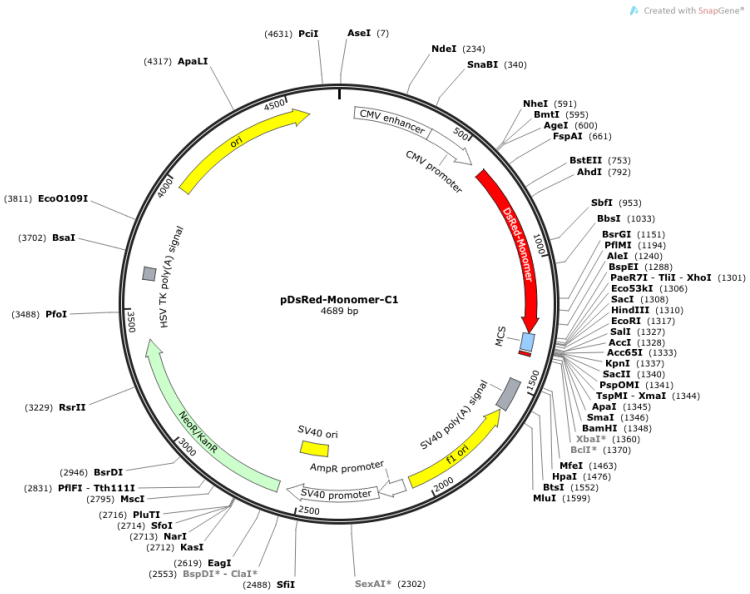

Figure 16 DsRed plasmid used to a create stably transfected MRC5 cell line

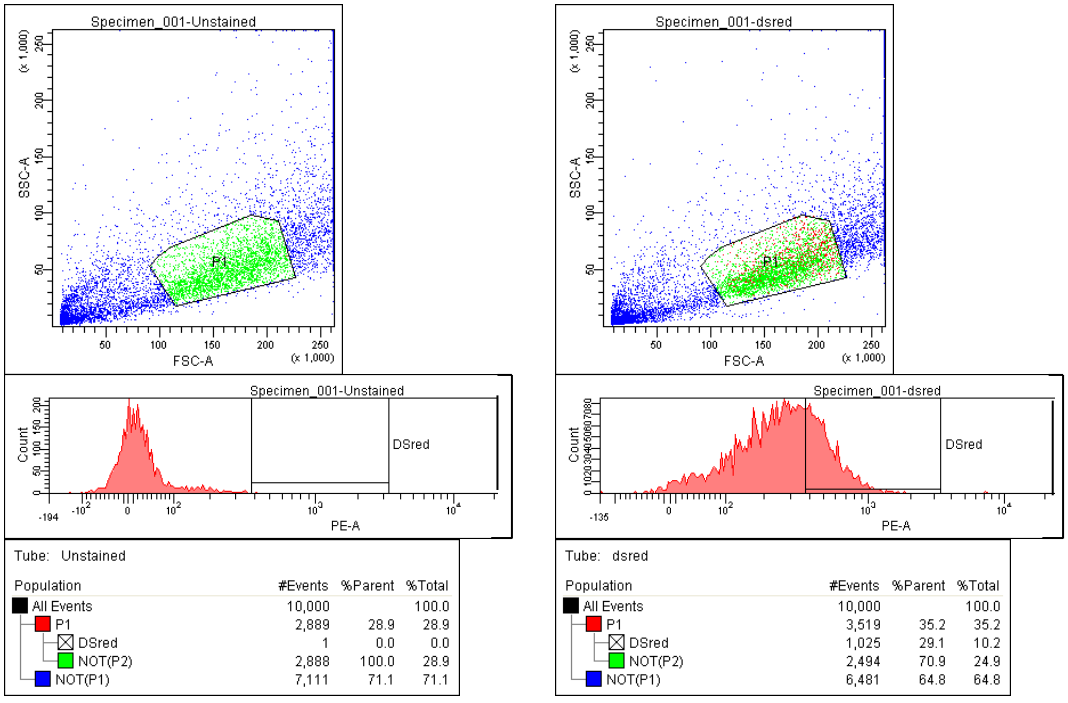

Figure 17 FACs plots for selection of DsRed MRC5 cells

2.3 Thermoresponsive polymers

The polymer chemistry for the NiPAAm polymers was carried out by Andrew Treherne and for the oxazoline polymers it was carried out by Adam Fisher and Tom Hartland, School of Chemistry, University of Southampton; for more detailed, methods see appendix.

2.3.1 Soluble polymer coatings

When working with the polymer, all solutions were pre-warmed to 37°C, to limit cooling of the polymer during handling.

The polymers which were used to coat the surface of a tissue culture dish were dissolved in isopropanol (isopropyl alcohol, IPA) (Sigma-Aldrich), and were subsequently applied at onto tissue culture plastic or glass coverslips and left to stand within a class 2 cell culture hood for a minimum of 1 hour to allow the IPA to evaporate.

2.3.1.1 Release of cell sheets

Polymer coated 12 well plates were seeded with 1ml of 6 x10^5 16HBEcells/ml for next day experiment or 4 x 10^5 16HBE cells/1ml for use within 48 hours or 5 x 10^5 HeLa cells/ml for next day experiment or 3 x 10^5 HeLa cells/ml for use within 48 hours. Once the cells reached confluence, microscopic images were taken. To release the cell sheets the medium was replaced with cold medium (straight from the fridge) and the cells were incubated at 20°C for 30 minutes, to allow dissolution of the polymer. The cells were flushed with a 1 ml Gilson pipette to lift any released cell sheets. Images were taken of these detached cell sheets.

2.3.1.2 Testing the polymer time lapse

To determine whether the polymer was remaining *in situ*, 30 µl of polymer at 1.3 mg/cm^2 was dropped into the middle of a 6 well tissue culture plate and dried within a class 2 cell culture hood for a minimum of 1 hour to allow the IPA to evaporate, leaving a visible edge. The polymer coated plates were placed into the heated chamber of a time lapse microscope (Leica DMI 6000B, with heated chamber). 3ml of 37°C or 20°C 16HBE media was added to the well, while time-lapse was running at intervals of 141ms per image for 5 minutes. The resulting images were analysed visually to determine whether the polymer was still attached.

2.3.2 Poly(2-alkyl-2-oxazoline) polymers covalently attached to a glass surface

In summary, glass coverslips were cut to size with a diamond tipped pen (1cm x 2cm). The slides were submerged in concentrated sulphuric acid: hydrogen peroxide 3:1 v/v (piranha

solution) to thoroughly clean the slides and hydroxylates the surface for silane attachment. After an hour they were washed with water, then ethanol. The slides were immersed in (3-aminopropyl)triethoxysilane (38µl) in freshly distilled ethanol (5ml) for 1 hour. They were then washed in ethanol before being heated to 80°C for another hour.

2-Alkyl-2-oxazoline (259.81mmol) was mixed with acetonitrile (44ml), and methyl p-toluenesulfonate (0.261ml, 1.73mmol). This was split into 3ml aliquots, in microwave vials. Each vial was microwave irradiated for 15 min (ramp time 20 min; 135°C; 130 psi). The polymer solution was then split into two vials with 0.030ml of triethylamine and 1.5ml of acetonitrile added. An amine-coated slide was added and the reaction mixture was left overnight at 60°C. The glass slide was then removed, rinsed with copious amounts of ethanol, and dried under a stream of nitrogen.

2.3.2.1 Contact angle goniometry

Contact angle goniometry was used to determine the addition of each functional group to the glass surface. This is a method for detecting changes on a surface. A 1µL droplet of distilled H_2O was placed on the surface and the angle where the droplet met the surface was measured. If a surface is hydrophilic this angle will be smaller and if the surface is hydrophobic it will be larger. This was performed using a Kruss DSA 100 drop shape analyser running SMARTDROP contact angle software on a windows PC.

2.4 Characterisation of cells on the polymer

To determine the biocompatibility of the cells on the oxazoline polymer coated coverslips various tests were carried out.

2.4.1 Fixing and fluorescent staining of cell sheets for ZO-1, E-cadherin and F-actin

Conjugation of ZO-1 mouse IgG1 (Invitrogen) and E-cadherin mouse IgG_1-k (Invitrogen) antibodies was carried out using Lightening-Link conjugation system (Innova Bioscience, Cambridge, UK). 1µl of LL-Modifier per 10µl of antibody was added to the antibody solution and gently mixed. The antibody solution was then added to the Lightening-Link mix and gently mixed. This was then incubated in the dark at room temperature for 3 hours. 1µl per 10µl of antibody of the LL-Quencher FD was added; this was then aliquoted and stored -20 until needed.

The F-actin was stained using a fluorescently labelled phalloidin, Acti-stain™ 555 phalloidin or Acti-stain™ 670 phalloidin, (cytoskeleton, Inc, Denver, USA) rather than an antibody. Phalloidin binds with high affinity to F-actin but not monomeric actin.

Cells were washed in PBS and fixed in 4% paraformaldehyde for ZO-1 and F-actin or with acetone: methanol 1:1 E-cadherin. The cells were permeablised for 15 minutes in perm-buffer (PBS, 0.1% triton X-100), before being blocked for 1 hour in block-buffer (PBS, 1% BSA, 0.1% Tween 20). The antibodies and phalloidin were diluted in block-buffer; ZO-1 conjugated alexa647 (1 in 1000; 0.77µg/ml) and F-actin (1 in 500), E-cadherin conjugated Alexa488 (1 in 500). The antibodies and phalloidin were incubated overnight, washed with perm-buffer and mounted using prolong gold plus DAPI (diamindino-2-pheylindole) (Invitrogen) nuclear counterstain. Fluorescent Z stack images were taken using either fluorescent light microscope (Leica DMI 6000B) and deconvoluted using the Leica software, or using confocal microscope (Leica SP5 laser scanning confocal microscope)

2.4.2 Cell adhesion

To ensure that all cells were at the same density on the varying surfaces an adhesion assay was used to determine the necessary seeding efficiency.

2.4.2.1 Calcein staining

To enable analysis of the cells they need to be fluorescently labelled, Calcein is a cell permanent dye. In live cells, the non-fluorescent calcein acetoxymethylester (calcein AM, Invitrogen) is converted to the green fluorescent calcein anion after acetoxymethylester hydrolysis by intracellular esterases. Trypsinised cells were resuspended at a concentration of $1x10^6$ cells/ml, 2mM calcein AM was added and incubated in the dark at room temperature for 30 minutes, allowing the dye to enter the cells. The cells were then washed 3 times by centrifugation to remove any excess dye.

2.4.2.2 Fluorescent plate reader

To validate the adhesion assay, initial experiments were performed in a 96 well plate where cell number could be assessed using a fluorescent plate reader. A black flat bottomed 96 well tissue culture plate was coated with several ECM proteins. 50µl of 1% collagen (pureCol, 97% type I collagen, (Advanced BioMatrix (Tucson, AZ, USA), 0.2% porcine skin gelatin (Sigma-Aldrich), 50µg/ml Human fibronectin (Sigma-Aldrich) or1mg/ml BSA were added to the wells and incubated at 37°C with 5% CO_2 for a minimum of 30 minutes. The BSA was used as a negative control; cells should not bind to this, as it is not an ECM

protein. $3x10^4$ calcein stained cells were added to these ECM coated wells or plain wells. At different time points (5, 15, 30, 45 and 60 minutes) 3 of these wells were washed 3 times to remove any cells that were not adhered to the surface. A standard curve (Figure 18) was set up by adding $3x10^3$ cells to $3x10^4$ into 8 wells. The plate was then read in the plate reader (Labsystems Multiskan Ascent plate reader) at 490nm excitation and 520nm emission. The standard curve was created and the interpolated cell numbers calculated using GraphPad Prism (GraphPad software, La Jolla, CA, USA).

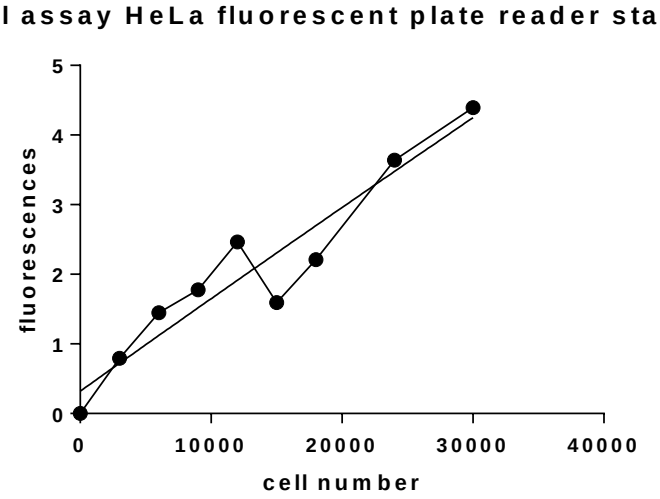

Figure 18 Standard curve from the plate reader.
Calcein stained HeLa cells at known concentrations between 3 x 10^3 and 3 x 10^4 were added in to three rows of a black 96 well plate. The plate was read in a fluorescent plate reader at 420nm, the average readings were taken and the standard curve determined

2.4.2.3 Microscopic analysis

A clear flat bottom tissue culture plastic 96 well plate was set up as in 2.4.2.2. The centre of the well was imaged using a fluorescent microscope (Leica DMI 6000B) and the cell number within this image counted using image J. This was corrected for the area of the well using the following equation.

(Area of the image / area of the well) x 100 = percentage of the area of the well within the image.

(Number of cells counted/ percentage of area imaged) x 100 = corrected cell number.

2.4.2.4 Microscopic analysis on glass coverslips

The oxazoline polymers were attached to glass coverslips, therefore any characterisation needs to be carried out on glass. Therefore a well needed to be created on the glass coverslip.

Coverslips were coated with ECM proteins; these were allowed to dry fully. They were attached to a glass slide using water surface tension; 6.4 mm diameter cloning rings (Sigma-Aldrich) were attached to the coverslip using silicone grease (Sigma-Aldrich) (Figure 19).

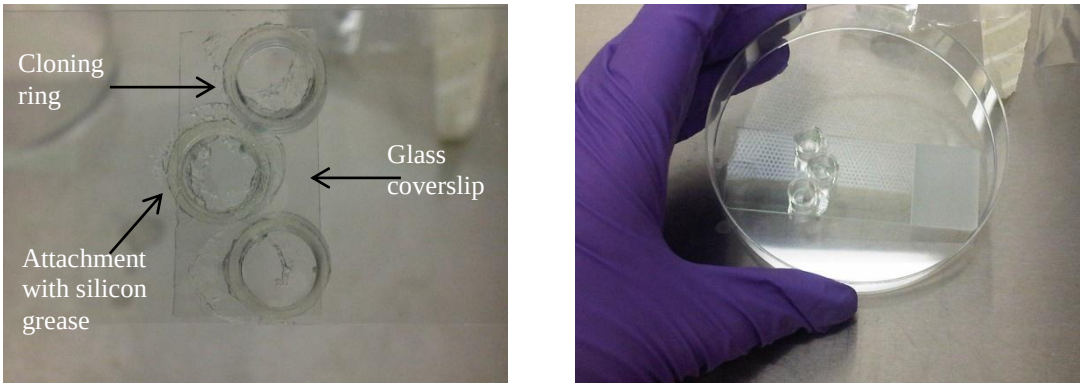

Figure 19 Set up of adhesion assay on coverslips
The coverslips were attached to the glass slide using water tension, the cloning rings were held in place using silicon grease.

$3x10^4$ calcein stained cells were added into each cloning ring; these were washed at 15, 30, 45 and 60 minutes removing any unattached cells. They were imaged (Leica DMI 6000B) and the cell number calculated using image J, the cell number was corrected for the area of the cloning ring.

(Area of the image/ area of the cloning ring) x 100 = percentage of area imaged

(Number of cells counted/ percentage of area imaged) x 100 = corrected cell number.

2.4.3 Cell motility

Initial experiments were carried out to optimise the density of cells needed on each surface to allow attachment of single cells to arrive at the same cell number. The coated glass coverslips were secured in place in 6 well plate using silicon grease on the corner of the glass. Two cloning rings were attached to the coated glass using silicon grease. The cells

were seeded inside the cloning rings. After 1 hour the wells were washed to remove unadhered cells. The plate was then placed into the time-lapse microscope and images taken at 10 minute intervals over a 17 hour period. The movement of 10 cells per well were monitored and the distance travelled measured using the mtrackj plugin for Image J software (**imagej**.nih.gov/ij/).

2.4.4 Co-culture on oxazoline polymers

To distinguish between the GFP 16HBE cells and the MRC5 cells when seeded together on the oxazoline polymer coated glass coverslips, the MRC5 cells were stained with cell tracker orange.

2.4.4.1 CMRA orange staining

2µl of 10mM CMRA orange in DMSO (Invitrogen) was diluted in 998µl of PBS for a 20µM solution. The MRC5 cells were washed in warm PBS, and then the 20µM cell tracker solution was added inside the cell ring. The cells were then incubated for 30 minutes at 37ºC. The CMRA orange solution was removed and warm media added to the MRC5 cells which were incubated for a further 30 minutes.

To determine cell selectivity of the oxazoline coated surfaces, two cloning rings were attached to the coated glass surfaces with silicon grease. $5x10^3$ MRC5 cells loaded with cell tracker orange and $5x10^3$ 16HBE cells transfected with GFP were seeded together within the cloning ring in 50% MRC5 medium and 50% 16HBE medium. They were incubated for 1 hour before being washed by removing the cloning rings, flooding the well and gently agitating the well. The media was replaced and the cells grown for 2 days before being imaged at x 5 magnification and the number of green or orange cells counted using the plugin cell counter for Image J (**imagej**.nih.gov/ij/).

2.4.5 Measurement of stress responses

To determine whether the polymer was causing a stress response within the cells, the phosphorylation of p38 MAP kinase (p38) was investigated using western blotting. 1ml of 4×10^5 16HBE cells/ml was seeded in a 12 well plate or 200µl of 2.5×10^4 PBEC's/ml within a cloning ring. The next day, these were placed in starvation medium, Ultraculture (Lonza,Wokingham, UK) supplemented with Penicillin/streptomycin for 16HBE or BEBM (Lonza) supplemented with 1% 100x ITS (10µg/ml bovine insulin, 5.5µg/ml transferrin, and 5ng/ml sodium selenite) (Sigma-Aldrich) and 1.5µg/ml BSA for PBEC's and incubated

overnight. The cytokines TNFα (1ng-100ng/ml) (PeproTech, London UK) or IL-1β (1ng-10ng/ml) (PeproTech,) were added in fresh starvation medium for 30 minutes for western blotting or 24 hours for IL-8 ELISA.

For western blotting, the 12 wells were lysed in 100µl and the cloning rings in 50µl of warm lysis buffer (62.5mM Tris-HCl, pH 6.8 (Tris base, Sigma-Aldrich), 10% glycerol (Sigma-Aldrich), 2% SDS (Sigma-Aldrich), dH_2O) plus (100µl/ml) phostop (phosphatase inhibitor, Roche Applied Science, Burgess Hill, UK) and (20µl/ml) protease inhibitor cocktail (complete tablet, Roche Applied Science)) and removed by systematic scraping of the well using a 1 ml pipette.

For ELISA the supernatants were collected, centrifuged for 7 minutes at 400 x *g* to remove cell debris. They were re-aliquoted and frozen at -20°C (section 2.4.6).

The lysed samples were sonicated using a probe sonicator (Soniprep 150, MSE, London, UK) for 10-15 seconds to shear the DNA. The protein concentration was read using a NanoDrop spectrophotometer (NanoDrop, ND-1000, Labtech international, Uckfield, UK) and the samples normalised to the concentration of the lowest sample using sample buffer (62.5mMTris-HCL pH6.8, 10%glycerol, 5% β-mercaptoethanol (Sigma-Aldrich), 2% SDS, 0.01% bromophenol blue(Sigma-Aldrich)). 30µl of sample in sample buffer was denatured for 5 minutes at 95°C within a heated block (Techne Dri-block DB-2P).

2.4.5.1 Sodium dodecyl sulphate polyacrylamide gel electrophoresis (SDS-PAGE)

SDS PAGE separates proteins on the basis of their size. A 12.5% resolving gel (3.1ml dH2O, 4.17ml acrylamide (30% Acrylamide/Bis-Acrylamide, BioRad, Hertfordshire, UK), 2.5ml 1.5M Tris-HCL pH 8.8,100µl 10% SDS, 50µl 10% Ammonium persulphate (Sigma-Aldrich), 5µl TEMED (N,N,N',N'-tetramethylethylenediamine) (Sigma-Aldrich) with a 4% stacking gel (3ml dH2O, 0.7ml acrylamide, 1.25ml 0.5M Tris-HCL pH6.8, 50µl 10% SDS, 25µl 10% ammonium persulphate, 10µl TEMED) were used. Glass plates were washed with methanol and inserted into the casting frame. The resolving gel was gently pipetted between the two glass plates and levelled with water saturated isopropanol. This stops oxygen blocking the polymerisation of the gel. After 45 minutes the isopropanol was removed and the gel washed with water. The stacking gel was gently pipetted on top of the resolving gel and the 10 well comb carefully placed into the stacking gel. This was left for another 45 minutes to set. The stacking gel concentrates all the proteins so they start at the same place before being resolved, so that they can then be separated by size alone.

5µl of molecular weight marker (Precision plus proteinTM standards, KaleidoscopeTM, Bio-rad) and 20µl of denatured sample in sample buffer were added into the wells. The tank (mini-protean tetraTM cell, Bio-rad) was topped up with running buffer (25mM Tris-HCl, 192mM glycine, 0.1% (w/v) SDS, pH 8.3) to the fill line. Electrophoresis was performed at 140V, 400ma (PowerPac^{TM} HC, 250v, 3.0A, 300W, Bio-rad) until the dye front had travelled to the end of the gel.

2.4.5.2 Western blotting

The resolving gel was removed from the casing and placed into cold transfer buffer for 15 minutes. During this time the PVDF (GE healthcare amersham^{TM}, UK) membrane was pre-wetted with methanol (Sigma-Aldrich), and then transferred to transfer buffer (25mM Tris, 192mM glycine (Sigma-Aldrich), 0.1%SDS, 20% (v/v) methanol pH 8.3) along with filter paper (Bio-Rad) and scotchbrite sponges. A transfer cassette was then set up (Figure 20)

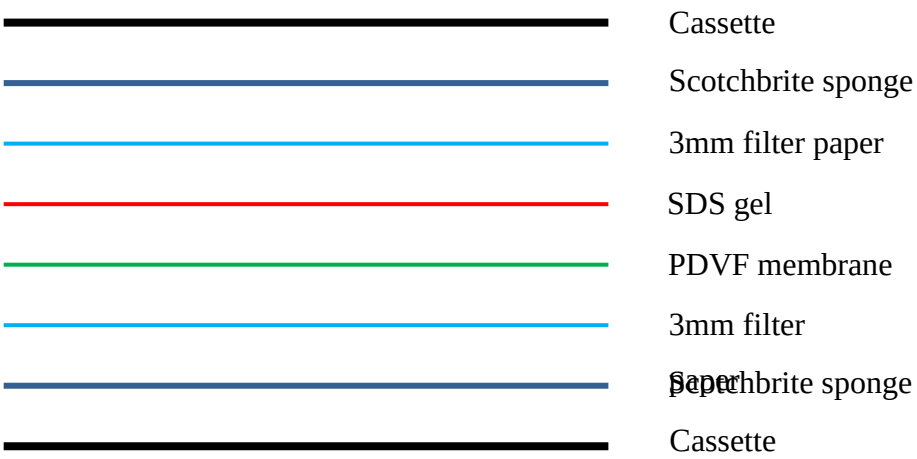

Figure 20 Set up of the western blotting cassette

The cassette was inserted into the transblot tank (bio-rad) containing an ice pack, with the membrane closest to the anode and the gel closest to the cathode; electrophoresis was performed for 90 minutes at constant 100v.

Once transferred, the blots were washed in 10ml 1xTBS Tween (Tris buffered saline/0.1% Tween 20) buffer (Sigma-Aldrich), followed by ponceau staining (ponceau s solution, Sigma-Aldrich) to detect all transferred protein. The membrane was blocked using 5% milk (Marvel, Dublin, ROI) in TBS/Tween (blocking buffer) for 30 minutes. 10 µl of rabbit polyclonal anti-phosphorylated p38 or pan p38 antibody in 10 ml 5% BSA (Bovine serum

albumin fraction V, Sigma-Aldrich) 1xTBS 0.1% Tween 20, was added to the membrane and incubated at 4°C overnight with shaking (Stuart Geneflow mini orbital shaker SSM1). The membrane was then washed in TBS/Tween for 15minutes and twice more for 5 minutes each wash. 7.5 µl of secondary antibody, swine anti-rabbit immunoglobulins/Horse radish peroxidase (HRP) (cell signalling, NEB, Hitchin, UK) in 15 ml blocking buffer per blot was added, and incubated at room temperature for 1 hour with shaking. The membrane was washed in TBS/Tween for 15minutes followed by 4 washes at 5 minutes each.

Bound antibody was detected using enhanced chemiluminescence. 2ml ECL+ solution (GE healthcare amersham^{TM}, blotting detection system) was added to the membrane for 5 minutes. The Enhanced chemiluminescence (ECL) solution is oxidised in the presence of HRP and H_2O_2 producing light, this light can be detected by an X-ray film.The ECL was removed, and the membrane wrapped in Clingfilm and taped into an X-ray film cassette. The membrane was exposed to hyperfilm ECL (GE healthcare) in a dark room for 90 seconds initially then immediately developed.

The membrane was stripped of antibody by incubating at 50°C in stripping buffer (100mM β-mercaptoethanol, 2% (w/v) SDS, 62.5mM Tris pH6.7) for 30 minutes and re-probed for the loading control in this case pan p38 (cell signalling).

2.4.5.3 Densitometry

The western blot films were analysed by densitometry. This analyses the intensity of the bands allowing a semi-quantitative analysis of the protein concentrations detected by the antibody. The films were scanned and processed using Image J. The density of the bands were calculated, from this information the percentage change between the phosphorylated p38 and the loading control could be determined.

2.4.6 ELISA enzyme-linked immunosorbent assay IL-8, IL-6 and IP-10

A sandwich ELISA was used to analyse IL-8, IL-6 and IP-10 release. All ELISA kits were DuoSet ELISA Development Systems (R&D systems, Abingdon, UK) and were performed according to the manufacturer's instructions. The basic protocol can be seen in Figure 21

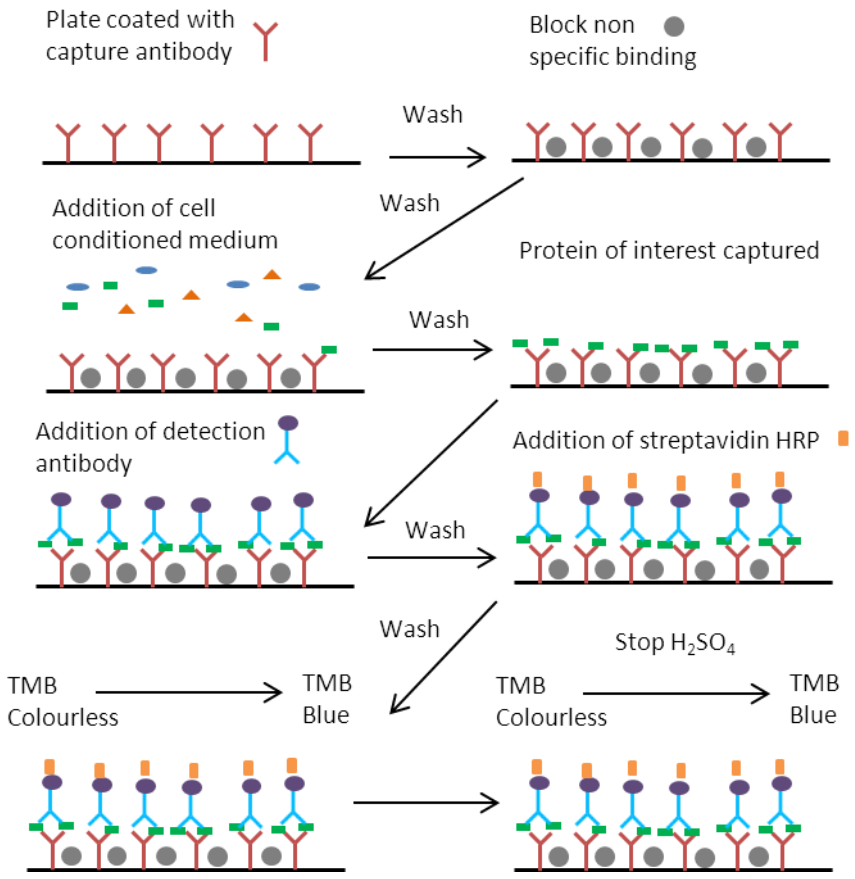

Figure 21 Schematic showing ELISA methodology
The plate was coated with capture antibody, excess was removed by washing, non-specific binding was blocked using a blocking buffer, and the excess was washed off. The cell conditioned medium was added, this was washed to remove non-specific binding. The protein of interest was captured on the capture antibody; the detection antibody was then added. Excess antibody was removed and streptavidin HRP is added. Excess streptavidin HRP was washed off and TMB was added, this underwent a colour change and was stopped with H_2SO_4. The colour change was then read in a colourmetric plate reader.

2.4.7 ELISA IL-8

The following shows an example of the protocol used for the IL-8 ELISA. 96 well Nunc Maxisorp plates (Nunc, Life technologies) were coated in the provided capture antibody at a dilution of 1 in 180 in PBS (All volumes are 50µl unless stated). This was incubated overnight at room temperature, and then washed with wash buffer (PBS, 0.05% Tween 20). It was then blocked using 150µl of block buffer per well (PBS, 1% BSA) at room temperature for 1 hour. The stored supernatants removed from stimulated cells were diluted 1 in 15 for 16HBE's in reagent diluent (TBS, 0.1% BSA, 0.05% Tween 20). The block buffer was removed and the plate washed to remove excess buffer. Standards were prepared from the supplied stock, by serial dilution making 7 standards from 2000pg/ml to 31.25pg/ml (in duplicate). The supernatant and standards were added (all in duplicate) and incubated overnight at 4°C, along with 2 wells contain reagent blanks (reagent diluent).

The plates were then washed and incubated with 1 in 180 diluted detection antibody in reagent diluent for 2 hours at room temperature. This was washed to remove excess antibody and the streptavidin HRP (diluted at 1 in 200 in reagent diluent) was added and incubated for 20 minutes at room temperature. The plate was washed to remove excess streptavidin HRP. The TMB solution was added and incubated at room temperature for 20 minutes. There should be a colour difference between the lowest concentration standard and the blank; this shows the reaction has occurred. The reaction was stopped using 25µl 1M sulphuric acid (H_2SO_4), the absorbance was measured at 450nm and at 570nm (labsystems multiskan Ascent plate reader). The 570nm reading was subtracted from the 450nm reading; this removes the absorbance of the plate. The standard curve was constructed on inbuilt software and the cytokine levels interpolated. The curve was constructed according to the 'four parameters logistic curve' setting.

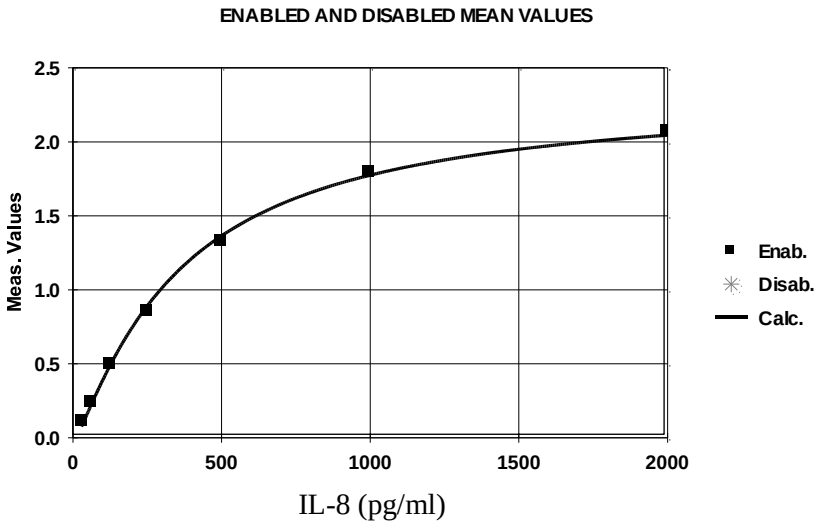

Figure 22 example of an IL-8 ELISA standard curve

2.5 Levitation within the Sonotweezers device

To reduce the need for manipulation of the cell sheet with the membrane the Sonotweezers device was used to levitate cells from the UpCell dish.

The Sonotweezer used are a half wavelength device (the chamber height is half a wavelength); this means that at resonance there is a pressure node and a velocity antinode in the centre of the chamber. The device consists of a PDMS microfluidic channel with an acoustic transducer on a piezoelectric substrate. It is the change in conformation of the piezoelectric substrate when a current is passed over it that causes the acoustic wave in the fluid.

2.5.1 Sonotweezers for levitation of cells from the UpCell dish

The cell ring was secured on the UpCell dish with silicon grease. 30µl of 3.33 x 10^3cells/ml of HeLa cells were seeded in to the cell ring on the UpCell dish. These were grown for 24 hours before being stained with CMRA orange. The warm media was removed and the cells incubated at 20ºC for 45 minutes and the cell ring removed. The UpCell dish was then placed on the device above the piezoelectric transducer, with a glass reflector placed on top. Between the cells and the reflector was a PDMS mat increasing the height to half a wavelength above the cells (Figure 23). The Piezoelectric transducer was attached to the signal generator (Model TG103 TTI, Cambridgeshire, UK) which was switched on at a frequency of 1.66mHz and an amplitude of 3.5 Volts peak to peak (Vpp) forming half a wavelength across the device.

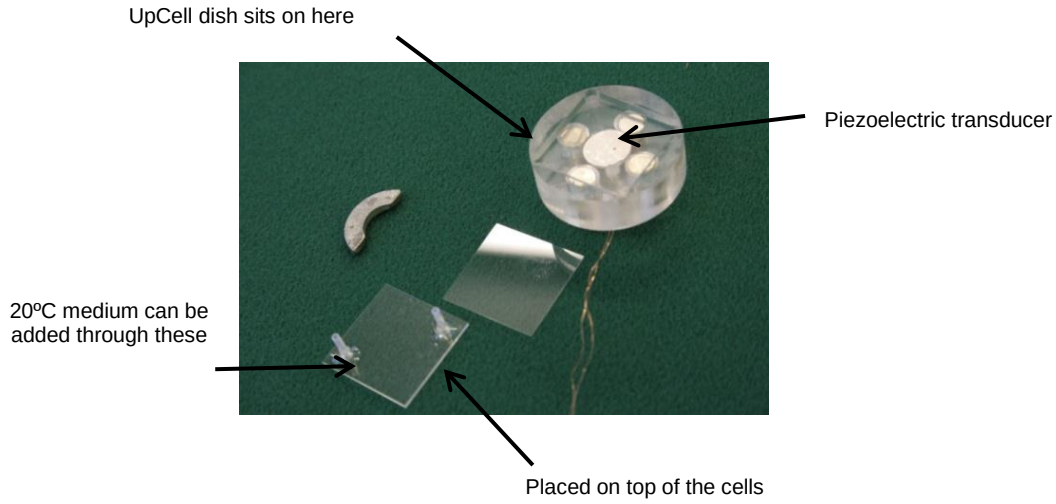

Figure 23 Sonotweezers device used for levitating cells from a thermoresponsive surface. The device is a half wavelength in height.

2.5.2 Sonotweezers device for prolonged levitation

To ensure that the medium has the correct CO_2 concentration it was incubated at 5% CO_2 for 1 day before the experiment was undertaken. The device was autoclaved to ensure sterility. The incubator cabinet for the device was maintained at to 37ºC. The device was set up within a class two laminar flow hood. 5% CO_2 was injected into the media bottle and a stirring ball was added into the cell suspension syringe. 2.5ml of CMRA orange stained cells at a concentration of 2 x 10^5cells/ml was added into the syringe. Once all tubes have been attached the device is removed and taken to the microscope. The system is then filled with media and any bubbles removed from the system using the syringe attached to the bubble trap. The transducer is then attached to the signal generator and the electrical connectivity checked. The device was switched on at amplitude of 17Vpp with a sweeping

frequency of 910 kHz to 930 kHz in 50ms which creates half a wavelength across the device. The syringes are attached to a syringe pump 0.5ml of cells and a rate of 60ml/hour was introduced into the system. The syringes are removed from the syringe pump and the peristaltic pump turned on at a rate of 0.01ml/minute. To reduce bubbles the syringes attached to the bubble trap are placed into the syringe pump and placed on suck at a rate of 0.06ml/hour (Figure 24). Images were taken of the cells as they entered the device and after they had been levitated for 5 days.

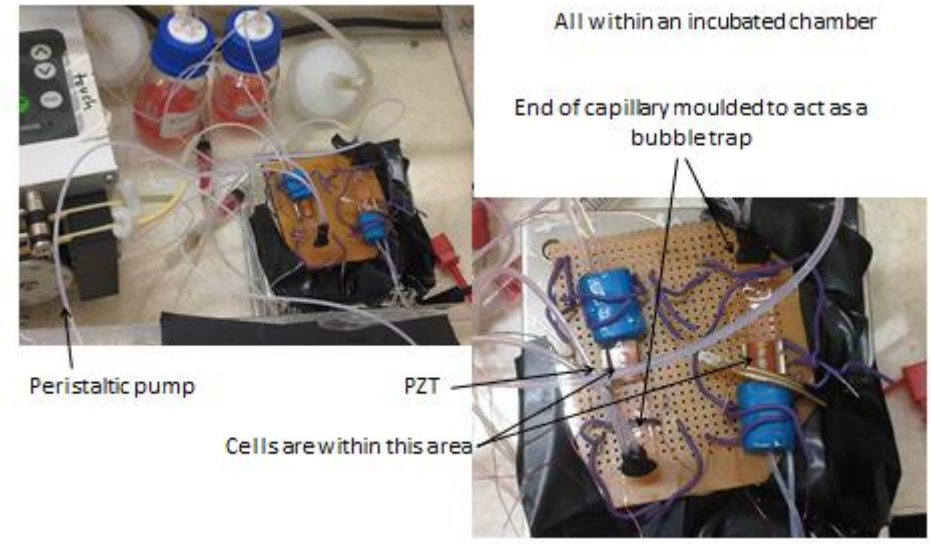

Figure 24 Sonotweezers device for prolonged levitation.
A half wavelength acoustic tweezers device.

2.6 6 well Sonotweezers device

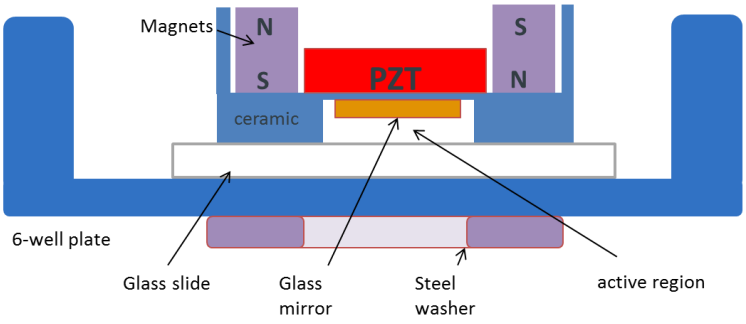

Figure 25 Schematic of 6 well Sonotweezers device.
A half wavelength acoustic tweezers device.

2.6.1 Loading cells into the device

A glass slide (without any frosted glass) (Life technologies) was cut into 4 pieces to fit within a 6 well plate using a diamond tipped pen. The glass was sterilised using 100% isopropanol (Sigma-Aldrich), and then allowed to air-dry within the cell culture hood. The

glass was held in position by the addition of silicon grease to each corner before it was placed on the base of the well; 3ml of cell specific medium was added in to the well. The device was sterilised by spraying with 70% IMS which was allowed to evaporate before the mirror was cleaned with 100 % isopropanol. A sterilised device was placed on top of the glass and held in place by a washer under the well. The connecters were attached to the devices; the plate holding the devices was moved to the heater chamber of the time lapse microscope where they were connected to the signal generator. A small LED on the transducer lit up if there was a current going through the device. This ensured that if a wire was damaged it could be rectified before cells were added. The devices were turned on and allowed to equilibrate while the cells were trypsinised. 10µl of 5x 10^5 cells /ml were added into the gap between the transducer and the glass slide using a gel loading tip (Figure 25). For immunofluorescent staining unlabelled cells were added, for the viability test the cells were stained with Cell tracker blue as this colour doesn't overlap with the 7AAD spectrum (Figure 26). 7AAD (Sigma-Aldrich) was made up in 50µl DMSO and 950µl PBS, this was added into the well close to the entrance of the device at a 1 in 100 dilution for 10 minutes before the cells were imaged to show the cell viability within the device.

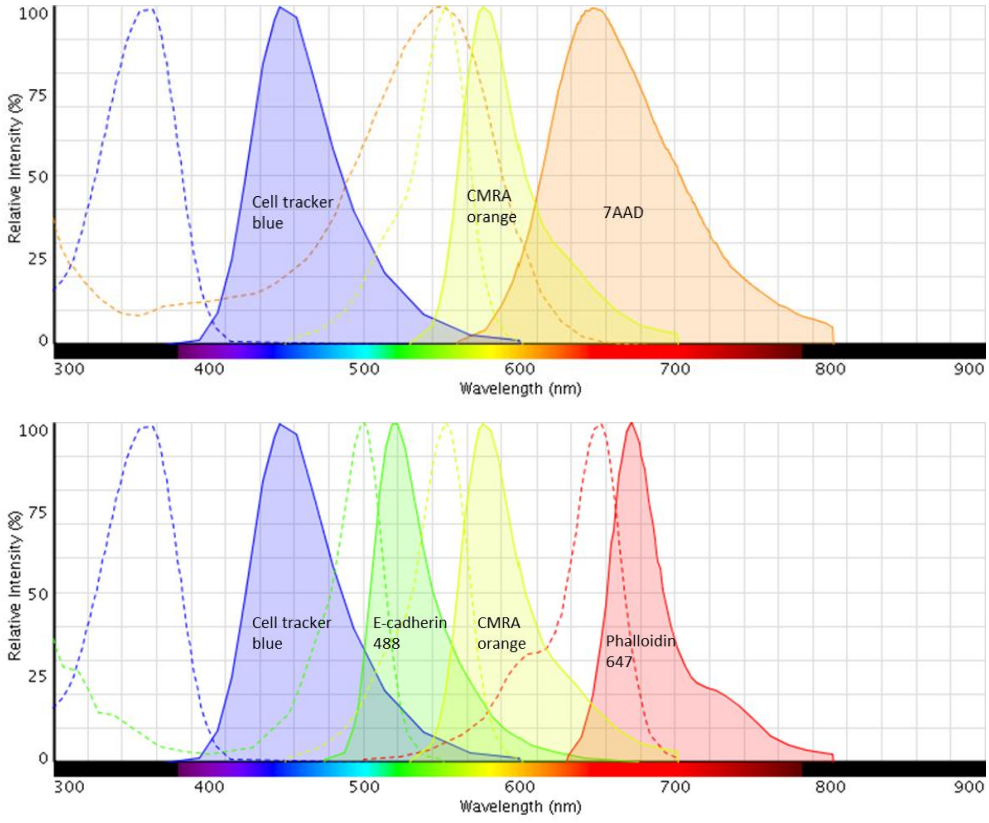

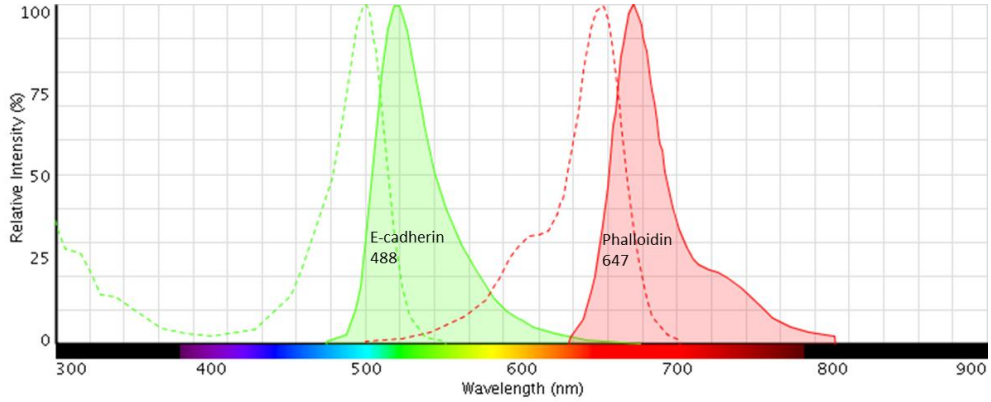

Figure 26 spectra for visualisation via cell tracker dyes and immunofluorescent staining of levitated 16HBE cells. Cell tracker blue can be used for viability studies as it does not cross over the 7AAD spectra, neither of the cell tracker dyes can be used when staining for E-cadherin and F-actin using Phalloidin, but E-cadherin and Phalloidin do not cross spectra.

2.6.2 Levitation within the Sonotweezers device with and without calcium

5 devices were set up within a 6 well plate, 2 wells contained Low calcium MEM (Life technologies) plus 10% FBS and 1% penicillin (50units/ml)/streptomycin mix (20µg/ml) with 5mM EGTA (Sigma-Aldrich). The remaining 3 wells contained calcium containing MEM. 10µm fluorescent Fluoresbrite yellow green microspheres (Polysciences, Inc. Pennsylvania, USA) were added to one device. Cell tracker blue stained cells were added to one device with the low calcium medium and added to one device with normal medium. Unstained 16HBE cells were added to the remaining two devices. They were levitated for 24 hours and images recorded every 10 minutes using the time-lapse microscope. 7AAD was added for 10 minutes to the cell tracker blue cells before the cells were imaged to determine the cell viability within the device.

2.6.3 Levitation within the Sonotweezers device with and without cytochalasin D

1 mg Cytochalasin D (Life Technologies) was dissolved in 500µl of DMSO (Sigma-Aldrich) to make a stock of 2mg/ml. 1µl/ml of this stock was added to the 16HBE medium to make a final concentration of 2µg/ml. The cytochalasin D containing 16HBE medium was added into two wells, while plain 16HBE media was added into a further two wells. One well of each condition had cell tracker blue 16HBE cells added while the other two wells had non-stained 16HBE cells added. These cells were levitated for 6 hours and images recorded every 10 minutes using the time-lapse microscope. 7AAD was added for 10 minutes to the cell tracker blue cells before the cells were imaged to determine the cell viability within the device.

2.6.4 Levitation within the Sonotweezers device with and without an E-cadherin neutralising antibody

The E-cadherin neutralising monoclonal antibody Mouse SHE78-7 (Life Technologies) was used to block the formation of the adherens junctions. 5µg/ml was added to the 3mls of 16HBE medium surrounding two of the Sonotweezers devices. The other two wells contained plain 16HBE medium. One well of each condition had cell tracker blue 16HBE cells added while the other two wells had non-stained 16HBE cells added. These cells were levitated for 6 hours and images recorded every 10 minutes using the time-lapse microscope. 7AAD was added for 10 minutes to the cell tracker blue cells before the cells were imaged to determine the cell viability within the device.

2.6.5 Measuring agglomerate areas over a set time period

Time lapse images were extracted from the microscope as AVI files and opened in ImageJ with the Bio-Formats plugin. Using the time series analyser V2 plugin the area of the aggregates was measured. This involved setting the scale of the image, drawing around the agglomerate and saving the area that was delineated. This was carried out for each time point. The area was then calculated for each time point. The percentage of the starting area was then calculated.

(Area of the agglomerate/ area of the starting agglomerate) x 100= % of starting area

2.7 Creation of Co-Cultures

2.7.1 Creation of co-cultures in transwells

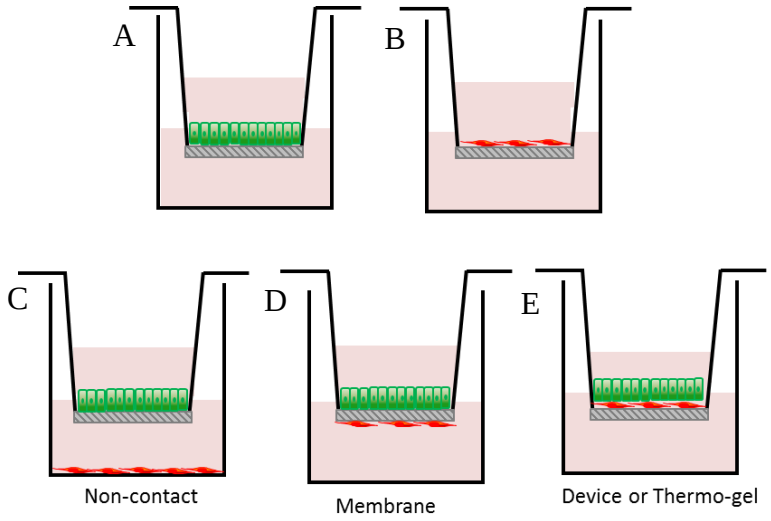

Figure 27 Schematic of co-cultures
A shows 16HBE alone in the apical compartment. B shows MRC5 alone in the apical compartment. C shows the non-contact co-culture, here the MRC5 cells are seeded on the bottom of the well and the 16HBE cells were seeded within the apical compartment. D shows the membrane co-culture, here the MRC5 cells were seeded on the underside of the transwell and the 16HBE cells were seeded within the apical compartment. E shows the cell-sheet co-culture, here c16HBE cell sheet created within the Sonotweezers or on the thermo-gel are added on to the top of a confluent layer of MRC5 cells on the apical compartment of the transwell.

2.7.1.1 Non-contact co-culture

50µl of $1x10^6$ MRC5 cells/ml was added onto the base of the transwell plate and incubated at 37ºC for 2 hours. A fresh collagen coated transwell was placed over the MRC5s and seeded with 200µl of $0.75x10^6$ 16HBE cells/ml.

2.7.1.2 Membrane co-culture

Both sides of the Transwell were collagen coated with 100µl of 1 in 100 collagen diluted in dH_2o and incubated at 37ºC for 20 minutes. The collagen solution is removed and the transwell turned upside down and seeded with 50µl of $1x10^6$ MRC5 cells/ml. This was incubated at 37ºC for 2 hours to allow the MRC5 cells to attach to the base of the well. After 2 hours the MRC5 coated transwells were gently washed with HBSS, and then placed into the holding plate. 200µl of $0.75x10^6$ 16HBE cells/ml were added on to the top of the transwell.

Both of these co-cultures were incubated for 6 days and the TER read every day. The TER was read using chopstick electrodes placed either side of the transwell to record the electrical resistance caused by the barrier formed within the cells. They were media change on day 3 and day 5.

2.7.2 Using Sonotweezers to create a co-culture

$3x10^4$ MRC5 cells were seeded on to a transwell and allowed to achieve confluence.10µl of $1x10^5$ 16HBE cells/ml were levitated for 2 hours within the Sonotweezers device before being dropped, the device removed and the aggregate captured using a wide bore pastette. The agglomerate was transferred on the transwell containing a confluent layer of MRC5 cells.

2.7.3 Co-culture created using the thermo-gel

$3x10^4$ MRC5 cells were seeded on to a transwell and allowed to achieve confluence. A 6% poly(2-isopropyl-2-oxazoline-co-2-butyl-2-oxazoline)-carboxymethylcellulose (P*i*PrOx-co-*n*BuOx-CMC) gel was made up in 16HBE medium, 100µl of the gel was added under 100µl of medium into a 96 well plate and centrifuged at 300g for 5 minutes to reduce any meniscus that was formed. This was then incubated at 37ºC for 30 minutes. $3x10^5$ 16HBE cells in 50µl of 16HBE medium were gently added on to the top of the gel. The cells were then incubated for 2 hours at 37ºC. The cell aggregates formed where then captured using a wide bore pastette and placed onto a transwell containing a confluent layer of MRC5 cells.

2.7.4 Poly (I:C) treatment

A 1mg/ml stock solution was diluted to a working concentration of 20µg/ml; 10µl of this working stock was added to the 200µl of medium on the top of the co-culture transwells giving a challenge concentration of 1µg/ml. The TER was measured 1, 6 and 24 hours after challenge. The apical and basal medium was collected and centrifuged for 7 minutes at 400 x *g* to remove cell debris. These supernatant were then used for IL-6, IL-8 and IP-10 ELISAs.

2.8 Statistical analysis

All data analysis and graphs were performed using GraphPad Prism. To determine whether the data was normally distributed the Shapiro-Wilk test was carried out. If this states yes, to passed normality test then a parametric test would be carried out. If this states no, to passed normality test then a non-parametric test is carried out.

For comparison of groups that are normally distributed the T test or one way ANOVA test or Two way ANOVA was used. If the data was not normally distributed then the Kruskal-Wallis test was used. Multiple comparisons were carried out using Tukey's multiple

comparison test for normally distributed data and Dunn’s multiple comparisons test if the data was not normally distributed.

3. Creating multi-layered cell culture models

Current cell culture methods have produced a large amount of information using a single cell type, but a tissue is made up of several cell types. Co-culture models have been developed to bridge this gap allowing investigation of the cross talk between cell types, particularly how this influences normal homeostasis and how this is disrupted in disease. These current co-culture models as described in chapter 1 are usually limited by the space between the varying cell types; there is either a gap filled by medium or thick matrix, for example a 4mm thick collagen gel (Pageau et al., 2011) or a transwell membrane polymer which is 10µm thick (Corning, 2012) with 0.4µm pores. This contrasts with the in vivo state where the cells are in intimate contact. Another difficulty is that the various cell types also grow at different rates for example it takes 21 days for differentiation of primary bronchial epithelial cells to occur. Fibroblasts or endothelial cells would not be able to survive in culture for this length of time and have different medium requirements.

One way to develop better tissue constructs is to use cell sheet engineering. Cell sheet engineering is a technique whereby cell layers are grown to confluence, released from their culture surface and stacked on top of another cell type, essentially making a cell "sandwich". This maintains cell-cell interactions which are especially important for epithelial cells that elaborate numerous adhesive junctions. The method of cell sheet engineering investigated within this project was to grow cells on a thermoresponsive surface. The most commonly used thermoresponsive polymer is N-isopropyl acrylamide (NiPAAm) covalently attached to tissue culture dishes. NiPAAm has a lower critical solution temperature (LCST) between 37°C and 20°C. At 37°C the polymer is compact allowing for cell attachment, however when the temperature is dropped to 20°C the polymer is rapidly hydrated, changing confirmation and releasing the cells. There are many papers describing the use of this polymer with a commercial product, Nunc UpCell surface, For example Kushida *et al* investigated MDCK and renal tubule epithelial cell release and the maintenance of cell polarity on tissue culture dishes with NiPAAm covalently attached via E-beam radiation (Kushida et al., 2005). Using the UpCell protocol cells are grown to confluence and then covered with the provided membrane before incubating at 20°C which allows the polymer to undergo its conformational change so releasing the cell sheet. The membrane is used to facilitate the release of the cells from the dish; it ensures the maintenance of the structural integrity of the sheet, and prevents it folding on itself (Figure 28).

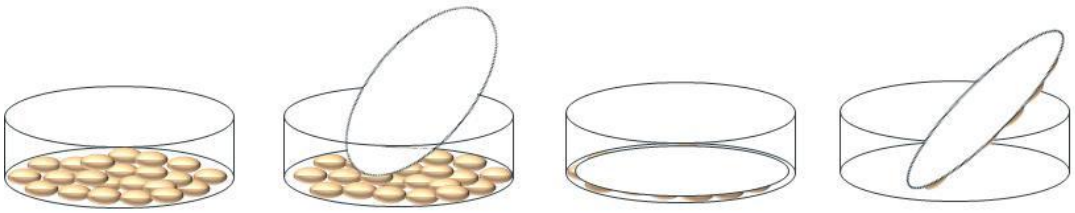

Figure 28 Schematic showing the release of a cell sheet from the UpCell dishes.
Cell are grown to confluence, the provided membrane is placed over the cells and incubated at 20°C for 30 minutes. The membrane is peeled off the dish with the cells attached it is then placed onto the next cell layer. After incubating for a further 30 minutes at 37°C the membrane is removed leaving behind the intact cell sheet.

A large number of cell types have been released from a NiPAAm coated surface. These include Endothelial cells, bovine aorta endothelial cells (BAEC's) (Okano et al., 1995), human aortic endothelial cells (HAEC's) (Harimoto et al., 2002), human umbilical vein endothelial cells (HUVECs) (Sasagawa et al., 2010)), primary human fibroblasts (Takezawa et al., 1990) and fibroblast cell lines such as 3T3, human skeletal muscle myoblasts (Sasagawa et al., 2010), hepatocytes (rat) (Okano et al., 1995), epithelial cells (MDCK (Madin Darby canine kidney)) (Kushida et al., 2000), and primary rat lung cells (Nandkumar et al., 2002). These are generally poorly adherent cell types that do not form cohesive sheets of cells with the exception of the MDCK epithelial cell line. These cell sheet constructs are mainly used for medical applications, for repairing damaged tissue with a graft being the main focus of the cell sheet work (Matsuura et al., Cerqueira et al., 2013, Sachiko et al., 2013, Fujita et al., 2012, Zhou et al., 2010, Shimizu et al., 2002, Von Recum et al., 1998, Yang et al., 2006). There are some papers that investigate the use of cell sheets for solely research purposes (Harimoto et al., 2002). All these papers have found that by placing the sheets of cells on top of one another they maintain their coherent sheets.

3.1 Creating multi-layered cell culture models

The models of the airway mucosa described in the literature are all quite complicated with the addition of cells on either side of membranes or imbedded within matrix gels. To determine whether the cell types of interest (i.e. epithelial cells and fibroblasts) would organise themselves into distinct layers, GFP-16HBE and DsRed-MRC5 cells were seeded together (Figure 29 A-B) or GFP-16HBE single cell suspension was seeded on top of a confluent layer of DsRed-MRC5 cells (Figure 29C-D). Both these methods produced islands of 16HBE cells surrounded by strands of MRC5 cells both in contact with the base of the culture dish. Even when the epithelial cells were placed onto a confluent layer of fibroblasts the single epithelial cells found a gap in the fibroblast cell layer and moved the fibroblasts out of the way as seen in the z-stacks which also show that there is no definition of layers between the two cell types. Thus, alternative strategies were investigated to create multi-layered cell constructs.

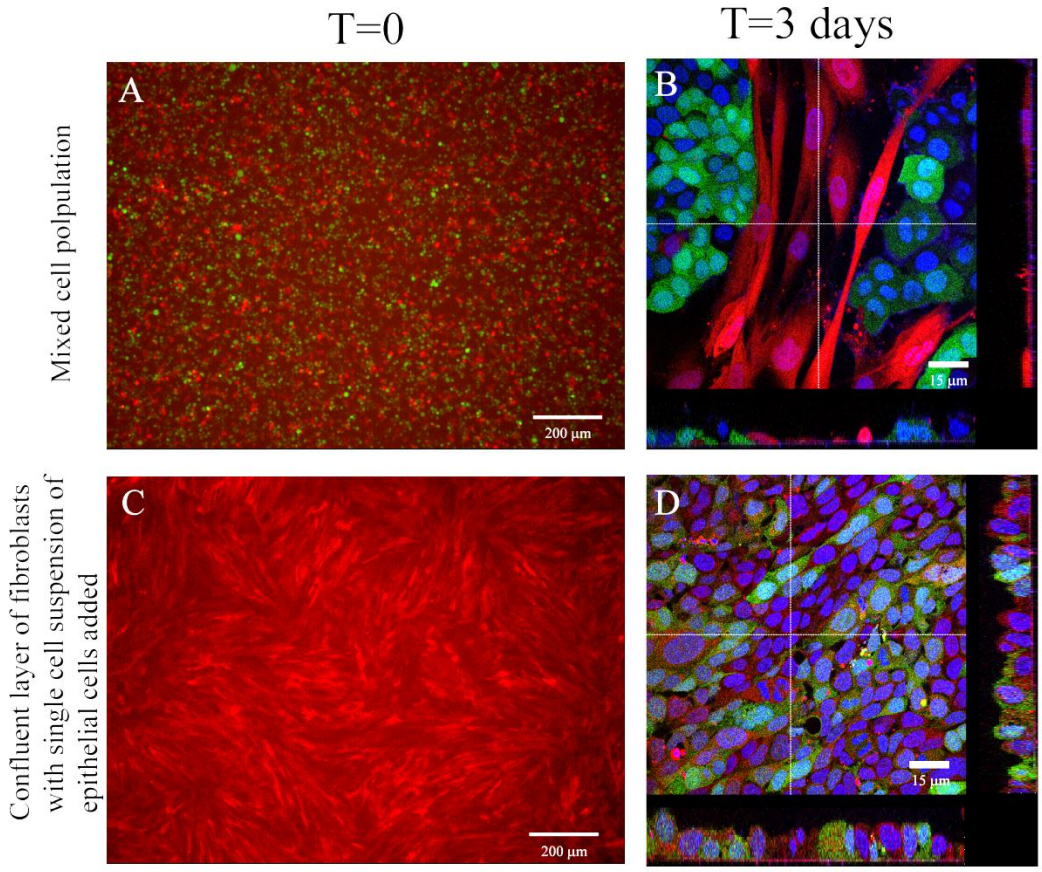

Figure 29 Co-culture of GFP 16HBE and DsRed MRC5 cells.
A mixture of GFP 16HBE and DsRed MRC5 cells were seeded together on to a transwell panel A shows the cells as they were initially seeded and panel B) shows the cells after 3 days. Here the 16HBE cells have formed islands surrounded by MRC5 cells. In panels C and D, a Single cell suspension of GFP 16HBE cells was seeded on top of a confluent layer of DsRed MRC5 cells on a transwell. C) Shows the MRC5 layer before the 16HBE cells were added, D) shows the cells after 3 days, the two cell types have mixed with both having contact with the base of the transwell. Scale bar shows either 200µm (A and C) or 15µm (B and D).

3.2 Cell sheet engineering

Cell sheet engineering has been carried out using a thermoresponsive polymer, generally based on the polymer NiPAAm (Takezawa et al., 1990). Therefore UpCell dishes with covalently attached NiPAAm were used to investigate the growth and release of 16HBE cells on a thermoresponsive surface. If successful, a NiPAAm based polymer, designed to coat the surface of a well or transwell, would be investigated.

3.2.1 UpCell: a model system

A 35mm UpCell dish and a control 35mm standard tissue culture dish were seeded with 8 $x10^5$ 16HBE cells and grown to confluence overnight. The 16HBE cells grown on the UpCell dish had the same morphological appearance under a phase microscope as those on tissue culture plastic (Figure 30A and B). To assess the ability of the cell sheet to be removed from the thermoresponsive polymer, the medium was removed and the cells incubated with the provided membrane for 30 minutes at 20ºC. The membrane and attached cells were then removed using forceps. The removal of the membrane from the control removed small areas of cell, with the majority left on the dish (Figure 30 C). The removal of the membrane from the UpCell dish also gave patchy release, with a large proportion of cells left behind (Figure 30 D).

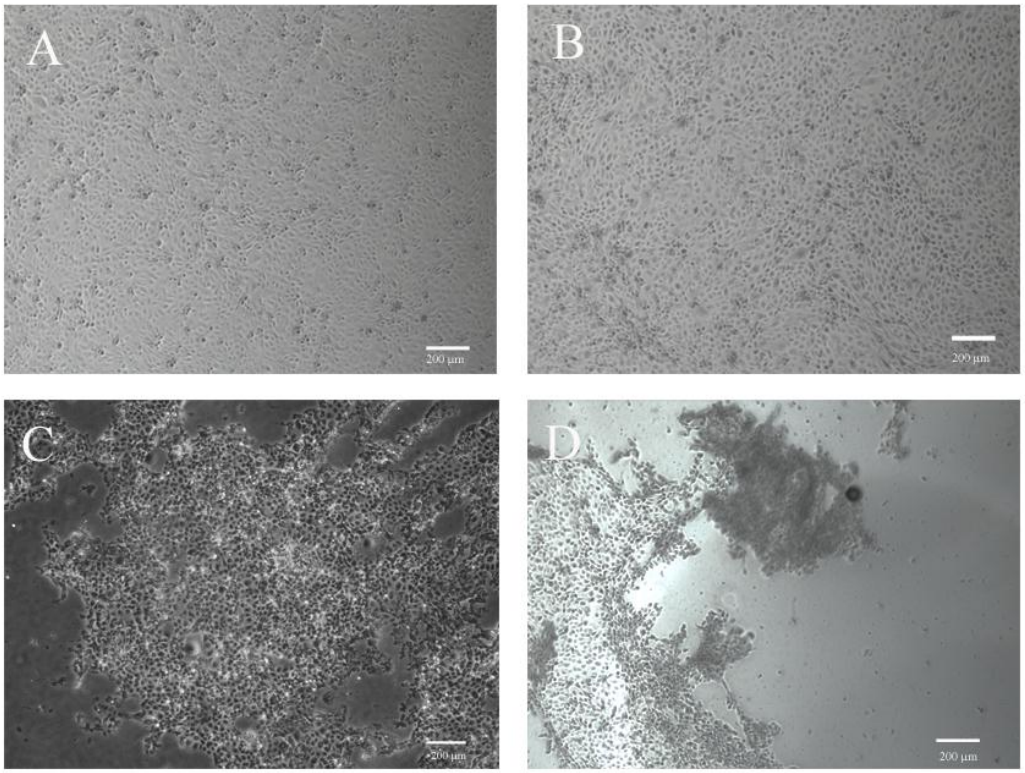

Figure 30 Growth of 16HBE cells on an UpCell surface tissue culture plastic dish.
16HBE cells were seeded onto a tissue culture dish A) and an UpCell dish B) and grown to confluence. Following the manufacturer's protocol for the UpCell dish the membrane was placed onto the cells and was then incubated at 20°C for 30 minutes. C) Shows what was left behind after the membrane was removed from the tissue culture plastic dish and D) shoes what remained on the UpCell dish. Scale bar shows 200µm.

16HBE's are a strongly adhesive cell type, and are difficult to detach even with trypsin. To determine whether the protocol was sub-optimal or bronchial epithelial cells were too strongly adherent to be released from these surfaces, the experiment was repeated using MRC5 fibroblasts. Much of the literature investigates fibroblast cells, where spontaneous release of the cells is recorded. To determine whether this occurred with MRC5 cells, they were grown on the UpCell dish and incubated at 20ºC for 30 minutes without the membrane. The MRC5 cells have the same morphological appearance on the UpCell dish compared to the tissue culture dish. After 30 minutes the cells had rounded up in to small aggregates of cells, no longer attached to the dish. Spontaneous release was achieved however the cells did not release as a sheet (Figure 31).

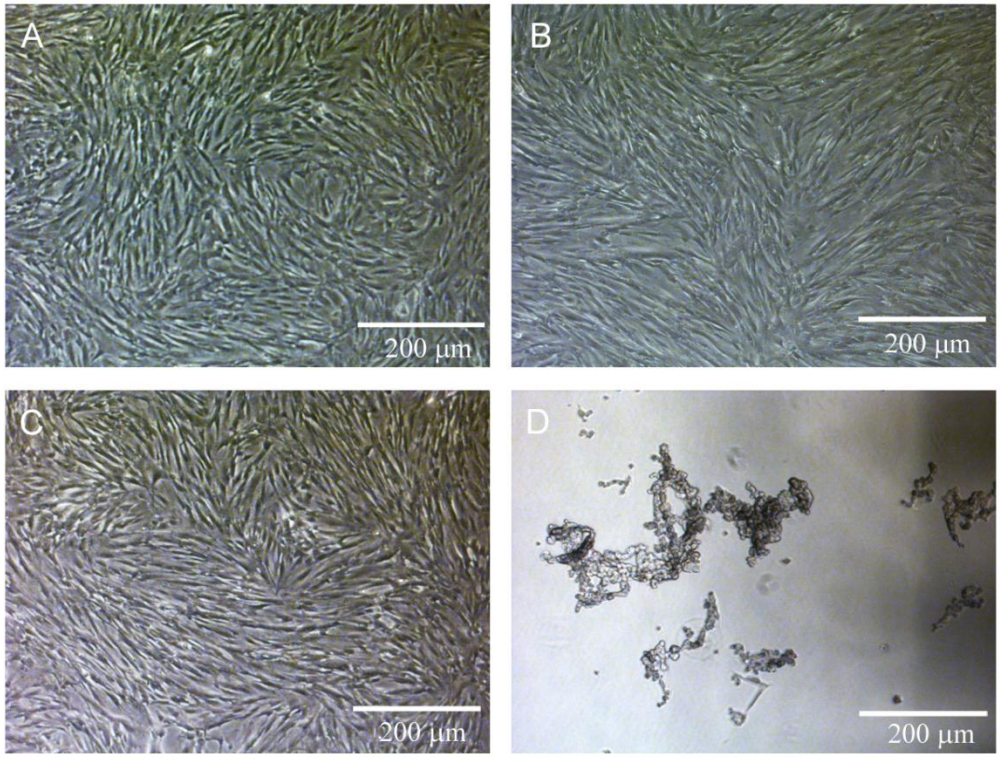

Figure 31 MRC5 cell release from the UpCell surface.
MRC5 cells were grown to confluence on A) a tissue culture plastic dish and on B) the UpCell dish. They were incubated at 20ºC for 30 minutes and the MRC5 cells on C) the control tissue plastic dish did not change conformation or release from the dish, on D) they spontaneously released from the UpCell dish. Scale bar shows 200µm.

The spontaneous release of the MRC5 cells suggests that the thermoresponsive surface is allowing cell detachment. To determine whether epithelial cells could be release HeLa cells were used. These are less adherent than 16HBE cells. An UpCell dish and a tissue culture dish were seeded with 6 x 10^5 HeLa cells, these grew to confluence overnight (Figure 32A and B). The medium was removed and the cells incubated at 20°C with the membrane on top of the cells. When the membrane was removed only part of the cell sheet came with it; Figure 32 C shows an area where the cell sheet was removed. However the majority of the cell sheet although released from the dish, did not adhere to the membrane (Figure 32D), this left the cell sheet folded in the dish.

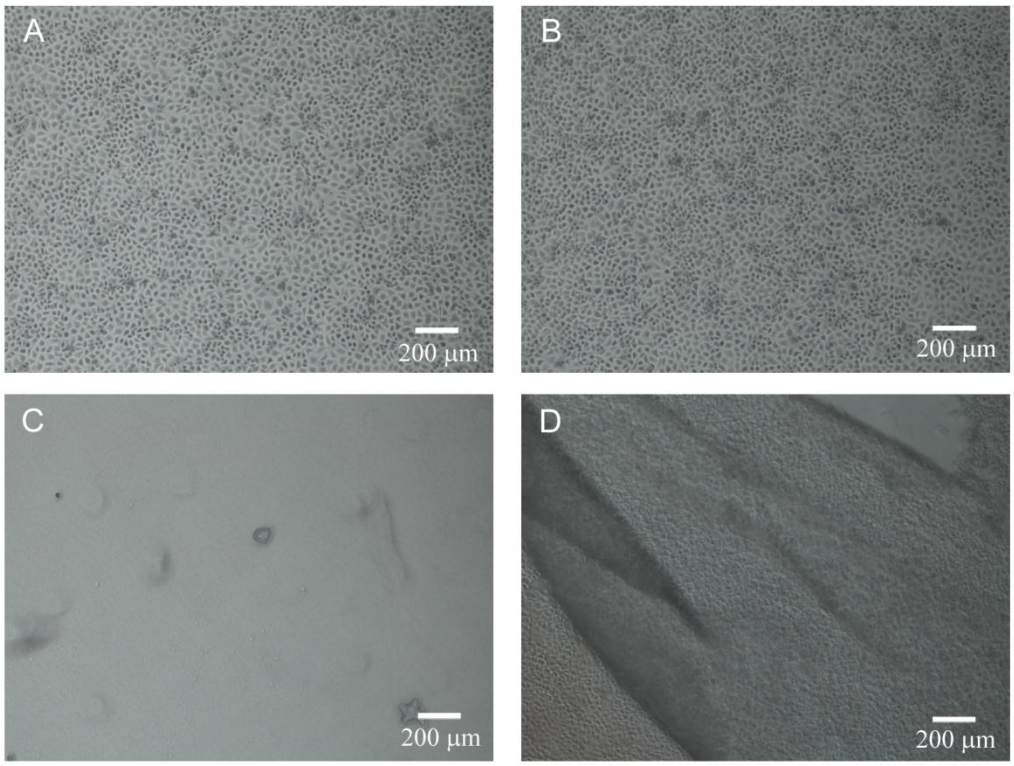

Figure 32 HeLa cell adherence and release from an UpCell dish.
There is no difference in morphology of the cells grown on tissue culture plastic (A) or the UpCell dish (B). The cells were incubated at 20°C with the membrane for 30 minutes; removal of the membrane gave partial release of the cells. C shows an area where cells were removed whereas D shows an area where cells did not adhere to the membrane, leaving the cell sheet folded in the dish. Scale bar shows 200µm.

From the preliminary studies it seemed that 16HBE cells did not release from the dish, the HeLa cells were released from the dish, but did not attach to the membrane and the MRC5 cells spontaneously released from the dish. This suggested that the protocol was not optimised for the more adhesive cell types. To keep the sheet intact the whole cell sheet needs to be attached to the membrane and released. Upon discussion with technical support at Nunc, another protocol was suggested better suiting these more adherent cell types.

The new protocol omitted the use of the membrane during the incubation at 20ºC, allowing visualisation of the cells (Figure 33). The cells were deemed ready to adhere to the membrane when those at the edge of the sheet had begun to round up. At this point the medium was removed and 50µl of cold medium added. The membrane was then placed on top of the cells for one minute before being removed with forceps and placed on to the next surface.

Figure 33 Schematic depicting the modified UpCell protocol.
Once the cells were confluent they were incubated at 20°C until the cells at the edge begin to round up. The membrane was placed on top of the cells for one minute before being removed and placed onto the next surface.

HeLa cells were used to investigate this modified protocol. After 30 minutes incubation at 20ºC, all the cells appeared to be rounded up (Figure 34 B) suggesting that they were released from the polymer but some of the cell-cell interactions appear to have been disrupted. All of the HeLa cells were removed using the membrane leaving no cells on the UpCell dish (Figure 34 C).

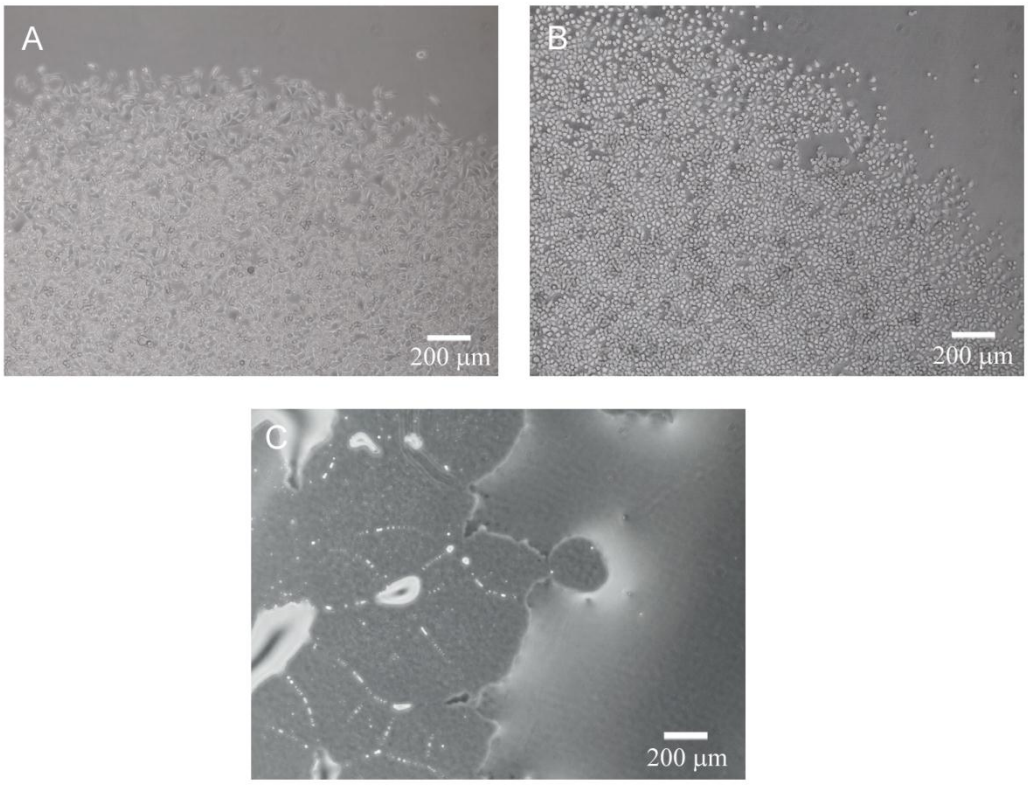

Figure 34 Release of HeLa cells from an UpCell dish following the improved protocol.
HeLa cells were seeded as a droplet on to an UpCell dish and incubated for 1 hour before the well was flooded with medium and the cells grown overnight A) shows the edge of the sheet at 37°C. The cells were then incubated at 20ºC for 30 minutes B) shows the edge of the sheet after incubation at 20°C, before the membrane was placed on top. The cells near the edges have rounded up showing that the cell sheet was partially disrupted. The membrane was then placed on to the cells for 1 minute and removed C) Shows the UpCell dish after the membrane has been removed, No cells were remaining. Scale bar shows 200µm.

The modified protocol was then repeated using 16HBE cells. However in this case incubated at 20ºC for 45 minutes, the edges of the 16HBE cell sheet began to round up (Figure 35 A) as expected from the manufacturers guidance. Furthermore the whole cell

sheet was removed using the membrane, leaving no cells behind (Figure 35 B). Okano *et al* have suggested that cells need metabolism to actively detach from the NiPAAm surface and that incubating at too low a temperature may block the release of cells (Okano et al., 1995). Consistent with this cooling on ice for 30 minutes did not stimulate the rounding up of the cells (Figure 35 C), whereas this was observed when incubated at 20ºC.

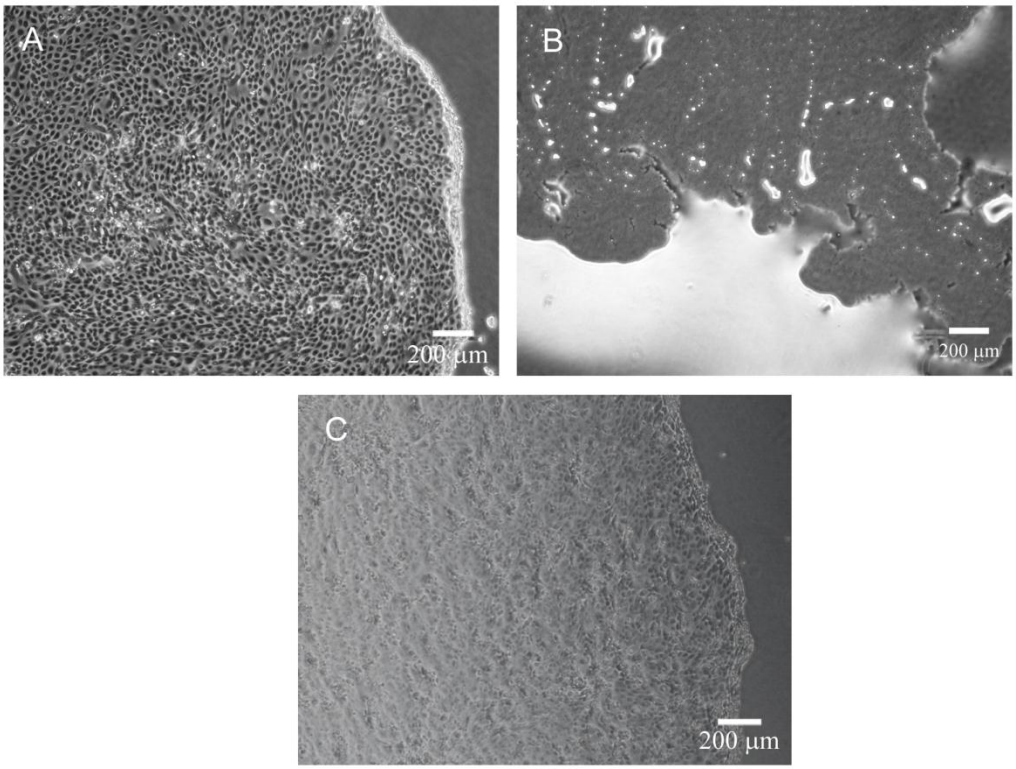

Figure 35 Release of 16HBE cells from an UpCell dish following the improved protocol.
16HBE cells were seeded at a confluent density in a droplet, they were left to adhere for 1 hour before the well was flooded with medium, and incubated at 37ºC overnight. A) Shows cells incubated at 20ºCfor 45 minutes, the edges have begun to round up. B) Shows the UpCell dish incubated at 20ºC after the membrane has been removed, no cells were remaining. C) Shows cells incubated for 30 minutes on ice, the edges have not rounded up. Scale bar shows 200µm.

To investigate detachment of the cells from the membrane after release from the thermoresponsive surface, the sheet was placed on to a glass coverslip. After 1 hour at 20°C the cell sheet was released from the membrane (Figure 36), however it was folded and not completely adhered to the glass coverslip, suggesting that it did not adhere sufficiently to the membrane.

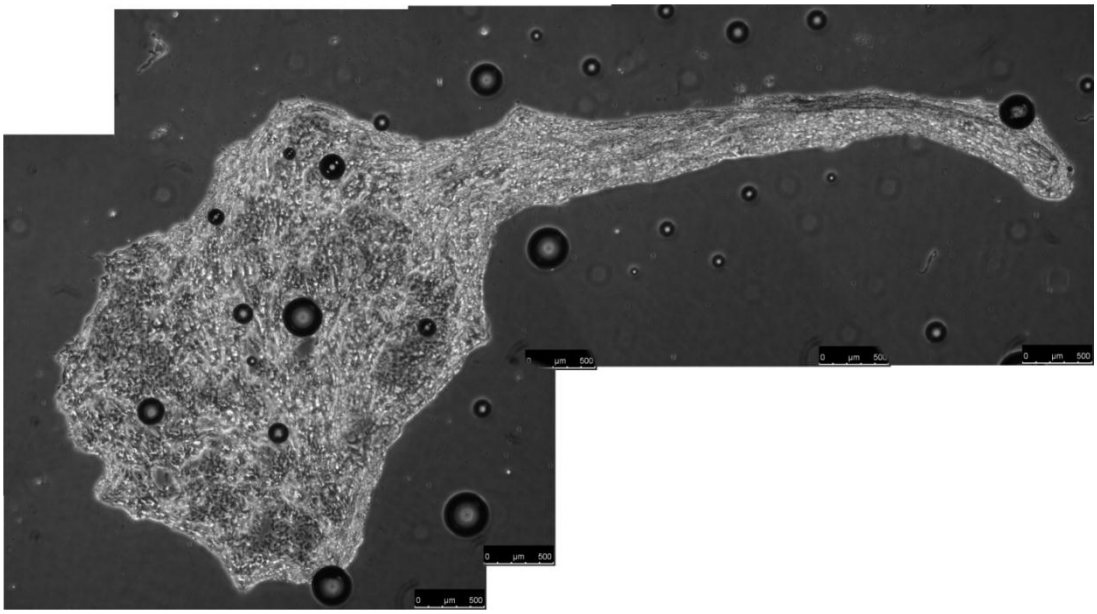

Figure 36 16HBE cells released from the UpCell membrane.
The membrane with 16HBE cells attached was placed on to a glass coverslip and incubated for 1 hour at 20°C allowing the cells to adhere to the glass and release from the membrane. Scale bar shows 500µm.

The released cell sheet was immunofluorescently stained for ZO-1 and F-actin. Two controls on glass coverslips were included, one in which cells were maintained at 37°C and one where the cells were incubated at 20°C for 105 minutes, equivalent to the time for release from the UpCell dish and attachment to the next surface. Figure 37 A, B and C show the cells maintained at 37ºC; here the ZO-1 (A) was located within the tight junctions surrounding the cell. The F-actin forms a belt around each cell and linking with other cells at points of cell-cell contact. D, E and F show the cells which were cooled at 20ºC for 105 minutes, here the ZO-1 was more punctate and did not form around the whole of every cell. The F-actin also seemed less uniformly located around the edges of the cells. G, H and F show the cells that have been released from the UpCell dish and reattached to a glass slide. The ZO-1 here is also punctate with areas where there was no staining. The F-actin appears less defined and there was more diffuse staining seen.

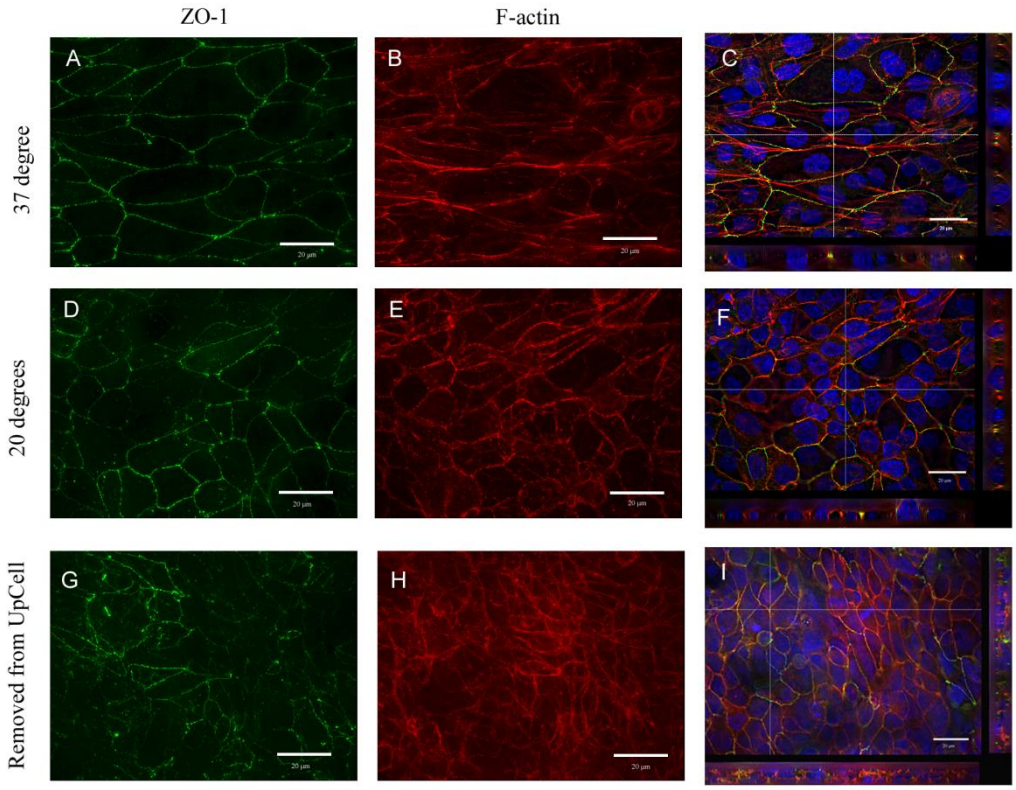

Figure 37 The effect of releasing the cell sheet on ZO-1 and F-actin distribution.
16HBE cells were grown on glass coverslips and an UpCell dish. A, B, C show 16HBE cells on a glass coverslip that were maintained at 37°C. D, E, F show 16HBE cells on a glass coverslip that were incubated at 20°C for 105 minutes to simulate the incubation time for the UpCell release. G, H, I show 16HBE cells grown on an UpCell dish incubated for 45 minutes at 20ºC before the cell sheet was removed using the membrane. The membrane was then incubated on a glass coverslip for 1 hour at 20ºC to allow the cells to attach to the glass coverslip. All the cell conditions were then fixed using 4% paraformaldehyde and immunofluorescently stained for ZO-1 and F-actin. Images taken using a fluorescent light microscope. Scale bars show 20µm, n=1.

Closer inspection of the cells in the reattached sheet suggested that they were smaller than those that had not been released. To determine the size variation achieved by releasing the cells from the polymer the average area of the cells was calculated using image J. A representative 10 cells per cell sheet were used which did not share a border if possible (Figure 38).

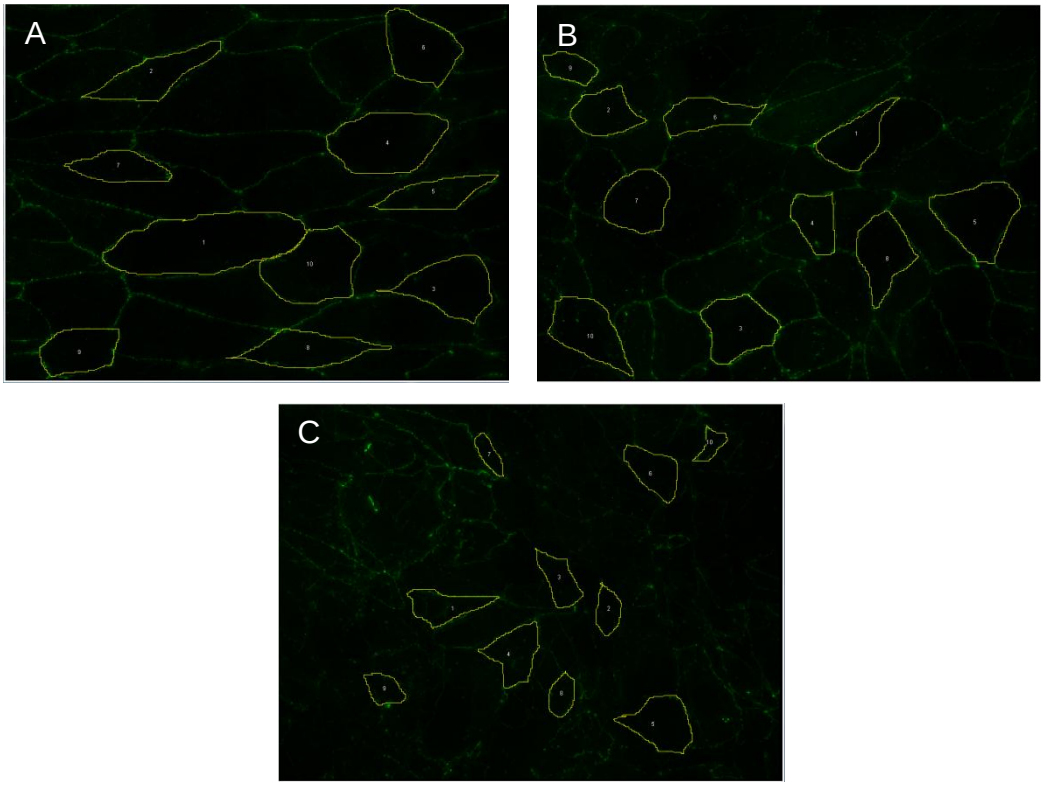

Figure 38 ZO-1 stained cells used to determine cell areas.
These images show ZO-1 staining; the highlighted cells are those which were measured for area calculation. A) Shows the cells maintained at 37ºC. B) Shows cells cooled to 20ºC for 105 minutes. C) Shows cells that were released from the UpCell dish and re-adhered to a glass coverslip.

The cells that remained at 37ºC had an average area of 1256.3µm^2 ± 696.4µm^2. The cells that were cooled for 105 minutes tended to be smaller having an average area of 845.9µm^2 ± 277.4 µm^2 however this difference was no statistically significant. The average area for a 16HBE cell on a surface is approximately 900µm^2 (Adams and Schubert, 2007). The released cells had an average area of 399.7µm^2 ± 211.8 µm^2. There was a significant difference between the released cells and either those incubated at 37ºC ($P<0.001$) and 20ºC ($P<0.005$). The statistical analysis used was the one way ANOVA with Tukey's multiple comparisons test (Figure 39).

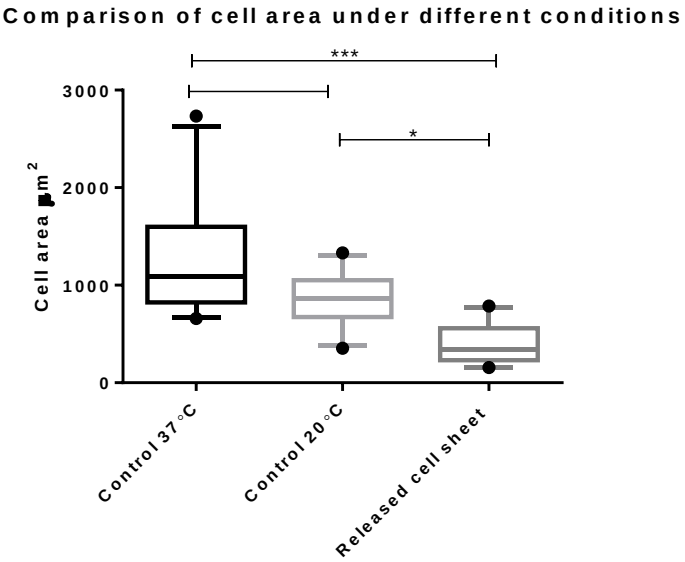

Figure 39 Area of 16HBE cells incubated at different temperatures or released from the UpCell dish. The areas of 10 cells per condition were calculated using image j. Data shows the median plus the 10-90 percentiles. The statistical analysis used was one way ANOVA with Tukey's multiple comparisons test. *** =p<0.001 and *=p<0.05 n=3

Cooling the bronchial epithelial cell sheet caused slight disruption to the tight junctional organisation, but not enough to disrupt the cell sheet. There was no significant difference between the sizes of cells within the cooled cell sheet and the control. This suggests that a change in temperature has minimal effect on the adhesion of the cell sheet to the surface. The cell sheet released from the polymer maintained its tight junctions, however the cells had contracted. This contraction may be due to the loss of cell-matrix interactions which allows the cytoskeleton to contract.

3.3 Levitating cells from the UpCell dish within the Sonotweezers device.

Having established that the 16HBE cells will release from the UpCell dish the next step was to investigate its use in the Sonotweezers device to avoid using the membrane provided. Cellular release without the membrane was tested by flushing with a 1ml pipette. This showed that although the sheet was released from the thermoresponsive surface it was folded (Figure 40).

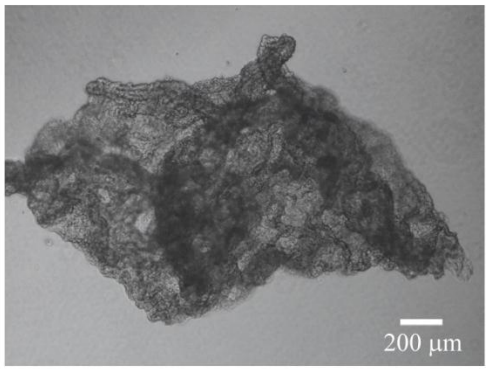

Figure 40 A 16HBE cell sheet released from the UpCell dish by flushing with a 1ml pipette.
16HBE cells were seeded in a droplet on an UpCell dish, after one hour the well was flooded with medium and incubated at 37ºC overnight. The cells were then incubated at 20ºC for 45 minutes before being flushed with a 1ml pipette to release the sheet from the thermoresponsive surface. Scale bar shows 200µm.

We therefore postulated that the use of the Sonotweezers device could be advantageous as it may keep this released sheet flat. To test this we first needed to determine whether cells could be released from the thermoresponsive polymer within the Sonotweezers device, Therefore HeLa cells were seeded at a cell density that would result in the attachment of isolated single cells on the UpCell dish; these were chosen for initial studies as they were less adhesive than 16HBE cells. After attachment of the cells overnight, the dish was incubated at 20ºC for 45 minutes then added into the device; cold medium was added through the microfluidic channels to maintain the temperature. The transducer was switched on at resonate frequency. This frequency had been determined using 10µm fluorescent polystyrene beads which were shown to be levitated. This approach only resulted in the levitation of 2 cells within the field of view; the circles show cells that moved to the nodal plane (Figure 41). Repetition did not increase this number.

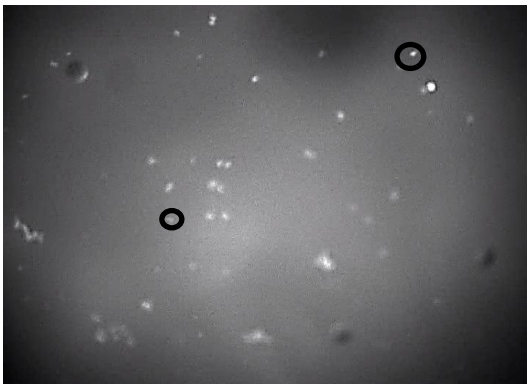

Figure 41 Single HeLa cells cooled on an UpCell dish and levitated within the Sonotweezers device.
HeLa cells were seeded at a low density in a droplet and incubated for one hour to allow attachment of the cells. The dish was then flooded with medium and incubated at 37ºC overnight. The dish was incubated for 30 minutes at 20ºC before the Sonotweezers device was placed on the dish. Cool medium was gently added into the device before it was switched on at resonant frequency. The cells circled show two cells that were levitated within the device. The majority of cells were not released from the UpCell surface using the Sonotweezers device.

3.4 Discussion

The creation of an *in vitro* model simply by the addition of a mixture of cell types in single cell suspension which would organise themselves as they would *in vivo* does not occur due to cell motility. The epithelial cells formed islands surrounded by the fibroblasts. Nandkumar *et al* also saw this with primary cells from Wistar rat lungs where patches of epithelial cells were surrounded by fibroblasts; this was noted on both tissue culture plastic and the UpCell dish (Nandkumar et al., 2002). It appears that the requirement for attachment to the surface outweighs any signals that would lead to a more complex organisation. To overcome this cell sheet engineering was attempted using the thermoresponsive polymer coated UpCell dishes. Ito *et al* showed that hepG2 and NIH3T3 cell sheets maintained their distinct layers for 24 hours after cell sheet manipulation, but when added together there was random organisation of the two cell types (Ito et al., 2007). Kim *et al* showed that hepatocytes and endothelial cells maintained their separate sheets after 3 days growth together (Kim et al., 2012). In the present study the UpCell dishes allowed the attachment of 16HBE and HeLa cells to the surface without the addition of extracellular matrix. Upon cooling the HeLa cells lost all their cell-cell junctions, the MRC5 cells released spontaneously forming aggregates of cells and the 16HBE cells took an extended time period for the polymer underneath the cohesive cell sheet to become hydrated causing problems with the release. The method used by Kushida *et al* was the closest to the method implemented for 16HBE cell sheet release. They incubated MDCK (Madin-Darby Canine Kidney Epithelial) cells for 1 hour at 20ºC before the medium was removed, the membrane was placed onto the surface of the cells. The membrane and cells were peeled off the polymer and placed on to a fresh dish. To allow attachment to the next dish the cells were incubated for a further 30 minutes at 20ºC (Kushida et al., 2001). Much of the initial work on tight junctions was carried out on this cell type making it comparable to the bronchial epithelial cell line. The 16HBE cell sheets were incubated for 45 minutes or until the edges had rounded up to achieve release and incubated for 1 hour to allow the cell sheet to attach to the next dish. Metabolic activity appears to be required for cell release as it was not observed at 4ºC. This was consistent with Okano *et al* who revealed that cell detachment of BAEC and rat hepatocytes was inhibited by the addition of sodium azide (Okano et al., 1995). Once a sheet of 16HBE cells was released with the aid of the membrane it was observed that a cohesive sheet had been retained as demonstrated by the presence of tight junctions. These tight junctions were slightly disrupted by the cooling process needed for the conformational change of the polymer; however they were not sufficiently disrupted to cause degradation of the cell sheet. The size of the released sheet

was shown to be decreased. This is probably due to the interactions of the actin cytoskeleton with the focal adhesions which bind to the surface of the polymer via integrins. The actin fibres are interspersed with myosin II molecular motor proteins (Peterson et al., 2004) these allow the fibres to contract. It has been shown that when the connection between the actin fibres and the focal adhesions weaken the myosin II molecular motors induce contraction of the fibres (Kumar et al., 2006). This has been noted when investigating cell sheet engineering (Nandkumar et al., 2002). Wei *et al* investigated the cytoskeleton in sheets of cells released from a surface using dispase. They noted that all parts of the cytoskeleton (F-actin, intermediate filaments and micro tubules) were involved in the contraction of the released cells sheet; however the F-actin played the greatest role (Wei et al., 2013). The use of the membrane maintains the integrity of the sheet once released as it keeps the sheets flat preventing them from folding. When cooled to achieve release from the polymer the HeLa cells appeared to lose their cell to cell contacts, with all cells rounding up. This shows that the behaviour of all cell types cannot be determined from the study of only one type, as each cell type will behave differently on these polymers.

It was evident that HeLa cells required less force to obtain release from the UpCell dish; therefore they were used to investigate the release of cells using the Sonotweezers device. The device was unable to levitate single HeLa cells from the surface of the UpCell dish. Takamizawa *et al* (Takamizawa et al., 2002) and Weder *et al* (Weder et al., 2010) both investigated the force needed to release BAEC (bovine aortic endothelial cells) and 3T3 (rat fibroblasts) using either a lever motor system to draw up a coverslip and sense the drawing force or the cantilever of an AFM microscope. The use of the lever motor enabled investigation of a sheet of cells whereas atomic force microscopy permitted analysis of a single cell. Takamizawa *et al* reported that the strength needed to release a sheet of BAEC was 230nN/cell at 37ºC and 14nN/cell at room temperature, compared to control experiments using tissue culture plastic in which 225+/-38nN was required at 37ºC and 160nN +/- 50nN at room temperature to obtained release. Weder *et al* reported that 3T3 fibroblasts grown on NiPAAm required 270nN at 37ºC and 19nN to be released compared to the control of 3T3 cells grown on glass which required 230nN at 37º and 200nN at 27ºC to be released. The sheer force needed to release the cells from NiPAAm has also being investigated. Tang *et al* investigated this by covalently attaching NiPAAm to a microfluidic device (Tang et al., 2012); this device was designed with various channels that obtained increasing sheer strength when media was flown through the device. This was also

investigated using 3T3 fibroblasts and BAECs. Media of decreasing temperatures was added over an hour, after which all the cells had released at the lowest force of 3.24dyn/cm^2 (0.324N/M^2). The need for forces to release the cells was contrary to the spontaneous release from the surface that was originally believed. The ultrasonic forces, created within the device are likely to be in the region of 0.02 to 0.1nN/cell, orders of magnitude less than the forces required for release from the thermoresponsive surface.

In summary the 16HBE cells can be released from a thermoresponsive surfaces as a coherent sheet with little disruption to the tight junctions. However, it was impossible to release them using the Sonotweezer device as the forces provided were insufficient.

The rest of this thesis will follow two pathways in the investigation of how to release sheets of cells from thermoresponsive polymers in a more controlled fashion and to investigate the creation of sheets of cells within the Sonotweezers device.

4. Levitating sheets of bronchial epithelial cells within the Sonotweezers device

Although the device did not provide enough force to levitate cells from the thermoresponsive polymer, an alternative strategy was adopted in which the device was used to form bronchial epithelial cell sheets.

The formation of cell sheets within ultrasonic devices has been observed for neural cells (Bazou et al., 2005a), the prostate epithelial cell line (PZ-HPV-7) the cancerous prostate epithelial cell line (DU-145) (Bazou et al., 2006a), chondrocytes (Bazou et al., 2006b) and HepG2 (liver hepatocellular carcinoma) (Edwards et al., 2007). These studies have focused on the formation of the adherens junctions. Adherens junctions in epithelial cells are made up of the transmembrane protein E-cadherin which forms a homodimer with an adjacent cell, in a calcium dependant manner. Within the cell the E-cadherin binds to β and then α-catenin, which in turn binds to the actin cytoskeleton (Figure 42). N-cadherin (neural-cadherin) carries out the same function as E-cadherin (epithelial-cadherin) but in neural cells.

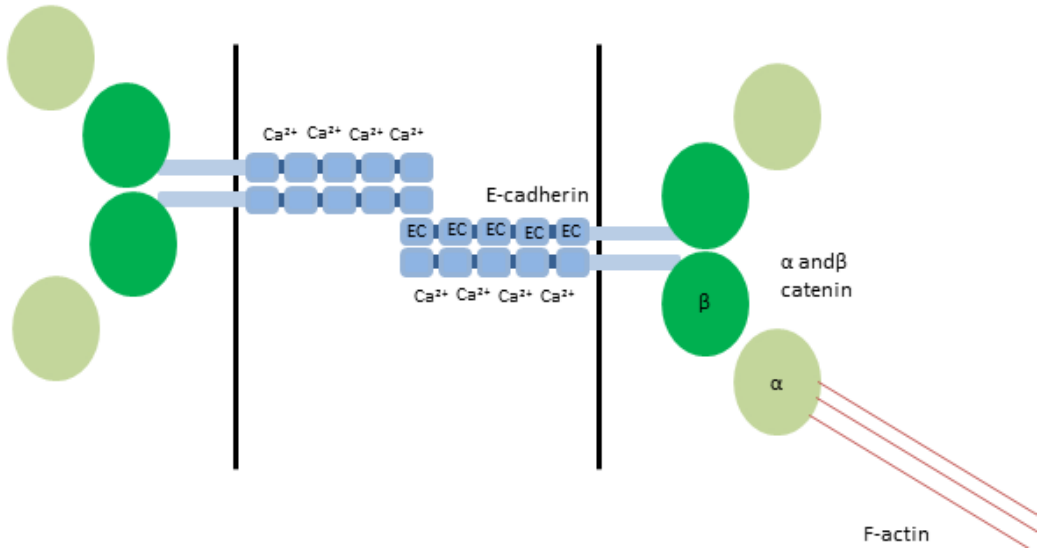

Figure 42 Schematic of the composition of the adherens junction

When Bazou *et al* levitated C6 neural cells within a half wavelength ultrasonic device, the cells came together forming 2D aggregates within 30 seconds. The morphology of the cells changed during 1 hour of levitation suggesting cell-cell contacts were forming. To investigate this after 1 minute, 8 minutes, 30 minutes and 60 minutes of levitation cell aggregates were collected and immunofluorescently stained for neural cell adhesion

molecule (NCAM), N-cadherin and F-actin. After 1 minute of levitation there was a weak NCAM signal that was discontinuous at the cell-cell interface. After 8 minutes levitation the staining was more continuous and after 30 minutes there was a strong signal that was evenly distributed at sites of cell-cell contact suggesting the adherens junctions had formed. The F-actin staining after 1 min showed a discontinuous punctate distribution around the surface of the cells. After 8 minutes the F-actin had accumulated at the interface between the cells, after 30 minutes there was a strong signal associated with the cell-cell contacts (Bazou et al., 2005a). This suggested that within 1 hour well organised cell-cell contacts had started to form.

Bazou *et al* also investigated the E-cadherin/catenin complex and F-actin localisation during cell-cell contact in a prostate epithelial cell line (PZ-HPV-7) and a prostate cancer cell line (PV145) when levitated for1 hour. They noticed that cell morphology for both cell types changed during the 1 hour levitation. After 1 hour the E-cadherin within PZ-HPV-7 changed from a ring type distribution around the edge to accumulating at areas of cell-cell contact. DU145 also had the ring type distribution at the edge of the cell however this did not change within the 1 hour of levitation. The F-actin staining was no different between both cell types, after 1hour of levitation it accumulated at the cell-cell interface. The α-catenins originally showed a diffuse distribution throughout the cells with a little accumulation at cell edge for both cell types. After levitation for 1 hour the α-catenin in both cell types accumulated at the cell-cell interface. The β and γ catenins in PZ-HVP-7 cells accumulated at the cell-cell interface after 1 hour levitation whereas the DU145 had diffuse cytoplasmic staining (Bazou et al., 2006a). This suggests that for this epithelial cell type, junctions do begin to form when the cells are not in contact with the ECM, however there is no information as to whether these cells begin to polarise. There is a marked difference between the epithelial cells and cancerous cells in their junctional protein localisation. Cancer cells have mutated to allow for uncontrolled growth and are frequently not dependent on cell-cell interactions for their survival.

Bazou *et al* also investigated the behaviour of chondrocytes that were levitated for 1 hour. After 30 seconds 2D cell aggregates were formed. When the 2D aggregates were removed after 1 minute of levitation they disassociated whereas those removed after 1 hour remained as a sheet. The F-actin was distributed in a ring like pattern at the cell surface following 1 minute levitation. After 1 hour the F-actin had accumulated at the cell-cell contact interface. Gap junctions were also suggested to have formed after one hour as

CMFRA dye passed from a stained population to an unstained population during levitation (Bazou et al., 2006b).

Edwards *et al* investigated HepG2 cells levitated over 1 hour. The HepG2 cells formed a 2-D aggregate within 30 seconds and by 10 minutes the morphology of the cells had changed losing their roundness. The F-actin staining became localised at regions of cell-cell contact after 4 minutes, becoming more defined at the cell-cell interface after 11 minutes (Edwards et al., 2007).

Although all these papers investigate the formation of cell sheets the morphology of the cells when levitated was not the same as the cells grown on a solid substrate.

None of these groups investigated cells levitated over 1 hour. The initial cell-cell contacts were observed but they did not determine whether the cells became polarised and formed an epithelial barrier. Cell polarisation is thought to be dependent upon integrin matrix interactions allowing the cells to determine their apical and basal sides and on tight junction formation which regulates lateral membrane diffusion of proteins.

The aim of this chapter is to create levitated sheets of bronchial epithelial cells within a Sonotweezer device.

4.1 Capillary microfluidics device

4.1.1 Levitating 16HBE cells over 5 days

An existing Sonotweezers device that allowed levitation over a prolonged time period was used to investigate the formation of sheets within a standing wave. A flat capillary with a height of 0.5mm was attached to a piezoelectric transducer the ends of the capillary were attached with microfluidics for a continuous media supply. Two devices were set up, the transducers were set with a sweeping frequency around the resonate frequency (910 kHz-930 kHz) (Figure 43). This allowed for variation between the two transducers and allowed some variation over time for the transducer, maintaining levitation over the time period required. 5 Days was initially chosen as this is the time taken for tight junctions to form completely when 16HBE cells are grown on a transwell (data not shown).

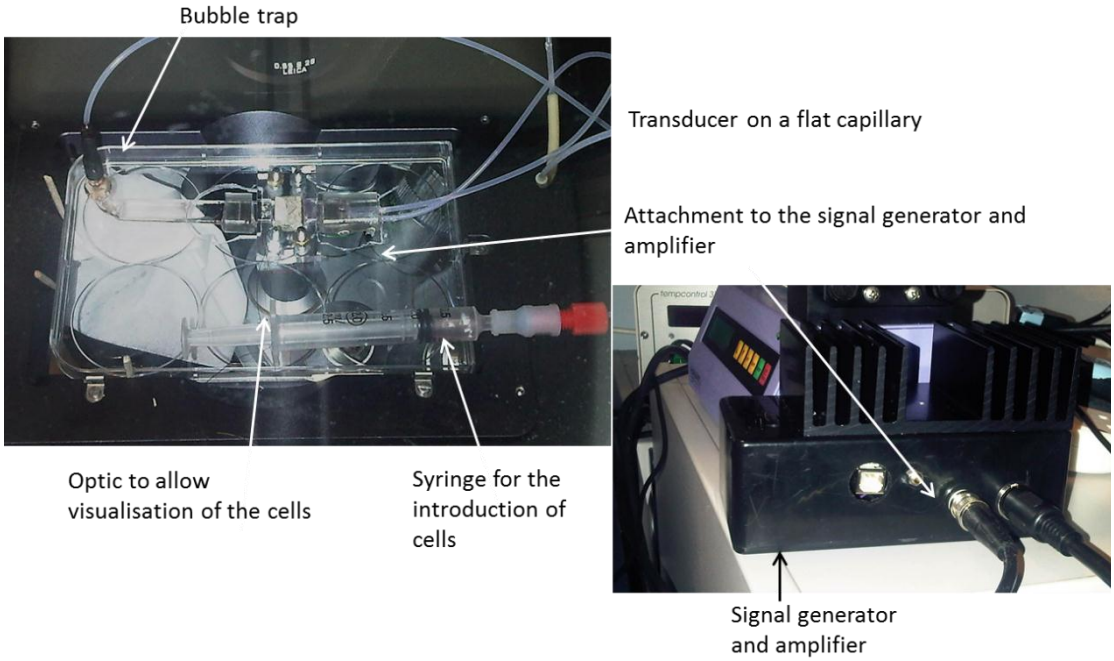

Figure 43 capillary device within time-lapse microscope heated chamber.

When CMRA orange stained 16HBE cells were injected into the device, aggregates formed almost instantly at acoustic hotspots. The cells came together, then started to contract forming a 3D aggregate after 2 days (Figure 44A), rather than a sheet one cell thick. After 5 days levitation, cells appear to move out of the 3D aggregate and start to form a monolayer 'skirt' around the aggregate (Figure 44B).

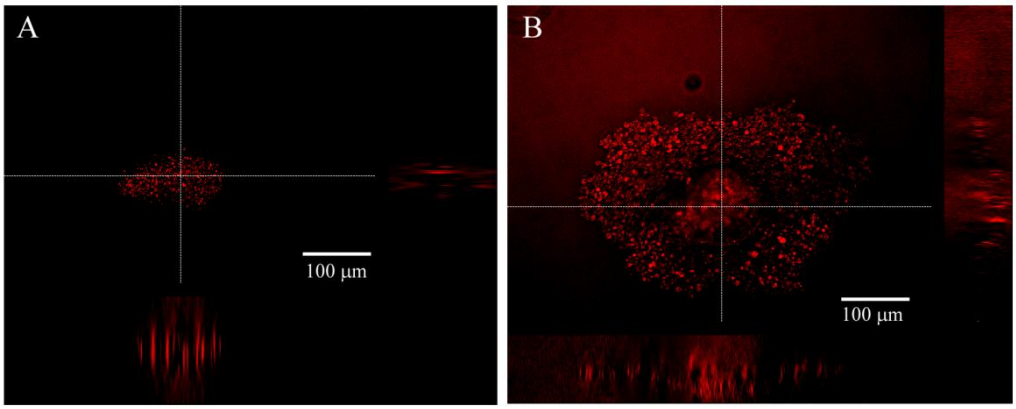

Figure 44 Z stacks taken during the 5 day levitation of 16HBE cells within the capillary Sonotweezers device.

The contraction of the agglomerate after 2 days suggested that there are some cellular interactions are occurring, possibly due to contraction of the actin cytoskeleton.

4.2 Chamber Sonotweezers device

4.2.1 A Sonotweezers device which fits into a 6 well plate

The original capillary device was not suited to our needs due to difficulties in retrieving the cells from the device after levitation. Bubbles were also a problem as they caused streaming which can damage the cells. To overcome these problems a device which was not microfluidic was designed, this is closer to the original design (Figure 23) that was used for the release of cells from the thermoresponsive polymers. This fits into a 6 well plate (Figure 47), allowing up to 6 experiments to run at one time. The device had an active region of 10 x 10 x 0.5 mm, which was resonant at 2.0 MHz, the addition of a mirrored surface allowed improved visualisation of the cells when using an epi-fluorescent microscope. The cells were introduced into the active area of the device using a flat gel loading tip. There was an LED located on the top of the device allowing visualisation of the current entering the PZT, which flashed showing the sweep frequency that is used to maintain constant levitation (Figure 45) .

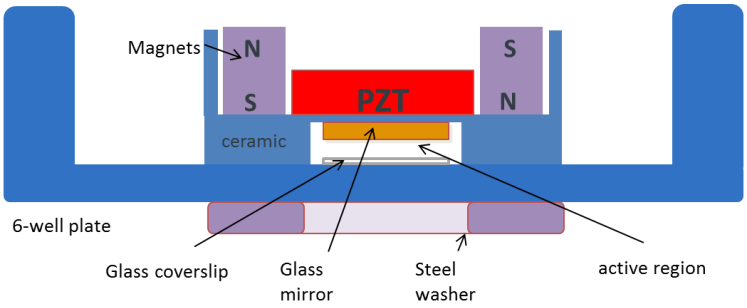

Figure 45 The 6 well Sonotweezers device initial design.

Since the acoustic resonance achieved with a coverslip as the reflector was not strong enough to maintain levitation, the glass was modified to use a glass slide which is much thicker than a coverslip (Figure 46). This provided improved reflection of the standing wave allowing levitation of the 16HBE cells and beads over a prolonged time period.

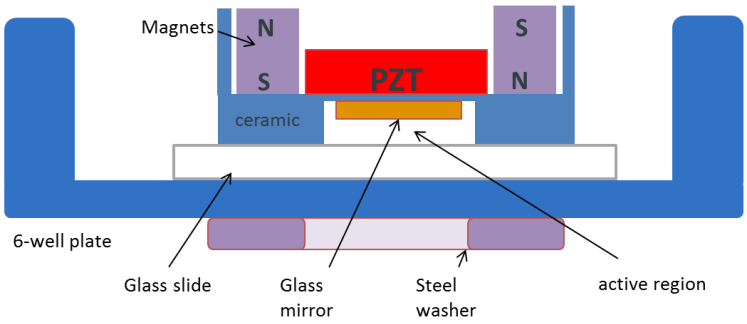

Figure 46 The 6 well Sonotweezers device with glass slide reflector.

Figure 47 The 6 well Sonotweezers device sits within the environmental chamber of a time lapse microscope.

Initial experiments were carried out to determine whether the contraction of the cells seen within the capillary device was a function of the device or a function of the cells, both 10µm polystyrene beads and CMRA orange stained 16HBE cells were levitated for 24 hours. Figure 48 shows that the cell aggregate significantly contracted ($P<0.005$) over the 24 hours. However this did not occur with the beads suggesting that the contraction was a function of the cells behaviour. The error bars are much larger for the beads due to the weaker lateral forces as a consequence of the lower density of the beads compared to the cells.

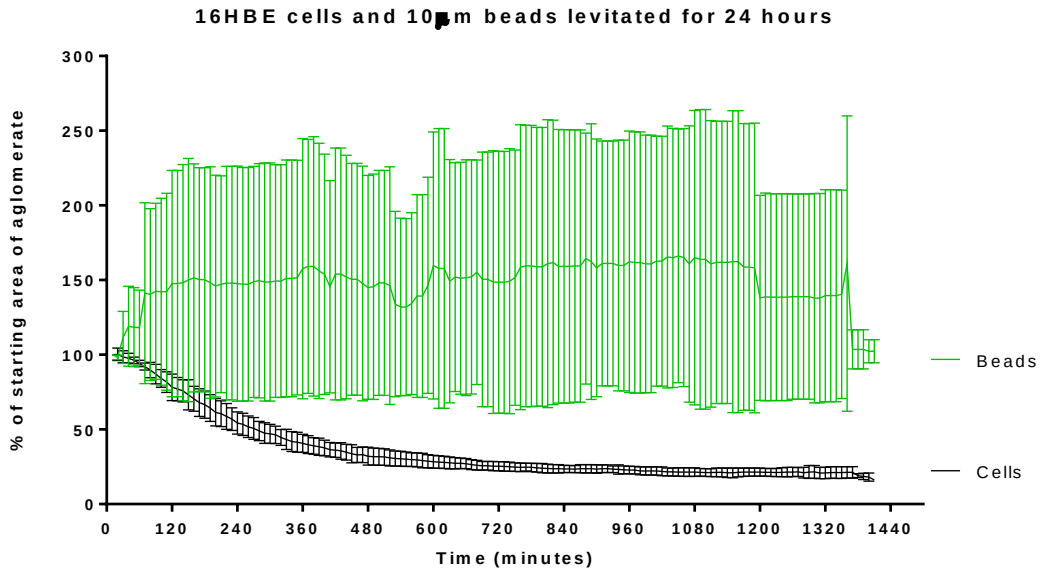

Figure 48 16HBE cells and 10µm polystyrene beads were levitated for 24 hours and the area of the aggregates measured.
Statistical analysis using two-way Anova with Sidak's multiple comparison shows no significant difference between the starting and finishing area of the bead agglomerate, however the cell agglomerate has significantly contacted ($P<0.005$) n=3.

The 16HBE cell aggregate that formed within the device over 24 hours was captured and immunofluorescently stained for F-actin and the cell nuclei. This confirmed the 3D structure seen within the device shown by the Z-stack in Figure 49.

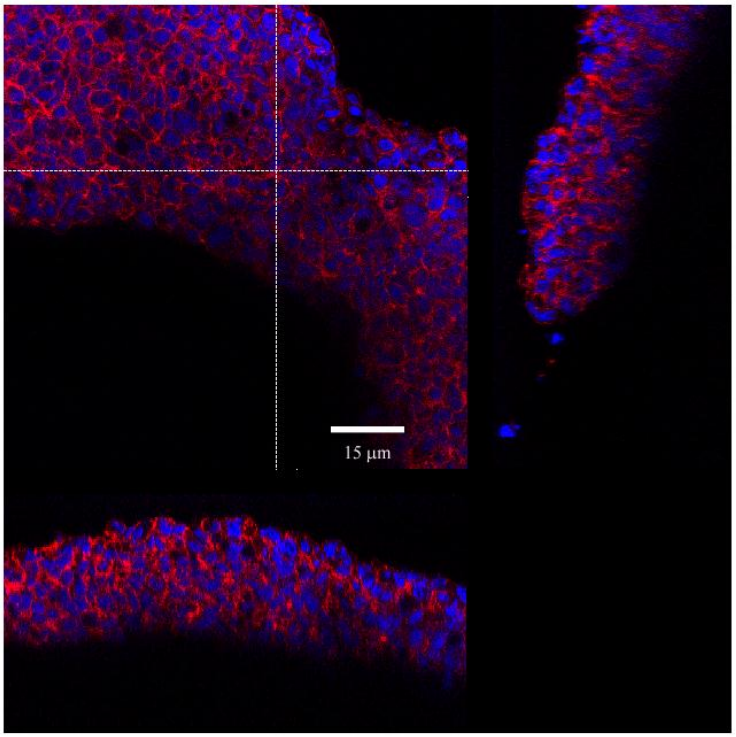

Figure 49 Immunofluorescent staining of the 16HBE aggregate levitated over 24 hours.
The cell aggregate was fixed with acetone:methanol (1:1) and stained using Phalloidin (red) to show F-actin and Dapi (blue) to show the nuclei. Image taken using a confocal microscope, representative of 3 aggregates. Scale bar shows 15µm.

To determine when the aggregation occurred and when junctions were forming, the cells were levitated for set time periods before being fixed and immunofluorescently stained for the adherens junctional protein E-cadherin and the actin cytoskeleton. To help inform which time points to study using the devices, 16HBE cells were first grown to confluence on a glass coverslip, deprived of calcium for 4 hours to disrupt the formed junctions before calcium was added to promote the reformation of the adherens junctions. At 0, 1, 2 and 6 hours the cells were fixed and immunofluorescently stained for E-cadherin and F-actin (Figure 50). This showed that at 0 hours the E-cadherin was diffuse and barely visible and the F-actin was a pericellular ring. The cells were rounded with gaps between them as there were no cell-cell contacts formed. After 1 hour the E-cadherin started to move to the cell-cell junctions. The F-actin also moved to the cell-cell contacts and the cells started to flatten. After 2 hours the E-cadherin was located at areas of cell-cell contacts. The F-actin surrounded the cell where there were cell-cell contacts and the cells were more spread with few gaps visible between the cells. After 6 hours the E-cadherin was located at the cell-cell junctions as was the F-actin. By this time the cells formed a coherent cell sheet with all the cells flat and spread. As these experiments suggested that adherens junctions had formed within 6 hours, the formation of adherens junctions within the Sonotweezers device was studied at times up to 6 hours.

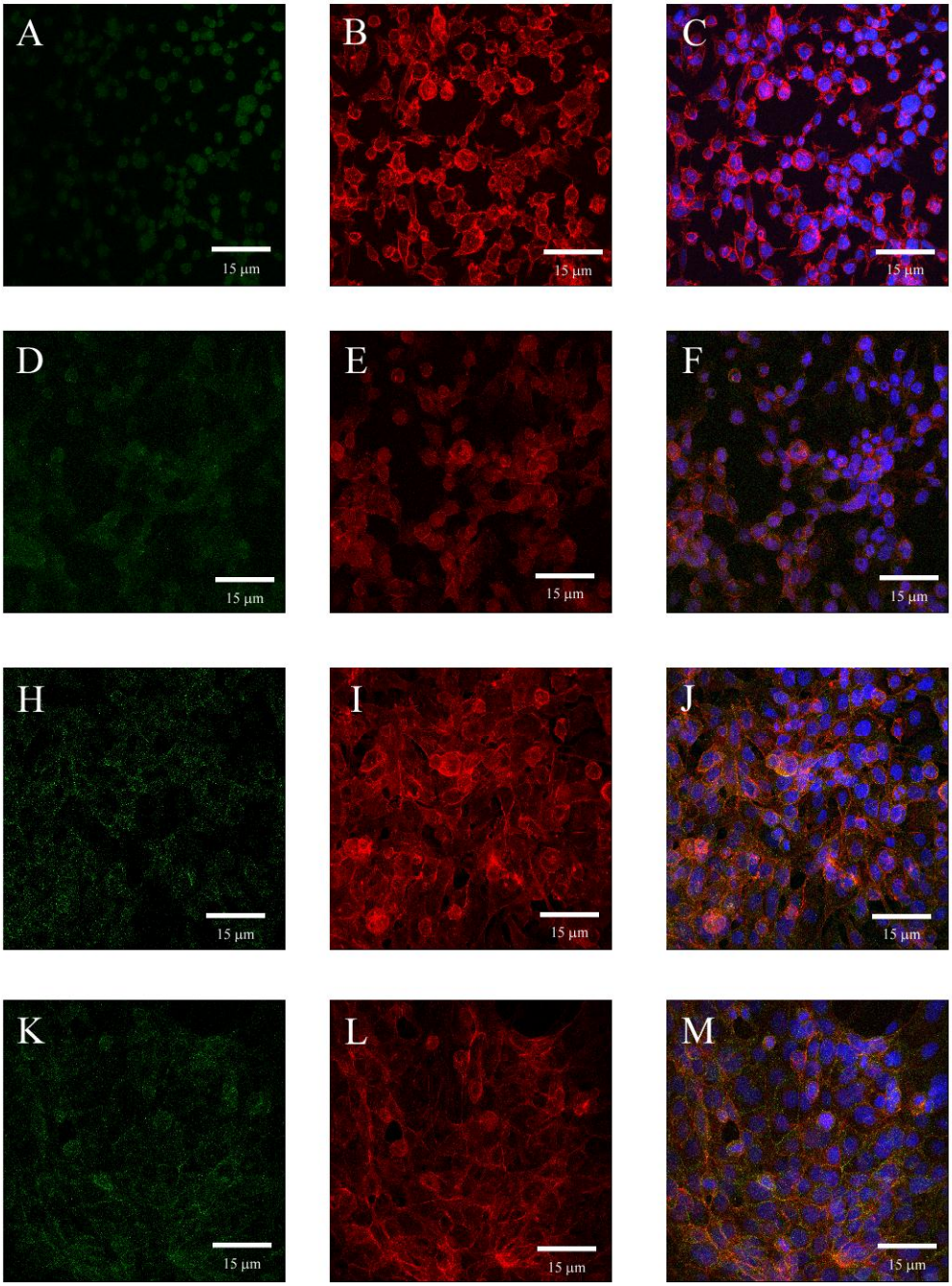

Figure 50 16HBE were grown on glass coverslips before their junctions were disrupted be the removal of calcium. The junctions were then allowed to reform by the addition of calcium. A, B and C show cells immediately after their junctions had been disrupted (t=0) by the removal of calcium. D, E and F show cells after 1 hour with calcium. H, I and F show cells after 2hours with calcium. K, L and M show cells after 6 hours with calcium. The E-cadherin staining is shown in green and the phalloidin F-actin staining is shown in red. The final row shows the overlay including the nuclear counter stain dapi. Images taken on a confocal microscope, representative of 3 repeats. Scale bar shows 15µm.

4.2.2 16HBE cells levitated for 1 hour

After levitation for 1 hour the 16HBE cell aggregate remained as monolayer similar to the beads with little variation in agregate size (Figure 51) with no significant difference from the aggregate starting size.

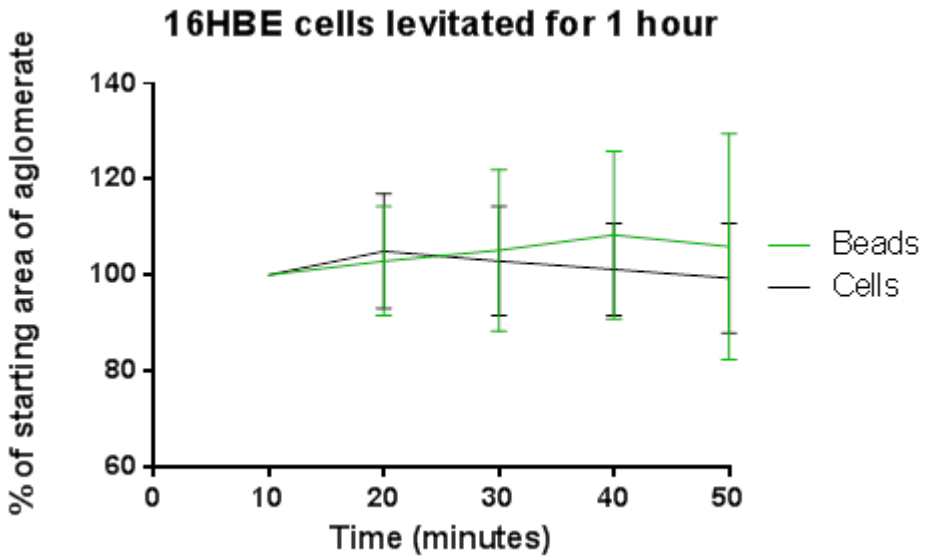

Figure 51 Area of 16HBE and 10µm polystyrene bead agglomerates during 1 hour levitation within the Sonotweezers device. Statistical analysis using two-way Anova with Sidak's multiple comparison test showed no significant difference between areas of the bead and the cell agglomerates or between the starting and finishing area of either aggregate n= 10.

After 1 hour of levitation, the cell sheet was fragile when removed from the device, the aggregates that were captured and immunofluorescently stained showed that the adherens junctions had not yet formed (Figure 52). This was expected as the E-cadherin was not located at the junctions within the control, where the cells are in optimal conditions. When levitated the formation of the junctions might be expected to be delayed as there are no cell-matrix intractions. Interestingly examination of the Z-stack showed that the nuclei are not in one layer (Figure 52D) suggesting that the cells pack together to accommodate the nuclei.

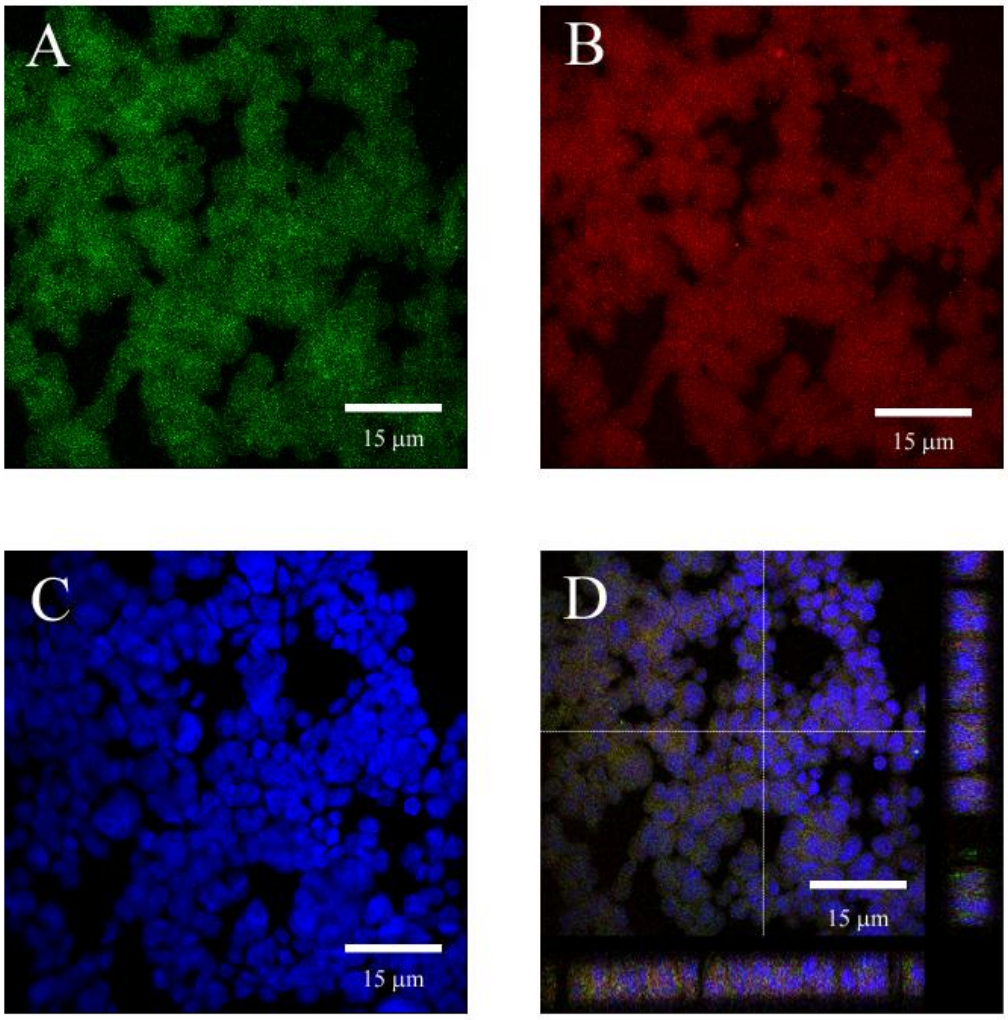

Figure 52 immunofluorescent staining of 16HBE cells levitated within the Sonotweezers device for 1 hour. A) Shows E-cadherin staining, B) Shows F-actin staining, C) shows the nuclei staining and D) Shows the overlay and Z-stack. The aggregates were fixed using acetone:methanol (1:1). The Images were taken using a confocal microscope, representative of 3 aggregates. The scale bar shows 15µm.

The addition of 7AAD for 10 minutes during levitation showed that there was no decrease in cell viability, Figure 53 shows only 1 red cell which has taken up the dead cell stain 7AAD.

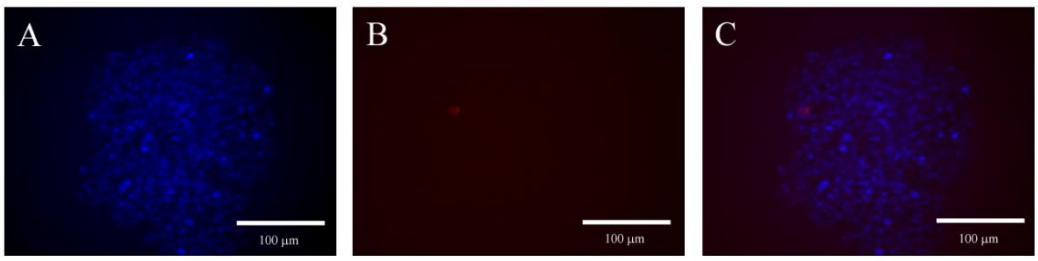

Figure 53 16HBE cell viability after 1 hour levitation within the Sonotweezers device. 16HBE cells stained with cell tracker blue were levitated for 50 minutes before 7AAD was added for the final 10 minutes of levitation. A) Shows the cell aggregate, B) Shows the cells stained with 7AAD and C) Shows an overlay of both channels. The scale bar shows 100µm.

4.2.3 16HBE cells levitated for 2 hours

After 2 hours levitation the cell aggregates started to significantly contract ($p<0.05$) (Figure 54).

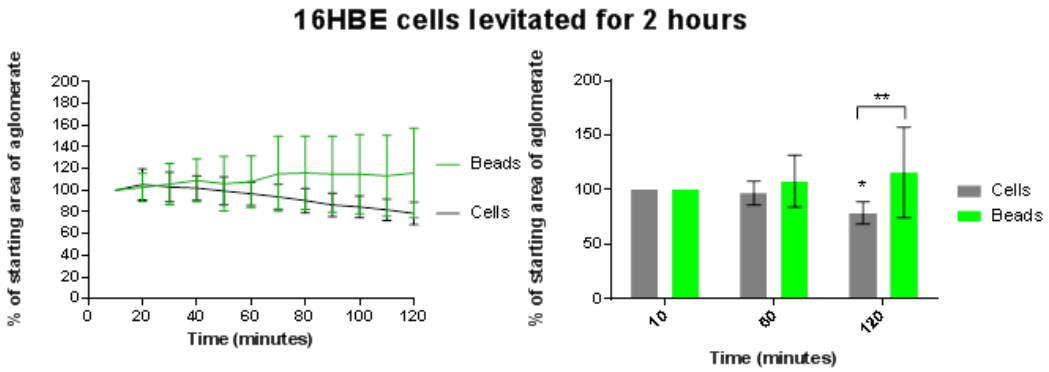

Figure 54 Contraction of the 16HBE cell aggregate after 2 hours levitation within the Sonotweezers device. Statistical analysis using two-way Anova with Sidak's multiple comparison test showed no significant difference between the starting and finishing area of the bead agglomerate. There was a significant difference between the starting area and finishing area of the cell agglomerate ($p<0.05$). The variation in area between the two agglomerates is also significantly different at 120 minutes ($p<0.005$) n=8.

This coincides with the appearance of E-cadherin at the cell-cell junctions and rearrangement of the actin cytoskeleton from diffuse staining to a pericellular ring (Figure 55).

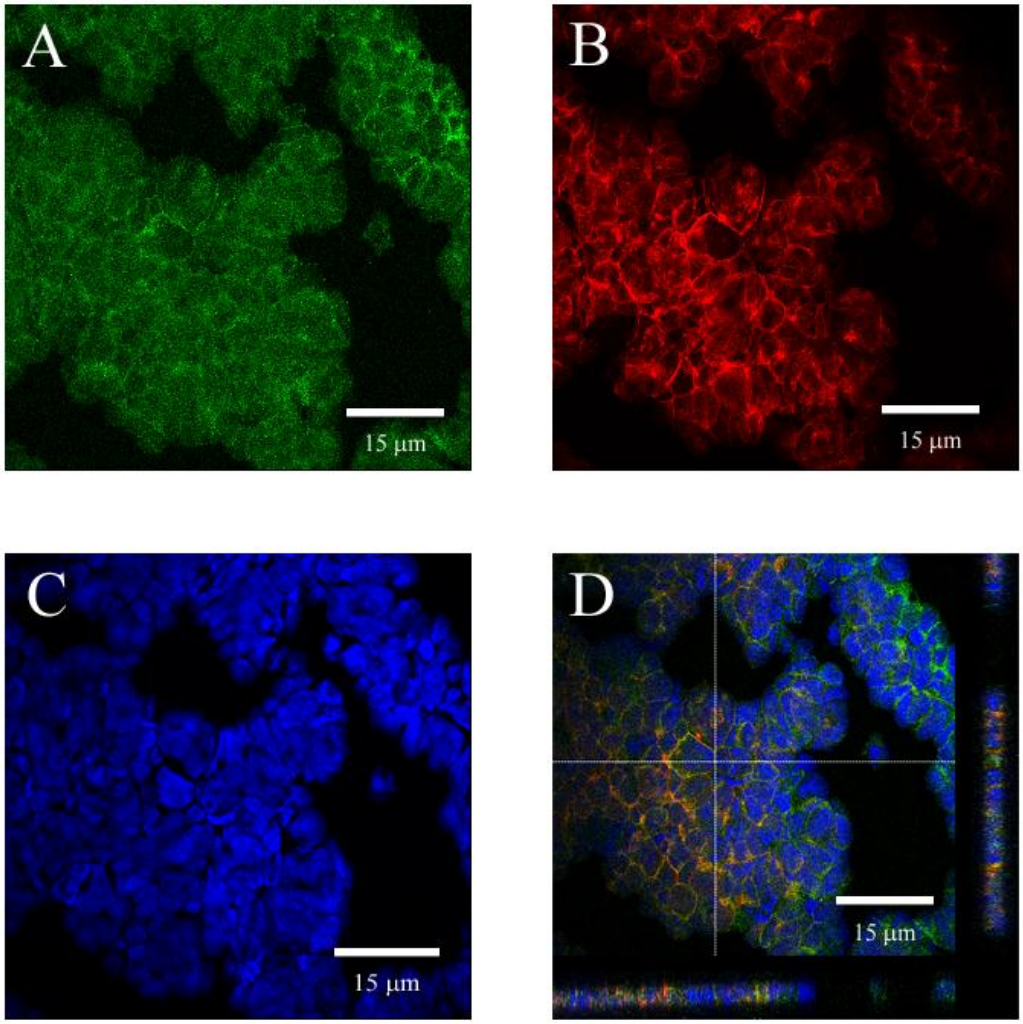

Figure 55 Immunofluorescent staining of the 16HBE cell aggregate formed after 2 hours levitation within the Sonotweezers device. A) Shows the E-cadherin staining, B) Shows the F-actin Staining, C) Shows the nuclei staining and D) Shows the overlay and Z-stack. The aggregates were fixed using acetone:methanol (1:1). The Images were taken using a confocal microscope, representative of 3 aggregates. The scale bar shows 15µm.

The cell nuclei distribution within the aggregate was more compact than after one hour levitation; they were not forming a 3D structure as the nuclei were arranged in one layer. The nuclei appear to have packed into the most structurally stable arrangement.

The viability of the cells was still high with very little red 7AAD staining seen (Figure 56).

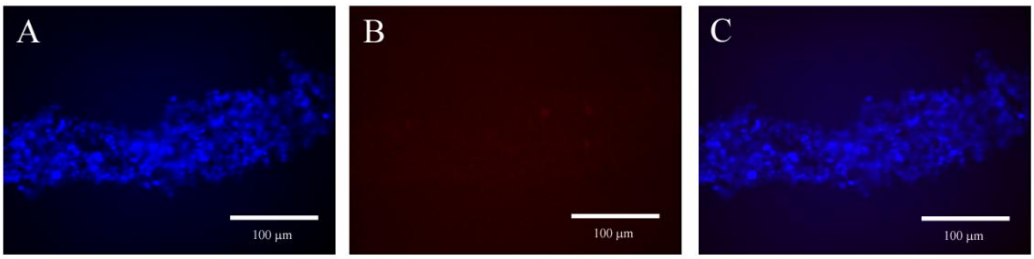

Figure 56 Cell viability of 16HBE cells levitated for 2 hours within the Sonotweezers device.
16HBE cells stained with cell tracker blue were levitated for 110 minutes before 7AAD was added for the final 10 minutes of levitation. A) Shows the cell aggregate, B) Shows the cells stained with 7AAD and C) Shows an overlay of both channels. The scale bar shows 100µm.

4.2.4 16HBE cells levitated for 6 hours within the Sonotweezers device

After 6 hours levitation the aggregate had significantly contracted to 50% of its starting size (Figure 57).

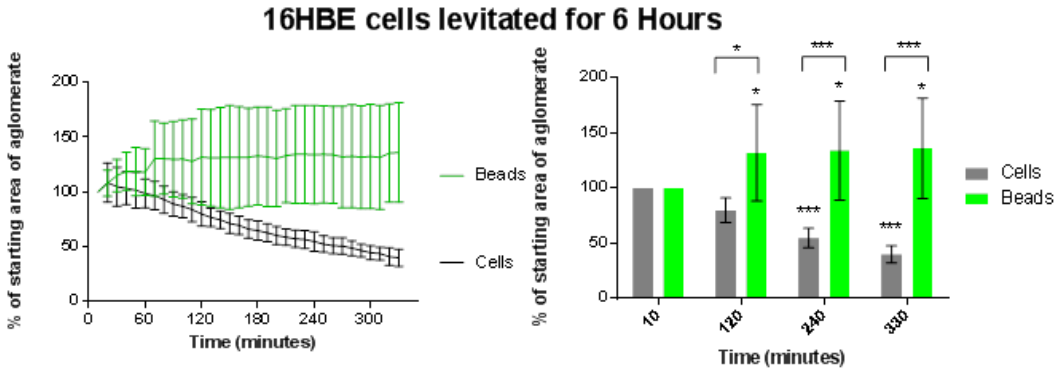

Figure 57 Contraction of the 16HBE cell aggregate during 6 hours levitation.
Statistical analysis using two-way Anova with Sidak's multiple comparison test showed a significant decrease in cell agglomerate size at 240 minutes and 330 minutes ($P<0.001$). There was a significant difference between cell agglomerate and bead agglomerate at 120 minutes ($P< 0.05$), 240 minutes and 330 minutes ($P<0.001$) n=5.

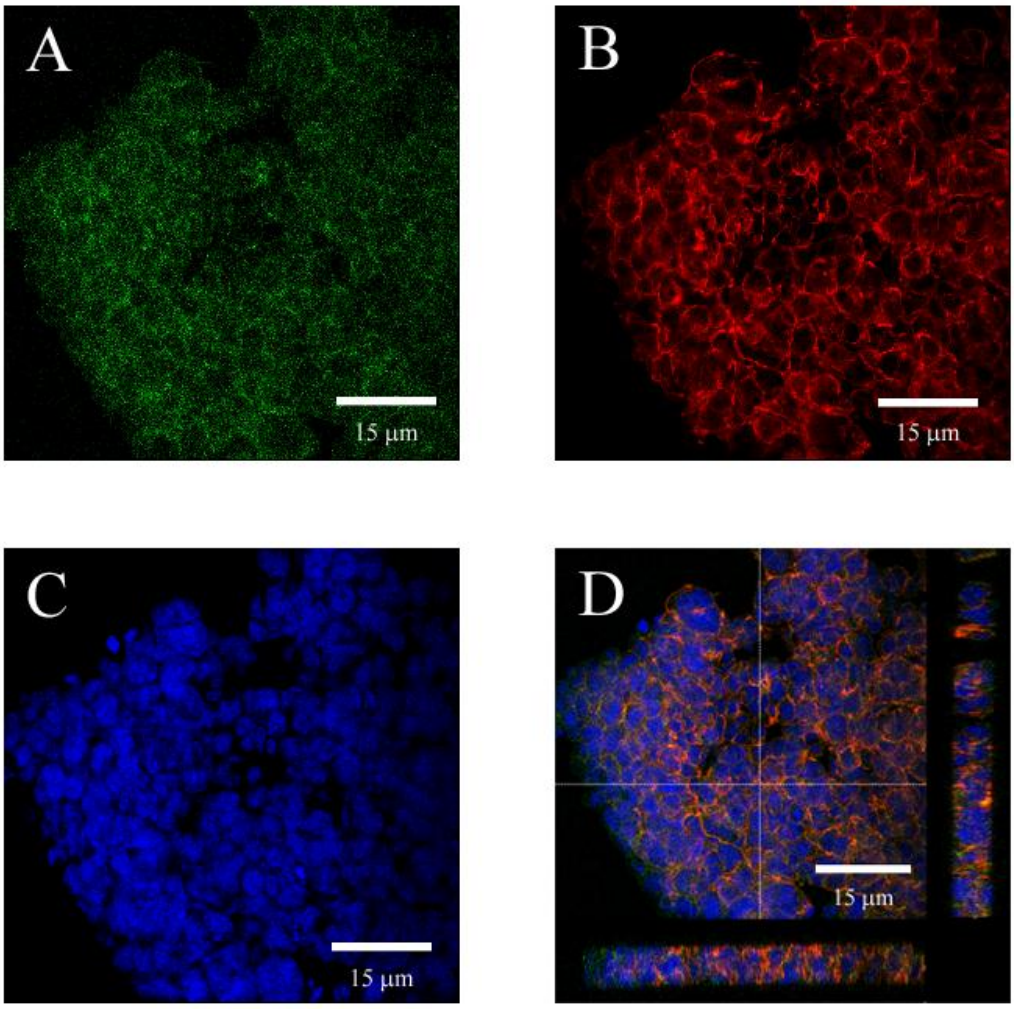

Figure 58 Immunofluorescent staining of cell aggregates levitated for 6 hours within the Sonotweezers device. A) Shows the E-cadherin staining, B) Shows the F-actin Staining, C) Shows the nuclei staining and D) Shows the overlay and Z-stack. The aggregates were fixed using acetone:methanol (1:1). The Images were taken using a confocal microscope, representative of 3 aggregates. The scale bar shows 15µm.

The nuclei were very compact (Figure 58 C) and the organisation was 3D as there was more than one layer of nuclei in the z stack (Figure 58 D). The cells had also become more compact and the staining of the F-actin formed a pericellular ring. The adherens junctions were still diffuse but were located at the cell-cell junctions.

The cell viability had significantly reduced with an increase in red 7AAD staining seen in the aggregates (Figure 59).

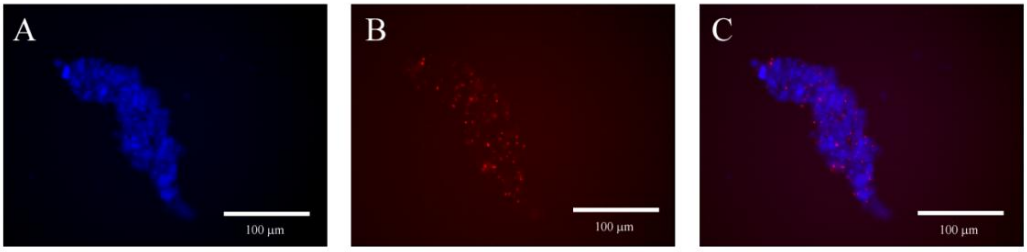

Figure 59 Cell viability of 16HBE cells levitated for 6 hours within the Sonotweezers device. 16HBE cells stained with cell tracker blue were levitated for 350 minutes before 7AAD was added for the final 10 Minutes of levitation. A) Shows the cell aggregate, B) Shows the cells stained with 7AAD and C) Shows an overlay of both channels. The scale bar shows 100µm.

4.2.5 16HBE cells levitated for 24 hours with and without calcium

The adherens junctions are calcium dependent; therefore removing the calcium from the medium should prevent their formation, allowing us to determine whether the contraction is caused by the formation of the junctions.

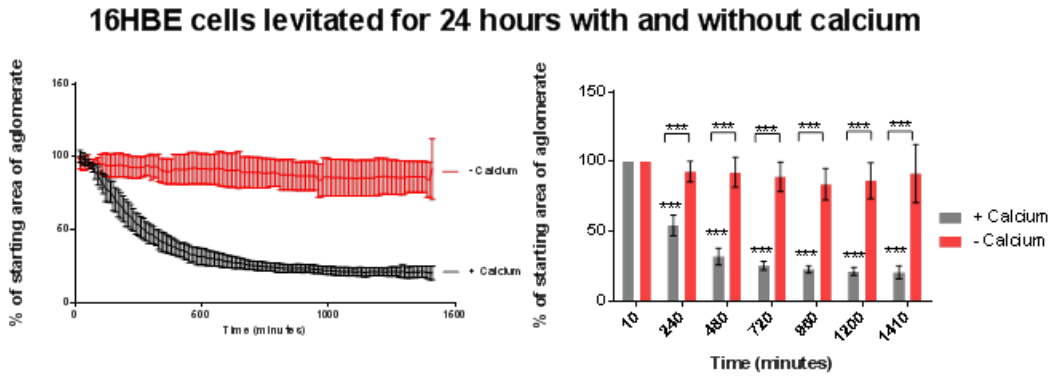

Figure 60 16HBE cells levitated within the Sonotweezers device for 24 hours with and without calcium. Statistical analysis using two-way Anova with Sidak's multiple comparison test showed a significant contraction when calcium is present at 240,480, 720,960,120 and 1410 minutes (P<0.001). However there was nosignificant contraction when calcium was removed when comparing the 1st and last aggregate areas. There was a significant difference between the cells with or without calcium at 240, 480, 720, 960, 1200 and 1410 minutes (P<0.001). n=3.

Blocking the formation of the adherens junctions by the removal of Ca^{2+} significantly blocked the contraction of the cells into the 3D agregate (Figure 60). This suggests that the formation of the adherens junctions and attachment of the actin filaments caused the contraction of the cells. Once the cells have been dropped, the compact agregate remained intact, however the cells without calcium did not maintain any structure (Figure 61).

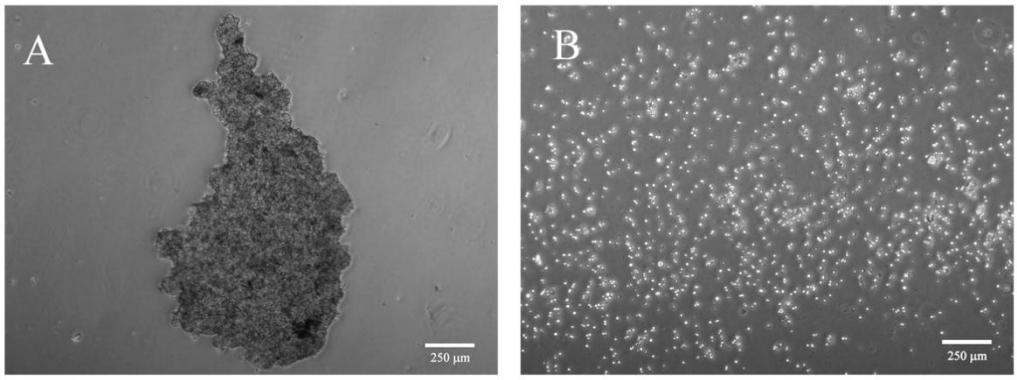

Figure 61 16HBE cells levitated for 24 hours with and without calcium after release from levitation. A) Shows the aggregate formed when calcium was present. B) Shows the cells after release from levitation when calcium was not present. Scale bar shows 250µm.

However there was a decrease in cell viability with or without the addition of calcium in the medium when the cells were levitated for 24 hours. The cells at the edge of the compact agregate had the the most 7AAD staining, however there was staining through out the whole agregate. This suggested that 24 hours was too long for the 16HBE cells to be levitated.

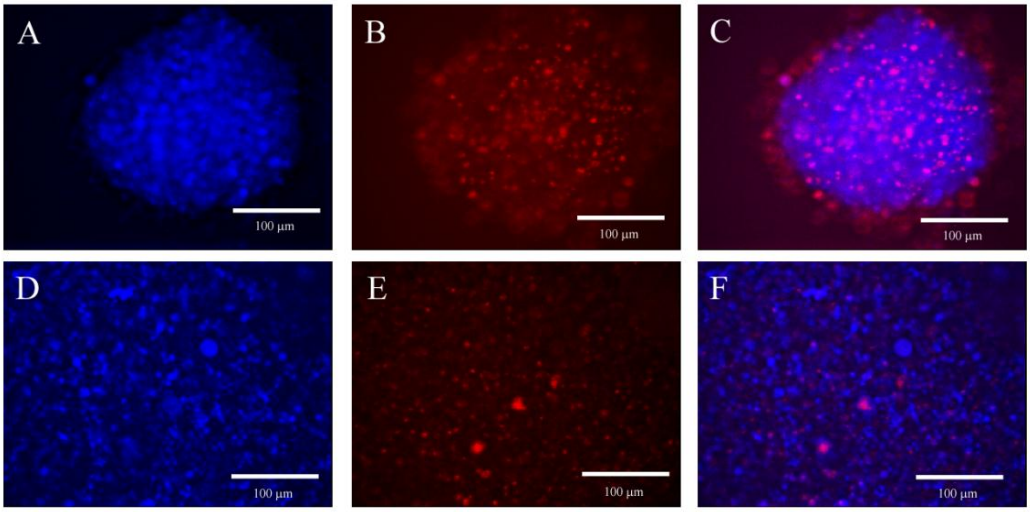

Figure 62 cell viability of 16HBE cells levitated within the Sonotweezers device with and without calcium for 24 hours. 16HBE cells stained with cell tracker blue were levitated for 1430 minutes before 7AAD was added for the final 10 Minutes of levitation. A, B and C show the cells with calcium and C, D and E show cells without calcium. A and D) show the cell aggregates, B and E) show the cells stained with 7AAD and C and F) show an overlay of both channels. The scale bar shows 100µm.

4.2.6 16HBE cells levitated for 6 hours with and without cytochalasin D

To determine whether the cellular contraction was a function of the actin cytoskeleton contracting once junctions were formed cytochalasin D (CD) was added to disrupt the

formation of the actin cytoskeleton. This would also allow us to keep the cells a sheet for a longer time period. Furthermore as the action of CD is reversible, sheets maintained with CD could be used for subsequent cell sheet engineering.

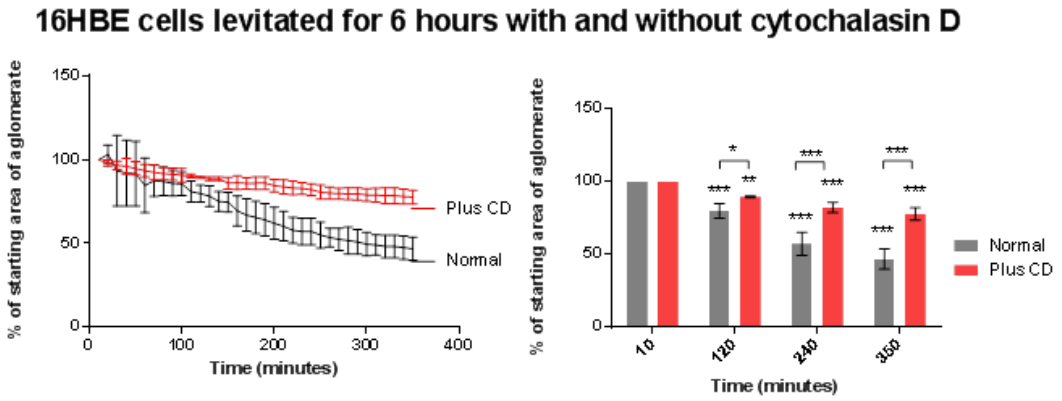

Figure 63 16HBE cells levitated for 6 hours with or without cytochalasin D (2µg/ml) aggregate area. Statistical analysis using two-way Anova with Sidak's multiple comparison test showed both with or without cytochalasin D the agglomerates significantly contracted ($P<0.001$). However there was a significant difference between the contraction of the agglomerate without cytochalasin D and the agglomerate formed with cytochalasin D ($P<0.001$). n=4.

The CD significantly decreased the contraction of the aggregate over 6 hour's levitation (Figure 63), suggesting that it is the assembly of the actin filaments causing the contraction of the aggregate.

The immunofluorescent staining of the captured aggregate levitated with CD shows disperse E-cadherin staining which has started to locate to the cell-cell junctions. The F-actin was diffuse and had not formed the pericellular ring seen in Figure 58, suggesting that the lack of contraction was due to the dysregulation of the actin cytoskeleton (Figure 64).

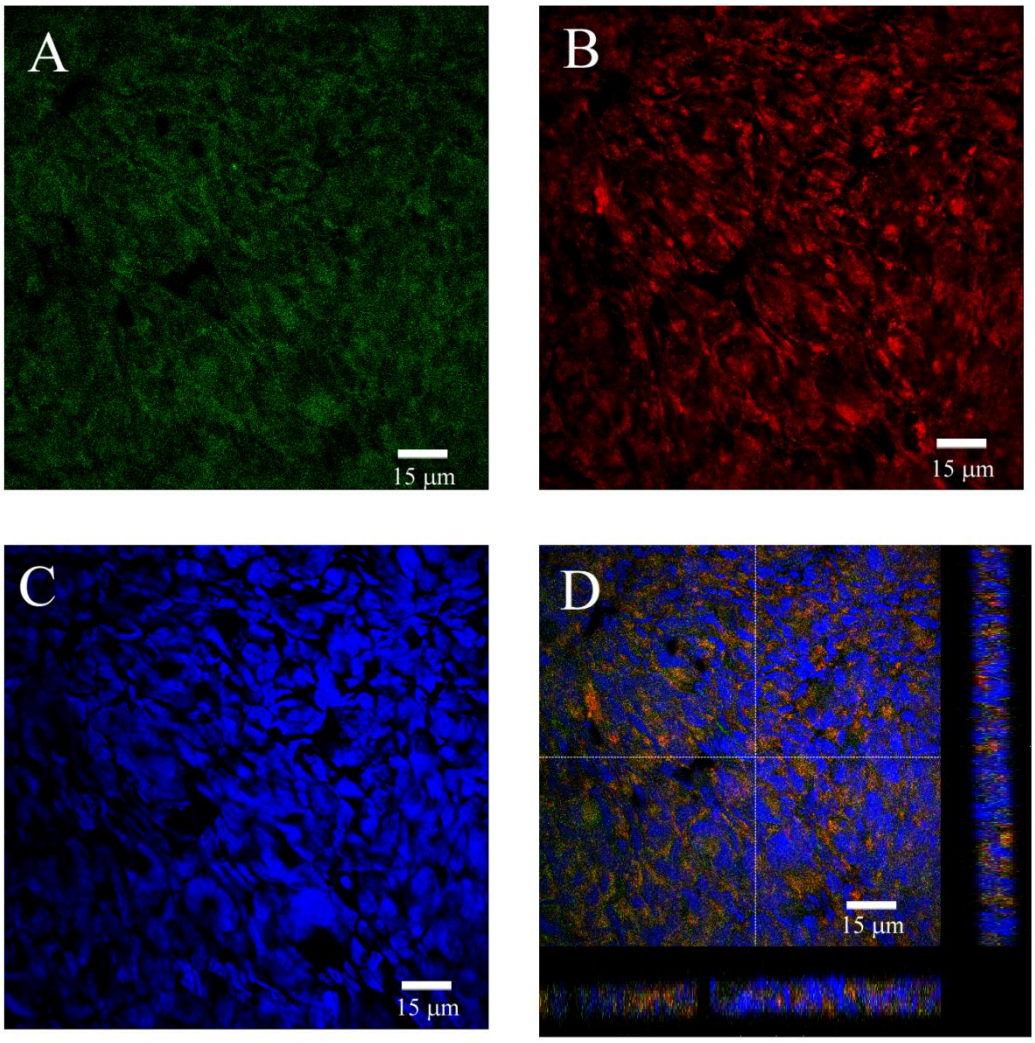

Figure 64 Immunofluorescent staining of cell aggregates levitated for 6 hours with Cytochalasin D within the Sonotweezers device. A) Shows the E-cadherin staining, B) Shows the F-actin Staining, C) Shows the nuclei staining and D) Shows the overlay and Z-stack. The aggregates were fixed using acetone:methanol (1:1). The Images were taken using a confocal microscope, representative of 3 aggregates. The scale bar shows 15µm.

However the viability of the cells was decreased over the 6 hours with the CD, therefore it was concluded that use of CD for 6 hours to keep the cells as a sheet was too long.

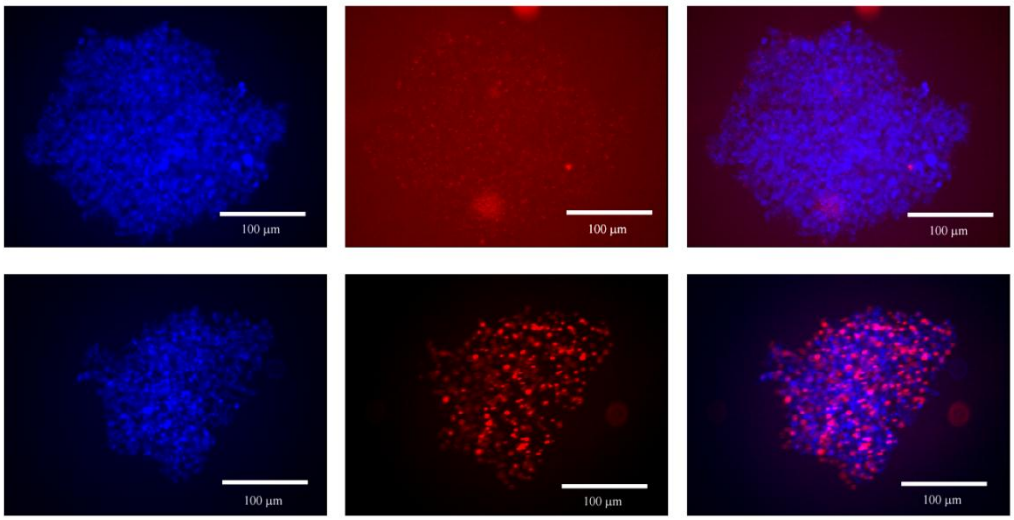

Figure 65 16HBE cell viability after been levitated for 6 hours with or without cytochalasin D.
16HBE cells stained with cell tracker blue were levitated for 350 minutes before 7AAD was added for the final 10 Minutes of levitation. A, B and C show the cells without CD and C, D and E show cells with CD. A and D) show the cell aggregates, B and E) show the cells stained with 7AAD and C and F) show an overlay of both channels. The scale bar shows 100µm.

4.2.7 16HBE cells levitated for 6 hours with and without an E-cadherin neutralising antibody

To confirm that the adherens junction contributed to the development of the contraction of the cell sheet, an E-cadherin neutralising antibody was added into the media during levitation.

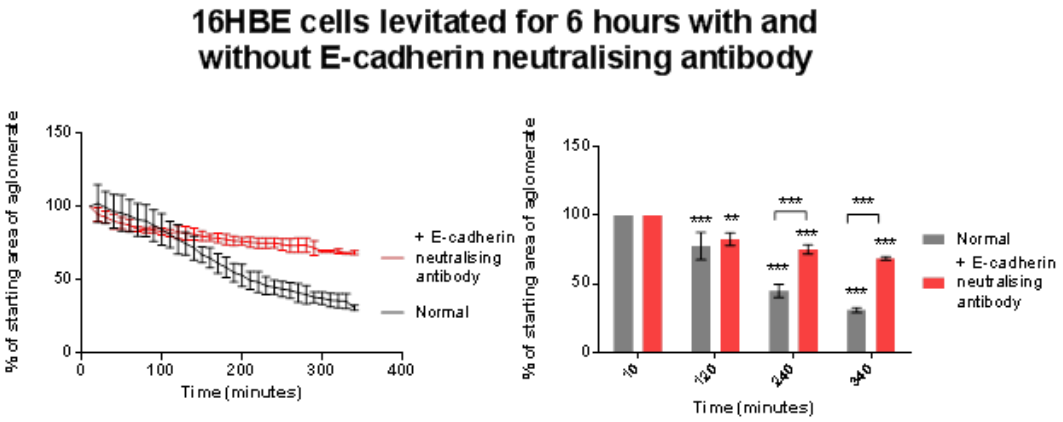

Figure 66 16HBE cells levitated for 6 hours with or without E-cadherin neutralising antibody.
Statistical analysis using two-way Anova with Sidak's multiple comparison test showed that there was significant contraction of both agglomerates ($P<0.001$). However there was a significant difference between the two agglomerated at 240 and 340 minutes ($P<0.001$). n=3.

After levitation for 6 hours the cellular contraction was significantly decreased when the adherens junctions formation was prevented by the neutralising antibody to E-cadherin (Figure 66).

Furthermore the aggregate disintegrated when released from levitation as no cell-cell junctions were formed (Figure 67).

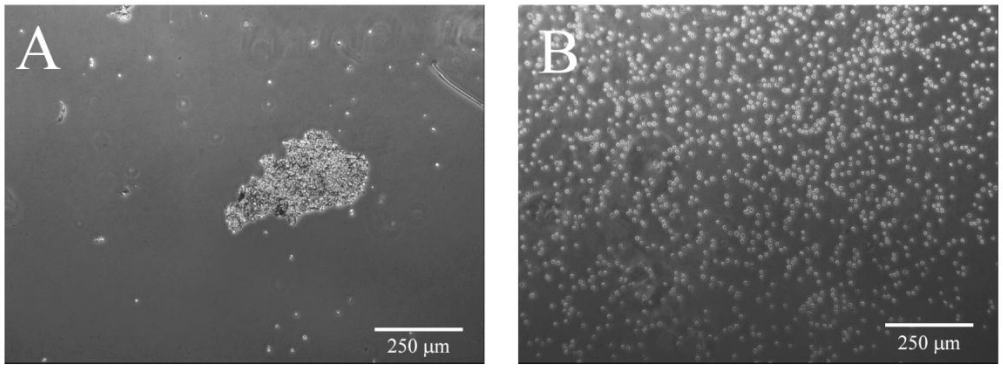

Figure 67 cells after dropped with and without E-cadherin neutralising antibody
A) shows 16HBE cells levitated within the device for 6 hours without the antibody, B) shows 16HBE cells levitated for 6 hours with the addition of the antibody. Scale bar shows 250µm.

Consistent with what we have seen in other levitation experiments, the cells have started to lose viability when levitated for 6 hours (Figure 68).

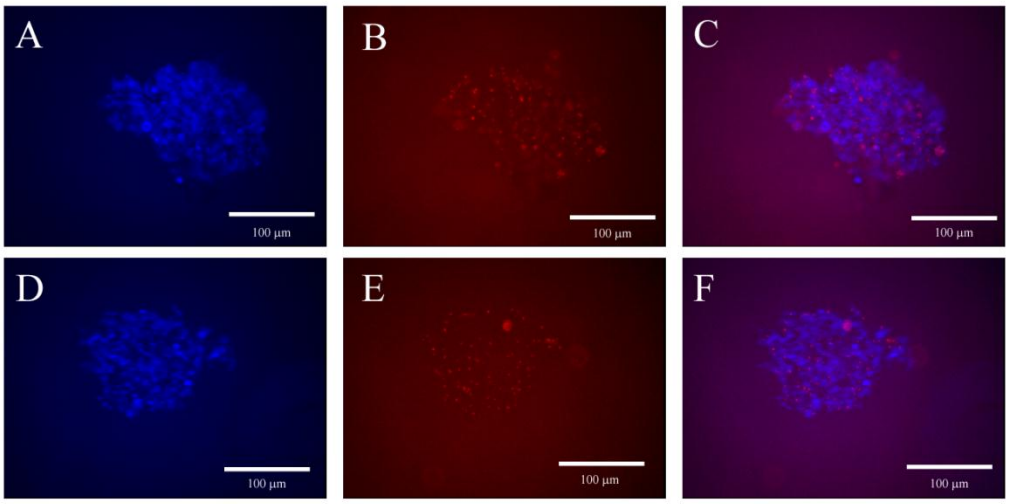

Figure 68 16HBE cell viability when levitated in the Sonotweezers device with or without an E-cadherin neutralising antibody. 16HBE cells stained with cell tracker blue were levitated for 350 minutes before 7AAD was added for the final 10 Minutes of levitation. A, B and C show the cells without the E-cadherin neutralising antibody and C, D and E show cells with the E-cadherin neutralising antibody. A and D) show the cell aggregates, B and E) show the cells stained with 7AAD and C and F) show an overlay of both channels. The scale bar shows 100µm.

4.3 Co-culture using the levitated cell sheet

From our results we have shown that 16HBE cells levitated for 2 hours form adherens junctions but remain as a monolayer. To determine whether a multi-layered cell culture model could be created, the 16HBE cell sheet formed within the device after two hours was placed onto a confluent layer of MRC5 cells within a transwell.

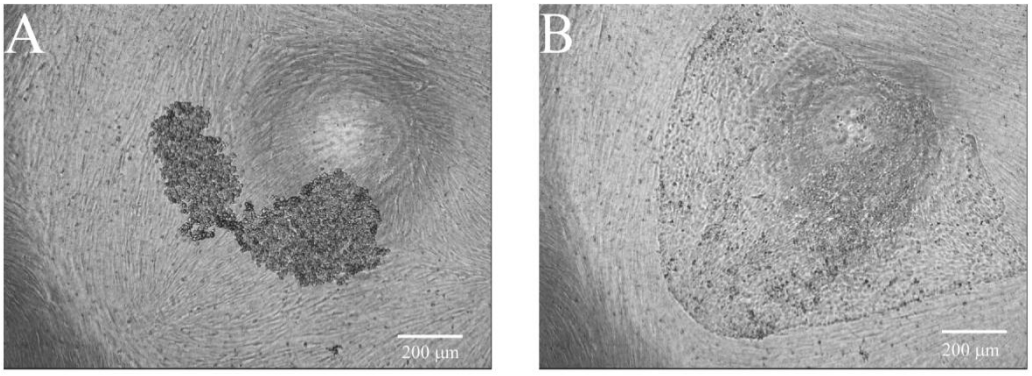

Figure 69 Aggregate created in the Sonotweezers device on a confluent MRC5 layer.
16HBE cells were levitated for 2 hours before being captured and placed on to a confluent layer of MRC5 cells (A). These were allowed to grow for 3 days (B); the 16HBE cell layer grew across the top of the confluent MRC5 layer. Scale bar shows 200µm.

The 16HBE cell aggregate moves out across the MRC5 cell layer, moving as a sheet of cells rather than as individuals (Figure 69). To determine whether the CMRA orange stained MRC5 layer was still beneath the layer GFP 16HBE cell layer the transwell was fixed and imaged using the confocal microscope (Figure 70). The z-stack shows that the red MRC5 are underneath the green 16HBE cells without any disruption to their cell layer.

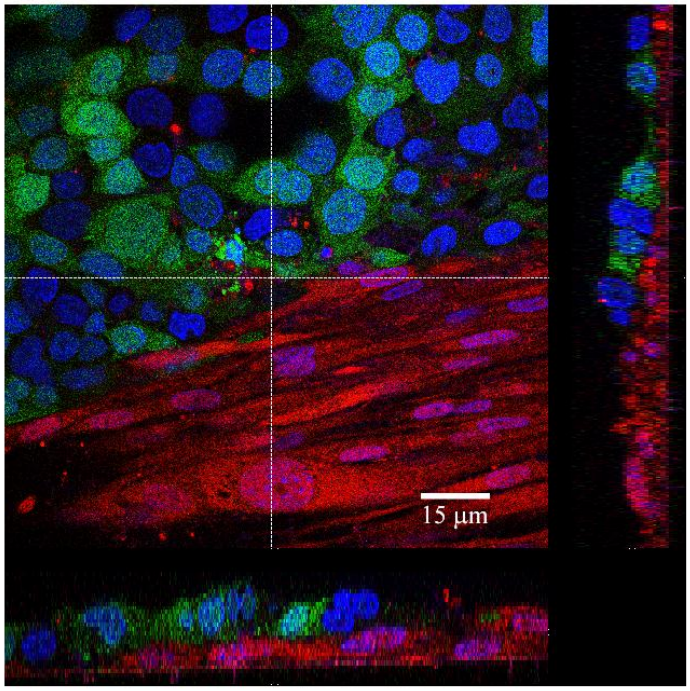

Figure 70 Co-culture created using a 16HBE cell aggregate formed within the Sonotweezers device placed onto a confluent layer of MRC5 cells within a transwell. GFP 16HBE cells were levitated for 2 hours within the Sonotweezers device. They were then captured and placed onto a confluent layer of CMRA orange stained MRC5 cells. These were grown for 3 days before being fixed using acetone:methanol (1:1). Image taken using a confocal microscope, representative of 2 co-cultures. Scale bar shows 15µm.

4.4 Discussion

This chapter attempted to determine whether 16HBE would create a cohesive sheet within the Sonotweezers device and whether these cell sheets could be used to create a multi-layered cell culture model.

Initially the cells were levitated for 5 days to allow tight junctions to form. The 16HBE cells formed a 2D aggregate within 30 seconds consistent with the literature. To the best of our knowledge there were no other epithelial cell lines levitated over 5 days, as the majority of experiments lasted only 1 hour (Bazou et al., 2006a). However during that time the cells lost the desired monolayer configuration and formed 3D aggregates. These 3D aggregates appeared to be similar to spheroids formed by other methods. Liu *et al* compared HepG2 aggregates created in the ultrasound trap with spheroids created in a classical way (Liu et al., 2007). The aggregates were levitated for 30 minutes before being placed into a suspension dish for 3 weeks. The control spheroids were formed by the gyrotatory-mediated method. The ultrasound method gave increased cell proliferation during the 1st 3 hours plateauing between 3 and 21 days. It also gave a slight increase in albumin secretion and a slight increase in P450-1A1 activity. This suggests that there were no detrimental effects of forming the spheroid in the ultrasound standing wave. Spheroids

of bronchial epithelial cells have been investigated as a 3D model. Wu *et al* investigated the differentiation of PBECs into glandular acini (the mucous gland located within the submucosa) by growing PBECs on matrigel to produce spheroids (Wu et al., 2012). Gamarra *et al* investigated cilliary beat frequency; they formed spheroids with the cilia on the outside. Current research on spheroids shows that they can be made with the inside being either the apical or basal side of the cells. The orientation of the cells within the spheroid formed in the device is not yet known. The method which forms the apical side of the cell in the lumen is growth on top of matrigel which provides matrix contact to the basal cells. Growing cells in an environment where the cells don't want to adhere to the surface orientates them with the apical side out. However spheroids were not what was needed for the current model being investigated.

To assess the switch from a sheet to a 3D spheroid, the levitation time was varied and formation of the adherens junctions was measured. Wallace *et al* showed that 16HBE cells fully formed their adherens junctions after 6 hours when grown on glass (Wallace et al., 2010) consistent with our controls. They grew their cells for 3 days before disrupting the junctions by removing calcium whereas in the current work cells were seeded at confluent density and left to adhere overnight. The pattern of the cell staining was similar with the E-cadherin appearing at the site of cell-cell contact after 2 hours and by 6 hours the junctions being fully formed. Bazou *et al* found that after one hour levitated prostate epithelial cells started to form their adherens junctions (Bazou et al., 2006a). In the current study after 1 hour levitation the 16HBE cells had not started to form their adherens junctions, however after 2 hours levitation the 16HBE cells remained sheet like and the adherens junctions had started to form. After 2 hours slight contraction had started to occur suggesting that it was the formation of the junctions and the associated actin filaments which caused the contraction that eventually lead to spheroid formation.

Cell viability within ultrasound devices have been investigated by many methods. When investigating single H9c2 cells within an ultrasound standing wave the viability was found to be unaffected between 0-15VPP (Ankrett et al., 2013), our device was run at 4VPP so falls nicely into the safe voltage range. However in the current work the cells were levitated for a longer time period and were allowed to form an aggregate. Many studies have used live dead stains during 12 hours levitation of the B cell line 721.221/HLA-Cw6 the presence of the live stain calcein AM and an intact membrane was monitored, and the viability was not reduced (Vanherberghen et al., 2010). These are non-adherent cells so

will not be influenced by the lack of contacts to a substrate. In the adherent COS-7 cell line the viability was also investigate using the live stain Calcein Am. The cells were levitated for up to 75 minutes, with no loss of viability (Hultstrom et al., 2007). Although the cells were only levitated for a short time period, the data was in line with our results. The dead stain used is generally trypan blue which only enters cells where the membrane is disrupted (Bazou et al., 2008). We used a dead stain but instead of trypan blue, 7AAD was used. This only enters cells where the membrane is disrupted, this could be visualised alongside the cell tracker blue added for visualisation allowing better images.

Reducing the calcium within the medium was used to block the formation of the calcium dependent adherens junctions. The reduction in contraction observed without calcium suggests that the contraction is dependent on the formation of the junctions. Consistent with our findings Brophy *et al* showed that hepatocyte spheroids do not form in calcium free medium and the unattached cells died within 24 hours (Brophy et al., 2009). In epithelial cancer cells it is thought that the adherens junctions are important for the aggregate formation which can invade neighbouring tissue (Kantak and Kramer, 1998).

The actin cytoskeleton binds to the adherens junctions forming tension throughout the cell sheet. To determine whether it was the assembly of the F-actin cytoskeleton attached to the adherens junctions which was pulling the cells into a 3D aggregate cytochalasin D (CD) was added. Cytochalasins are fungal metabolites (zygosporium masonii) that interfere with the assembly of F (filamentous) actin from G (globular) actin monomers (Brown and Spudich, 1981). The addition of CD has been shown to stop the formation of rat hepatocyte spheroids (Tzanakakis et al., 2001). Consistent with this when CD was added to the levitating cells sheets it also blocked the cellular contraction. This suggests that the contraction of our cell aggregates is similar to classical spheroids formation. Blocking the contraction with CD did not block the formation of the adherens junctions allowing collection of the sheet. Wei *et al* investigate the contraction of a sheet of MDCK cells released form a tissue culture dish using dispase. They found that the addition of CD reduced the contraction (Wei et al., 2013). It was noted that this did not completely block all contraction of the cell sheet. The current work is consistent with this as even with the addition of CD there was significant contraction of the cell aggregate. This is likely to be caused by the contraction of the intermediated filaments and the microtubules. Wei *et al* also found that blocking microtubules and intermediate filaments also blocked some contraction, suggesting that all the aspects of the cytoskeleton are involved in the contract.

Gipson *et al* showed reversibility of the effects of CD when investigating the blocking of migration of corneal epithelial cells in excised rat corneas with abrasions on them, removing the CD containing medium and replacing it with fresh medium allowed the wound to heal (Gipson et al., 1982). Therefore cell sheets can be maintained within the Sonotweezers device for longer without contracting before being removed and placed onto the next cell type.

E-cadherin neutralising antibody was used to block the formation of the adherens junctions, Kantak *et al* had used the same antibody to block adherens junction formation in aggregated suspension cultures of HSC-3 human carcinoma cells (Kantak and Kramer, 1998). They found that blocking the cell-cell junctions for 72 hours caused the cells to undergo apoptosis. In keeping with this the current results show a lack of cell-cell contacts and increase in cell death after levitation with the E-cadherin neutralising antibody over 6 hours. The actin cytoskeleton binds to the formed adherens junctions, therefore without the formation of the junctions we speculate that the cytoskeleton will not fully form. This will stop the cellular contraction of the levitated agglomerate. There is still some contraction seen, this however is likely to be due to the packing of the nuclei into the most efficient conformation.

Having discovered that after 2 hours levitation a coherent cell sheet could be formed and captured, this was used to create a co-culture. A sheet of cells moves differently to single cells. They have a collective motion known as plithotaxis (Trepat and Fredberg, 2011), the sheet moves as one. This is the motion seen in wound healing assays, where the edges of the wound move together covering the exposed area (Kurten et al., 2004). This movement relies on various forces within the sheet of cells acting on different cells within the sheet. It is this collective motion that we suggest allowed the preformed epithelial cell sheet to grow across the confluent fibroblast layer and remain as two defined layers.

In summary 16HBE cells will form a 3D aggregate similar to a spheroid over 5 days. However after just 2 hours levitation they form adherens junctions but have not yet reorganised their actin cytoskeleton so have not contracted allowing transfer to another cell layer forming a multi-layered cell culture model. The period of cell sheet formation can be extended by the addition of CD. The addition of an epithelial cell sheet onto a confluent fibroblast cell layer will maintain two distinct cell tiers as the epithelial cells grown across the surface of the fibroblasts.

5. Thermoresponsive polymers

This chapter investigates the use of novel thermoresponsive polymers and their biocompatibility.

The NiPAAm polymers used in this study were synthesized by Andrew Treharne, and the oxazoline polymers were synthesized and chemically characterised by Tom Hartland and Adam Fisher, School of Chemistry, University of Southampton.

16HBE cells have been shown to adhere to, proliferate on and be released from grafted NiPAAm polymers on commercially sourced tissue culture dishes (UpCell) allowing for the creation of a cell sheet engineered model of the airway mucosa to be investigated. This model would comprise of a layer of bronchial epithelial cells on top of a layer of bronchial fibroblasts to allow direct contact of the cell types as seen within the airways. PBECs when grown at ALI on transwells will differentiate into psuedostratified epithelium. Initial experiments will use undifferentiated bronchial epithelial cell lines which can be grown on tissue culture plastic, however as the model progresses transwells coated in a thermoresponsive polymer for the growth of PBECs at ALI will be required. As this format is not currently commercially available, two different types of polymer where synthesised and tested for their potential use for bronchial epithelial culture. The first was a NiPAAm based polymer created by free radical polymerisation initiated by AIBN (Azobisisobutyronitrile). This was a co-polymer of Poly(*n*-isopropyl acrylamide-co-methyl methacrylate-poly(ethylene glycol) methacrylate) (NiPAAm -co-MMA-co-PEGM) with a ratio of 70:10:20. MMA is hydrophobic and lowers the LCST of NiPAAm based polymers. Varghese *et al* showed that a co-polymer of MMA-NiPAAm did not lose its ability for L929 fibroblast cells to adhere to and proliferate on it (Varghese et al., 2010). PEG when part of a co-polymer with NiPAAm has previously been shown to accelerate the polymer transition from compact to hydrated (Kaneko et al., 1998) without changing the LCST (Yoshioka et al., 1994), it is also nontoxic and non-immunogenic (Zhang et al., 1998). Previous work in our laboratory using a 70:10:20 NiPAAm polymer has been shown to allow cell adhesion and detachment (unpublished data). In the current study the polymer was used as a coating rather than being covalently attached to the tissue culture surface as with the UpCell surface.

Another range of polymers, Poly(2-alkyl-2-oxazolines) were also tested. These have been shown to possess thermoresponsive properties. Oxazolines are formed by the living cationic ring-opening polymerization of 2 oxazoline monomers (Figure 71).

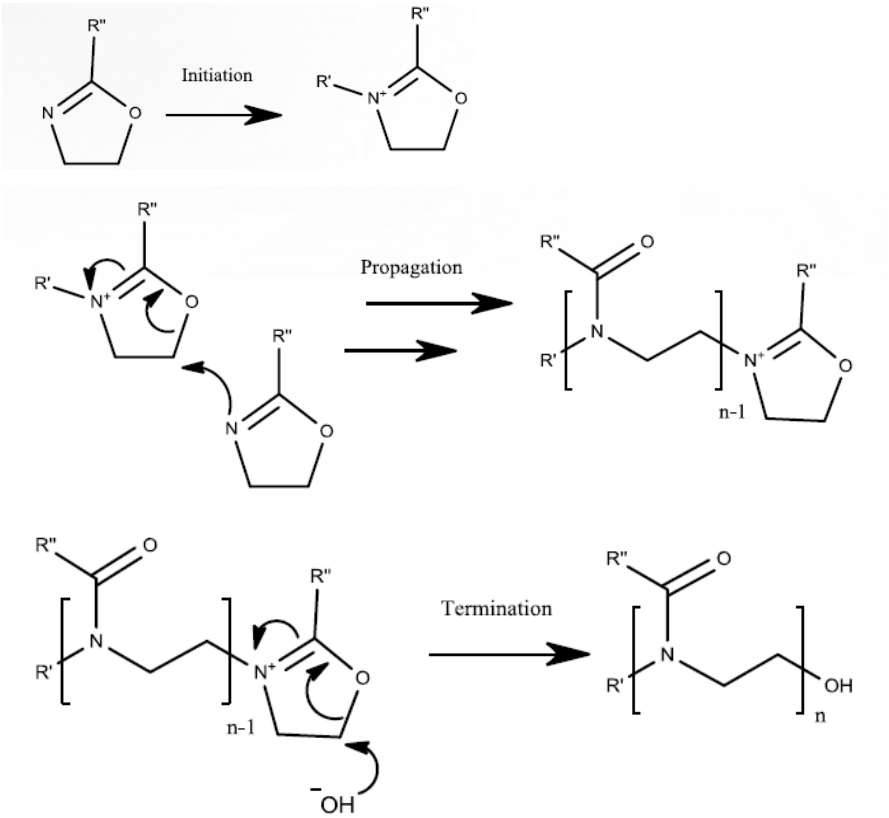

Figure 71 Schematic of the mechanism for the polymer creation.
The cationic ring opening polymerisation means that monomers are added sequentially giving a defined polymer chain length. (Adam Fisher)

The monomers are sequentially added enabling a defined chain length to be created, with a lower polydispersity index (PDI) than NiPAAm, resulting in a more reproducible polymer length. The polydispersity index is a measure of the variation in chain lengths created during polymerisation, the lower the value the less variation within the polymer.

Modification of the 2-position of the oxazoline ring can change the properties of the polymer created, such as the LCST (Christova et al., 2003). Lin *et al* were the first to report that poly(2-ethyl-2-oxazoline) (PEtOx) was thermoresponsive (Lin et al., 1988). It took 4 years from this initial discovery to develop a polymer with an LCST within the physiological range. This was poly(2-isopropyl-2-oxazoline) (P*i*PrOx) which has an LCST within the range 36°C-39°C (Uyama and Kobayashi, 1992) and is a structural isomer of NiPAAm (Aoshima and Kanaoka, 2008). The sensitivity of the phase transition of P*i*PrOx

was found to be more pronounced than that of NiPAAm (Hoogenboom, 2009), due to its lower PDI.

The polymer coatings that were created were a pure *i*PrOx polymer and a co-polymer comprised of P*i*PrOx and Bis*i*PrOx (Bis-isopropyl-oxazoline). The addition of Bis*i*PrOx introduces cross linkages with the aim of forming a more viscous coating.

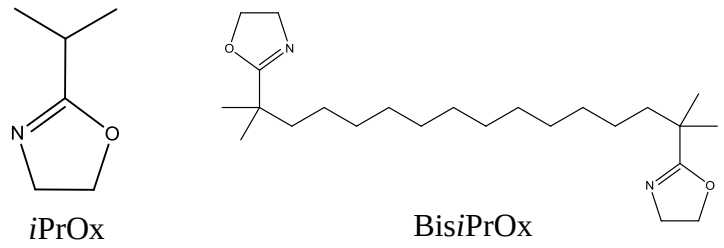

*i*PrOx Bis*i*PrOx

Figure 72 Schematic of *i*PrOx and Bis*i*PrOx.

Although there is an opportunity to utilise the LCST for cell sheet engineering there are only a handful of papers investigating cell behaviour on oxazolines. It has been shown that the attachment of Poly(2-ethyl-2-oxazoline) (PEtOx) to glass, allows the growth of HUVECs (human umbilical vein endothelial cells), and primary rat and sheep fibrocytes (Chang et al., 2002). HUVECs can adhere and spread on fibronectin coated PEtOx and poly(2-methyl-2-oxazoline) (PMeOx) attached to glass (Zhang et al., 2012). PEtOx has an LCST between 62°C and 65°C (Christova et al., 2003) therefore it would be in its hydrated hydrophilic state at physiological temperatures. Dworak *et al* showed that primary human dermal fibroblasts can adhere to, proliferate on and detach from P*i*PrOx and poly[(2-ethyl-2-oxazoline)-co-(2-nonyl-2-oxazoline)] covalently attached to glass (Dworak et al., 2014). They showed increased cell adhesion on P*i*PrOx polymer compared to tissue culture plastic, and found no detrimental effects of the two polymers on gene expression. Very little else is known about the biocompatibility of related polymers, in particular for the growth of cells.

Therefore the aim of this chapter was to determine the biocompatibility of these novel polymers.

5.1 Thermoresponsive polymers: NiPAAm based polymer NiPAAm-co-MMA-co-PEGM 70:10:20

The 70:10:20 NiPAAm co-polymer dissolved in isopropanol (IPA) was deposited at 1.3 mg/cm^2 on to tissue culture dishes by evaporation of the solvent. The cells adhered to and grew on the polymer without any change to their morphology compared to a tissue culture plastic control, when viewed using a phase microscope (Figure 73A and B). However after incubation at 20°C and flushing with a 1ml pipette, only a small area of cells was released (Figure 73 C). This was observed for both 16HBE (n=8) and HeLa (n=5) cell types. The pipette was used instead of the membrane because it was easier to determine cell release, when the sheet was not being transferred to another dish.

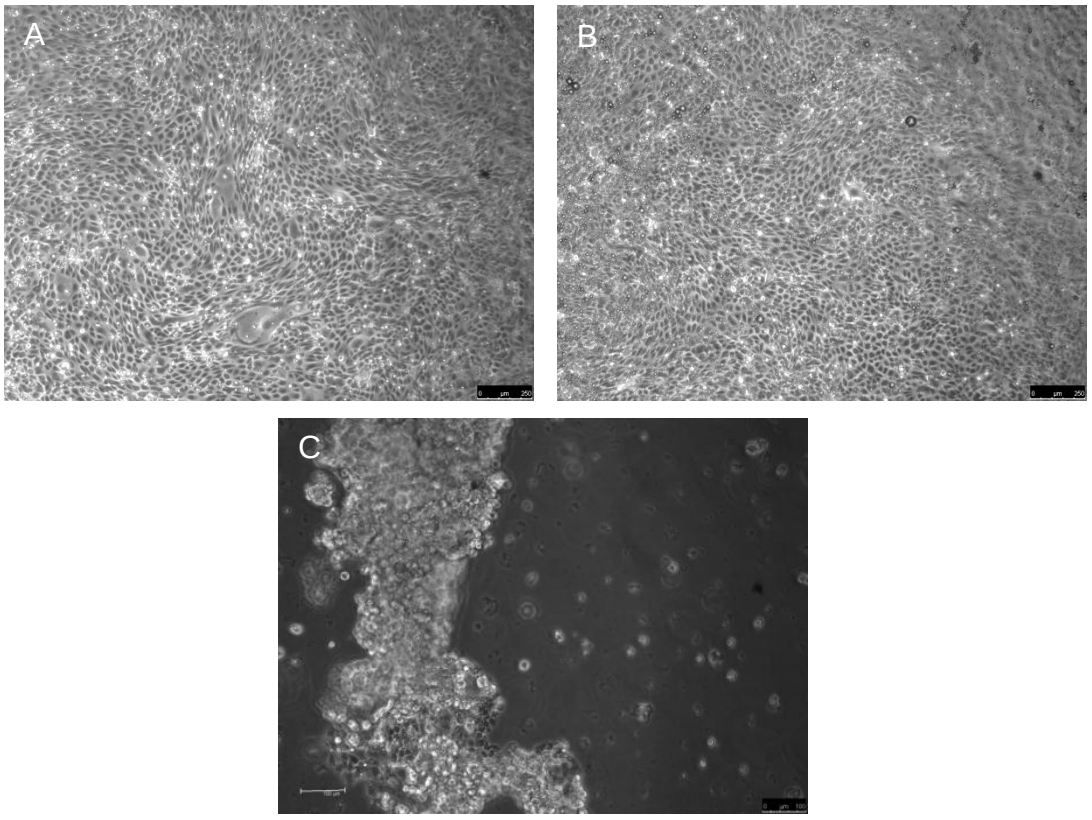

Figure 73 adherence and release of 16HBE cells from 70:10:20 NiPAAm co-polymer.
A) Shows 16HBE cells grown on 70:10:20 NiPAAm co-polymer coated tissue culture plastic. B) Shows 16HBE cells on collagen coated tissue culture plastic. C) Shows a small cell sheet released after incubation at 20°C for 45 minutes and flushing with a 1ml pipette. Scale bar 250µm.

As was demonstrated in the previous chapter 16HBE cells can be released from a NiPAAm polymer (Figure 35), therefore it was investigated whether the polymer was remaining *in situ*. When cells were added to the polymer coated well, it was noted that occasionally the medium became cloudy, at the end of the experiment white particulates were observed in

the medium and during microscopy balls of polymer were seen above the cells even though all liquids were above the LCST of the polymers, suggesting that the polymer was not remaining on the surface of the well (Figure 74).

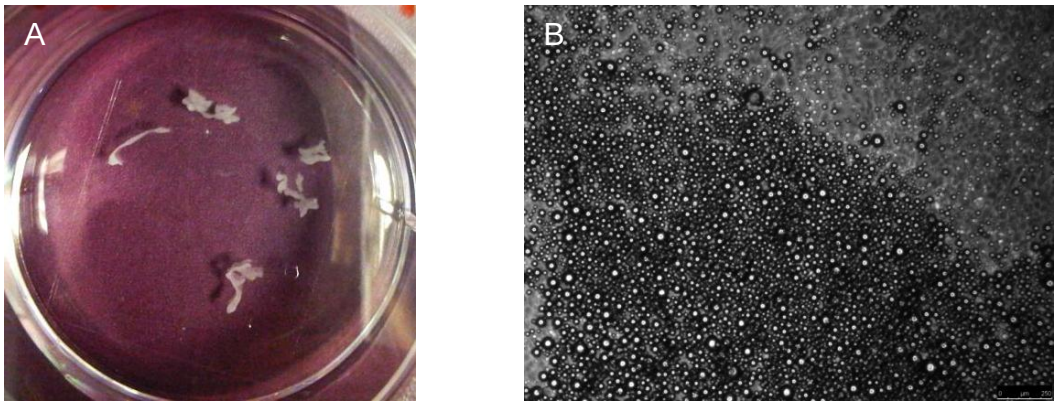

Figure 74 Aggregates and balls of polymer indicates that it is not remaining on the base of the well. A) Shows aggregated polymer in 37°C medium. B) Shows balls of polymer above a 16HBE cell sheet.

To test this possibility a 30µl droplet of polymer giving coverage of 1.3 mg/cm^2 was deposited on to a tissue culture well. This droplet did not fill the well, enabling focus on an edge to determine whether the polymer remained *in situ*. The addition of medium at 37°C was recorded using time lapse microscopy. The resulting images determined that the polymer aggregated together over time (Figure 75). This suggested that the polymer was easily hydrated, so when liquid was present the hydrophobic groups came together as there was nothing anchoring the polymers to the surface.

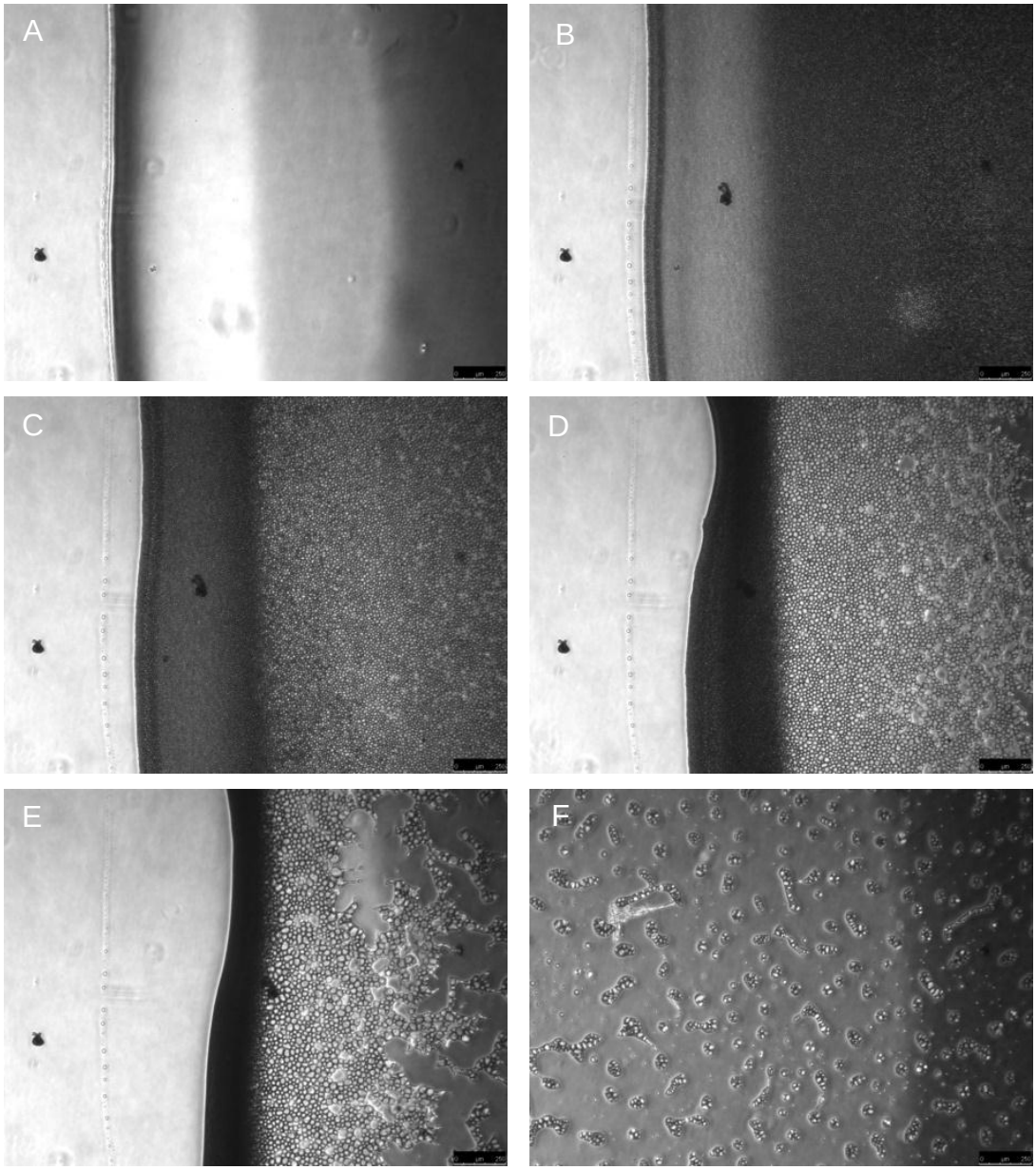

Figure 75 Time lapse images of the 70:10:20 NiPAAm co-polymer as 37°C medium was added.
A) Shows the edge of the polymer droplet when medium was initially added. B, C, D and E show the progression of the aggregation of the polymer during the 5 minute time-lapse. The edge moves closer to the centre of the image and the polymer in the centre aggregates together. F) Shows an image taken of the centre of the droplet after the 5 minute time-lapse has finished. The scale bar shows 250µM.

Four batches of 70:10:20 co-polymer were created, each batch aggregated differently (Figure 76). This is probably because the 70:10:20 NiPAAm co-polymer was formed via free radical polymerisation; this is an uncontrolled method, giving a high Polydispersity index (PDI). The resulting polymers may therefore vary in chain length, resulting in variable properties. Consequently it was decided to discontinue their use.

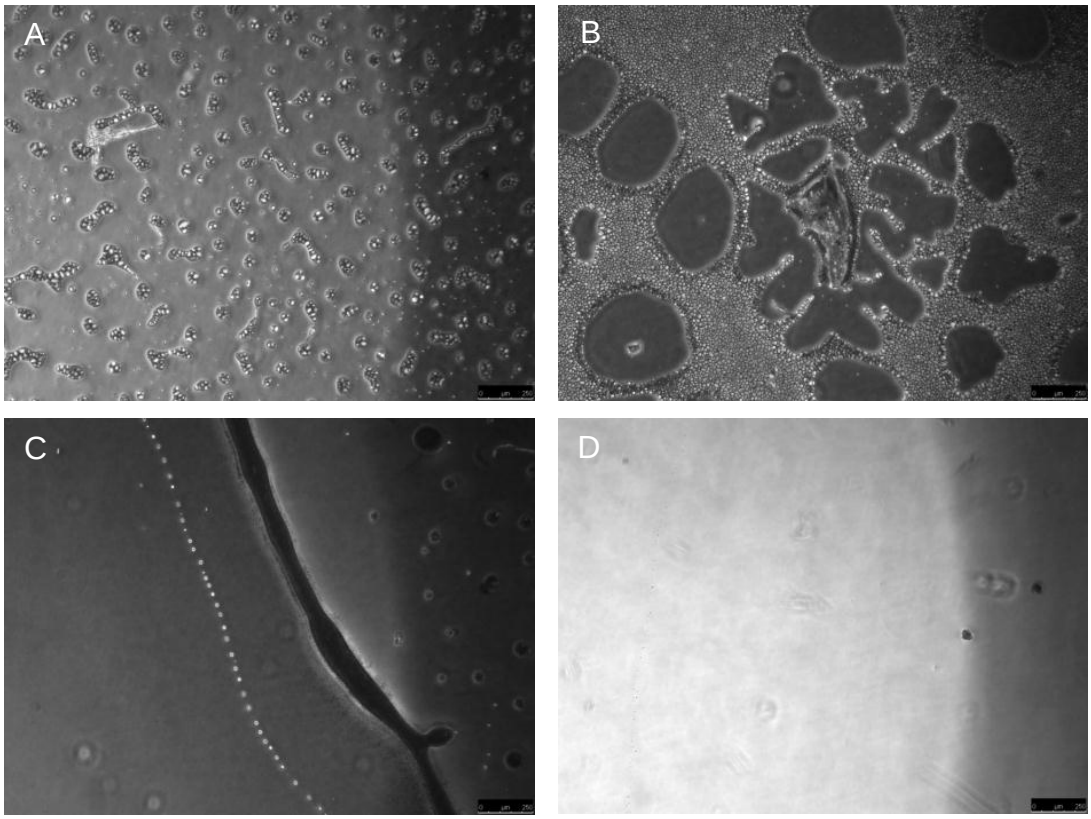

Figure 76 Batch variations of 70:10:20 NiPAAm co-polymer after 37°C medium was added.
A) Shows batch 1; this was previously used by a colleague (unpublished data). B) Shows batch 2 which was used for the majority of experiments, it gave patchy release of the 16HBE cells. C and D are batches 3 and 4, these were created to test the reproducibility of the polymer. Scale bar is 250µM.

5.2 Thermoresponsive polymers: Oxazolines

5.2.1 P*i*PrOx Polymer coatings

To avoid the PDI issues seen with the NiPAAm based polymers a polymer of P*i*PrOx was created. The first P*i*PrOx polymers produced were dissolved in isopropanol (IPA) and deposited onto the tissue culture plastic as the solvent evaporated, thus replicating the NiPAAm based polymer, with a view to using them to coat both tissue culture wells and transwells. These were shown to be thermoresponsive in PBS; at 20°C the polymer

dissolved giving a clear solution and whereas at 37°C the polymer precipitated out giving a turbid solution (Figure 77).

Figure 77 Demonstration of the thermoresponsive nature of P*i*PrOx.
A) shows P*i*PrOx with 300 repeating units dissolved PBS at 20°C.B) shows the same polymer at 37°C.

To determine the PDI, the polymer underwent Maldi-TOF (matrix-assisted laser desorption/ionisation time of flight) mass spectrometry. This allowed the determination of several parameters such as the number average molecular weight ($\boldsymbol{M_n}$) and the weight average molecular weight ($\boldsymbol{M_w}$). From these the PDI can be calculated. For P*i*PrOx this was found to be 1.06. The lower the PDI the more uniform the chain lengths are, for P*i*PrOx this was very low. The Maldi-TOF spectrum along with the PDI calculation can be found in the appendix.

The LCST was measured using a UV/VIS spectrometer equipped with a heating bath. The LCST was measured by noting the temperature where a sudden drop in transmission occurred (Figure 78).

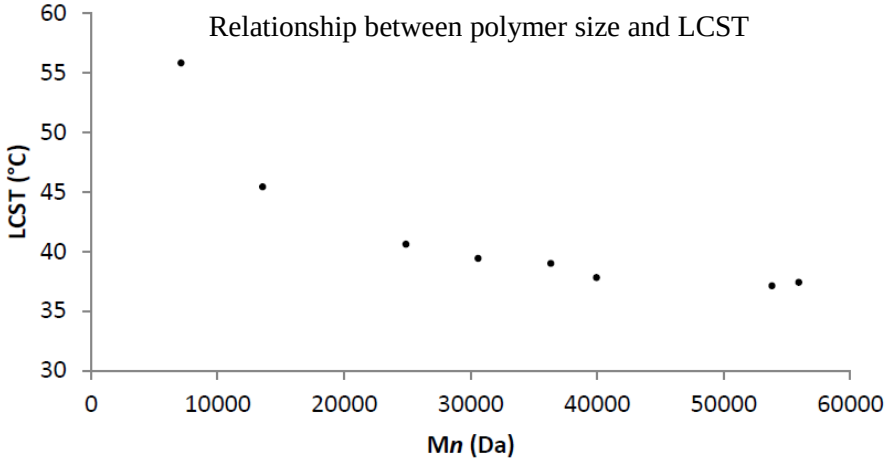

Figure 78 Relationship between LCST and molecular weight of P*i*PrOx.
The LCST was measured using a UV/VIS spectrometer equipped with a heating bath. The LCST was measured by noting the temperature where there was a sudden drop in transmission. This experiment was carried out by Adam Fisher.

There was a trend of LCST being dependent on the molecular weight, as the molecular weight increases the LCST appears to be less sensitive to the changes. Therefore a polymer of 200 repeating units (24888Mn) was used.

These oxazoline polymers were investigated to determine whether they aggregated when medium at 37°C was added. As with the PNiPAAm based polymer (Figure 75), the pure P*i*PrOx polymers also aggregated together (Figure 79).

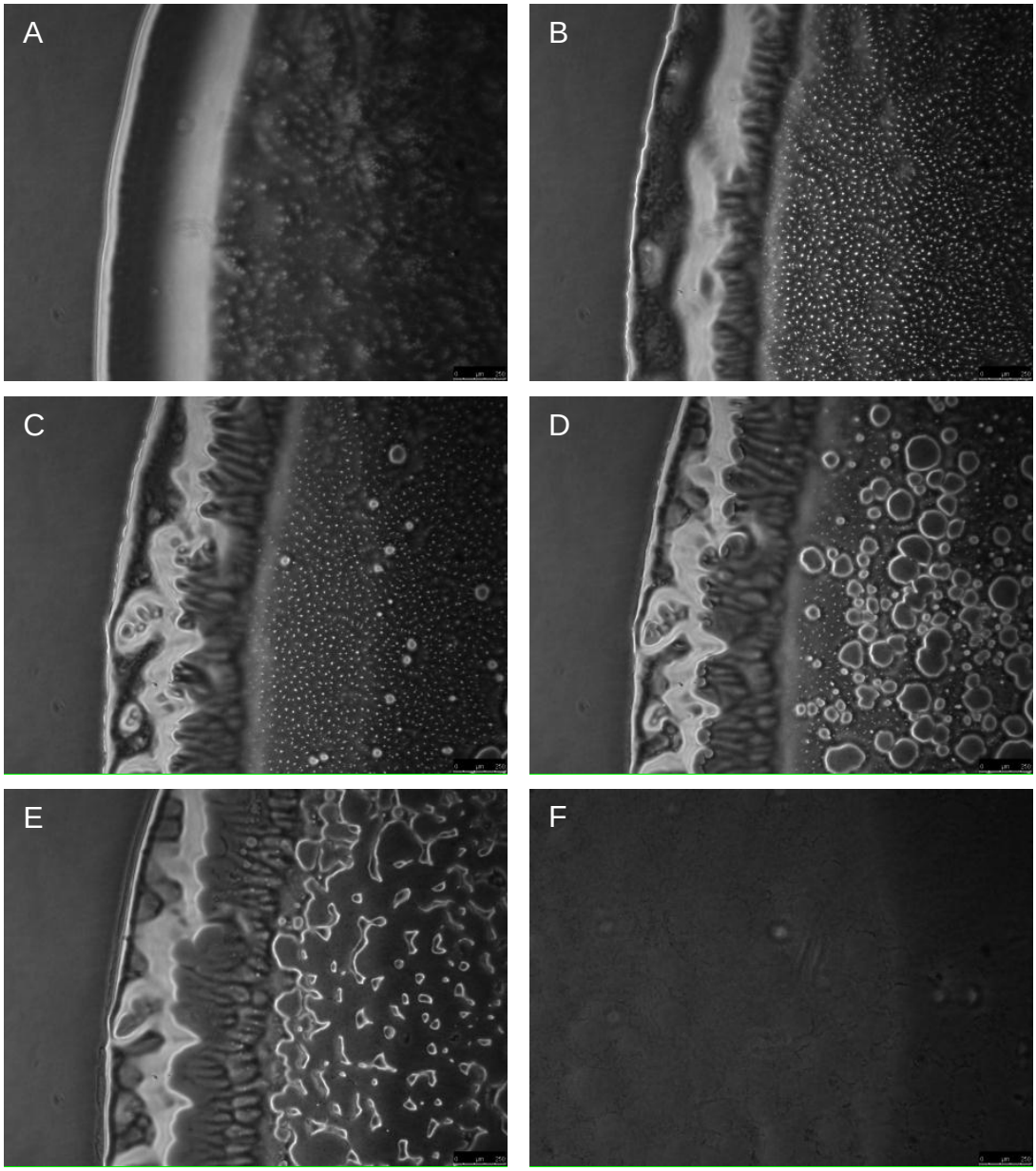

Figure 79 Time-lapse microscopy of P*i*PrOx 200 repeating units as 37°C medium was added.
A) Shows the polymer as liquid was first added, B, C, D and E show the progression of the polymer through the 5 minute time-lapse. F) Shows an image taken of the centre of the droplet after the 5 minute time-lapse has finished, in this case there was no polymer present. Scale bar 250µM.

To overcome the problem of the P*i*PrOx polymers aggregating during incubation with medium, a co-polymer Poly(*i*PrOx-co-Bis*i*PrOx) (Bis*i*PrOx) was created to provide a larger molecular weight by the addition of cross linkages, to create a more viscous solution. NMR (nuclear magnetic resonance) confirmed the addition of the Bis-oxazoline monomers. The NMR data can be found in the appendix.

Investigating the LCST of Bis*i*PrOx polymers with varying concentrations of Bis*i*PrOx showed that the transition occurred within the physiological range (Figure 80).

Polymer code	Repeating units	End groups	Estimated mass (kDa)	Percentage of bis-oxazoline	LCST (°C)
PiPrOx-Bis*i*PrOx 1	1334	CH3, OH	174.1	6.18	Insoluble
PiPrOx-Bis*i*PrOx 2	102	CH3, OH	11.8	0.60	34.2
PiPrOx-Bis*i*PrOx 3	102	CH3, OH	11.9	1.39	31.4
PiPrOx-Bis*i*PrOx 4	102	CH3, OH	12.0	1.29	29.3
PiPrOx-Bis*i*PrOx 5	102	CH3, OH	12.3	2.54	28.7
PiPrOx-Bis*i*PrOx 6	102	CH3, OH	12.8	3.75	28.2

Figure 80 Co-polymers using Bis-oxazoline and their corresponding characteristics. This experiment was carried out by Adam Fisher.

The Bis*i*PrOx polymer composed of 1334 repeating units with 6.18% Bis*i*PrOx, remained *in situ* as 37°C medium was added (Figure 81). The polymer layer was hydrophobic enough to block the diffusion of water into the polymer layer.

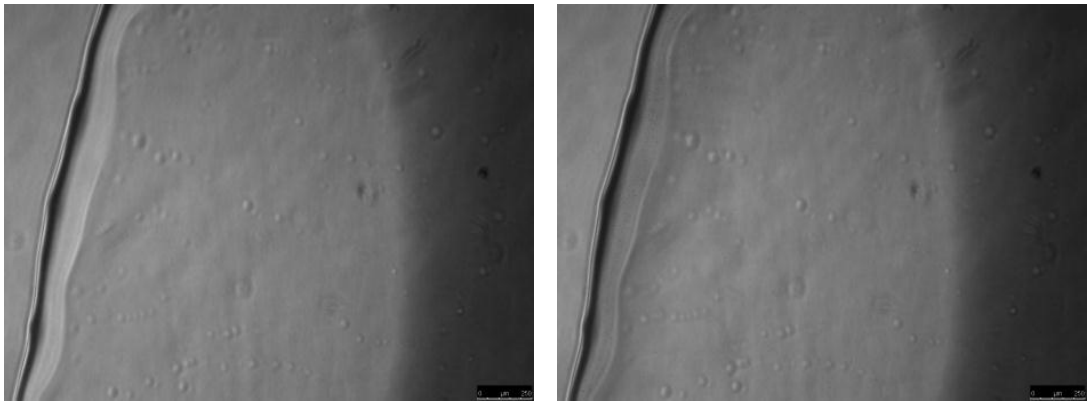

Figure 81 Time-lapse images of Bis*i*PrOx with 37°C medium added.
A) Shows the polymer immediately after 37°C medium was added. B) Shows the polymer at the end of the 5 minute time-lapse. There was no difference between the images. Scale bar 250µM.

Although the polymer was insoluble when the LCST was tested, it was shown to be thermoresponsive on the tissue culture plastic at 20°C (Figure 82). Thus a 30µl droplet of polymer (1.3 x 10mg/cm^2) dissolved into the medium after 25 minutes at room temperature.

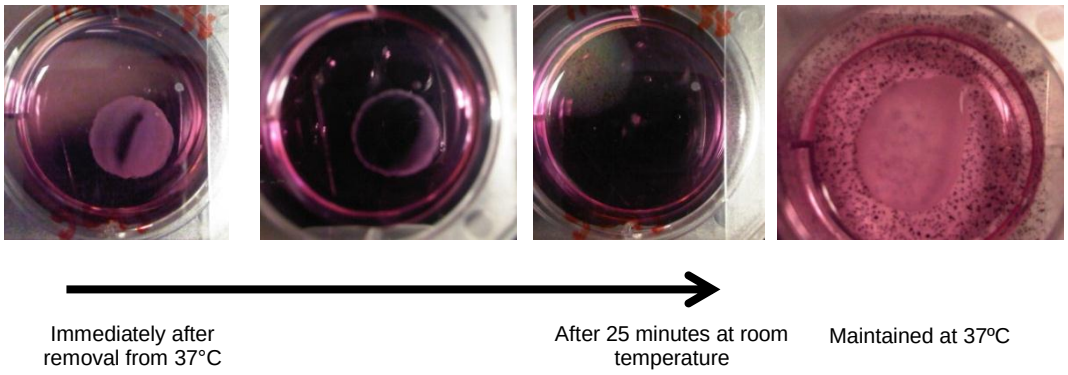

Figure 82 Bis*i*PrOx at 20°C dissolving into 20°C medium.
A) Shows the polymer as it was removed from 37°C. B) Shows the polymer after 15 minutes at 20°C. C) Shows the polymer fully dissolved after 25 minutes.

As the Bis*i*PrOx polymer remained *in situ* and dissolved below its LCST, it was used as a culture surface for HUVEC, 16HBE and HeLa cells. These cell types were used due to their varying adhesive properties. There is limited knowledge on the growth of cells on oxazolines, HUVEC have been shown to adhere to PEtOx and PMeOx, and their use here gives a direct comparison to the literature. HeLa are weakly adherent and 16HBE are very adherent. These cells were grown over night and monitored using the time-lapse microscope; the images in Figure 83 were taken after 24 hours. The cells on the polymer appear rounded whereas the control cells have flattened and formed a confluent cell sheet. This suggests that the Bis*i*PrOx polymer was too hydrophobic to support cell adhesion.

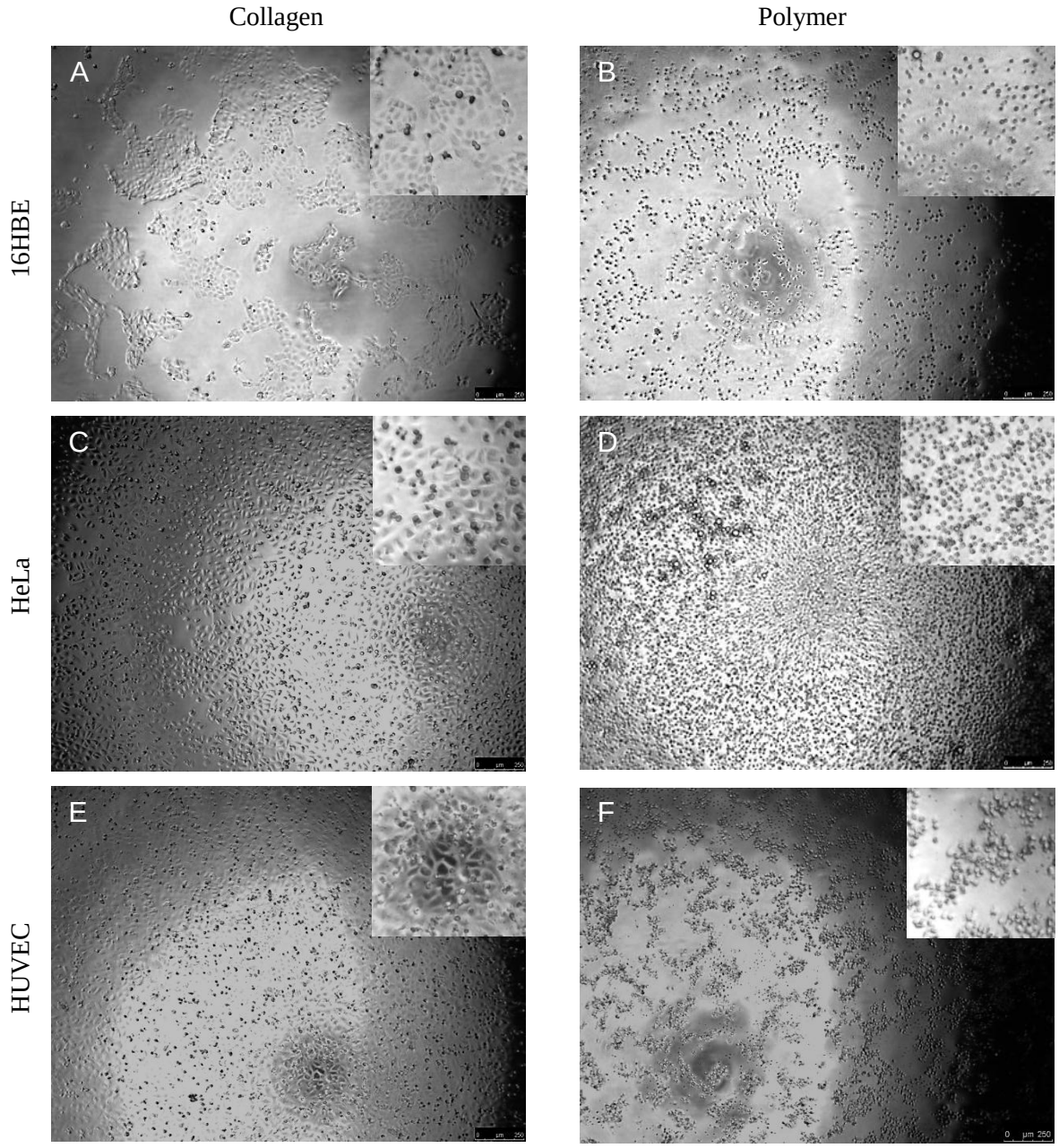

Figure 83 16HBE, HeLa and HUVEC cells plated on BisIPrOX.
16HBE, HeLa and HUVEC (2 x 10^4) cells were seeded to a 96 well plate either coated with collagen or Bis*i*PrOx and grown overnight. A) and B) show 16HBEcells, C) and D) show HeLa cells and E) and F) show HUVEC's None of these cells adhere to the polymer suggesting it was to hydrophobic. The image in the top right hand corner shows an enlarged area of the well. Scale bar is 250µM

As the cells failed to adhere well to the polymer surface, it was postulated that cell adhesion could be improved by use of ECM proteins as a coating on the polymer surface. Three coatings were tested: A 2% type I collagen gel (collagen was used for general 16HBE cell culture); the use of a gel may create a barrier between the hydrophobic polymer and the cells, a 2% gelatin solution (used for general HUVEC culture) and 50µg/ml Fibronectin (an ECM protein that is abundant in serum). Within the control wells

the 16HBE cells were spread and flat, whereas on the ECM coated Bis*i*PrOx the cells are rounded. This suggested that the addition of ECM proteins did not improve the cell adhesion for 16HBE cells to the Bis*i*PrOx polymer (Figure 84).

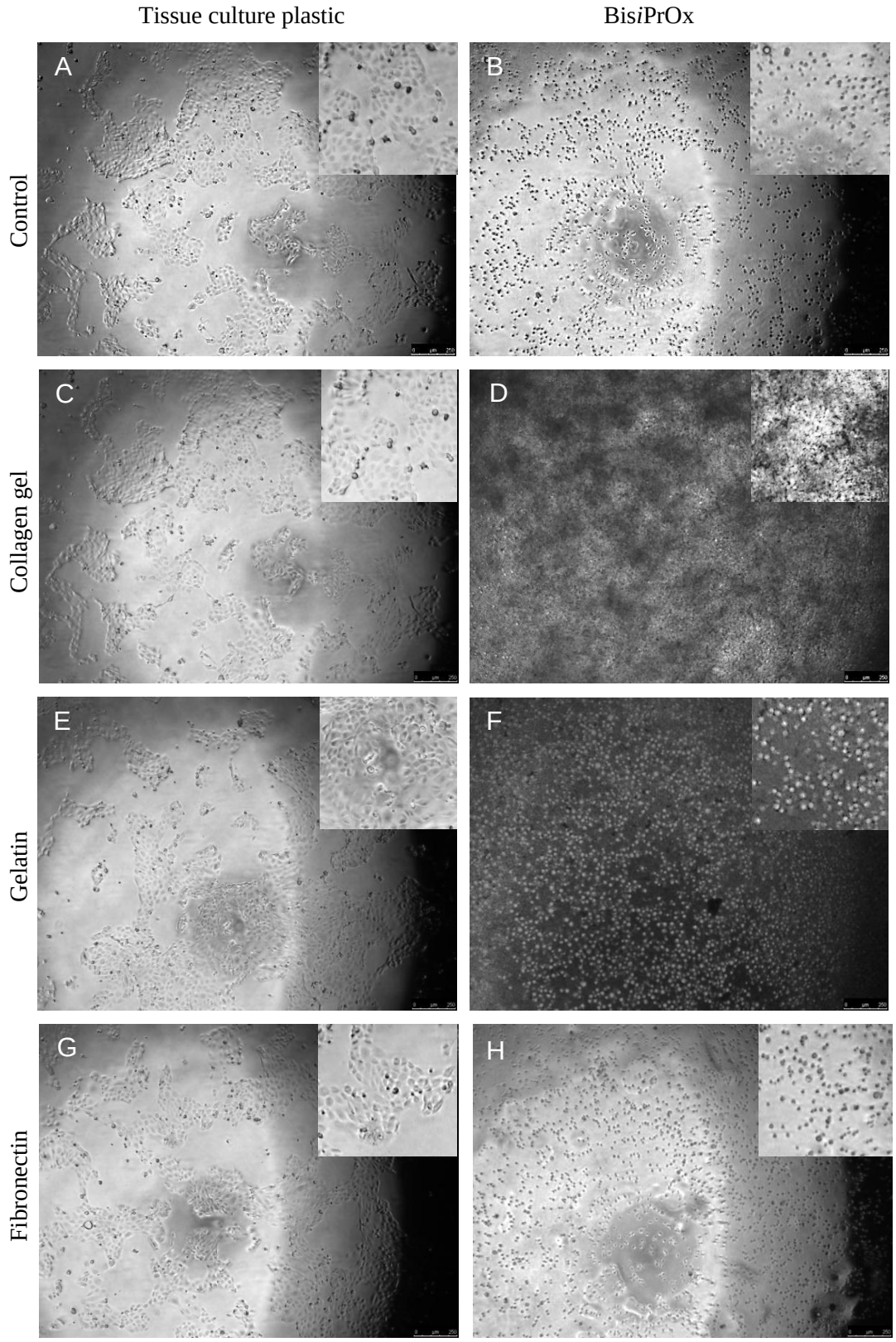

Figure 84 The effect of ECM on Bis*i*PrOx and 16HBE cell adhesion.
16HBE cells (2 x 104 cells) were grown overnight in a 96 well plate coated with various ECM proteins or Bis*i*PrOx coated and various ECM proteins. A) 1 in 100 collagen, B) *BisiPrOx*. C) type I collagen gel D) Bis*i*PrOx coated with collagen gel. E) Gelatin F) Bis*i*PrOx coated with gelatin. G) Fibronectin, H) Bis*i*PrOx coated with fibronectin. The addition of the ECM proteins does not improve the adhesion of the 16HBE cells to the Bis*i*PrOx polymer. The image in the top right hand corner is an enlarged image of the well. Scale bar shows 250µm.

5.2.2 Oxazolines covalently attached to a glass surface

As the oxazoline polymers aggregated together, when used as a coating, it was decided to attach the oxazoline polymer to a surface. Since the Bis*i*PrOx co-polymer was too hydrophobic to allow cell adhesion it was disregarded. Glass was chosen as a suitable surface; it can easily fit into the microwave tubes used for polymerisation and can be transferred into the ultrasonic device once release has been optimised. The method used involved 'polymerisation on the surface'. Since different cell types have different requirements for surfaces to allow growth. We investigated four oxazoline polymers with a range of hydrophobicities using; 2-methyl-2-oxazoline (MeOx), 2-ethyl-2-oxazoline (EtOx), 2-isopropyl-2-oxazoline (*i*PrOx) and 2-*n*-butyl-2-oxazoline (*n*BuOx). MeOx was the most hydrophilic through to *n*BuOx being the most hydrophobic.

To covalently attach the polymers to glass, they were polymerised and terminated using amine functionalised glass coverslips. This facilitated a reproducible and scaleable procedure allowing the synthesis of several batches of coatings. The slides were characterised using contact angles and X-ray Photoelectron spectroscopy (XPS). Contact angle measurement involves measuring the angle of the edges of a droplet of water placed on a surface, the higher the contact angle the more hydrophobic the surface being tested. Figure 85 shows the contact angles for the oxazoline polymers attached to glass. There was a difference of 15-20 degrees from the amine surface and those with polymer attached, suggesting the attachment had been successful. This also highlights the variation in hydrophobicity of the range of oxazoline polymers investigated. (More data can be found in the appendix).

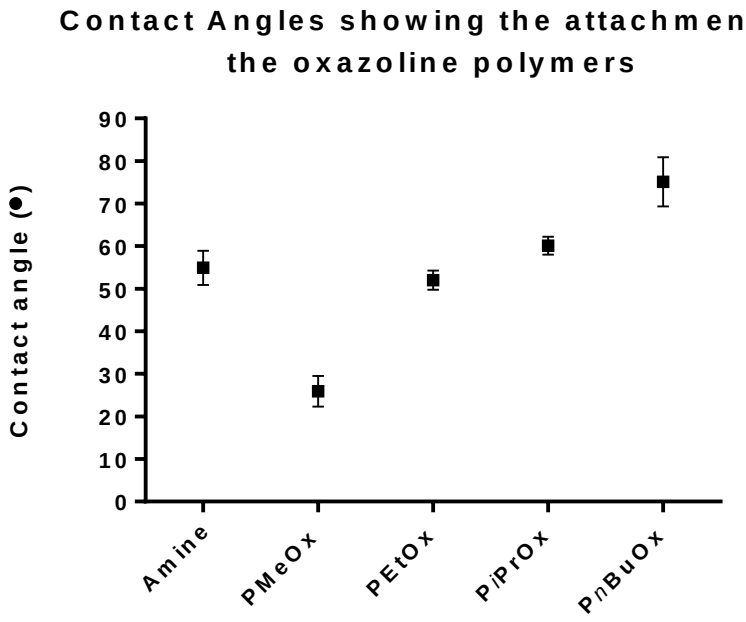

Figure 85 Contact Angles for the polymer surfaces.
Error bars show standard deviation, n=10

To demonstrate the reproducibility of this method, three batches of polymer coated glass coverslips were synthesised for characterisation of the cell behaviour. Each batch was characterised using contact angles (Figure 86).

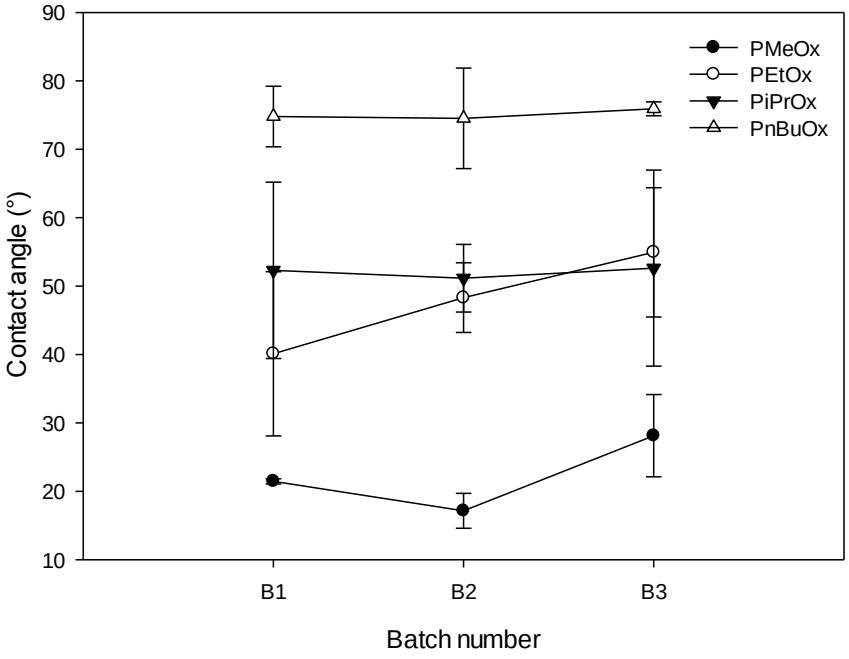

Figure 86 Contact Angles for the polymer batches.
Error bars show standard deviation, n=3

To test the biocompatibility of the polymer surfaces 16HBE and MRC5 cell lines were grown to confluence on the functionalised glass coverslips. Figure 87 shows that there were no morphological changes seen in the phase contrast images compared to a glass control. Immunofluorescent staining of the confluent cells demonstrated that the morphology remained the same, with the 16HBE cells forming tight junctions and creating a cobble stone pattern. The MRC5 cells formed a filamentous pattern with their actin filaments forming longitudinally throughout the cell, suggesting that the polymer surfaces were biocompatible for both cell types. However it was noted that, the growth of both 16HBE and MRC5 cells at day 3 varied on the 4 polymers surfaces (Figure 87). As there could be several reasons for this, we started by investigating the adhesion of the cells to the polymer surfaces.

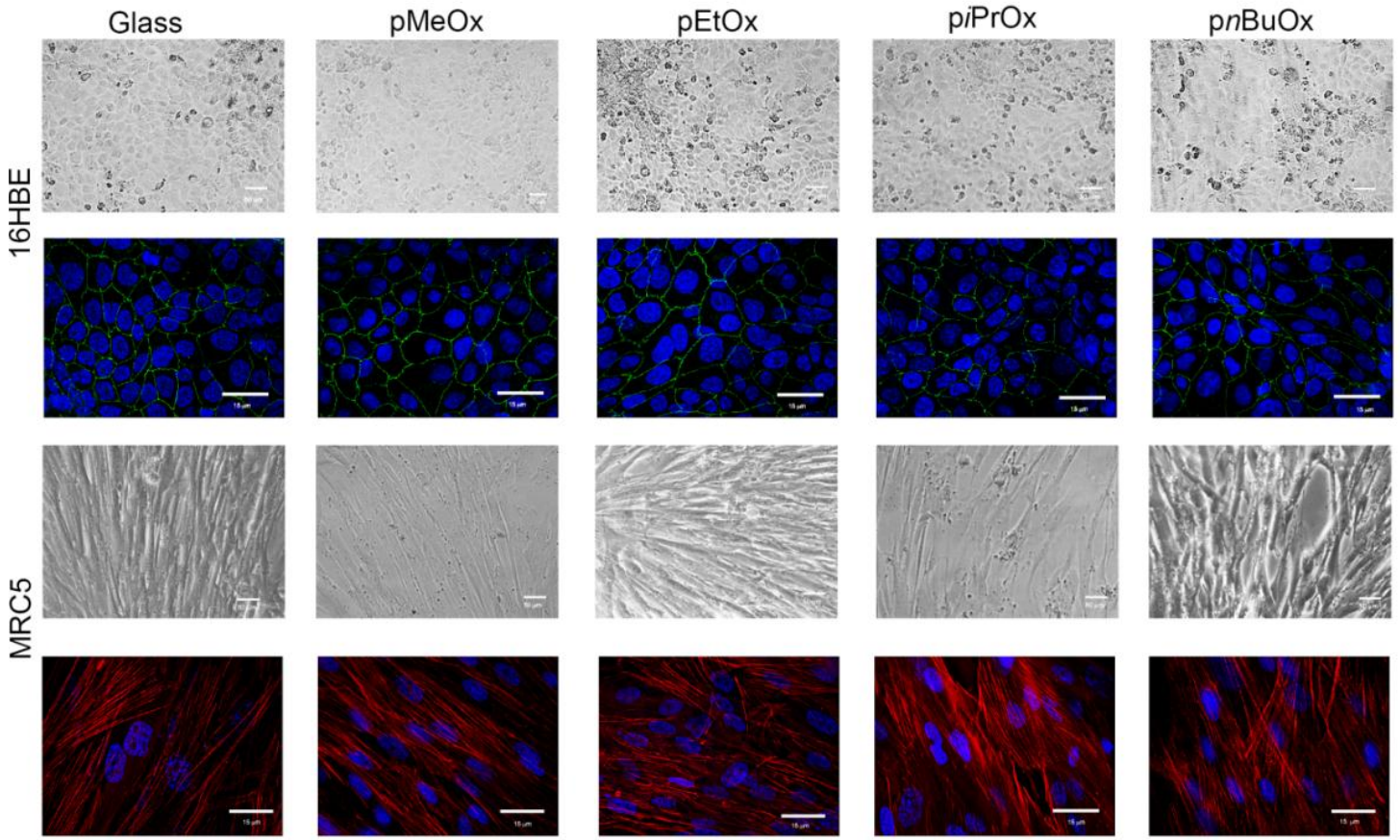

Figure 87. Immunofluorescently stained images of 16HBE and MRC5 cells grown to confluence over 5 days on the oxazoline polymer surfaces. Both cell types were fixed using 4% paraformaldehyde. 16HBE cells were stained with ZO-1 for tight junction formation and dapi counter stain. The MRC5 fibroblast cells stained using phalloidin for the F-actin cytoskeleton and dapi counter stain. The fluorescent images were taken using a confocal microscope. All images are representative of 3 repeats. Scale bar represents 15µm.

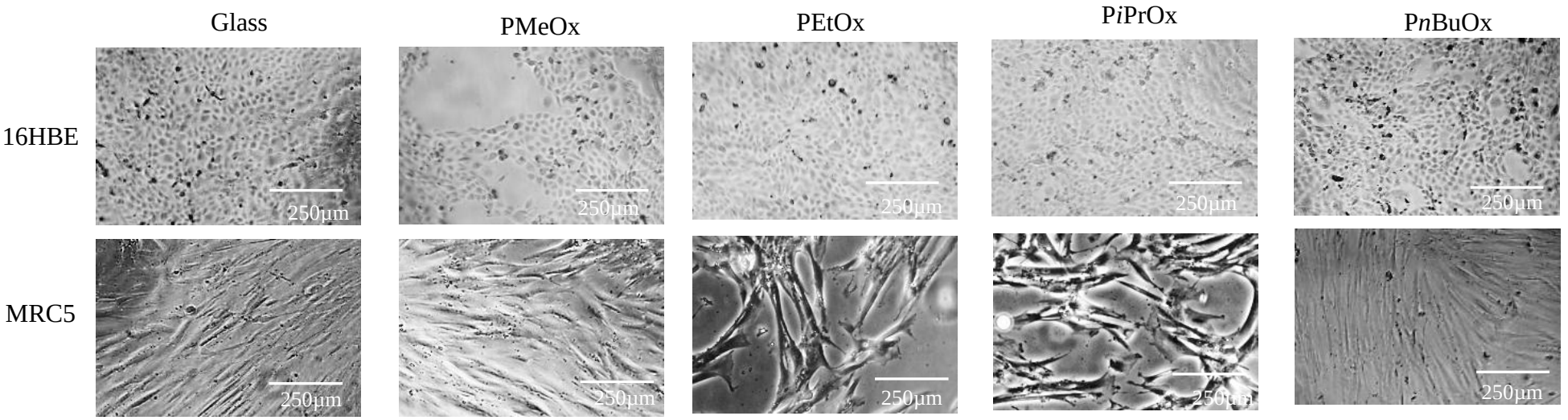

Figure 88 16HBE and MRC5 on the oxazoline polymers after 3 days growth.
There was a variation in confluence at day 3 for both cell types on the four oxazoline surfaces. Scale bar shows 250µm n=6.

5.3 Cell biocompatibility of the oxazoline surfaces

To determine whether there was a difference between the polymer surfaces the cell behaviour was monitored. Adhesion of the cells on to the polymers was important because seeding efficiency will be a determinant of starting cell number for growth experiments and without information from the integrins which mediate cell-matrix adhesion, the cells can apoptose (Frisch and Francis, 1994).

The conventional method for analysing cell adhesion would be to seed fluorescently labelled cells of a known concentration into a black 96 well plate for a set time period. The wells are washed to remove all unadhered cells. A standard curve of known cell concentrations is seeded into the same plate; this plate is then read in a fluorescent plate reader. From the standard curve the remaining adhered cell number can be interpolated. As the adhesion of cells to polymer coated glass was to be investigated, a comparable method which could be carried out without the use of the fluorescent plate reader needed to be developed. Fluorescent microscopy was used investigated as an alternative method to obtain cell number information for wells of various sizes allowing the polymer coated glass to be analysed.

5.3.1 Adhesion assay protocol optimisation

Black plates are used for fluorescent data, as this blocks any fluorescence leak signal into the surrounding wells, which may skew the results. As it would be beneficial to carry out the microscopic analysis on the same plate as the plate reader data, to allow for a direct comparison of techniques, a clear plate and black plate were first compared to assess the magnitude of leakage of signal between wells (Figure 89). Both plates were seeded with calcein labelled HeLa cells between 3×10^3 and 3×10^4 and the fluorescence measured.

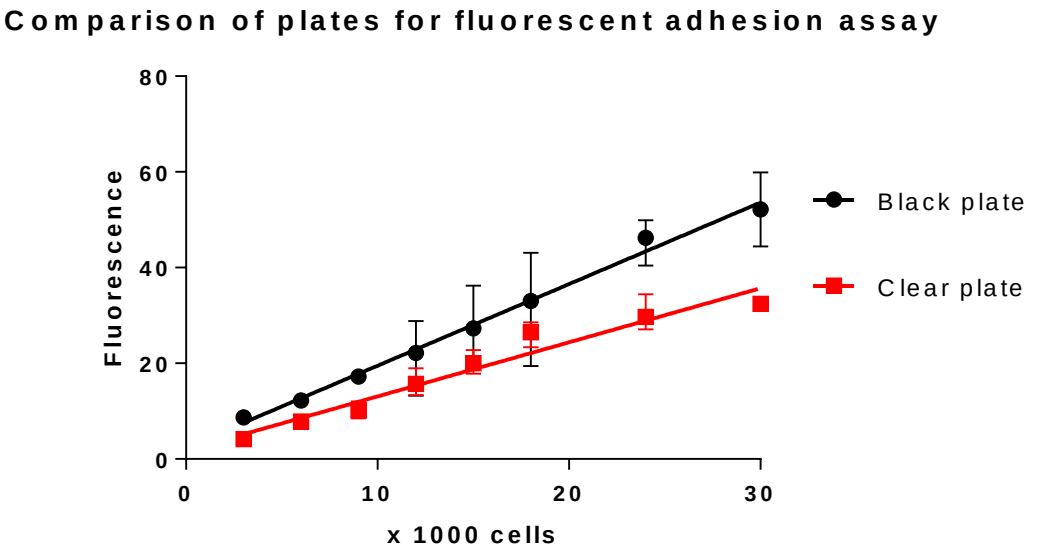

Figure 89 Comparison of black and clear 96 well plates for the standard curve of fluorescently labelled HeLa cells. A black and a clear 96 well plate were seeded with known concentrations between 3 x 10^3 and 3 x 10^4 calcein stained HeLa cells. Although there is a difference in the readings they follow the same pattern so a clear plate can be used for future experiments. This was repeated 3 times within one experiment, the points represent the mean and the error with the error bars showing the range.

Figure 89 shows the standard curves for fluorescently labelled cells read in a clear or a black plate. The black plate reads higher fluorescence as there is no loss of light from the well. The two readings follow a linear relationship; this allows a comparison of the fluorescence and cell number. As the relationship is linear an unknown cell number can be interpolated even from the clear plate, so allowing fluorescent analysis and microscopic analysis to be carried out within the same plate.

5.3.2 Adhesion assay 16HBE

As the main cell line of interest was 16HBE, the adhesion assay was developed using this cell type. The plate was analysed using the fluorescent plate reader and via microscopy to give a direct comparison of the two methods. As can be seen in Figure 90, these two methods gave similar results, the cell adhesion improved over the hour incubation and the ECM coatings of collagen and gelatin provided superior surfaces. The BSA did not improve adhesion to the plate; 16HBE cells appear to need an ECM coating to adhere more rapidly.

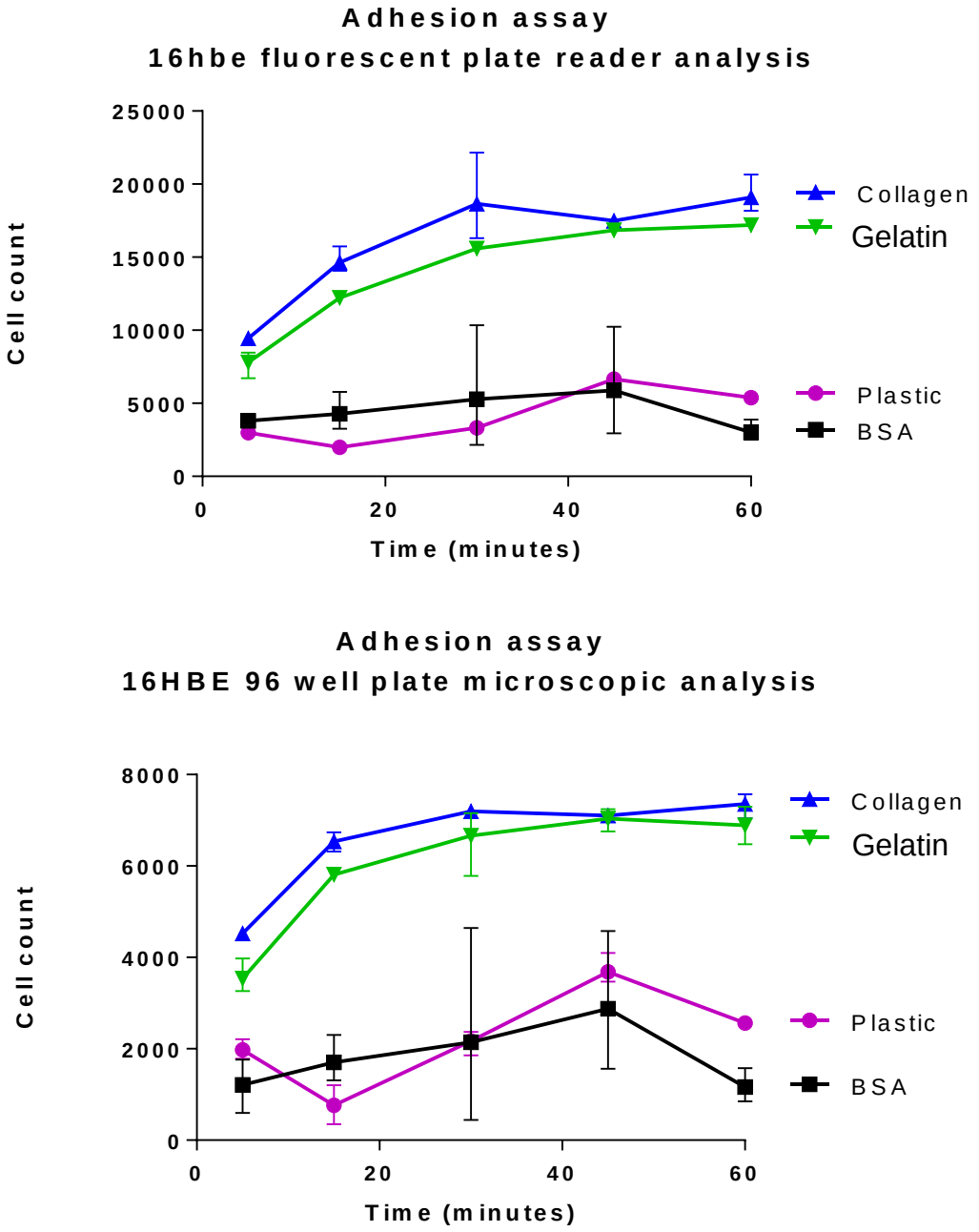

Figure 90 Adhesion assay for 16HBE cells in a clear plate both fluorescent plate reader and microscopic analysis. 3 x 10^4 Calcein stained 16HBE cells were added to the wells of a clear 96 well plate coated in various ECM proteins and washed at various time intervals 5, 15, 30, 45 and 60 minutes. The plate was read in the fluorescent plate reader and the standard curve created before the cell number was interpolated. The same plate was transfer to the microscope and images were taken. The cell count was carried out using image j and the total cell count calculated. This was repeated 3 times within one experiment, the points represent the mean and the error with the error bars showing the range n=2.

There were some discrepancies between the cell numbers determined by the two methods. The cell number obtained via microscopic analysis is an average of 7370 cells for collagen at 60 minutes, whereas fluorescent analysis showed 19102 cells. To investigate this discrepancy, the standard curve for the microscopic method was analysed. This showed

that the cell number plateaued after 12000 cells had been added (Figure 91) whereas the fluorescence gave a linear relationship (The standard curve from the fluorescent plate reader analysis can be found in the methods). This means that cell numbers above 12000 cannot be accurately counted.

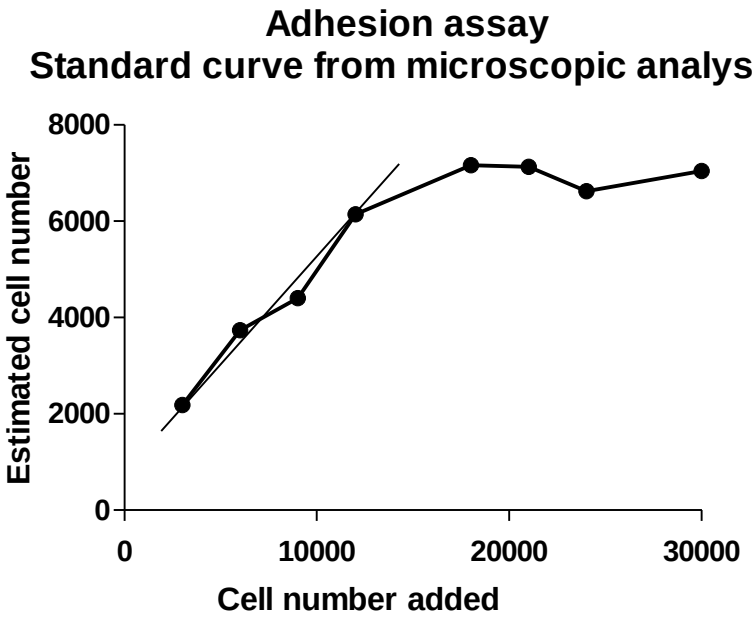

Figure 91 Standard curve created via microscopic analysis.
3 x 10^3 to 3 x 10^4 calcein stained 16HBE cells were added into 8 wells of a 96 well plate, this was repeated 3 times. Microscopic images were taken at 5 times magnification. The cell number was analysed using image J and the total cell count calculated from this.

The cell numbers calculated via counting are approximately half the number of cells added. This is because the Image J programme struggles to determine single cells (Figure 92).

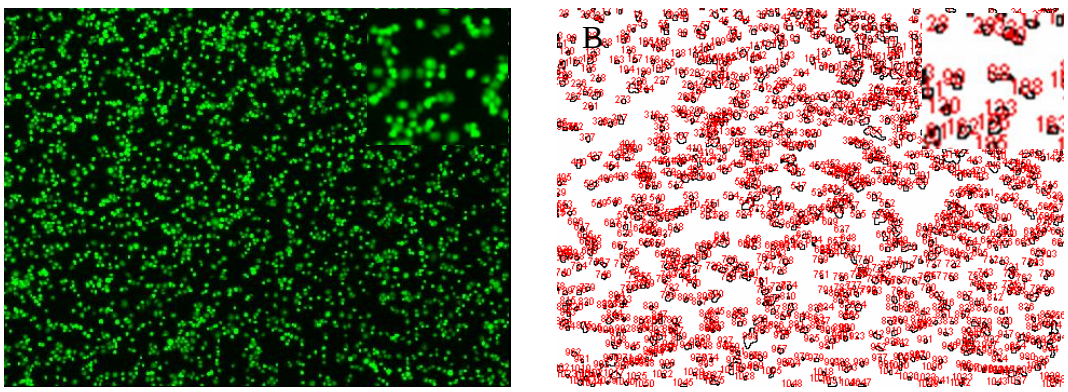

Figure 92 comparison of calcein stained 16HBE cell adhesion assay original image and cell count image. The images are from collagen coated glass at 45minutes which was the highest cell count obtained during the adhesion assay. The enlarged areas in the right hand corner are of the same area.

Although the numbers produced by the two methods are different, the patterns seen are the same. Therefore the information obtained shows which surface was more suited for rapid adhesion. As a result the microscopic counting method was used to provide information for the adhesive properties of cells on the polymer coated glass.

5.3.3 Adhesion assays on glass

The adhesion assay was then carried out using the coverslips with 16HBE cells (Figure 93). This produced comparable data to the original 96 well plate microscopic analysis, where the total number of cells on a collagen coated surface was between 6000 and 8000 cells on both tissue culture plastic and glass. In each experiment BSA and the plain dish or glass provided little adhesion for 16HBE cells.

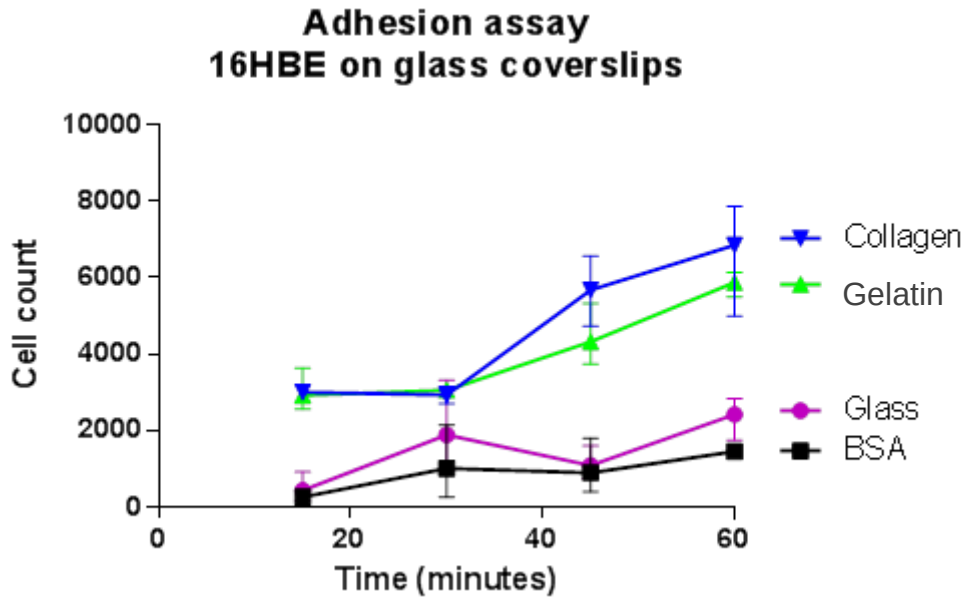

Figure 93 16HBE adhesion assay on glass coverslips.
Calcein stained 16HBE cells were seeded inside cloning rings attached to glass coverslips coated in various ECM proteins. The cloning rings were removed and the whole area washed at various time points 15, 30, 45 and 60 minutes. Images were taken of the area and the cell number counted using image j. from this the total cell number was calculated. This was repeated 3 times within one experiment the points represent the mean and the error with the error bars showing the range n=1.

The largest variation between glass and the ECM coated surfaces was seen at 60 minutes; hence this time point was used to investigate the adhesion of 16HBE and MRC5 cells on the four oxazoline polymers.

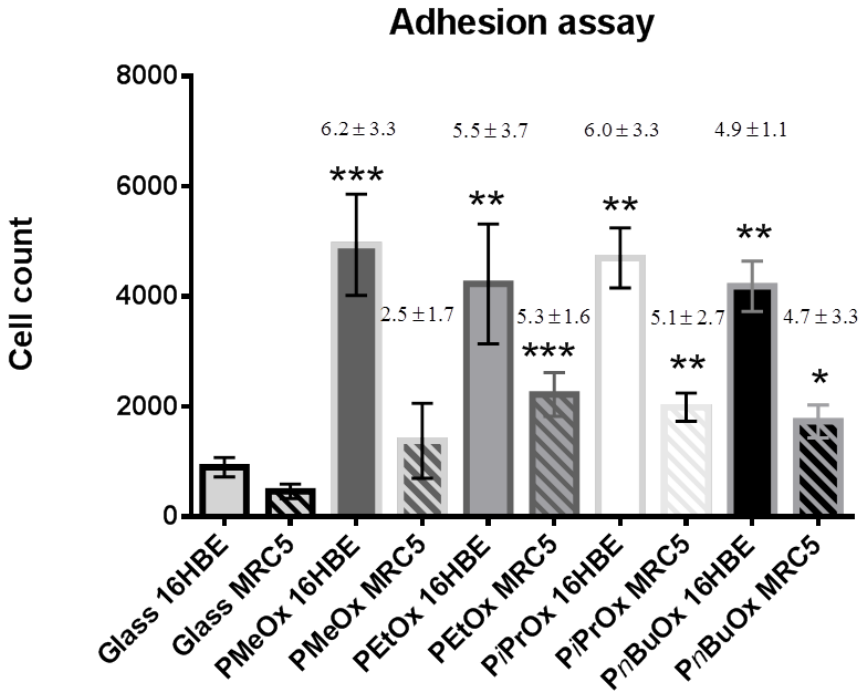

Figure 94. Adhesion assay for both 16HBE and MRC5 on the oxazoline polymers.
Bars represent mean ± Standard deviation, N=3, statistical analysis using two-way ANOVA and Dunnett's multiple comparison. Numbers above show the fold increase compared to the plain glass control. * p<0.05, ** p<0.005, *** p<0.001. numbers above are the mean fold increase ± standard deviation.

There was a significant increase in adhesion to the polymers compared to the glass surface alone for the two cell types with the exception of MRC5 cells on PMeOx. The 16HBE cells were approximately twice as adhesive as the MRC5 with around $4x10^3$ 16HBE cells adhering compared to $2x10^3$ MRC5 cells. The 16HBE cells adhered best to the PMeOx surface with a fold increase of 6.2 ± 3.3. The MRC5 cells had their greatest increase in adhesion on the PEtOx polymer at 5.3 ± 1.6 fold increase compared to the glass control. The biggest difference between the two cell types was seen on PMeOx with 16HBE having a 6.2 ± 3.3 fold increase whereas the MRC5 cells only have a 2.5 ± 1.7 fold increase. This is the lowest increase for the MRC5 and the highest for the 16HBE (Figure 94).

5.3.4 Cell motility

The motility of the cells was investigated to determine how the cells behaved on the polymer surfaces (Figure 95). The cell motility was measured by time lapse microscopy using imagej for analysis as described in the methods section. This showed that 16HBE cells tended to form groups of cells whereas fibroblasts moved more randomly. 16HBE cells were significantly less motile on the PMeOx than on the plain glass control, P*i*PrOx or

P*n*BuOx. The cells also had a slightly reduced motility PEtOx surface but this was not significant. The MRC5 cells moved around more than the 16HBE cells. There was reduced motility on PEtOx, P*i*PrOx and P*n*BuOx compared to the plain glass control and PMeOx which provide weaker adhesive surfaces (Figure 95).

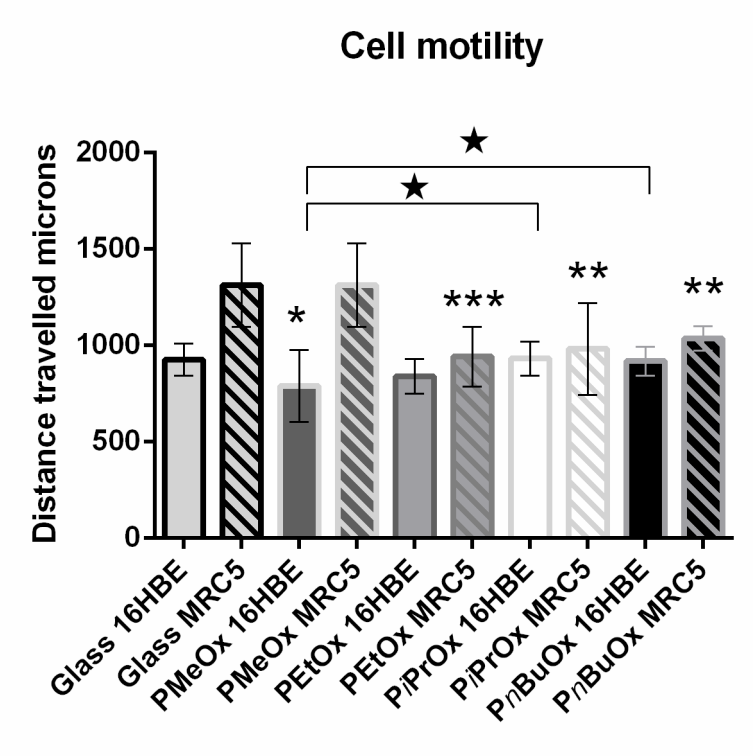

Figure 95 Cell motility of 16HBE and MRC5 on oxazoline polymers
Bars represent mean ± Standard deviation, N=3, statistical analysis using two-way ANOVA and Dunnett's multiple comparison. *p<0.05, ** p<0.005, *** p<0.001.

From these experiments, it appeared that the surfaces exhibited differing properties in supporting cell adhesion, motility and growth. Suggesting they may be used for selection of individual cell types from a mixture of cells for example tissue digestion.

5.3.5 Co-culture

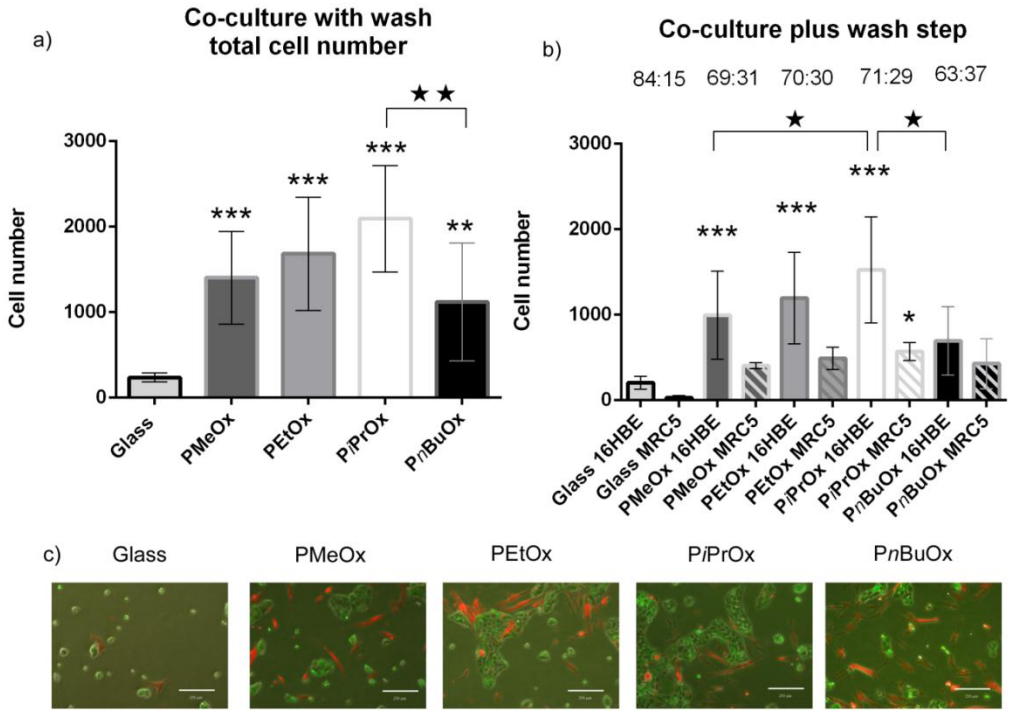

Figure 96 Co-culture with a wash step.
a) Shows the total cell number on each polymer surface, b) shows the number of each cell type on each polymer surface and the ratio of the two cell types. c) shows the microscope images of the co-culture on the polymer surfaces where 16HBE are shown in green and the MRC5 are shown in red, images taken using a fluorescent light microscope. Scale bar 250µm * show statistical differences compared to the control and ★ shows the statistical difference between the polymer surfaces n=3.

To determine whether the variation in cell adhesion and motility could be used to select for a specific cell type from a mixture of cells, equal numbers of 16HBE and MRC5 cells were allowed to adhere for one hour before the unadhered cells were washed off and then left to grow for 2 days. All the polymer surfaces had a significantly greater cell number than the glass control (Figure 96a). The largest total cell count was found on the P*i*PrOx, which had significantly more cells than P*n*BuOx. When looking at the two cell types the P*i*PrOx had a significantly greater cell number for both cell types compared to the glass control. P*i*PrOx also had a significantly greater number of 16HBE's than PMeOx and P*n*BuOx. The P*i*PrOx provides the second most adhesive surface for both cell types. The P*n*BuOx provides the worst surface for 16HBE cells; the cell number was not significantly greater than the glass control. As a result there was a reduced proportion of 16HBE to MRC5 cells on this surface 63:37 compared to the 70:30 seen on the other 3 polymer surfaces (Figure 96c). The Adhesion to the P*n*BuOx was equivalent to PEtOx for 16HBE and the motility was similar to the other polymers suggesting that the on P*n*BuOx growth is reduced for 16HBE. The PMeOx surface although most adhesive for the 16HBE did not provide such a good

growth environment due to the reduced motility of the cells on the surface. The MRC5 cells were the least adhesive and most motile on PMeOx however this did not sufficiently hinder the growth of the adhered cells that were left behind after the wash step.

5.4 Cellular stress

As the novel P*i*PrOx polymer could be used as a thermoresponsive cell culture surface, it was further investigated to determine if it caused any stress to the cells. This was carried out using western blotting for the phosphorylation of p38 mitogen-activated protein kinase (p38). P38 is activated by environmental stress and inflammatory cytokines, its activation occurs via phosphorylation of Threonine 180 and Tyrosine 182 (Cuenda and Rousseau, 2007). This activation enhances substrate access and increases enzymatic activity. This activation can occur within minutes and has a rapid turnover. P38 is involved in transcription regulation, chromatin remodelling, mRNA stability, protein synthesis, regulation and cytoskeleton reorganisation.

To determine a positive control for cellular stress 16HBE cells were treated with TNFα and IL-1β before being lysed and western blotted for phosphorylated p38. To overcome the issue of cell number these were normalised to the lowest protein concentration. Figure 97 shows that there was no significant difference between those treated with TNFα and IL-1β and the control due to a high baseline phosphorylation of p38.

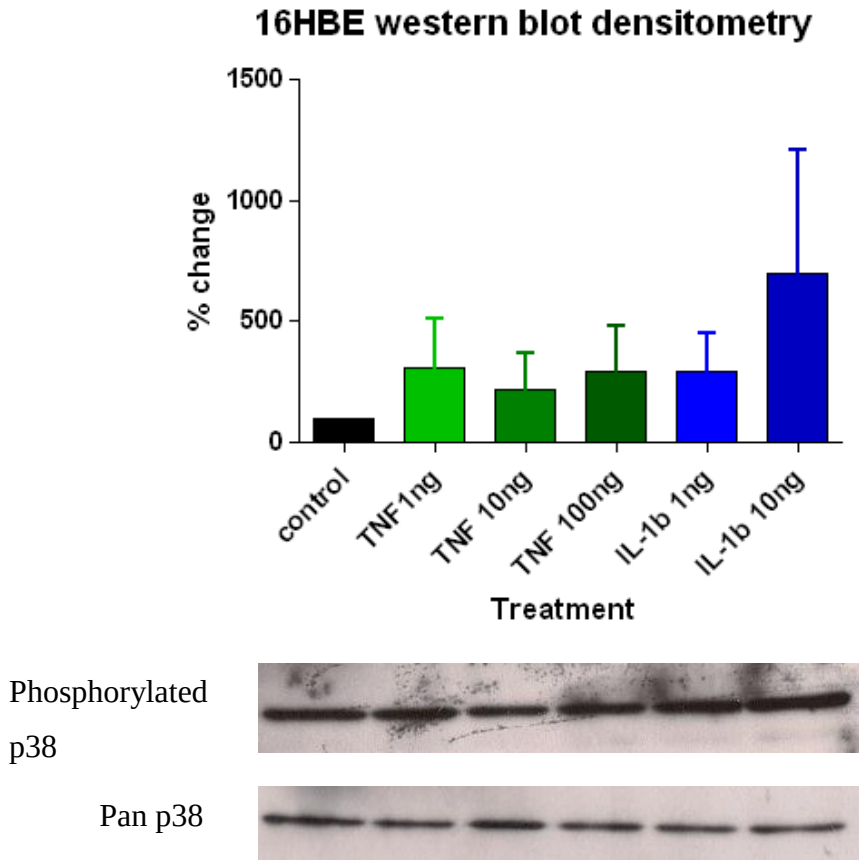

Figure 97 16HBE cells treated with TNFα and IL-1β western blot analysis.
16HBE cells were grown to confluence in a 12 well plate. They were serum starved overnight before being treated with TNFα or IL-1β for 30 minutes. The cells were lysed and analysed for phosphorylate and pan p38 via western blotting. The densitometry was normalised to the loading control. Statistically analysed using Friedman's 1 way repeated ANOVA with Dunn's correction. P=0.0982.

The initial western blotting (n= 8) gave variable results as can be seen by the error bars (Figure 97). To determine whether this was related to the cell type or the cytokines, 16HBE cells were treated for 24 hours before being analysed for IL-8 release using ELISA (Figure 98). IL-8 is a chemotactic peptide for neutrophils (Baggiolini et al., 1989); it is produced by epithelial cells in response to IL-1β and TNFα (Baggiolini et al., 1989). This showed that the cytokines were having an effect on the 16HBE cells, but this was not reflected in their p38 activation.

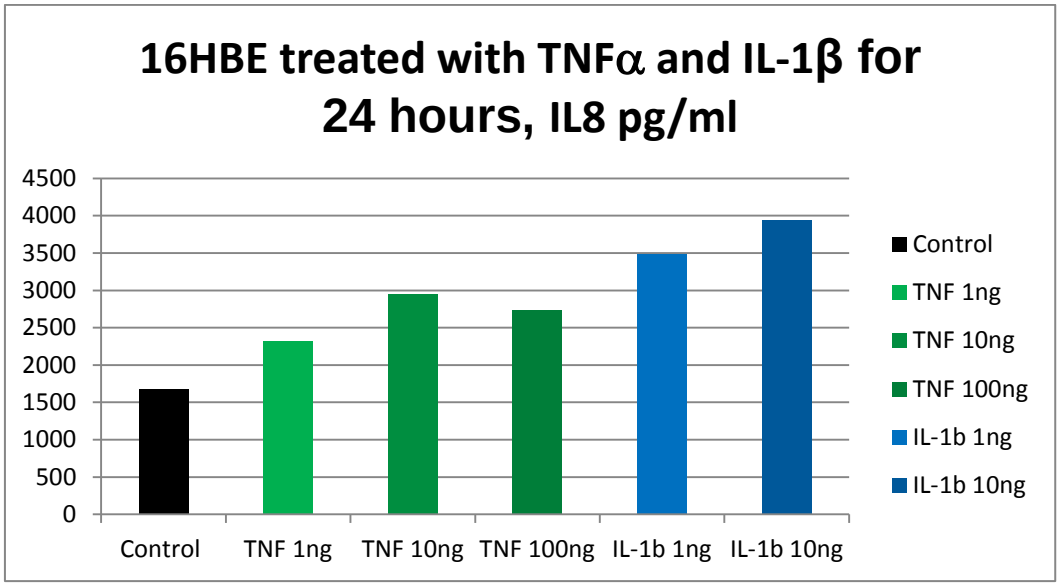

Figure 98 IL-8 release from 16HBE cells treated for 24 hours with TNFα and IL-1β.
16HBE cells were grown to confluence in a 12 well plate before being serum starved overnight. They were treated with 1ng, 10ng or 100ng TNFα or 1ng or 10ng of IL-1β for 24 hours. The cell conditioned media was collected and analysed for IL-8 concentration by ELISA n=1.

16HBE cells have high baseline phosphorylated p38 possibly due to the use of the SV40 large T antigen proto-oncogene used to transform the cells. Therefore another cell type was needed to analyse the environmental stress caused by this novel surface. Healthy PBEC monolayers were investigated for p38 phosphorylation. Healthy PBECs were treated with TNFα and IL-1β for 30 minutes; before undergoing lysis and western blot analysis of p38 phosphorylation (Figure 99).

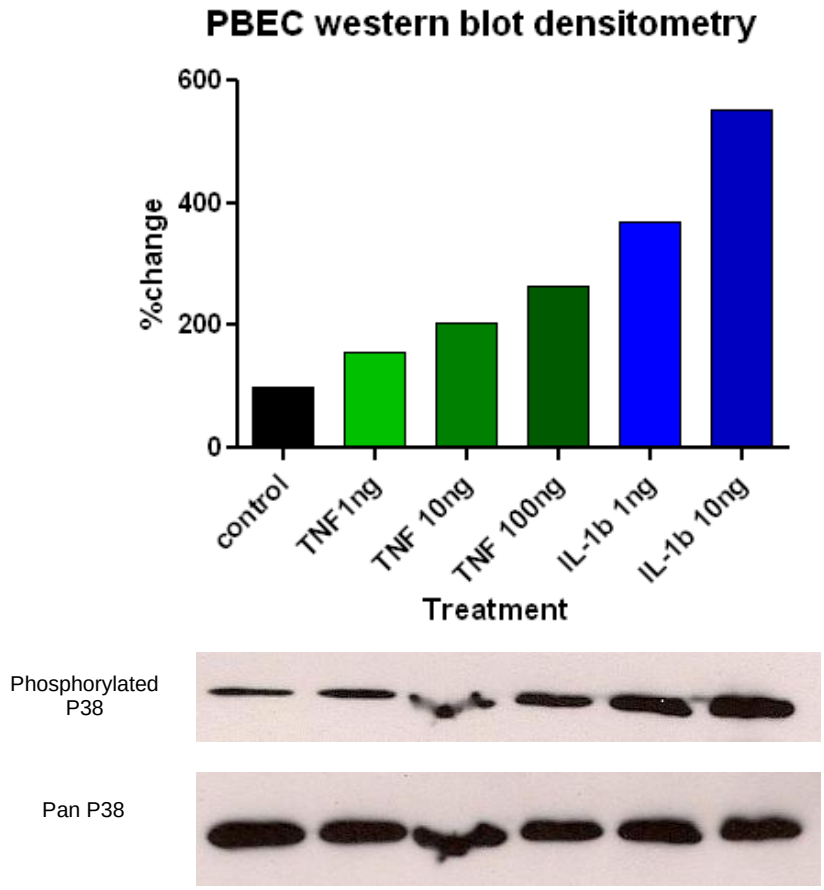

Figure 99 PBEC's treated with TNFα and IL-1β western blot analysis for Phosphorylated p38. PBEC's were grown to confluence as monolayers in a 96 well plate. They were serum starved overnight and treated with TNFα and IL-1β for 30 minutes. The cells were lysed and analysed using western blotting looking for variation in phosphorylated p38. The densitometry was normalised to the loading control (n=1).

The western blot shows that there were low baseline levels of phosphorylated p38, and the stimulation by the cytokines causes a marked increase. The TNFα causes a stepwise rise of p38 phosphorylation with the addition of more cytokine. The IL-1β causes a larger increase, also stepwise with concentration of cytokine. Therefore these cells were used to determine whether the P*i*PrOx polymer caused any stress to epithelial cells. IL-1β gave a greater response, and was used as a positive control for p38 phosphorylation on the polymer coated coverslips.

5.4.1 Cellular responses to P*i*PrOx

Healthy PBEC's were grown to confluence within cloning rings (Figure 100), to cover all aspects of the release from a thermoresponsive polymer, the following treatments were set up, collagen coated glass or P*i*PrOx (not collagen coated) at 20°C or 37°C either plain or

treated with 10ng of IL-1β. The lysed samples were normalised to the smallest protein concentration to remove any discrepancy in cell number.

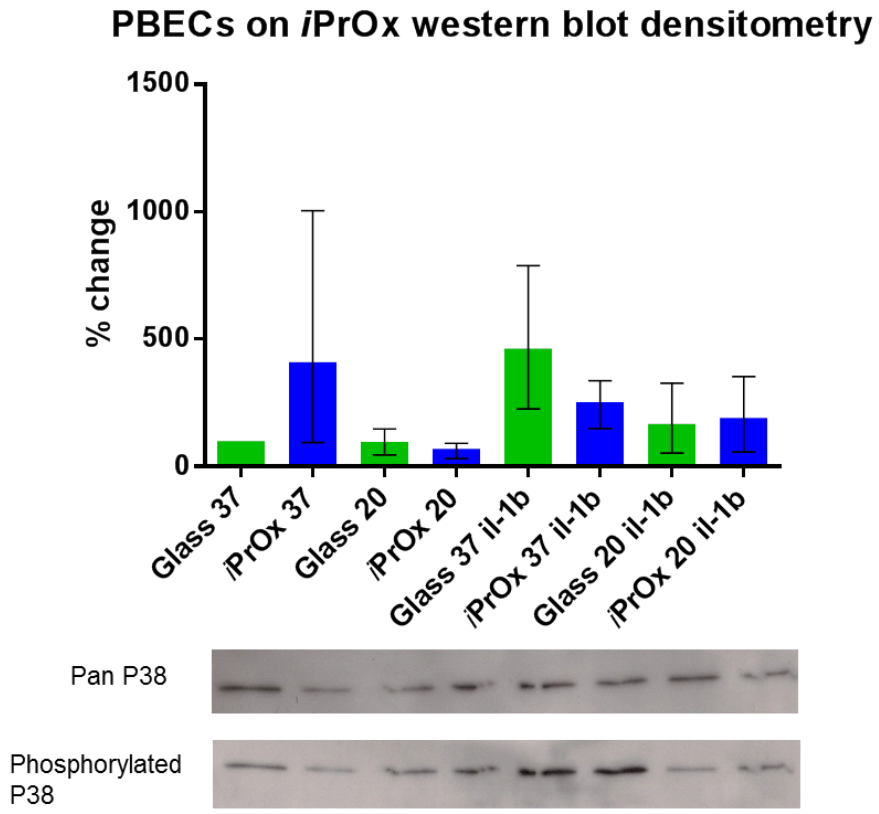

Figure 100 Western blot analysis of PBEC's grown on P*i*PrOx.
PBECs were grown as monolayers within cloning rings before being serum starved overnight and treated with temperature for 105 minutes and IL-1β for 30 minutes before being lysed and analysed via western blotted. The densitometry was normalised to the loading control.

The graph shows that there was no significant difference between the phosphorylation of p38 on collagen coated glass and P*i*PrOx at 37ºC although there is an increase. The cells can activate phosphorylation on the P*i*PrOx as shown by increase in phosphorylation when stimulated with IL-1β at 20ºC however there is not an increase at 37ºC.

5.5 Thermoresponsiveness of P*i*PrOx covalently attached to glass

As 16HBE cells will grow to confluence on the P*i*PrOx coated glass (Figure 87), they were used to determine whether P*i*PrOx was thermoresponsive when covalently attached to the glass. The UpCell protocol was followed. Neither the glass control nor the P*i*PrOx allowed the cells at the edges to round up, as seen on the UpCell (Figure 101).

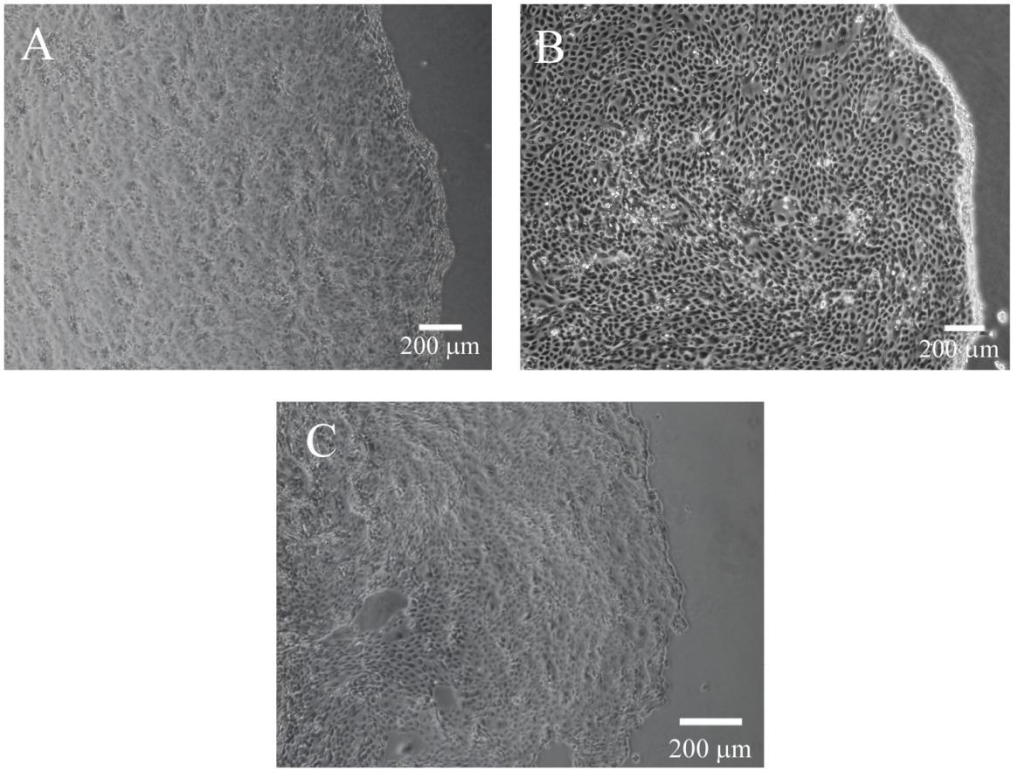

Figure 101 16HBE cell sheets after incubating at 20°C for 45 minutes.
16HBE cells were grown on a glass coverslip (A), an UpCell dish (B) and P*i*PrOx coated glass (C). The edge of the cell sheet has rounded up on the UpCell dish (A), but not on the *i*PrOx coated glass (C) suggesting that there is no thermoresponsive activity. Scale bar is 200µM

After incubation and removal of the membrane there was a large proportion of cells left behind on both the control (Figure 102 A) and the P*i*PrOx (Figure 102 C), although there are less cells left behind on the P*i*PrOx. This suggested that this polymer was not thermoresponsive when attached to the glass or that the protocol for the NiPAAm based polymers was not optimal for oxazoline based polymers.

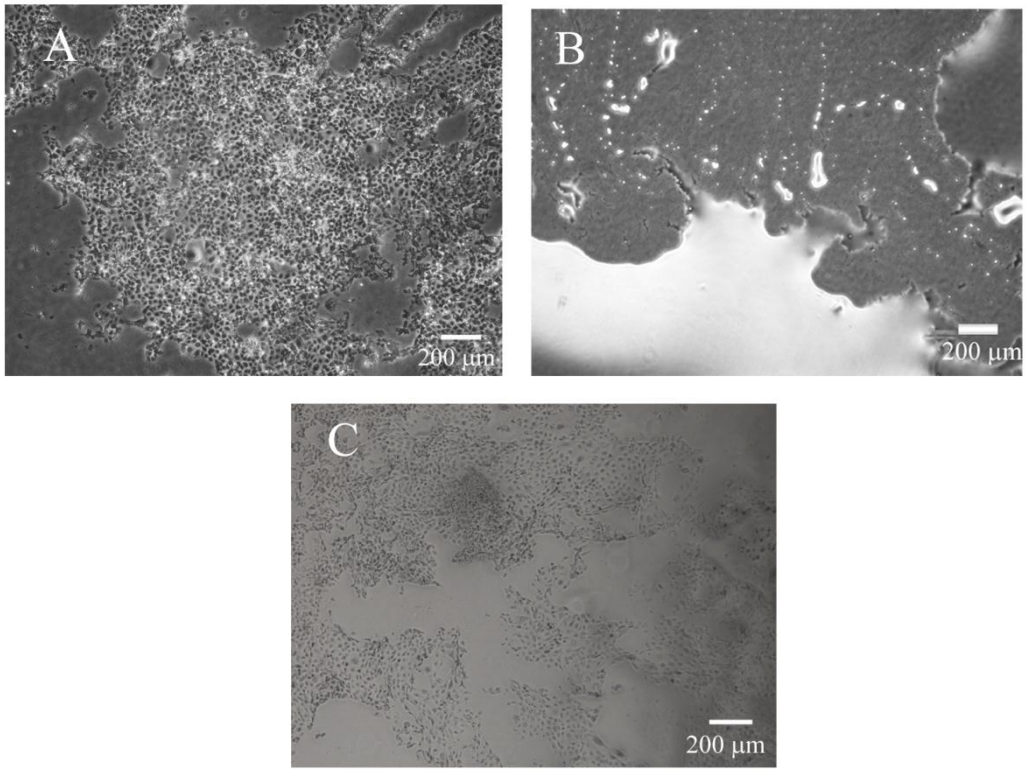

Figure 102 Comparison of cell release between UpCell, Glass and P*i*PrOx.
Confluent 16HBE cells on UpCell, glass and P*i*PrOx were incubated at 20°C for 45 minutes before the UpCell membrane was placed on the cell surface for one minute and removed. A) Shows cells remaining on a glass coverslip. B) Shows no cells remaining on the UpCell dish. C) Shows cells remaining on P*i*PrOx coated glass. N=1

5.1 Discussion

This present work attempted to determine whether a novel thermoresponsive polymer surface was biocompatible and could facilitate the formation and release of a bronchial epithelial cell sheet, which could be used to create a 3D model of the airways.

In previous studies on NiPAAm polymers Takezawa *et al* coated tissue culture dishes with pure NiPAAm (100µg/cm^2) and NiPAAm-co-collagen (200µg/cm^2) (Takezawa et al., 1990). They found that pure NiPAAm when not covalently attached to the dish did not support cell growth but did remain *in situ*. However while it remained on the surface it was too hydrophobic to allow cell attachment. A co-polymer NiPAAm -co-MMA-co-PEGM at a ratio of 70:10:20 was also created that could be coated on to a tissue culture dish. The 70:10:20 NiPAAm co-polymer used in the present study was deposited on to the base of tissue culture wells at 1.3 mg/cm^2 (1300µg/cm^2), a much higher concentration than Takezawa *et al*, however the 70:10:20 NiPAAm co-polymer did not remain *in situ*. It is

unlikely that a lower concentration of polymer would not have prevented this. Because of the nature of the polymer even in its compact form it has some interaction with water, causing the hydrophobic regions to gather together forming the balls of polymer shown in Figure 74. These are not micelles as they do not contain a distinct hydrophobic or hydrophilic region. There was also a large batch variation in the polymer due to the high PDI caused by the free radical polymerisation.

To overcome the polymerisation issues, a new polymer based on poly(2-isopropyl-2-oxazoline) (P*i*PrOx) was synthesised. This has an LCST within the physiological range (Uyama and Kobayashi, 1992), but a much lower PDI than NiPAAm. The P*i*PrOx coating behaved in the same way as the NiPAAm as it did not remain *in situ*. To decrease the interactions with water a co-polymer Bis*i*PrOx was created to form viscous solution. The Bis*i*PrOx co-polymer did not aggregate when used as a coating on the tissue culture plastic dish, as it was too viscous to allow any water molecules to penetrate it, preventing the "balling up" seen in all other polymer coatings. The Bis*i*PrOx co-polymer was shown to be thermoresponsive when coating the base of the dish. This was unexpected as there was no LCST data for this polymer, as it would not dissolve in PBS at room temperature for the measurements to be carried out. The Bis*i*PrOx co-polymer, however, did not support adhesion of 16HBE, HeLa or HUVEC cells because it was too hydrophobic.

When synthesised on a glass surface covalently linked oxazoline polymer surfaces supported growth of 16HBE and MRC5 cell lines. It has previously been shown that primary sheep and rat fibrobrocytes and HUVECs will grow on PEtOx (Chang et al., 2002), HUVECs will adhere and spread on bottle-brush brushes of PMeOx and P*n*PrOx when pre-coated in fibronectin (Zhang et al., 2012), and primary human dermal fibroblasts will adhere to and proliferate on P*i*PrOx and a co-polymer poly[(2-ethyl-2-oxazoline)-co-(2-nonyl-2-oxazoline)] (Dworak et al., 2014). This shows that a variety of cell types will adhere and grow on oxazoline polymer surfaces. The morphology of the cells was not affected by growth on the oxazoline polymers.

The current study has shown that 16HBE and MRC5 vary in their ability to achieve confluence when grown on the 4 oxazoline surfaces. This is also a problem for NiPAAm. When Nash *et al* investigated spin coating NiPAAm on to Thermanox plastic discs, they investigated 7 different cell lines and found that SW480 (colorectal cancer cell line) cells had slight growth impedance whereas HaCat (human keratinocyte cell line) cells had 50%

less cell growth than the control (Nash et al., 2011). Zhang *et al* have shown that protein absorption was lower on PMeOx and PEtOx at 6ng/cm^2 compared to P*n*PrOx at 90ng/cm^2 (Zhang et al., 2012). This lower protein absorption could explain why cell growth on the PMeOx and PEtOx surfaces was lower at day 3 than P*i*PrOx.

To determine a reason for the variation in cell growth, the adhesion of 16HBE and MRC5 cells to the covalently attached oxazoline surfaces was explored. A range of methods to study the adhesion of cells to various polymer coated surfaces has been utilised within the literature. Lagunas *et al* investigated the optimum density of RGD peptides on a surface using NIH/3T3 (mouse embryonic fibroblasts). These cells were washed with PBS after 1 hour to remove non adherent cells, before fixing and immunofluorescent staining for focal adhesion contacts. These focal adhesion points were then counted and a threshold value of RGD peptides on the surface calculated. 4pmol/cm^2 provided successful cell adhesion and spreading (Lagunas et al., 2012). Poly(N-isopropyl acrylamide)-grafted polycaprolactone films have been investigated to determine whether the addition of collagen could increase cell adhesion, while maintaining cell release from the thermoresponsive surface, using 3T3 fibroblasts. The cells were grown for 2 days before washing with PBS to remove any unadhered cells. The cells underwent fixation before being imaged using phase-contrast. They noted that cell adhesion was increased at 37ºC and that a sheet could be released by reducing the temperature (Xu et al., 2010). On oxazoline polymers P*i*PrOx and a co-polymer poly[(2-ethyl-2-oxazoline)-co-(2-nonyl-2-oxazoline)] the adhesion was measured after 2.5, 4, 8, 24, 48 and 72 hours. This was measured using the Almarblue method (Dworak et al., 2014). Here they found that the cell adhesion was comparable to the TCP control. However there was lower adhesion for the co-polymer at 2.5 hours compared to the P*i*PrOx. They also remarked that PiPrOx appeared to support cell growth better than the control. We saw that PiPrOx also supported cell growth better than our glass control and the other polymers investigated. All these studies were carried out over a longer time period than the current study, where the initial cell adhesive qualities of the polymer were investigated. Allen *et al* studied three co-polymers of NiPAAm and N-Tert-Butylacrylamide, with varying hydrophobicities (50:50 contact angle 56.53º, 63:35 contact angle 54.35º and 85:15 contact angle 52.98º). Thus the 85:15 polymer is similar to PEtOx (contact angle 52.01±2.22) while 50:50 and 63:35 polymers are in-between the PEtOx and P*i*PrOx (contact angle 60.13 ±2.10) polymers. They found that MRC5, HeLa, 1BR3 (primary fibroblast) and HASMC (aortic smooth muscle) all exhibited decreased cell adhesion with increasing hydrophilicity of the surface (Allen et al., 2003). In the current

study decreased adhesion was observed using PMeOx, the most hydrophilic surface. However PEtOx was the most cell adhesive surface whereas its hydrophobicity was equivalent to the least cell adhesive NiPAAm-acrylamide surface.

Once adherence of cells to a surface has been achieved, it is essential that they are able to move around to make cell to cell contacts; without these contacts the cells may apoptose (Kantak and Kramer, 1998). Using the co-polymers of NiPAAm and N-tert-butylacrylamide (50:50 contact angle 56.53º, 63:35 contact angle 54.35º) described above Allen *et al* found that there was an increase in cell motility with an increase in hydrophilicity of the surface (Allen et al., 2006). In the current study MRC5 cells were more motile with increasing hydrophilicity of the polymers as they were most motile on PMeOx covalently attached to glass, the most hydrophilic surface tested. The 16HBE cells did not follow this pattern, as they were most motile on P*n*BuOx the most hydrophobic (contact angle 75.09 ± 5.77) surface and the least motile on PMeOx the most hydrophilic surface. The fibroblasts were slightly more mobile than the 16HBE cells on all the polymers. For both 16HBE and MRC5 cells the surface which the cells adhered to least supported the highest motility of the cells.

The variation in adhesion and motility between the 16HBE and MRC5 cells on the polymer surfaces hinted that they could be used to preferentially select for a specific cell type. This has previously been utilized by Tsuda *et al* in the creation of co-cultures on NiPAAm and NiPAAm-co-*n*-butyl methacrylate patterned tissue culture dishes. At 27ºC primary rat hepatocytes were seeded on to the hydrophobic dehydrated co-polymer, but did not attach to the NiPAAm. At 37ºC bovine carotid endothelial cells were seeded which attached to the NiPAAm in its hydrophobic state (Tsuda, 2005). To investigate cell selectivity on the four oxazoline polymer surfaces covalently attached to glass, 16HBE and MRC5 cells were seeded together and allowed to adhere for one hour before being washed, taking advantage of the adhesion variation and allowed to grow for two days. A similar method was used by Gengec *et al* to select L1210 mouse leukaemia cells when mixed with healthy human leukocytes. They found that by changing the polymer coating they could preferentially select the leukaemia cells (Gengec et al., 2014). We found that P*n*BuOx selected a higher proportion of MRC5 cells than 16HBE cells, making it a candidate for a cell selective surface. The greatest cell number for both cell types was found on the P*i*PrOx surface, making it a polymer with the potential to increased cell growth.

The cellular stress caused by P*i*PrOx was explored. Other groups have investigated the cytotoxicity of cells on NiPAAm. Vihola *et al* investigated the cytotoxicity of NiPAAm for Caco-2 (human epithelial colorectal adenocarcinoma) and Calu-3 (human airway epithelial) cell lines at both 20ºC and 37ºC using the MTT test and LDH release. The MTT test measures a decrease in mitochondrial activity of the cells and LDH release measures severe cell damage. After treatment with NiPAAm both cell types had an LDH of less than 10% indicating that the cell membrane was intact. The MTT test indicated a slight increase in mitochondrial activity. These results suggest that NiPAAm is relatively non-toxic at concentrations below 10mg/ml in both Caco-2 and Calu-3 cell cultures (Vihola et al., 2005). The cytotoxicity of the NiPAAm polymer in a whole organism has been investigated. Malonne *et al* investigated the effects of ingestion of the polymer in mice. It was reported that at a concentration of 2000mg/kg body weight there were no toxic effects after 28 days when looking at changes in clinical signs, body weight and food consumption, haematology, clinical chemistry and absolute organ weight (Malonne et al., 2005). There was no significant difference in cellular stress on the P*i*PrOx polymer surface compared to the collagen coated glass control this could be further decreased by the addition of a collagen coating over the polymer surface.

PEtOx and PiPrOx display thermoresponsive behaviour in solution analogous to that of PNiPAAm (Uyama and Kobayashi, 1992). Although we did not observe this behaviour after covalent attachment to the glass surfaces, there is the potential to further develop these for cell sheet growth and harvesting. Dworak *et al* have shown that human dermal fibroblast cell sheets have been released from P*i*PrOx and a co-polymer poly[(2-ethyl-2-oxazoline)-co-(2-nonyl-2-oxazoline)] by temperature reduction (Dworak et al., 2014). Dworak *et al* use the same method to attach the polymers to the glass; however we postulate that they achieved greater coverage of polymer due to the use of a dilute solution incubated for 3 days with stirring, whereas in the current study a more concentrated solution was used overnight with no stirring.

In Summary the four oxazoline polymers provided a suitable cell culture surface for 16HBE and MRC5 cells with no adverse effects on cell morphology and PBECs incurred no increase in cellular stress when grown on the P*i*PrOx. There was a variation in adhesion and motility for the cells on each polymer and between the two cell types allowing for cell selectivity. There is the potential to further functionalise these polymers giving a large

scope for more tailored cell culture surfaces. There is also the possibility of creating a thermoresponsive surface using P*i*PrOx.

6. Thermo-gels and cell sheet engineering.

The Thermo-gel used for this work was synthesised and characterised by Adam Fisher, School of Chemistry, University of Southampton.

Although there was the possibility to release cells from *i*PrOx attached to glass, this was still not suited to our model of interest as it was unreliable and complex. Also the use of a membrane for transfer was still required to maintain the integrity of the sheet; therefore we investigated whether a thermo-gel based on the *i*PrOx polymer could be used to suspend bronchial epithelial cells and allow them to form junctions in a similar fashion to the Sonotweezers.

A thermo-gel is an aqueous polymer system that undergoes solution (sol)-to-gel transition as the temperature increases. Bokias *et al* created a thermo-gel using NiPAAm as the thermoresponsive component. Linear NiPAAm polymers were attached to the polysaccharide carboxymethylcellulose (CMC) (a hydrophilic ionic ether of cellulose) backbone (Bokias et al., 2001). Lu *et al* used the same thermo-gel when investigating a biodegradable injectable hydrogel to aid protein delivery. They carried out a cytotoxicity test using the MTT assay on HEK 293T cells which were grown on tissue culture plastic before various concentrations of the polymer gel were added to the media. There was no significant decrease in cell viability with concentrations between 0.1-2.0mg/ml (Lü et al., 2011).

The Oxazoline thermo-gelling polymer (P*i*PrOx-co-*n*BuOx-CMC) was created following the method used by Bokias *et al*. It was comprised of a CMC backbone with linear P*i*PrOx-co-*n*BuOx arms. CMC is a biodegradable polymer which has no toxicity (Vasile et al., 2004) and is FDA approved. It is a hydrophilic ionic ether of cellulose, which is biodegradable and biocompatible. The use of CMC also reduces any hydrogen bonding interactions with side chains allowing for dissolution in neutral liquids (Bokias et al., 2001). The P*i*PrOx-CMC had a gelation temperature ranging from 58ºC to no gelation, depending upon the concentration of P*i*PrOx added. The addition of *n*BuOX reduced the gelation Temperature (LCST) to 29ºC making it suitable for use within a cell culture environment. Rheology was used to investigate the gelation temperature by measuring the stiffness of the gel and its variation over the temperature range. Reducing the concentration

by weight of the polymer reduced the gelation temperature. A 6% gel in MEM was deemed suitable for cell culture.

The aim of this work was to use the thermo-gel will be used to aid in cell sheet engineering by allowing the formation of a sheet of cells on its surface, which can sediment through the gel upon decreasing the temperature and centrifugation (Figure 103). This presents a high throughput method for cell sheet engineering.

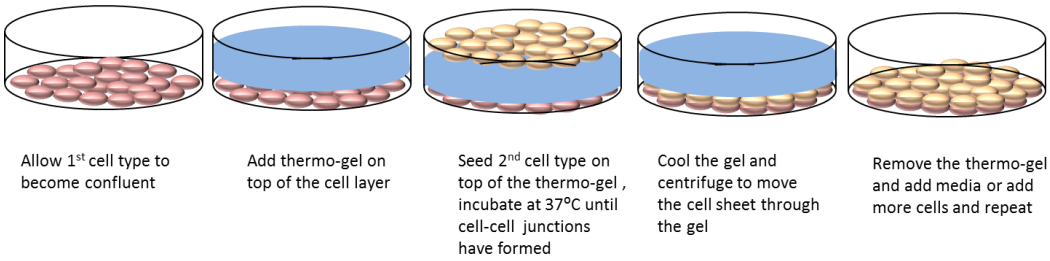

Figure 103 Schematic of the proposed method for the use of the thermo-gel for cell sheet engineering.

This chapter will focus on the initial cell interactions with the oxazoline thermo-gel and a comparison of co-culture models created using various methods.

6.1 Biocompatibility

To determine the biocompatibility of the thermo-gel, 3 x 10^4 16HBE cells were seeded in a 96 well plate and allowed to adhere to the surface overnight. 100µl of the thermo-gel was added on top of the cells and incubated for 2 hours. The gel was then removed and the cells stained with 7AAD dead stain. Figure 104 shows that very few cells had died during the incubation with the gel. As the gel was biocompatible it was used to allow cells to form a sheet on its surface.

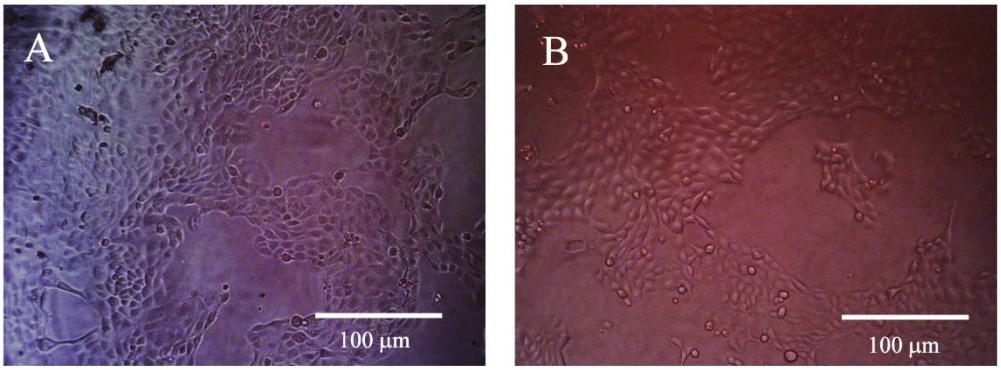

Figure 104 Biocompatibility of the Thermo-gel.
16HBE cells were seeded in a 96 well plate and allowed to adhere overnight. 100µl of thermo-gel was placed on top (A) for two hours, B remained with medium on top. After 2 hours the gel was removed and the dead stain 7AAD placed on top for 10 minutes.

The 1.5 x 10^4 16HBE cells were seeded on to the top of the thermo gel and incubated at 37ºC for 2 hours. 2 hours was chosen based on experiments in the Sonotweezers device, as this was the time when adherens junctions started to form but the actin cytoskeleton had not started to contract as shown in (Figure 54). Under these conditions, the cells did not form a confluent layer on top of the thermo-gel. Instead they formed aggregates (Figure 105 and Figure 106). The aggregates had a similar morphology to those created in the Sonotweezers device suggesting that although they had not formed a sheet they had started to form cell-cell contacts and thus may function in a similar way to the Sonotweezers formed aggregates.

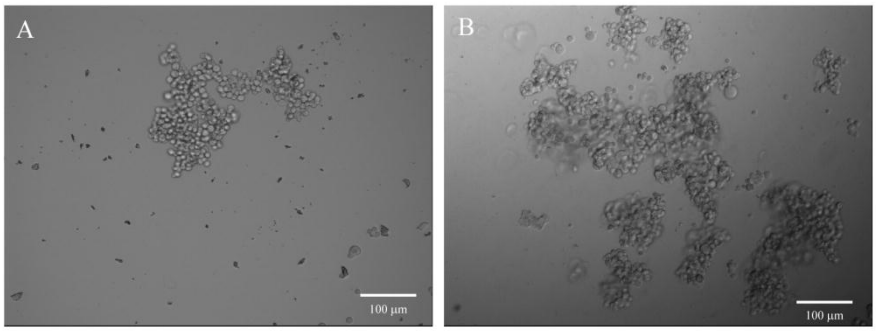

Figure 105 Comparison of aggregates created by levitation within the Sonotweezers device and seeding on to the thermo-gel. 16HBE cells were levitated for 2 hours within the Sonotweezers device before being dropped (A) or seeded on top of the Thermo-gel for 2 hours before being removed (B).

6.2 Formation of co-cultures

To determine whether the aggregates formed on the gel would form a co-culture they were captured with a pastette and transferred onto a confluent layer of MRC5 cells within a transwell. The aggregated grew across the cell layer in a similar way to the Sonotweezers created aggregates (Figure 106)

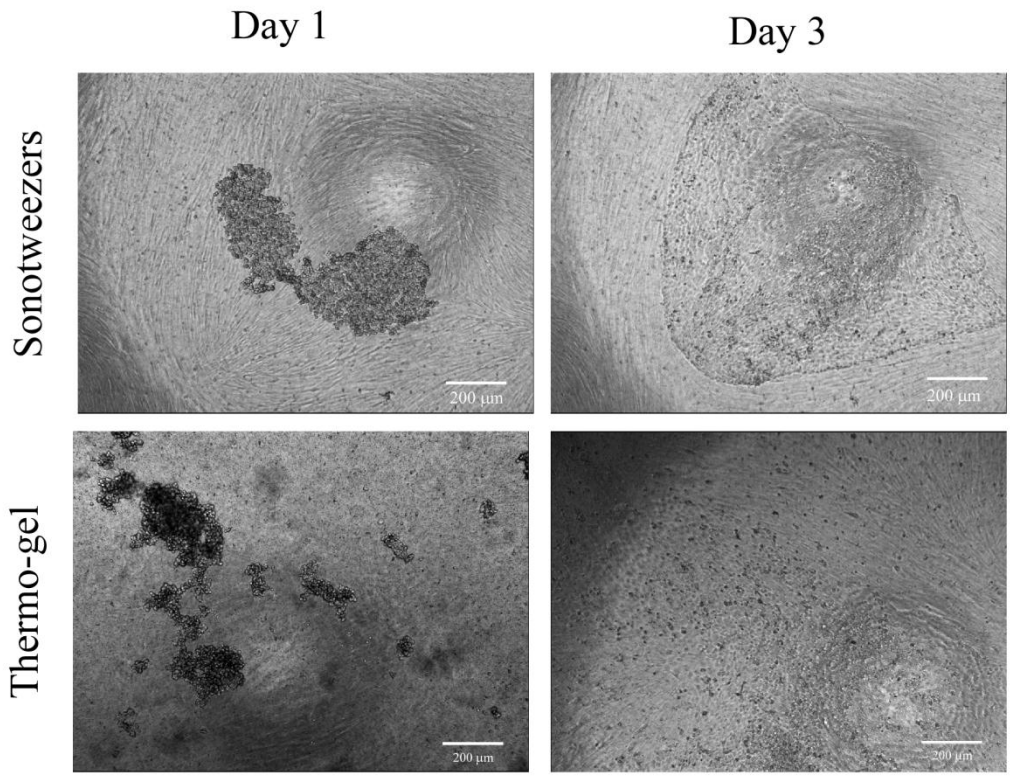

Figure 106 Comparison of phase images of Sonotweezer and Thermo-gel aggregates at day 1 and day 3. MRC5 cells were seeded onto a transwell and allowed to adhere overnight at 37ºC. 16HBE cells were either levitated within the Sonotweezers device for 2 hours (images from Figure 69) or seeded on to the thermo-gel and incubated for 2 hours. The aggregates formed where then transferred onto the confluent MRC5 cell layer. Phase images were taken at day 1 and day 3 of the culture. Scale bar shows 200µm.

The epithelial cell aggregates formed on the thermo-gel grew across an MRC5 fibroblast layer similarly to those formed within the Sonotweezers. However the leading edge of the cells was not as well defined, most likely due to the increase in aggregate number, as various aggregates meet rather than a single aggregate growing across the whole fibroblast layer.

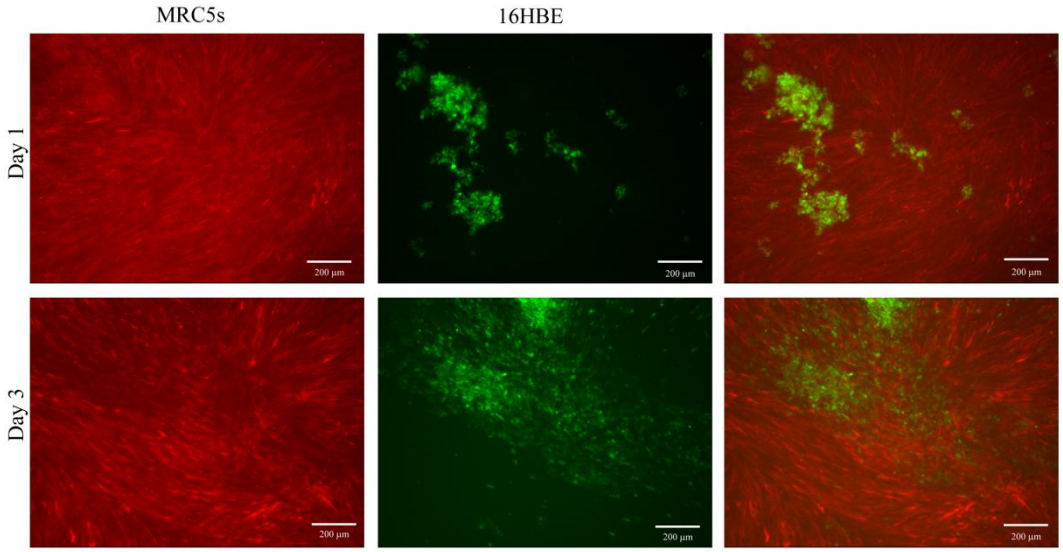

Figure 107 Thermo-gel co-cultures at day1 and day 3 of culture. DsRed MRC5 cells were seeded onto a transwell and allowed to adhere overnight at 37ºC. GFP 16HBE cells were seeded on to the thermo-gel and incubated for 2 hours. The aggregates formed were then transferred onto the confluent MRC5 cell layer. Fluorescent images were taken at day 1 and day 3 of the co-culture. Images were taken using a fluorescent light microscope, representative of 2 repeats. Scale bar shows 200µm.

Use of GFP-16HBE cells and DsRed MRC5 cells showed that the 16HBE cells grew across the top of the MRC5 layer (Figure 107), as seen with the co-culture created using the cell sheet from the Sonotweezers device.

The epithelial cell aggregates were allowed to grow until they formed a confluent sheet on top of the fibroblasts. After 10-14 days, the TER was measured and found to be around 1000Ω. However when these cell-sheet co-cultures were imaged using confocal microscopy, the MRC5 cells were reduced in number and some of the 16HBE cells were in contact with the transwell membrane (Figure 108).

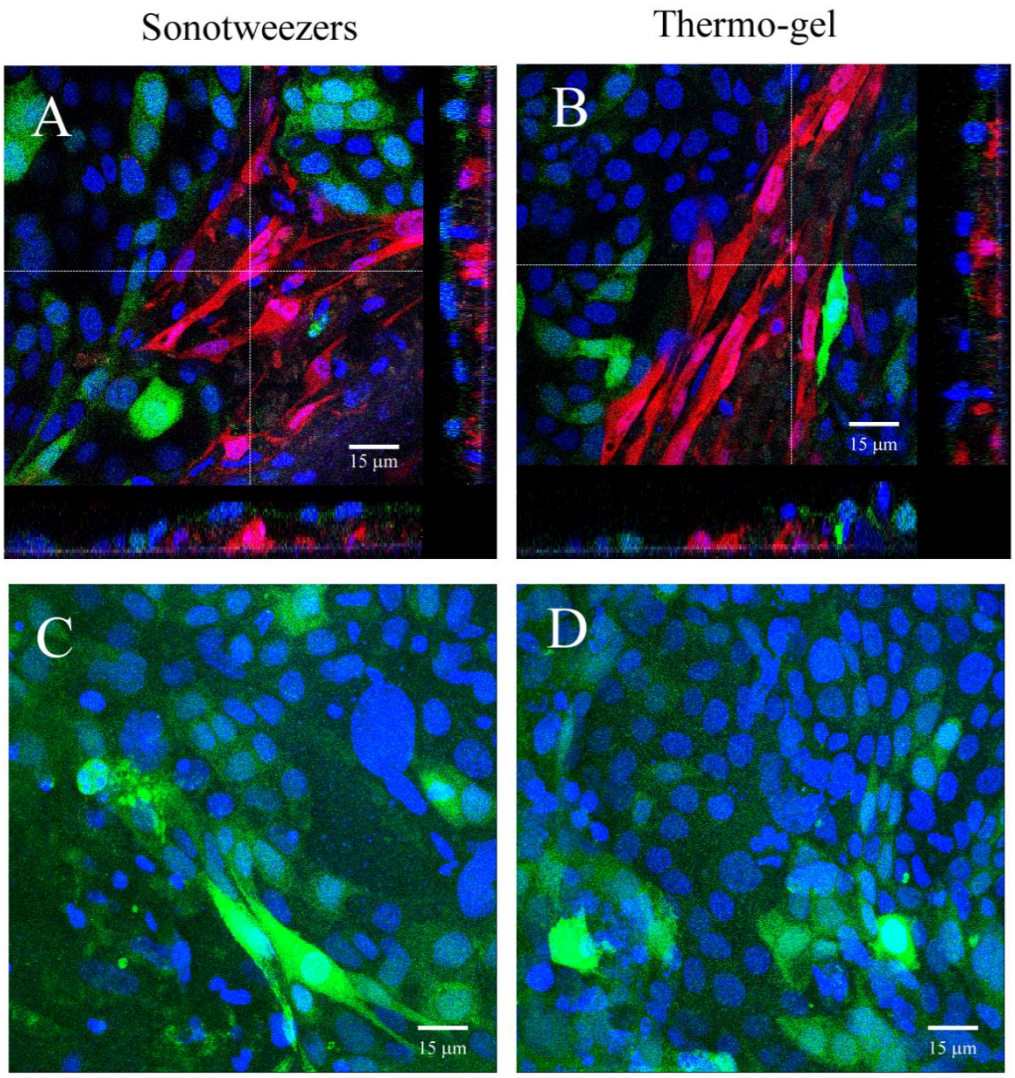

Figure 108 Cell-sheet co-cultures at day 10. A cell sheet of GFP 16HBE cells created either in the Sonotweezers device for 2 hours or on the thermo-gel for 2 hours was then placed on to a confluent DsRed MRC5 layer on a transwell. The cells were then grown for 10 days before being fixed using acetone:methanol (1:1) and the nuclei stained using dapi and imaged using a confocal microscope. A and B show the area next to the transwell membrane. C and D show the confluent 16HBE layer over the MRC5 cells. Representative of 2 repeats. Scale bar shows 15µm.

Although there was not a complete layer of MRC5 cells underneath the 16HBE cells, the fibroblasts were still in close contact with the 16HBE cells and, most importantly, the epithelial cell sheet was continuous over the fibroblast layer. This is in contrast with the initial studies using single 16HBE cells which formed islands of epithelial cells surrounded by fibroblasts (Figure 29). Therefore it was decided to assess the function of the co-cultures.

6.3 Comparison of co-cultures

As co-cultures could be created using both the Sonotweezers device and the thermo-gel producing cultures with TER readings of around 1000Ω suggesting they formed a barrier, their responses were compared with the current co-culture methods used. To test the new co-culture systems with the existing co-cultures they were stimulated with the viral mimic Poly (I:C).

Six conditions were set up within transwells (Figure 109): monoculture controls of 16HBE cells (A) or MRC5 fibroblasts (B) seeded in the apical compartment, a non-contact co-culture with MRC5 cells on the base of the well and 16HBE cells within the apical compartment (C), a membrane co-culture with MRC5 cells on the base of the transwell and 16HBE cells within the apical compartment (D) and the cell-sheet co-cultures created using the device or the thermo-gel (E). These were grown until a barrier had formed for the cell-sheet co-cultures or 6 days for the rest. On day 6 the cells were stimulated with 1µg/ml of Poly (I:C) the TER was read at 1, 6 and 24 hours. After 24 hours the supernatants were harvested for analysis using ELISA.

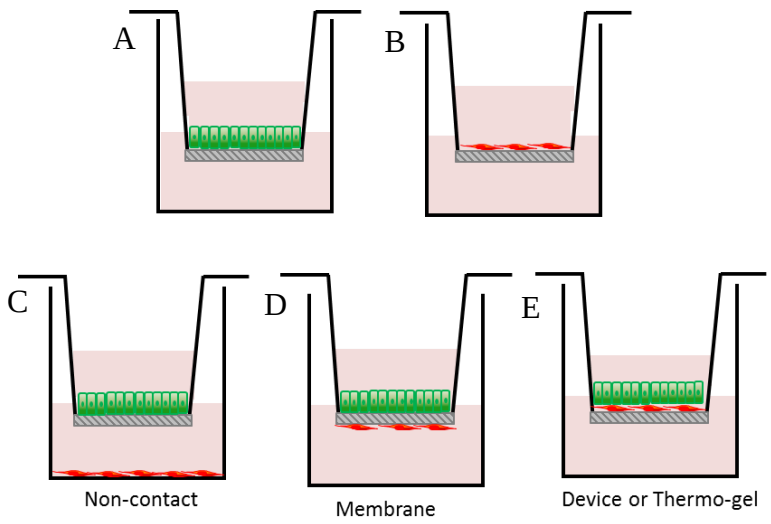

Figure 109 Schematic representation of co-cultures used.
A shows 16HBE alone in the apical compartment. B shows MRC5 alone in the apical compartment. C shows the non-contact co-culture, here the MRC5 cells are seeded on the bottom of the well and the 16HBE cells were seeded within the apical compartment. D shows the membrane co-culture, here the MRC5 cells were seeded on the underside of the transwell and the 16HBE cells were seeded within the apical compartment. E shows the cell-sheet co-culture, here c16HBE cell sheet created within the Sonotweezers or on the thermo-gel are added on to the top of a confluent layer of MRC5 cells on the apical compartment of the transwell.

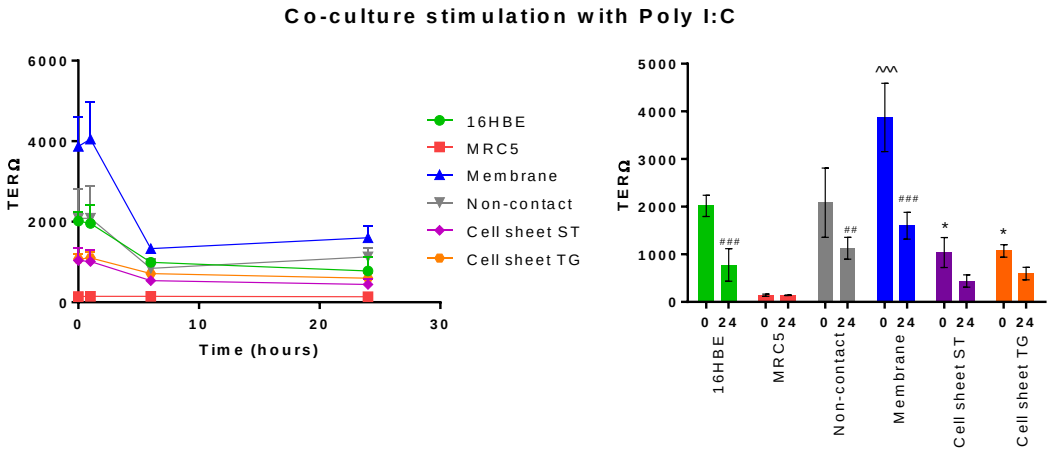

Figure 110 TER decrease with Poly(I:C) stimulation.
1µg/ml of Poly(I:C) was added to the apical compartment of the co-cultures, the TER was read at 1 hour, 6 hours and 24 hours after stimulation. # shows significant decrease compared to control. ^ shows significantly higher than all conditions at that time point. * Shows significant decrease compared to all conditions at that time point.

The TER readings showed that without stimulation the membrane co-culture had a significantly higher reading than all other models. Suggesting it had the tightest barrier due to the interaction of the MRC5 and 16HBE cells. The MRC5 cells did not form a barrier as they do not form the elaborate cell-cell junctions seen in epithelial cell sheets. The cell-sheet co-cultures had a significantly lower TER than all other models containing epithelial cells. We postulate that this may be due to the lower number of 16HBE cells which were added as sheets. Stimulation with Poly(I:C) caused a significant decrease in TER reading after 24 hours for 16HBE, non-contact and membrane co-cultures. Although not a significant decrease in TER for the cell-sheet co-cultures, there is still a downward trend.

The supernatants from the stimulated and control wells were harvested from the apical and basal compartments and analysed using ELISA for interleukin 6 (IL-6) and Interferon -γ-inducible protein 10 (IP-10 CXC10) cytokine release to determine whether the different co-culture configurations affected the response to the viral mimic.

In all models, challenge with poly IC increased apical IL-6 release with a significant increase for 16HBE and MRC5 monocultures. However, there was a trend for the total amount of IL-6 released from the cell sheet ST (Sonotweezers) or Cell sheet TG (thermo-gel) co-cultures to be greater when stimulated with poly (I:C) compared to all conditions, with a significant increase from the Cell-sheet ST. It was also notable that the baseline IL-6 was higher in the non-stimulated cell-sheet ST or cell-sheet TG co-culture models. This may be because the MRC5s detected the SV40 large T antigen that was used to

immortalise the 16HBE cells. Thus, when comparing the percentage change in response to poly IC, the increase was similar in all co-culture conditions.

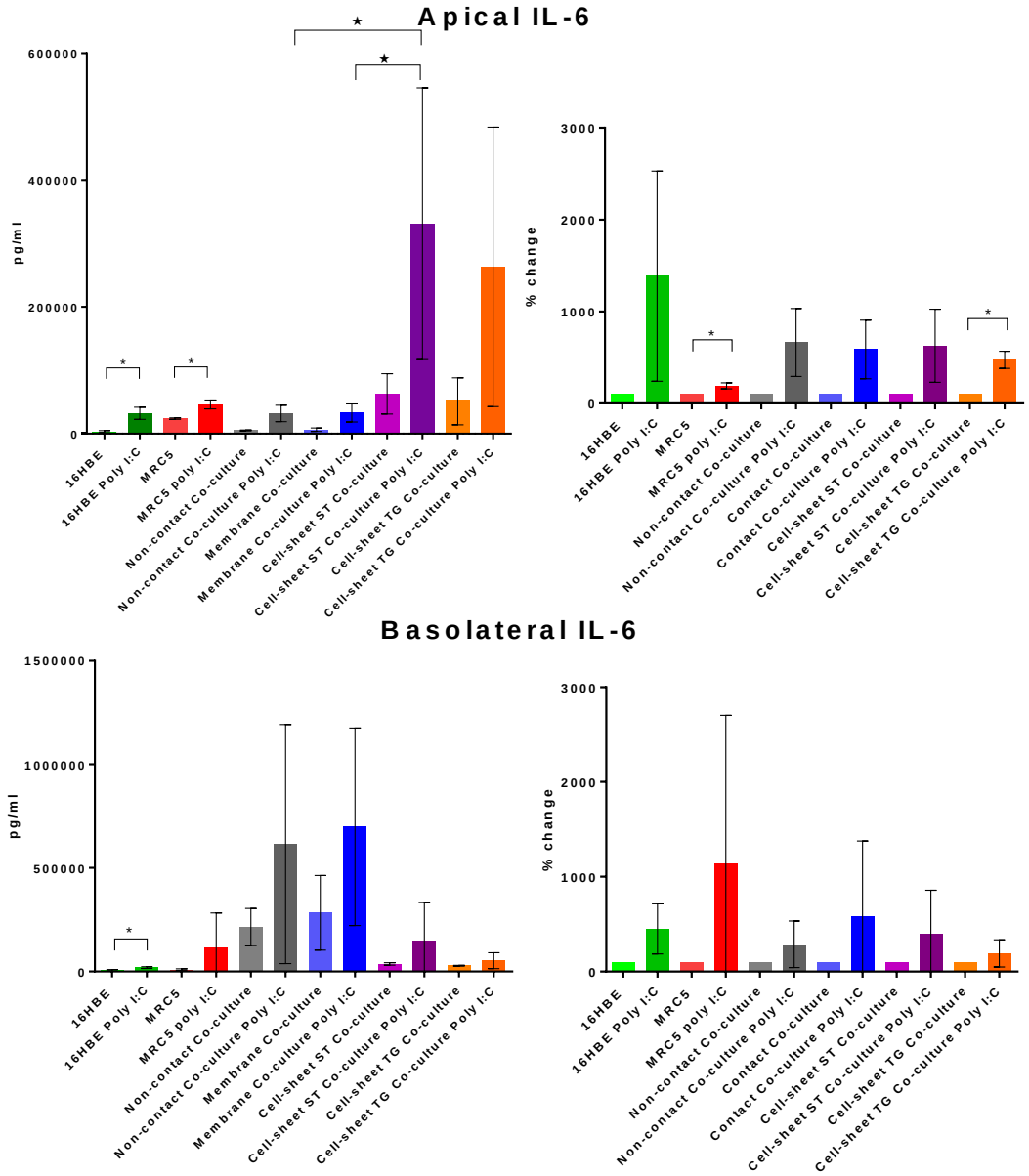

Figure 111 Apical and Basolateral release of IL-6 from various constructions of co-cultures. Statistical analysis carried out using t test to determine the difference between control and poly(I:C) stimulation or Two way Anova with Tukey's multiple comparison to compare the effect of the co-cultures. N=3

There was also an increase in basolateral IL-6 release in all conditions challenged with poly IC. Similar to that observed in the apical compartment of the cell-sheet co-cultures, the

baseline basolateral release of IL-6 in the non-contact and membrane co-cultures was higher, consistent with the fibroblasts sensing the viral antigen in the epithelial cells. As a consequence, the percentage increase of IL-6 in the co-cultures was similar. In summary, there was greater apical release of IL-6 from the cell sheet co-cultures compared to the membrane and non-contact models. This was possibly due to the fibroblasts being on the apical side of the transwell so releasing their cytokines into the apical compartment.

There was a trend for an increase in apical IP-10 in response to poly (I:C) in the membrane and non-contact co-cultures, but no effect in the cell sheet models. In contrast, the pattern of basolateral release of IP-10 in response to poly (I:C) was reversed, with the cell sheet cultures releasing more IP-10 than the membrane or non-contact models. This suggests that the direct contact between the epithelial cells and the fibroblasts changes the direction of release of the cytokine. However, overall the amounts of IP-10 released basolaterally was higher for all conditions.

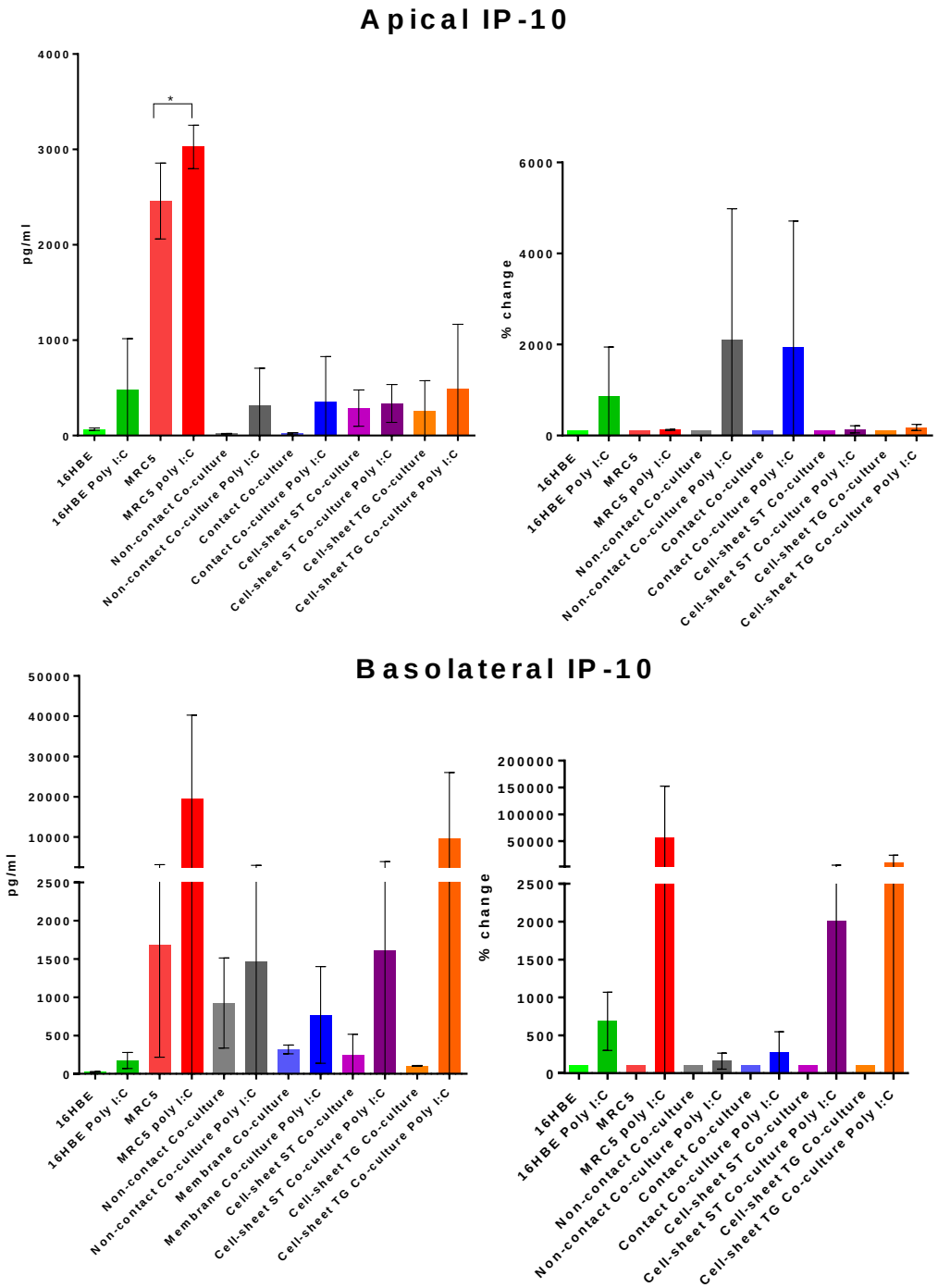

Figure 112 Apical and Basolateral release of IP-10 from various constructions of co-cultures. Statistical analysis carried out using t test to determine the difference between control and poly(I:C) stimulation or Two way Anova with Tukey's multiple comparison to compare the effect of the co-cultures. N=3

6.4 Discussion

This chapter investigated the use of a Thermo-gel to aid in the creation of a cell sheet engineered co-culture model and how the cell sheet co-cultures differ from conventional co-culture systems.

Current cell sheet engineering involves the removal of a cell sheet from a thermoresponsive polymer coated surface. As discussed in chapter 3 this method is not well suited for our model of interest due to the large forces needed to release the epithelial cells from the surface. The use of a thermo-gel would reduce these forces as the cells are not fully attached to the gel compared with when they are on a solid surface. To the best of our knowledge a thermo-gel has never been investigated to create a cell sheet. The thermo-gel was not stiff enough to allow the formation of a single cohesive sheet, possibly due to the 16HBE cells not being able to adhere efficiently to the soft surface. Pelham *et al* investigated the behaviour of rat kidney epithelial cells on a soft collagen coated polyacrylamide surface. On the soft surface they showed irregularly shaped focal adhesions which were highly dynamic whereas on a stiff surface they had normal morphology and were more stable, suggesting that the stiffness of a surface causes morphological changes in the cells (Pelham and Wang, 1997). The 16HBE cells formed aggregates on the gel surface which were similar to those seen in the Sonotweezers device suggesting that adherens junctions had started to form between those cells which were in contact.

The formation of a sheet over the confluent layer of fibroblasts was similar to that seen by the cell sheet formed in the Sonotweezers device. The sheets of cells moved using plithotaxis (Trepat and Fredberg, 2011) moving as one across the confluent fibroblast layer. However after 10 days the MRC5 cells are no longer a confluent layer. This may be due to fibroblast cell death over time, or because the 16HBE cells sense the stiff membrane under the fibroblasts and prefer to adhere to this. Regardless of the reorganization of the fibroblast layer, the epithelial cell sheet remained continuous and there were still areas of close contact between the different cell types. Therefore, the cell-sheet co-culture models were used to investigate their cytokine release when stimulated with Poly (I:C). Poly (I:C) is an artificial double stranded RNA viral mimic composed of 1 strand of Inosines and 1 strand of cytidines. Comstock *et al* showed that Poly (I:C) disrupted tight junctions in 16HBE cells (Comstock et al., 2011) and similar responses were observed in the co-culture models. Ritter *et al* showed that primary small airway epithelium when stimulated with Poly (I:C) secrete increased levels of IL-6 and IP-10 (Ritter et al., 2005). IL-6 is a cytokine

that supports the differentiation of B cells (Hirano et al., 1986) and IP-10 is a chemoattractant for activated T lymphocytes (Taub et al., 1993). The present study showed that the total amount of IL-6 produced in the apical compartment of the cell-sheet co-cultures was higher than that in any other cell configuration and this tended to increase in response to Poly (I:C) stimulation. Further studies will be required to demonstrate a statistically significant increase. The 16HBE cells are virally transformed and it is likely that the MRC5 cells detected this viral antigen resulting in release of IL6 and IP-10. The larger amount of IL-6 released apically in the cell-sheet co-cultures may be due to the fibroblasts being in the apical compartment. In the other co-cultures where the basolateral total amount is greater the fibroblasts are located under the transwell in the basal compartment. The reverse was seen with the IP-10 where there was a much larger response seen in the basal compartment by the cell-sheet co-cultures. The IP-10 attracts lymphocytes from the circulation so might be secreted basally *in vivo*.

In summary, the use of an oxazoline based thermo-gel allows production of bronchial epithelial cell sheets which can be transferred onto a confluent layer of fibroblasts where the cell sheet grows across the fibroblasts creating a co-culture where the epithelial cells form an electrically tight barrier and the two cell types are in direct contact. Challenge of these co-culture models with poly (I:C) causes disruption of the epithelial barrier, as is the case with current co-culture models. The cell-sheet co-culture models increase their production of IL-6 and IP-10 after stimulation with Poly (I:C), with IL-6 being secreted mostly apically and IP-10 being secreted mostly basally. This is in contrast with current models.

7. Final discussion

The aim of this project was to create a multi-layered cell culture model for the study of asthma and other airway diseases using cell sheet engineering.

7.1 Overview

This current work showed that cohesive bronchial epithelial cell sheets could be created using either the Sonotweezers device or the thermo-gel P*i*PrOx-co-*n*BuOx-CMC; when these sheets were overlaid on to a fibroblast layer within a transwell, the epithelial cells grew across the top of the fibroblasts and created a barrier that responded to stimulation with enhanced cytokine release. This model represents an advance over the majority of models where co-cultures are created either using a transwell system where the cells are physically separated by the transwell membrane (Chowdhury et al., 2010), or using collagen gels which contain fibroblasts and are overlaid with epithelial cells (Hoang et al., 2012). In the former case, the membrane prevents intimate cell-cell contact and in the latter case, the dimensions of the gel are much larger than would be found *in vivo*.

The tissue engineering was split into two methods within this project, the use of the Sonotweezers device and the use of thermoresponsive polymers. However, in addition to the technical considerations, there were various biological hurdles which needed to be overcome to allow the best use of both methods.

7.2 Biological considerations

The most important part of this project was the use of epithelial cell sheets as a method for creating the desired co-culture model. From the study, it became evident that epithelial cells behaved differently when used as single cells or as a cohesive sheet of cells. These differences were largely attributable to the cell-cell and cell-matrix adhesive interactions. As shown in Figure 113, a mature epithelium has numerous cell-cell and cell-matrix contacts. Most central to the considerations of the current study were the adherens junctions (Gumbiner et al., 1988) and the focal adhesions, both of which link to the actin cytoskeleton (Burridge and Chrzanowska-Wodnicka, 1996).

Usually, when epithelial cells are seeded as a single cell suspension *in vitro*, their first contacts are with the matrix (eg. cell culture plastic coated with ECM such as fibronectin from serum). Formation of focal adhesions (Burridge and Chrzanowska-Wodnicka, 1996)

allows the cells to attach and move around until they come into contact with another cell, when cell-cell junctions are formed (Gumbiner et al., 1988). Initial studies placing a single cell suspension of epithelial cells onto a confluent layer of fibroblasts highlighted the need for the epithelial cells to form contacts with the substratum, as the epithelial cells took over the space previously occupied by fibroblasts. This is probably because the culture is highly dynamic with the less adherent fibroblasts moving around the culture dish, allowing the epithelial cells to find an area to attach to. For this reason, cell sheet engineering was adopted as a strategy for creating a multi-layered cell model.

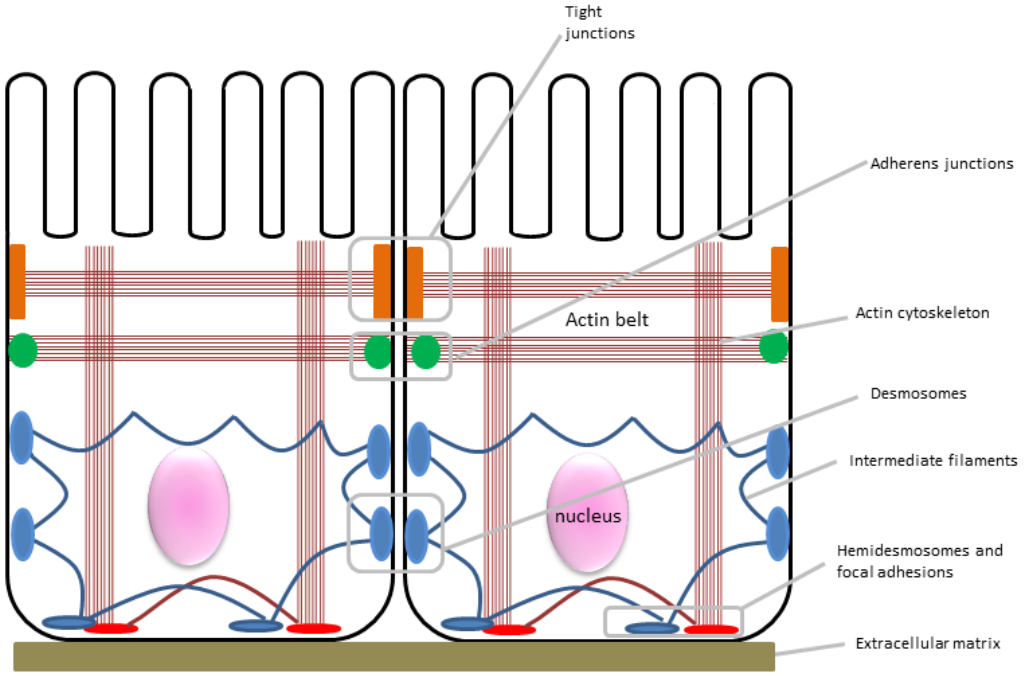

Figure 113 Schematic of cell-cell and cell-matrix interactions

The initial strategy involved development of a confluent layer of epithelial cells on a thermoresponsive polymer. However, releasing and transferring the cells was a significant hurdle as there was contraction of the cell sheet when released from the surface. This was again due to the adhesive properties of the epithelial cells and their links with the actin cytoskeleton. Epithelial cells bind to the tissue culture dish using hemidesmosomes and focal adhesions. These two junctions bind to the surface using integrins, which bind to a recognition site on the ECM coating the dish (Burridge and Chrzanowska-Wodnicka, 1996), often the amino acid sequence Arginine-Glycine-Aspartic acid (RGD) (Pierschbacher and Ruoslahti, 1984). The integrins through focal adhesions are also linked to the actin cytoskeleton (Burridge and Chrzanowska-Wodnicka, 1996) which helps maintain the structural rigidity of the cell sheet; without these links to the ECM, the actin cytoskeleton contracts (Wei et al., 2013). When releasing cell sheets from the UpCell dish,

disruption of the cell-matrix contacts caused contraction of the cell sheet and increased the risk of folding of the sheet (Wei et al., 2013). While folding could be minimised by using the membrane for lifting the cells, the risk of damage to the cell surface by the membrane (eg. damage to cilia on fully differentiated epithelium) was something that we wished to avoid through use of the Sonotweezer device. However, cell detachment and levitation from the polymer surface could not be achieved using either bronchial epithelial cells or poorly adhesive HeLa cells, since the forces required for release of cells from the polymer exceeded those generated by the Sonotweezers by almost three orders of magnitude (Takamizawa et al., 2002) (Tang et al., 2012) (Weder et al., 2010).

Having failed to optimise a protocol for creation and release of a mature cell sheet on a thermoresponsive surface using the Sonotweezers device, a second approach was adopted in which the device was used to levitate single cells in order to create a sheet. Here, the aim was to bring cells together to facilitate formation of cell-cell junctions, without the need for attachment to the ECM to allow the cells to move to find a neighbouring cell. The most important cell-cell junctions for this process are the adherens junctions (Gumbiner et al., 1988). Although the cells within the Sonotweezers device did make adherens junctions, they did not achieve the spread morphology of 16HBE cells on a tissue culture surface. Instead, cell aggregates were formed within the Sonotweezers device after 24 hours and by 5 days the cells had formed compact 3D structures. Again the interplay between cell-cell adhesion and assembly of the actin cytoskeleton was important for these effects (Gumbiner et al., 1988). From a control experiment where the cell junctions were disrupted by the removal of calcium (Chappuis-Flament et al., 2001) it was shown that 16HBE cells started to form adherens junctions after 2 hours and these were completely formed after 6 hours. Consistent with this, when cells were levitated in the Sonotweezer device for short time periods, they retained a 2D organization. To confirm that the adherens junctions formed at areas of cell-cell contact, the cells were captured after 1, 2 and 6 hours. After 2 hours the E-cadherin was localised at the areas of cell-cell contact but no contraction was seen, after 6 hours the E-cadherin was still localised at areas of cell-cell contact but the aggregate had contracted. This suggested that the optimal time point for the creation of a cell sheet without contraction of the actin cytoskeleton was 2 hours. The importance of the actin cytoskeleton was investigated using cytochalasin D (CD) which disrupts the actin cytoskeleton (Brown and Spudich, 1981); this allowed the formation of cell-cell contacts but not the contraction into a 3D aggregate. While use of CD would have prolonged the window for formation and transfer of the cell sheet, it was decided that this

was not an improvement in the method as several washing steps would be required to remove the CD from the cell sheet prior to placement on the fibroblasts, as the CD would also cause disruption of the fibroblast cytoskeleton. Also when levitating for longer than 2 hours, the cell viability decreased, probably due to programmed cell death which can occur when cells are detached from the matrix; this is known as anoikis (Frisch and Francis, 1994). Alternatively, Chen *et al* determined that cell shape could signal whether the cell would undergo apoptosis or survive. They investigated human and bovine capillary endothelial cells on a surface micropatterened with islands of varying sizes of ECM protein. This showed significantly increased cell death in cells which were rounded in morphology compared to those which had spread on the substrate (Chen et al., 1997). Based on all these considerations, minimizing the time for cell sheet formation was deemed the best way to retain viability and maintain a 2D structure.

Once an epithelial sheet was generated, its behaviour was compared to that of single cells. Time-lapse microscopy showed that the cells moved in a coordinated fashion similar to a wound healing response. In a scratch wound assay, the epithelial cells move across the scratched area with a collective motion known as plithotaxis (Trepat and Fredberg, 2011). Plithotaxis is the collective cell movement mediated by the physical forces across cell-cell junctions (Tambe et al., 2011). By exploiting this plithotactic response, it was possible for small cell sheets to be placed on top of, and grow over, a fibroblast layer to form a discrete epithelial cell layer over the fibroblast layer. Furthermore, the epithelial-fibroblast cultures had TER readings of between 800 and 1000Ω indicating that an electrically tight barrier had formed. The barrier formation suggested that the epithelial cells have structurally and functionally polarised forming a cohesive sheet across the whole of the transwell and that all cell-cell junctions had formed (Wan et al., 2000). This suggested that the model had achieved some of the key biological conditions that are relevant for the tissue of interest. In particular, the cell configuration in the cell-sheet co-culture created is biologically more relevant than current models which are separated by medium or a transwell membrane. However, while, the creation of the two distinct cell layers was initially seen, as the time progressed the fibroblast layer was no longer confluent, although it always remained underneath the 16HBE cell layer. This may be due to several reasons, for example, the fibroblasts may have reorganised themselves to a better approximation of their *in vivo* state, or they may not be creating mature collagen (Lyons and Schwarz, 1984) to support the epithelial cells. As a consequence, the epithelial cells may eventually ‘burrow’ through the

fibroblast layer to make attachments with the stiff Transwell membrane. Further work will be required to assess these possibilities (section 7.4).

The physical barrier properties of the bronchial epithelium are essential for protection of the internal milieu of the lung against the inhaled particles, bacteria, viruses etc. (Xiao et al., 2011). To determine whether the close contact of the epithelial cells and fibroblasts provided different information from current models, it was tested with the viral mimic, poly (I:C). The results showed that there was a difference in the direction that the cytokine IP-10 was secreted suggesting that the close contact does affect how the cell types interact with each other. Also the IL-6 results showed greater total IL-6 release within the apical compartment possibly due to the MRC5 detecting the SV40 large T antigen used to transform the 16HBE cells. This should not occur when primary cells are used.

7.3 Tissue engineering considerations

Several novel tissue engineering approaches were used in the current work. These were focussed on use of the Sonotweezers device to levitate cells and use of thermoresponsive polymers to find methods to create sheets of bronchial epithelial cells.

Although initial plans had aimed to use the Sonotweezers device to levitate a mature cell sheet, the strength of the integrin interactions with the base of the UpCell dish even when cooled was too great for the Sonotweezers device to levitate even single cells (Takamizawa et al., 2002) (Tang et al., 2012) (Weder et al., 2010). This led to the project following two different paths, the formation of cell sheets within the Sonotweezers device without any interaction with a surface, or the use of a novel thermoresponsive oxazoline based polymer.

Oxazolines are thermoresponsive polymers (Lin et al., 1988) which had not been characterised previously for use as a cell attachment surface. There were initially several problems with the use of the oxazolines as a surface, but this was solved by covalent attachment to glass coverslips. Consequently, methods also needed to be optimised for creation and use of a culture well on the glass surface and for subsequent analysis of cell characteristics. This was solved by the use of a cloning ring held in place by silicon grease. A range of oxazoline polymers MeOx, EtOx, *i*PrOx and *n*BuOx were shown to be biocompatible for both 16HBE and MRC5 cells. There are several factors which influence cell adhesion to a surface, the surface chemistry (in the case of the thermoresponsive polymers the wettability at different temperatures), the electrical charge, the surfaces

topology and the stiffness of the substrate. The surface chemistry and charge impact the adsorption of proteins on to the surface. The absorption of proteins then allows the adhesion using integrins which recognise the ECM proteins adsorbed on the surface. For example Choi *et al* have shown that when there is a dense coating of NiPAAm brush polymers on gold slides above the LCST there was absorption of serum proteins but when the polymer was incubated below its LCST the proteins were released aiding in the release of cell sheets from these thermoresponsive surfaces (Choi et al., 2012). Zhang *et al* investigated bottle brush oxazoline surfaces for protein absorption. P*n*PrOx was shown to allow absorption of serum proteins most efficiently out of PMeOx and PEtOx (Zhang et al., 2012). This is possibly why P*i*PrOx provides the best cell culture surface of the oxazoline polymer investigated within this thesis. Cell adhesion has been shown to be improved by a positively charged surface due to the ECM proteins being negatively charged. Lesny *et al* investigated the effect of charge on 2-hydro-xyethyl methacrylate (HEMA) based co-polymers. They found that rat bone marrow stromal cells had improved adhesion on the positively charged hydrogel compared to a negatively charged hydrogel (Lesný et al., 2006). The topology or roughness of the surface has been shown to have both positive and negative effects on cell adhesion. Macro-roughness where irregularities are in the range of 1-100µm have no effect on the cells as they are too large be detected by the cells (Bacakova et al., 2011). Micro-roughness with irregularities 100nm-1µm have been shown to be both positive. Sammons *et al* investigated the effect of surface micro-roughness of titanium dental implants on rat calvarial osteoblast cells. They found that a rough surface increase cell spreading, but that both rough and smooth surfaces allowed cell differentiation and calcification to occur (Sammons et al., 2005). Negative effects have been shown by Sader *at al* who investigated the micro-roughness of titanium on osteoblasts from the femora of Balb/c mice and found that on the rough surfaces the cells did not spread completely and had an altered cell morphology. The mechanisms to why there are differing cell adhesions is still unclear due to the difficulty of defining the types of topography (Bacakova et al., 2011). Nanoscale roughness is thought to have appositive effect on cell adhesion due to its similarity to ECM. Miller *et al* investigated the effect of nanoscale rough ness on a poly(lactic-co-glycolicacid) (PLGA) polymer surface. They showed that rat aortic smooth muscle cells and rat aortic endothelial cells had greater cell density on the nano-structured polymer surfaces compared to a smooth polymer surface (Miller et al., 2004). Variation in stiffness can modify cell adhesion (Pelham and Wang, 1997) and even cause stem cells to modify their differentiation. Engler *et al* showed that naïve mesenchymal stem cells became neurogenic on soft substrates, myogenic on stiffer

substrates and oestrogenic on rigid substrates mimicking the basement membranes found in those parts of the body. Although the release of a sheet of bronchial epithelial cells was not achieved using the polymers, Dworak *et al* have shown that fibroblasts will release from *i*PrOx (Dworak et al., 2014), however a different method of attachment was used. A dilute *i*PrOx solution was incubated for 3 days with stirring, whereas in the current study a more concentrated *i*PrOx solution was incubated overnight with no stirring. Although not useful currently as a thermoresponsive surface, the oxazoline polymers gave good cell viability and had good flexibility (Cesana et al., 2006) (Zarka et al., 2003), allowing modification to suit better the needs of this project. Thus, the thermoresponsive polymers were transformed into a thermo-gel. The use of the thermo-gel will be discussed after the Sonotweezers device as a lot of the information needed to create a cohesive 2D cell sheet was discovered using the Sonotweezers and then applied to the thermo-gel.

The Sonotweezers devices themselves evolved during this project as the biological aspects of forming cell sheets became more apparent. A microfluidic Sonotweezers device was initially used to allow for levitation over a prolonged period, however this was not needed once it was established that the optimum time for a sheet of cells to be formed was very short. The device progressed to a 6 well device; this allowed easy access to the cell sheets and visualisation of the formation of the cell sheets by the addition of a mirrored reflector under the transducer. There were however some problems with the devices as they needed constant maintenance with small wires becoming detached on a regular basis. In addition, they did not produce regular sized cell sheets with one larger sheet or several smaller sheets been produced in each device. The devices were also limited in that they could not be used under sterile conditions - the cells needed to be added when the devices were *in situ* as the devices cannot be moved without disruption of the cell sheets.

To the best of our knowledge, bronchial epithelial cells had not been levitated previously within an ultrasonic trap. As discussed previously, the loss of integrin-matrix signalling can cause anoikis. The effect on cell viability appears to be time dependent with very few dead cells within 1-2 hours of levitation compared to a much larger proportion seen by 24 hours. There is also the possibility that sonoporation was occurring over time. Carugo *et al* showed that sonoporation can occur without the need for a contrast agent suggesting that the effect of the ultrasound could cause small pores in the cell membrane (Carugo et al., 2011). If this occurred during cell sheet formation it could allow the influx of calcium ions which would be detrimental to the cell viability (Trump and Berezesky, 1995). From

immunofluorescent staining, it was determined that after 2 hours the cell sheet had started to form adherens junctions but that contraction had not occurred, making this the best time point for capture of the cell sheet. Although the Sonotweezers device was low throughput with only a small number of aggregates formed per device, it provided easy viewing of how the cells behaved without contact to the matrix. This visualisation meant that the time when the aggregate started to contract could be measured by analysing microscopy data. The devices also allowed easy access to the aggregates once they had been dropped as the devices could easily be removed from the tissue culture plate.

In view of the limitations of the Sonotweezer device, the thermo-gels were created to determine whether a high throughput system could be created to allow the formation of a cell sheet. Thus, the aim was to place the epithelial cells on the gel for 2 hours to allow adherens junctions to form before cooling to allow the gel to undergo a conformational change turning it into a solution; this would allow the cell sheet to sediment onto a second layer of cells by gravity or by the use of centrifugation. As with the Sonotweezer device, the thermo-gel was not stiff enough to allow the formation of a single sheet of flattened epithelial cells as seen on tissue culture plastic. However from the use of the Sonotweezers, we speculated that because the cells remained aggregated together after removal from the gel that they had started to form adherens junctions. This suggested that they would behave in a similar way to those sheets created within the Sonotweezers device and this turned out to be the case. Thus, thermo-gels offer a high through-put method for creating cell sheets with less manipulation needed compared to the Sonotweezers device. However visualisation of the cells on the thermo-gel surface during the 2 hours incubation was much more difficult than using the Sonotweezers as the gel becomes turbid above its LCST causing light scatter from the epi-fluorescent microscope. The thermo-gel also has some auto fluorescence making even stained cells harder to image.

The creation of cell-sheet co-cultures allows the direct contact of two different cell types setting it apart from current methods which have a separation of the cells either by medium, matrix or a transwell membrane (Blume and Davies, 2013). It was the knowledge that cells behave differently in sheets that allowed for the thinking that the smaller cell sheets formed within the device or on the thermo-gel could create these distinct layers. Cell sheet engineering has been a technique used for various cell types, with the majority of research into cardiac tissue for use in transplantation (Matsuura et al., 2013). Here the sheets are all of similar sizes and it was just the adherence of the sheets together which was important, so

the growth across another cell layer has not been investigated. This project showed that the epithelial cell sheet would grow across the top of the confluent fibroblast layer and would form an electrically tight barrier. This allowed the comparison of co-culture systems. The cell-sheet co-cultures currently take longer to achieve a barrier than already established methods as there were fewer 16HBE cells within the sheets. The formation of the co-cultures was generally slightly quicker using the thermo-gel as more small sheets could be created from 1x 96 well plate compared to the number of sheets created within several Sonotweezer devices. One set of thermo-gel created cell-sheet co-cultures achieved a barrier within 6 days, the same time period used for the conventional co-culture methods. Currently the co-cultures cannot be created without manipulation for transferring the cell sheets to the next cell layer.

The aim of this project was to recreate a complex tissue which is formed during embryogenesis. The development of the lung is dependent on epithelial-mesenchymal interaction. The epithelium is derived from the endoderm and the mesenchyme is derived for the mesoderm (Spooner and Wessells, 1970). The mesenchyme induces branching morphogenesis (Rudnick, 1933) and it promotes the epithelial patterning and differentiation (Shannon et al., 1998). The mesenchymal fibroblasts release growth factors such as epidermal growth factor (EGF) and transforming growth factor β (TGF-β). Where EGF is shown to promote morphogenesis and TGF-β was shown to inhibit it (Warburton et al., 2000) it is this balance of mediators which allows the formation of the lung tissue. It is this cross talk between the cells types which we are trying to recreate *in vitro*. So far the model that has been created is closer to the *in vivo* environment than those currently available. The model represents the top layer of the airway mucosa with an epithelial cell layer with a tight electrical barrier and the underlying mesenchymal fibroblast layer. An analysis of the extracellular matrix proteins created by the cells has not yet been carried out. So the creation of a basement membrane between these cell types cannot be determined. The use of 16HBE cells does not recapitulate the epithelial layer completely as this cell line does not create a psuedostratified epithelium and is more representative of basal cells. However the technology used here is transferable to primary cell types. Currently there is no addition of immune cells or endothelial cells showing the blood barrier or smooth muscle layer. However once the techniques are optimised the addition of extra cell layers will be possible.

7.4 Future work

The current project explored novel approaches for creating a tissue engineered construct of the airways. As there was little knowledge of the Sonotweezers and no information concerning the behaviour of bronchial epithelial cells on thermoresponsive polymers prior to beginning the project, much of the project was exploratory. While the project demonstrated the feasibility of the approach for modelling the airways, there is still much work to be done to create a robust system that has day-to-day utility. From the systems studied, it can be concluded that epithelial cell sheets can be created by aggregating cells into a 2D sheet-like structure either by levitation using the Sonotweezers or by seeding onto a thermoresponsive gel. However, neither approach is optimal. The Sonotweezers devices are currently low throughput and need improved sterile handling. This should allow the devices to be set up and used within a sterile environment or enable use of a class two hood prior to moving the device to an incubator. The reproducibility for the size and number of aggregates formed also needs to be improved perhaps by carefully evaluating the acoustic properties of the devices and minimising the effects of streaming. The reliability of the electrical connections also needs to be improved to stop the constant need for soldering small wires back onto the attachments.

As regards the thermo-gels, there are various ways to improve their behaviour. The biocompatibility of the thermo-gel for cell attachment may be improved by the addition of an integrin recognition sequence RGD (Pierschbacher and Ruoslahti, 1984). This may aid in the formation of a sheet of cells on the thermo-gel as the cells will recognise this sequence.

There also needs to be development of a robust method for manipulating the cells sheets to allow placement on the next sheet without the need for manual transfer, as in the current study. For the Sonotweezers, this will need to take into account the observation that not all the cells are levitated when they enter into the device, as transfer of single cells which behave differently from a sheet, may lead to disruption of the cell sheet beneath. One way to overcome this would be to have a defined area within the well that is not underneath the device while cells are levitating, then gently moving the device and the levitated cell sheet over to the confluent cell layer. There is also the possibility of creating a more complex device with several nodes; where different cell types could be added into each node and then manipulated by changing the frequency. However, it would be technically challenging to introduce the different cell types into the device at the set nodes without mixing. The

use of the thermo-gels is technically much simpler than the Sonotweezers; however creation of the co-cultures using the thermo-gels could also be improved. One simple solution would be to centrifuge the cell sheets through the liquefied gel within a transwell reducing the need for manipulation of the cell sheets, so providing a high throughput simple method for cell-sheet engineering. The centrifugation will need optimising to ensure that the cells are not damaged when they meet the next surface.

To overcome the long term reorganization of the cell sheet model that was observed over time, it will be important to ascertain why there appeared to be a decrease in fibroblasts seen under the cell-sheet co-cultures at 10 days. One possibility that needs to be excluded is preferential loss of fibroblasts by cell death. If this is the case, then optimisation of conditions for long term culture of the fibroblasts may be required. If fibroblast viability is not the problem, then it is possible that the epithelial cells burrow through the fibroblast layer to reach the plastic transwell, similar to that observed in the single cell cultures. However, is it noteworthy that in the cell sheet model, the epithelial layer remains continuous whereas in the single cell model, the epithelial cells form islands surrounded by fibroblasts. To prevent the 'burrowing' of epithelial cells through the fibroblast layer, creation of a 'basement membrane' could be tested by overlaying the fibroblast layer with Type IV collagen (Timpl, 1989). Another option would be to stimulate the fibroblast layer to produce its own mature collagen by the addition of ascorbic acid and copper ions before the epithelial cell sheet is transferred to the layer (Lyons and Schwarz, 1984). This would also provide a more robust surface for the epithelial cell sheet to be centrifuged onto when using the thermo-gel possibly aiding in cell viability during creation of the multi-layered cell sheet cultures.

Once the methodologies for creation of the cell sheet models have been optimised, their properties need to be characterised in detail. In this thesis, preliminary studies were undertaken testing the effect of the viral mimic, poly (I:C). Much more work is required to test responses to other challenges (viruses, cytokines, allergens, cigarette smoke etc); this might involve monitoring changes in cytokine responses, but may also require more detailed analysis of barrier properties at functional, morphological and ultra-structural level.

A major obstacle still to be overcome is the incorporation of primary cells into the model. Initially it would be necessary to determine the viability of PBECs when levitated or

cultured on the thermo-gel for two hours, whether they form a cohesive sheet, as with the cell line and whether this sheet will grow across a layer of primary fibroblasts. The next biological issue to be faced would be whether the PBECs will differentiate when on top of the fibroblast layer after formation in the device or on the thermo-gel. *In vivo*, fibroblasts provide factors that support growth of epithelial cells (Pohl et al., 2009), so it is possible that the co-culture will aid in the differentiation of the epithelium. However, it is noteworthy that the different cell types are currently cultured in specialised medium (Tamm et al., 2001) (Gray et al., 1996) which may not support the growth of the other cell type. One solution to this problem would be to compare growth of both cell types in different ratios of both media, to determine the ratio that supports both cell types best. Once optimised, this approach would allow comparison of cultures derived from asthmatic and non-asthmatic donors.

As soon as methodologies for a dual cell type co-culture cell sheet model have been established, the possibility of adding other cell types as sheets should be feasible. For example, endothelial cells could be added first, then a layer of fibroblasts then the epithelial cell layer to recapitulate the complex composition of cells in the airway by the addition of the blood barrier into the model. This could further be improved by the addition of a microfluidic system below the transwell to mimic the circulation, here circulatory immune cells could be flown through the device and the influx of immune cells into the tissue engineered construct be monitored under different conditions and between healthy and asthmatic patients similar to the microfluidics channels within to the lung on a chip device created by Huh *et al* (Huh et al., 2010).

8. References

ABERLE, H., BUTZ, S., STAPPERT, J., WEISSIG, H., KEMLER, R. & HOSCHUETZKY, H. 1994. Assembly of the cadherin-catenin complex in vitro with recombinant proteins. *Journal of Cell Science,* 107**,** 3655-3663.

ADAMS, N. & SCHUBERT, U. S. 2007. Poly(2-oxazolines) in biological and biomedical application contexts. *Advanced Drug Delivery Reviews,* 59**,** 1504-1520.

AKDIS, C. A. & AKDIS, M. 2011. Mechanisms of allergen-specific immunotherapy. *Journal of Allergy and Clinical Immunology,* 127**,** 18-27.

ALLEN, L. T., FOX, E. J., BLUTE, I., KELLY, Z. D., ROCHEV, Y., KEENAN, A. K., DAWSON, K. A. & GALLAGHER, W. M. 2003. Interaction of soft condensed materials with living cells: phenotype/transcriptome correlations for the hydrophobic effect. *Proceedings of the National Academy of Sciences,* 100**,** 6331-6336.

ALLEN, L. T., TOSETTO, M., MILLER, I. S., O'CONNOR, D. P., PENNEY, S. C., LYNCH, I., KEENAN, A. K., PENNINGTON, S. R., DAWSON, K. A. & GALLAGHER, W. M. 2006. Surface-induced changes in protein adsorption and implications for cellular phenotypic responses to surface interaction. *Biomaterials,* 27**,** 3096-3108.

ANKRETT, D., CARUGO, D., LEI, J., GLYNNE-JONES, P., TOWNSEND, P., ZHANG, X. & HILL, M. 2013. The effect of ultrasound-related stimuli on cell viability in microfluidic channels. *Journal of Nanobiotechnology,* 11**,** 20.

AOSHIMA, S. & KANAOKA, S. 2008. Synthesis of stimuli-responsive polymers by living polymerization: Poly(N-isopropylacrylamide) and poly(vinyl ether)s. *Wax Crystal Control: Nanocomposites, Stimuli-Responsive Polymers,* 210**,** 169-208.

ARNAOUT, M., MAHALINGAM, B. & XIONG, J.-P. 2005. Integrin structure, allostery, and bidirectional signaling. *Annu. Rev. Cell Dev. Biol.,* 21**,** 381-410.

AUGSTEIN, J., FARMER, J. B., LEE, T. B., SHEARD, P. & TATTERSA.ML 1973. Selective Inhibitor of Slow Reacting Substance of Anaphylaxis. *Nature-New Biology,* 245**,** 215-217.

BACAKOVA, L., FILOVA, E., PARIZEK, M., RUML, T. & SVORCIK, V. 2011. Modulation of cell adhesion, proliferation and differentiation on materials designed for body implants. *Biotechnology Advances,* 29**,** 739-767.

BAGGIOLINI, M., WALZ, A. & KUNKEL, S. L. 1989. Neutrophil-activating peptide-1/interleukin 8, a novel cytokine that activates neutrophils. *The Journal of clinical investigation,* 84**,** 1045-9.

BATEMAN, E. D., HURD, S. S., BARNES, P. J., BOUSQUET, J., DRAZEN, J. M., FITZGERALD, M., GIBSON, P., OHTA, K., O'BYRNE, P., PEDERSEN, S. E., PIZZICHINI, E., SULLIVAN, S. D., WENZEL, S. E. & ZAR, H. J. 2008. Global strategy for asthma management and prevention: GINA executive summary. *European Respiratory Journal,* 31**,** 143-178.

BAZOU, D., COAKLEY, W. T., HAYES, A. J. & JACKSON, S. K. 2008. Long-term viability and proliferation of alginate-encapsulated 3-D HepG2 aggregates formed in an ultrasound trap. *Toxicol In Vitro,* 22**,** 1321-31.

BAZOU, D., DAVIES, G., JIANG, W. G. & COAKLEY, T. 2006a. Rapid molecular and morphological responses of prostate cell lines to cell-cell contact. *Cell Commun Adhes,* 13**,** 279-94.

BAZOU, D., DOWTHWAITE, G. P., KHAN, I. M., ARCHER, C. W., RALPHS, J. R. & COAKLEY, W. T. 2006b. Gap junctional intercellular communication and

cytoskeletal organization in chondrocytes in suspension in an ultrasound trap. *Mol Membr Biol,* 23**,** 195-205.

BAZOU, D., FOSTER, G. A., RALPHS, J. R. & COAKLEY, W. T. 2005a. Molecular adhesion development in a neural cell monolayer forming in an ultrasound trap. *Mol Membr Biol,* 22**,** 229-40.

BAZOU, D., KUZNETSOVA, L. & COAKLEY, W. 2005b. Physical enviroment of 2-D animal cell aggregates formed in a short pathlength ultrasound standing wave trap. *Ultrasound in Medicine & Biology,* 31**,** 423-430.

BEASLEY, R., ROCHE, W. R., ROBERTS, J. A. & HOLGATE, S. T. 1989. Cellular Events in the Bronchi in Mild Asthma and after Bronchial Provocation. *American Review of Respiratory Disease,* 139**,** 806-817.

BECNEL, D., YOU, D., ERSKIN, J., DIMINA, D. & CORMIER, S. 2005. A role for airway remodeling during respiratory syncytial virus infection. *Respiratory Research,* 6**,** 122.

BISGAARD, H., BØNNELYKKE, K., SLEIMAN, P. M. A., BRASHOLT, M., CHAWES, B., KREINER-MØLLER, E., STAGE, M., KIM, C., TAVENDALE, R., BATY, F., PIPPER, C. B., PALMER, C. N. A. & HAKONARSSON, H. 2009. Chromosome 17q21 Gene Variants Are Associated with Asthma and Exacerbations but Not Atopy in Early Childhood. *American Journal of Respiratory and Critical Care Medicine,* 179**,** 179-185.

BLANCHOIN, L., BOUJEMAA-PATERSKI, R., SYKES, C. & PLASTINO, J. 2014. Actin Dynamics, Architecture, and Mechanics in Cell Motility. *Physiological Reviews,* 94**,** 235-263.

BLANK, F., ROTHEN-RUTISHAUSER, B. & GEHR, P. 2007. Dendritic cells and macrophages form a transepithelial network against foreign particulate antigens. *Am J Respir Cell Mol Biol,* 36**,** 669-77.

BLUME, C. & DAVIES, D. E. 2013. In vitro and ex vivo models of human asthma. *European Journal of Pharmaceutics and Biopharmaceutics,* 84**,** 394-400.

BOKIAS, G., MYLONAS, Y., STAIKOS, G., BUMBU, G. & VASILE, C. 2001. Synthesis and aqueous solution properties of novel thermoresponsive graft copolymers based on a carboxymethylcellulose backbone. *Macromolecules,* 34**,** 4958-4964.

BRESLOW, D. K., COLLINS, S. R., BODENMILLER, B., AEBERSOLD, R., SIMONS, K., SHEVCHENKO, A., EJSING, C. S. & WEISSMAN, J. S. 2010. Orm family proteins mediate sphingolipid homeostasis. *Nature,* 463**,** 1048-1053.

BREWER, J. M., CONACHER, M., HUNTER, C. A., MOHRS, M., BROMBACHER, F. & ALEXANDER, J. 1999. Aluminium hydroxide adjuvant initiates strong antigen-specific Th2 responses in the absence of IL-4- or IL-13-mediated signaling. *J Immunol,* 163**,** 6448-54.

BREWSTER, C. E. P., HOWARTH, P. H., DJUKANOVIC, R., WILSON, J., HOLGATE, S. T. & ROCHE, W. R. 1990. Myofibroblasts and Subepithelial Fibrosis in Bronchial Asthma. *American Journal of Respiratory Cell and Molecular Biology,* 3**,** 507-511.

BROPHY, C. M., LUEBKE-WHEELER, J. L., AMIOT, B. P., KHAN, H., REMMEL, R. P., RINALDO, P. & NYBERG, S. L. 2009. Rat hepatocyte spheroids formed by rocked technique maintain differentiated hepatocyte gene expression and function. *Hepatology,* 49**,** 578-586.

BROWN, H. M., STOREY, G. & GEORGE, W. H. 1972. Beclomethasone dipropionate: a new steroid aerosol for the treatment of allergic asthma. *Br Med J,* 1**,** 585-90.

BROWN, S. S. & SPUDICH, J. A. 1981. Mechanism of action of cytochalasin: evidence that it binds to actin filament ends. *The Journal of Cell Biology,* 88**,** 487-491.

BURCHARD, E. G., SILVERMAN, E. K., ROSENWASSER, L. J., BORISH, L., YANDAVA, C., PILLARI, A., WEISS, S. T., HASDAY, J., LILLY, C. M.,

FORD, J. G. & DRAZEN, J. M. 1999. Association Between a Sequence Variant in the IL-4 Gene Promoter and FEV1 in Asthma. *American Journal of Respiratory and Critical Care Medicine,* 160**,** 919-922.

BURRIDGE, K. & CHRZANOWSKA-WODNICKA, M. 1996. Focal adhesions, contractility, and signaling. *Annu Rev Cell Dev Biol,* 12**,** 463-518.

CAMBIER, S., MU, D.-Z., O'CONNELL, D., BOYLEN, K., TRAVIS, W., LIU, W.-H., BROADDUS, V. C. & NISHIMURA, S. L. 2000. A Role for the Integrin αvβ8 in the Negative Regulation of Epithelial Cell Growth. *Cancer Research,* 60**,** 7084-7093.

CANTERO-RECASENS, G., FANDOS, C., RUBIO-MOSCARDO, F., VALVERDE, M. A. & VICENTE, R. 2010. The asthma-associated ORMDL3 gene product regulates endoplasmic reticulum-mediated calcium signaling and cellular stress. *Human Molecular Genetics,* 19**,** 111-121.

CAPONI, P.-F., QIU, X.-P., VILELA, F., WINNIK, F. M. & ULIJN, R. V. 2011. Phosphatase/temperature responsive poly(2-isopropyl-2-oxazoline). *Polymer Chemistry,* 2**,** 306-308.

CARTER, W. G., RYAN, M. C. & GAHR, P. J. 1991. Epiligrin, a new cell adhesion ligand for integrin α3β1 in epithelial basement membranes. *Cell,* 65**,** 599-610.

CARTERSON, A. J., HONER ZU BENTRUP, K., OTT, C. M., CLARKE, M. S., PIERSON, D. L., VANDERBURG, C. R., BUCHANAN, K. L., NICKERSON, C. A. & SCHURR, M. J. 2005. A549 lung epithelial cells grown as three-dimensional aggregates: alternative tissue culture model for Pseudomonas aeruginosa pathogenesis. *Infect Immun,* 73**,** 1129-40.

CARUGO, D., ANKRETT, D. N., GLYNNE-JONES, P., CAPRETTO, L., BOLTRYK, R. J., ZHANG, X., TOWNSEND, P. A. & HILL, M. 2011. Contrast agent-free sonoporation: The use of an ultrasonic standing wave microfluidic system for the delivery of pharmaceutical agents. *Biomicrofluidics,* 5**,** 044108.

CATES, E. C., FATTOUH, R., WATTIE, J., INMAN, M. D., GONCHAROVA, S., COYLE, A. J., GUTIERREZ-RAMOS, J. C. & JORDANA, M. 2004. Intranasal exposure of mice to house dust mite elicits allergic airway inflammation via a GM-CSF-mediated mechanism. *J Immunol,* 173**,** 6384-92.

CERQUEIRA, M. T., PIRRACO, R. P., SANTOS, T. C., RODRIGUES, D. B., FRIAS, A. M., MARTINS, A. R., REIS, R. L. & MARQUES, A. P. 2013. Human Adipose Stem Cells Cell Sheet Constructs impact epidermal morphogenesis in full-thickness excisional wounds. *Biomacromolecules*.

CESANA, S., AUERNHEIMER, J., JORDAN, R., KESSLER, H. & NUYKEN, O. 2006. First Poly(2-oxazoline)s with Pendant Amino Groups. *Macromolecular Chemistry and Physics,* 207**,** 183-192.

CHANG, B.-J., PRUCKER, O., GROH, E., WALLRATH, A., DAHM, M. & RÜHE, J. 2002. Surface-attached polymer monolayers for the control of endothelial cell adhesion. *Colloids and Surfaces A: Physicochemical and Engineering Aspects,* 198–200**,** 519-526.

CHAPPUIS-FLAMENT, S., WONG, E., HICKS, L. D., KAY, C. M. & GUMBINER, B. M. 2001. Multiple cadherin extracellular repeats mediate homophilic binding and adhesion. *The Journal of cell biology,* 154**,** 231-243.

CHEN, C. S., MRKSICH, M., HUANG, S., WHITESIDES, G. M. & INGBER, D. E. 1997. Geometric Control of Cell Life and Death. *Science,* 276**,** 1425-1428.

CHOI, S., CHOI, B.-C., XUE, C. & LECKBAND, D. 2012. Protein Adsorption Mechanisms Determine the Efficiency of Thermally Controlled Cell Adhesion on Poly(N-isopropyl acrylamide) Brushes. *Biomacromolecules,* 14**,** 92-100.

CHOWDHURY, F., HOWAT, W. J., PHILLIPS, G. J. & LACKIE, P. M. 2010. Interactions between endothelial cells and epithelial cells in a combined cell model

of airway mucosa: effects on tight junction permeability. *Experimental Lung Research,* 36**,** 1-11.

CHRISTOVA, D., VELICHKOVA, R., LOOS, W., GOETHALS, E. J. & PREZ, F. D. 2003. New thermo-responsive polymer materials based on poly(2-ethyl-2-oxazoline) segments. *Polymer,* 44**,** 2255-2261.

COAKLEY, W. T., BAZOU, D., MORGAN, J., FOSTER, G. A., ARCHER, C. W., POWELL, K., BORTHWICK, K. A., TWOMEY, C. & BISHOP, J. 2004. Cell-cell contact and membrane spreading in an ultrasound trap. *Colloids Surf B Biointerfaces,* 34**,** 221-30.

COMSTOCK, A. T., GANESAN, S., CHATTORAJ, A., FARIS, A. N., MARGOLIS, B. L., HERSHENSON, M. B. & SAJJAN, U. S. 2011. Rhinovirus-induced barrier dysfunction in polarized airway epithelial cells is mediated by NADPH oxidase 1. *Journal of virology,* 85**,** 6795-6808.

CORNING, I. 2012. Transwell permeable supports manual.

COZENS, A. L., YEZZI, M. J., KUNZELMANN, K., OHRUI, T., CHIN, L., ENG, K., FINKBEINER, W. E., WIDDICOMBE, J. H. & GRUENERT, D. C. 1994. CFTR expression and chloride secretion in polarized immortal human bronchial epithelial cells. *Am J Respir Cell Mol Biol,* 10**,** 38-47.

CUENDA, A. & ROUSSEAU, S. 2007. p38 MAP-Kinases pathway regulation, function and role in human diseases. *Biochimica et Biophysica Acta (BBA) - Molecular Cell Research,* 1773**,** 1358-1375.

CULLUM, V. A., FARMER, J. B., JACK, D. & LEVY, G. P. 1969. Salbutamol: a new, selective beta-adrenoceptive receptor stimulant. *Br J Pharmacol,* 35**,** 141-51.

DAVIES, D. E. 2009. The Role of the Epithelium in Airway Remodeling in Asthma. *Proceedings of the American Thoracic Society,* 6**,** 678-682.

DE BOER, W. I., SHARMA, H. S., BAELEMANS, S. M. I., HOOGSTEDEN, H. C., LAMBRECHT, B. N. & BRAUNSTAHL, G. J. 2008. Altered expression of epithelial junctional proteins in atopic asthma: possible role in inflammation. *Canadian Journal of Physiology and Pharmacology,* 86**,** 105-112.

DE JONG, P. M., VAN STERKENBURG, M. A., HESSELING, S. C., KEMPENAAR, J. A., MULDER, A. A., MOMMAAS, A. M., DIJKMAN, J. H. & PONEC, M. 1994. Ciliogenesis in human bronchial epithelial cells cultured at the air-liquid interface. *American Journal of Respiratory Cell and Molecular Biology,* 10**,** 271-277.

DE PEREDA, J. M., ORTEGA, E., ALONSO-GARCÍA, N., GÓMEZ-HERNÁNDEZ, M. & SONNENBERG, A. 2009. Advances and perspectives of the architecture of hemidesmosomes: Lessons from structural biology. *Cell Adhesion & Migration,* 3**,** 361-364.

DONNADIEU, E., JOUVIN, M.-H., RANA, S., MOFFATT, M. F., MOCKFORD, E. H., COOKSON, W. O. & KINET, J.-P. 2003. Competing Functions Encoded in the Allergy-Associated FcεRIβ Gene. *Immunity,* 18**,** 665-674.

DREES, F., POKUTTA, S., YAMADA, S., NELSON, W. J. & WEIS, W. I. 2005. α-catenin is a molecular switch that binds E-cadherin-β-catenin and regulates actin-filament assembly. *Cell,* 123**,** 903-915.

DWORAK, A., UTRATA-WESOŁEK, A., OLESZKO, N., WAŁACH, W., TRZEBICKA, B., ANIOŁ, J., SIEROŃ, A. L., KLAMA-BARYŁA, A. & KAWECKI, M. 2014. Poly (2-substituted-2-oxazoline) surfaces for dermal fibroblasts adhesion and detachment. *Journal of Materials Science: Materials in Medicine***,** 1-15.

EDER, W., KLIMECKI, W., YU, L., VON MUTIUS, E., RIEDLER, J., BRAUN-FAHRLÄNDER, C., NOWAK, D. & MARTINEZ, F. D. 2004. Toll-like receptor 2 as a major gene for asthma in children of European farmers. *Journal of Allergy and Clinical Immunology,* 113**,** 482-488.

EDWARDS & HOWELL 2000. The chromones: history, chemistry and clinical development. A tribute to the work of Dr R. E. C. Altounyan. *Clinical & Experimental Allergy,* 30**,** 756-774.

EDWARDS, G. O., BAZOU, D., KUZNETSOVA, L. A. & COAKLEY, W. T. 2007. Cell adhesion dynamics and actin cytoskeleton reorganization in HepG2 cell aggregates. *Cell Commun Adhes,* 14**,** 9-20.

EVANS, M. J., VAN WINKLE, L. S., FANUCCHI, M. V. & PLOPPER, C. G. 1999. The attenuated fibroblast sheath of the respiratory tract epithelial-mesenchymal trophic unit. *American Journal of Respiratory Cell and Molecular Biology,* 21**,** 655-7.

FELDMAN, G. J., MULLIN, J. M. & RYAN, M. P. 2005. Occludin: structure, function and regulation. *Adv Drug Deliv Rev,* 57**,** 883-917.

FRANZ, C. M. & RIDLEY, A. J. 2004. p120 Catenin Associates with Microtubules: INVERSE RELATIONSHIP BETWEEN MICROTUBULE BINDING AND RHO GTPase REGULATION. *Journal of Biological Chemistry,* 279**,** 6588-6594.

FRISCH, S. & FRANCIS, H. 1994. Disruption of epithelial cell-matrix interactions induces apoptosis. *The Journal of Cell Biology,* 124**,** 619-626.

FUJITA, J., ITABASHI, Y., SEKI, T., TOHYAMA, S., TAMURA, Y., SANO, M. & FUKUDA, K. 2012. Myocardial cell sheet therapy and cardiac function. *Am J Physiol Heart Circ Physiol,* 303**,** H1169-82.

GAERTNER, F. C., LUXENHOFER, R., BLECHERT, B., JORDAN, R. & ESSLER, M. 2007. Synthesis, biodistribution and excretion of radiolabeled poly (2-alkyl-2-oxazoline) s. *Journal of controlled release,* 119**,** 291-300.

GALLI, S. J., TSAI, M. & PILIPONSKY, A. M. 2008. The development of allergic inflammation. *Nature,* 454**,** 445-454.

GENGEC, N. A., GULSUNER, H. U., ERBIL, H. Y. & TEKINAY, A. B. 2014. Selective adsorption of L1210 leukemia cells/human leukocytes on micropatterned surfaces prepared from polystyrene/polypropylene-polyethylene blends. *Colloids and Surfaces B: Biointerfaces,* 113**,** 403-411.

GIBSON, J. G., LODDENKEMPER, R., LUNDBACK, B. & SIBELLE, Y. 2013. *European Lung White Book.*

GIPSON, I. K., WESTCOTT, M. J. & BROOKSBY, N. G. 1982. Effects of cytochalasins B and D and colchicine on migration of the corneal epithelium. *Investigative Ophthalmology & Visual Science,* 22**,** 633-42.

GLYNNE-JONES, P., BOLTRYK, R. J. & HILL, M. 2012. Acoustofluidics 9: Modelling and applications of planar resonant devices for acoustic particle manipulation. *Lab on a Chip,* 12**,** 1417-1426.

GODDARD, P., HUTCHINSON, L. E., BROWN, J. & BROOKMAN, L. J. 1989. Soluble polymeric carriers for drug delivery. Part 2. Preparation and< i> in vivo</i> behaviour of< i> N</i>-acylethylenimine copolymers. *Journal of controlled release,* 10**,** 5-16.

GOLDMAN, R. D., CLELAND, M. M., MURTHY, P., MAHAMMAD, S. & KUCZMARSKI, E. R. 2011. Inroads into the structure and function of intermediate filament networks. *J Struct Biol*.

GONZALEZ-MARISCAL, L., BETANZOS, A. & AVILA-FLORES, A. 2000. MAGUK proteins: structure and role in the tight junction. *Semin Cell Dev Biol,* 11**,** 315-24.

GOPLEN, N., KARIM, M. Z., LIANG, Q., GORSKA, M. M., ROZARIO, S., GUO, L. & ALAM, R. 2009. Combined sensitization of mice to extracts of dust mite, ragweed, and Aspergillus species breaks through tolerance and establishes chronic features of asthma. *Journal of Allergy and Clinical Immunology,* 123**,** 925-932.e11.

GRAY, T. E., GUZMAN, K., DAVIS, C. W., ABDULLAH, L. H. & NETTESHEIM, P. 1996. Mucociliary differentiation of serially passaged normal human tracheobronchial epithelial cells. *American Journal of Respiratory Cell and Molecular Biology,* 14**,** 104-112.

GREEN, K. J. & JONES, J. C. 1996. Desmosomes and hemidesmosomes: structure and function of molecular components. *The FASEB Journal,* 10**,** 871-81.

GUMBINER, B., STEVENSON, B. & GRIMALDI, A. 1988. The role of the cell adhesion molecule uvomorulin in the formation and maintenance of the epithelial junctional complex. *The Journal of Cell Biology,* 107**,** 1575-1587.

GÜNZEL, D. & ALAN, S. 2013. Claudins and the modulation of tight junction permeability. *Physiological reviews,* 93**,** 525-569.

HAITCHI, H. M., POWELL, R. M., SHAW, T. J., HOWARTH, P. H., WILSON, S. J., WILSON, D. I., HOLGATE, S. T. & DAVIES, D. E. 2005. ADAM33 Expression in Asthmatic Airways and Human Embryonic Lungs. *American Journal of Respiratory and Critical Care Medicine,* 171**,** 958-965.

HARDYMAN, M. A., WILKINSON, E., MARTIN, E., JAYASEKERA, N. P., BLUME, C., SWINDLE, E. J., GOZZARD, N., HOLGATE, S. T., HOWARTH, P. H., DAVIES, D. E. & COLLINS, J. E. 2013. TNF-α–mediated bronchial barrier disruption and regulation by src-family kinase activation. *Journal of Allergy and Clinical Immunology,* 132**,** 665-675.e8.

HARIMOTO, M., YAMATO, M., HIROSE, M., TAKAHASHI, C., ISOI, Y., KIKUCHI, A. & OKANO, T. 2002. Novel approach for achieving double-layered cell sheets co-culture: overlaying endothelial cell sheets onto monolayer hepatocytes utilizing temperature-responsive culture dishes. *Journal of Biomedical Materials Research,* 62**,** 464-470.

HARTSOCK, A. & NELSON, W. J. 2008. Adherens and tight junctions: Structure, function and connections to the actin cytoskeleton. *Biochimica et Biophysica Acta (BBA) - Biomembranes,* 1778**,** 660-669.

HIRANO, T., YASUKAWA, K., HARADA, H., TAGA, T., WATANABE, Y., MATSUDA, T., KASHIWAMURA, S.-I., NAKAJIMA, K., KOYAMA, K. & IWAMATSU, A. 1986. Complementary DNA for a novel human interleukin (BSF-2) that induces B lymphocytes to produce immunoglobulin.

HOANG, A. T. N., CHEN, P., JUAREZ, J., SACHAMITR, P., BILLING, B., BOSNJAK, L., DAHLÉN, B., COLES, M. & SVENSSON, M. 2012. Dendritic cell functional properties in a three-dimensional tissue model of human lung mucosa. *American Journal of Physiology-Lung Cellular and Molecular Physiology,* 302**,** L226-L237.

HOGAN, S., KOSKINEN, A., MATTHAEI, K., YOUNG, I. & FOSTER, P. 1998. Interleukin-5–producing CD4+ T Cells Play a Pivotal Role in Aeroallergen-induced Eosinophilia, Bronchial Hyperreactivity, and Lung Damage in Mice. *American Journal of Respiratory and Critical Care Medicine,* 157**,** 210-218.

HOLGATE, S. T. 2008. The airway epithelium is central to the pathogenesis of asthma. *Allergol Int,* 57**,** 1-10.

HOLGATE, S. T., DAVIES, D. E., LACKIE, P. M., WILSON, S. J., PUDDICOMBE, S. M. & LORDAN, J. L. 2000. Epithelial-mesenchymal interactions in the pathogenesis of asthma. *Journal of Allergy and Clinical Immunology,* 105**,** 193-204.

HOLGATE, S. T., ROBERTS, G., ARSHAD, H. S., HOWARTH, P. H. & DAVIES, D. E. 2009. The Role of the Airway Epithelium and its Interaction with Environmental Factors in Asthma Pathogenesis. *Proceedings of the American Thoracic Society,* 6**,** 655-659.

HOLLOWAY, J. W., YANG, I. A. & HOLGATE, S. T. 2010. Genetics of allergic disease. *Journal of Allergy and Clinical Immunology,* 125**,** S81-S94.

HOLMES, K. C., POPP, D., GEBHARD, W. & KABSCH, W. 1990. Atomic model of the actin filament. *Nature,* 347**,** 44-49.

HONG, K. U., REYNOLDS, S. D., WATKINS, S., FUCHS, E. & STRIPP, B. R. 2004. Basal Cells Are a Multipotent Progenitor Capable of Renewing the Bronchial Epithelium. *The American Journal of Pathology,* 164**,** 577-588.

HOOGENBOOM, R. 2009. Poly(2-oxazoline)s: A Polymer Class with Numerous Potential Applications. *Angewandte Chemie International Edition,* 48**,** 7978-7994.

HOOGENBOOM, R. & SCHLAAD, H. 2011. Bioinspired Poly(2-oxazoline)s. *Polymers,* 3**,** 467-488.

HOVENBERG, H. W., DAVIES, J. R. & CARLSTEDT, I. 1996. Different mucins are produced by the surface epithelium and the submucosa in human trachea: identification of MUC5AC as a major mucin from the goblet cells. *Biochem J,* 318 (Pt 1)**,** 319-24.

HUH, D., MATTHEWS, B. D., MAMMOTO, A., MONTOYA-ZAVALA, M., HSIN, H. Y. & INGBER, D. E. 2010. Reconstituting Organ-Level Lung Functions on a Chip. *Science,* 328**,** 1662-1668.

HULTSTROM, J., MANNEBERG, O., DOPF, K., HERTZ, H., BRISMAR, H. & WIKLUND, M. 2007. Proliferation and viability of adherent cells manipulated by standing-wave ultrasound in a microfluidic chip. *Ultrasound in Medicine & Biology,* 33**,** 145-151.

HYDE, D. M., MILLER, L. A., SCHELEGLE, E. S., FANUCCHI, M. V., VAN WINKLE, L. S., TYLER, N. K., AVDALOVIC, M. V., EVANS, M. J., KAJEKAR, R., BUCKPITT, A. R., PINKERTON, K. E., JOAD, J. P., GERSHWIN, L. J., WU, R. & PLOPPER, C. G. 2006. Asthma: a comparison of animal models using stereological methods. *European Respiratory Review,* 15**,** 122-135.

ITO, A., JITSUNOBU, H., KAWABE, Y. & KAMIHIRA, M. 2007. Construction of Heterotypic Cell Sheets by Magnetic Force-Based 3-D Coculture of HepG2 and NIH3T3 Cells. *Journal of Bioscience and Bioengineering,* 104**,** 371-378.

ITOH, M., NAGAFUCHI, A., MOROI, S. & TSUKITA, S. 1997. Involvement of ZO-1 in Cadherin-based Cell Adhesion through Its Direct Binding to α Catenin and Actin Filaments. *The Journal of Cell Biology,* 138**,** 181-192.

J, G. 2000. Series: Basic Sciences: Host defence mechanisms of the respiratory system. *Paediatric Respiratory Reviews,* 1**,** 128-134.

JACQUOT, J., PUCHELLE, E., ZAHM, J. M., BECK, G. & PLOTKOWSKI, M. C. 1987. Effect of human airway lysozyme on the in vitro growth of type I Streptococcus pneumoniae. *Eur J Respir Dis,* 71**,** 295-305.

JAFFAR, Z., ROBERTS, K., PANDIT, A., LINSLEY, P., DJUKANOVIC, R. & HOLGATE, S. 1999. B7 Costimulation Is Required for IL-5 and IL-13 Secretion by Bronchial Biopsy Tissue of Atopic Asthmatic Subjects in Response to Allergen Stimulation. *American Journal of Respiratory Cell and Molecular Biology,* 20**,** 153-162.

JEFFERY, P. K. 2004. Remodeling and Inflammation of Bronchi in Asthma and Chronic Obstructive Pulmonary Disease. *Proceedings of the American Thoracic Society,* 1**,** 176-183.

KABESCH, M., TZOTCHEVA, I., CARR, D., HÖFLER, C., WEILAND, S. K., FRITZSCH, C., VON MUTIUS, E. & MARTINEZ, F. D. 2003. A complete screening of the IL4 gene: Novel polymorphisms and their association with asthma and IgE in childhood. *Journal of Allergy and Clinical Immunology,* 112**,** 893-898.

KANEKO, Y., NAKAMURA, S., SAKAI, K., AOYAGI, T., KIKUCHI, A., SAKURAI, Y. & OKANO, T. 1998. Rapid deswelling response of poly (N-isopropylacrylamide) hydrogels by the formation of water release channels using poly (ethylene oxide) graft chains. *Macromolecules,* 31**,** 6099-6105.

KANTAK, S. S. & KRAMER, R. H. 1998. E-cadherin Regulates Anchorage-independent Growth and Survival in Oral Squamous Cell Carcinoma Cells. *Journal of Biological Chemistry,* 273**,** 16953-16961.

KELLY, A. M., KALTENHAUSER, V., MÜHLBACHER, I., RAMETSTEINER, K., KREN, H., SLUGOVC, C., STELZER, F. & WIESBROCK, F. 2013. Poly(2-

oxazoline)-derived Contact Biocides: Contributions to the Understanding of Antimicrobial Activity. *Macromolecular Bioscience,* 13**,** 116-125.

KEVIN, M. 2011. The increasing challenge of discovering asthma drugs. *Biochemical Pharmacology,* 82**,** 586-599.

KIM, K., OHASHI, K., UTOH, R., KANO, K. & OKANO, T. 2012. Preserved liver-specific functions of hepatocytes in 3D co-culture with endothelial cell sheets. *Biomaterials,* 33**,** 1406-1413.

KNIGHT, D. 2001. Epithelium-fibroblast interactions in response to airway inflammation. *Immunol Cell Biol,* 79**,** 160-4.

KOCH, L., KUHN, S., SORG, H., GRUENE, M., SCHLIE, S., GAEBEL, R., POLCHOW, B., REIMERS, K., STOELTING, S. & MA, N. 2009. Laser printing of skin cells and human stem cells. *Tissue Engineering Part C: Methods,* 16**,** 847-854.

KOSTREWA, D., BROCKHAUS, M., D'ARCY, A., DALE, G. E., NELBOECK, P., SCHMID, G., MUELLER, F., BAZZONI, G., DEJANA, E., BARTFAI, T., WINKLER, F. K. & HENNIG, M. 2001. X-ray structure of junctional adhesion molecule: structural basis for homophilic adhesion via a novel dimerization motif. *EMBO J,* 20**,** 4391-8.

KRONEK, J., KRONEKOVÁ, Z., LUSTOŇ, J., PAULOVIČOVÁ, E., PAULOVIČOVÁ, L. & MENDREK, B. 2011. In vitro bio-immunological and cytotoxicity studies of poly(2-oxazolines). *Journal of Materials Science: Materials in Medicine,* 22**,** 1725-1734.

KUMAR, N. M. & GILULA, N. B. 1996. The gap junction communication channel. *Cell,* 84**,** 381-388.

KUMAR, R. K. & FOSTER, P. S. 2002. Modeling allergic asthma in mice: pitfalls and opportunities. *Am J Respir Cell Mol Biol,* 27**,** 267-72.

KUMAR, S., MAXWELL, I. Z., HEISTERKAMP, A., POLTE, T. R., LELE, T. P., SALANGA, M., MAZUR, E. & INGBER, D. E. 2006. Viscoelastic retraction of single living stress fibers and its impact on cell shape, cytoskeletal organization, and extracellular matrix mechanics. *Biophysical journal,* 90**,** 3762-3773.

KURTEN, R. C., CHOWDHURY, P., SANDERS, R. C., PITTMAN, L. M., SESSIONS, L. W., CHAMBERS, T. C., LYLE, C. S., SCHNACKENBERG, B. J. & JONES, S. M. 2004. Coordinating epidermal growth factor-induced motility promotes efficient wound closure. *American Journal of Physiology - Cell Physiology,* 288**,** C109-C121.

KUSHIDA, A., YAMATO, M., ISOI, Y., KIKUCHI, A. & OKANO, T. 2005. A noninvasive transfer system for polarized renal tubule epithelial cell sheets using temperature-responsive culture dishes. *Eur Cell Mater,* 10**,** 23-30.

KUSHIDA, A., YAMATO, M., KIKUCHI, A. & OKANO, T. 2001. Two-dimensional manipulation of differentiated Madin–Darby canine kidney (MDCK) cell sheets: The noninvasive harvest from temperature-responsive culture dishes and transfer to other surfaces. *Journal of Biomedical Materials Research,* 54**,** 37-46.

KUSHIDA, A., YAMATO, M., KONNO, C., KIKUCHI, A., SAKURAI, Y. & OKANO, T. 2000. Temperature-responsive culture dishes allow nonenzymatic harvest of differentiated Madin-Darby canine kidney (MDCK) cell sheets. *Journal of Biomedical Materials Research,* 51**,** 216-223.

LAGUNAS, A., COMELLES, J., MARTÍNEZ, E., PRATS-ALFONSO, E., ACOSTA, G. A., ALBERICIO, F. & SAMITIER, J. 2012. Cell adhesion and focal contact formation on linear RGD molecular gradients: study of non-linear concentration dependence effects. *Nanomedicine: Nanotechnology, Biology and Medicine,* 8**,** 432-439.

LARCHE, M., AKDIS, C. A. & VALENTA, R. 2006. Immunological mechanisms of allergen-specific immunotherapy. *Nat Rev Immunol,* 6**,** 761-771.

LECHNER, J. F., HAUGEN, A., MCCLENDON, I. A. & PETTIS, E. W. 1982. Clonal growth of normal adult human bronchial epithelial cells in a serum-free medium. *In vitro,* 18**,** 633-42.

LECKIE, M. J., BRINKE, A. T., KHAN, J., DIAMANT, Z., O'CONNOR, B. J., WALLS, C. M., MATHUR, A. K., COWLEY, H. C., CHUNG, K. F. & DJUKANOVIC, R. 2000. Effects of an interleukin-5 blocking monoclonal antibody on eosinophils, airway hyper-responsiveness, and the late asthmatic response. *The Lancet,* 356**,** 2144-2148.

LEE, J.-Y., PARK, S.-W., CHANG, H. K., KIM, H. Y., RHIM, T., LEE, J.-H., JANG, A.-S., KOH, E.-S. & PARK, C.-S. 2006. A Disintegrin and Metalloproteinase 33 Protein in Patients with Asthma. *American Journal of Respiratory and Critical Care Medicine,* 173**,** 729-735.

LEHNERT, B. E. 1992. Pulmonary and thoracic macrophage subpopulations and clearance of particles from the lung. *Environ Health Perspect,* 97**,** 17-46.

LEHRER, R. I., LICHTENSTEIN, A. K. & GANZ, T. 1993. Defensins: Antimicrobial and Cytotoxic Peptides of Mammalian Cells. *Annual Review of Immunology,* 11**,** 105-128.

LESNÝ, P., PŘÁDNÝ, M., JENDELOVA, P., MICHALEK, J., VACIK, J. & SYKOVA, E. 2006. Macroporous hydrogels based on 2-hydroxyethyl methacrylate. Part 4: growth of rat bone marrow stromal cells in three-dimensional hydrogels with positive and negative surface charges and in polyelectrolyte complexes. *Journal of Materials Science: Materials in Medicine,* 17**,** 829-833.

LI, X. & WILSON, J. W. 1997. Increased Vascularity of the Bronchial Mucosa in Mild Asthma. *American Journal of Respiratory and Critical Care Medicine,* 156**,** 229-233.

LIEN, E., SELLATI, T. J., YOSHIMURA, A., FLO, T. H., RAWADI, G., FINBERG, R. W., CARROLL, J. D., ESPEVIK, T., INGALLS, R. R., RADOLF, J. D. & GOLENBOCK, D. T. 1999. Toll-like Receptor 2 Functions as a Pattern Recognition Receptor for Diverse Bacterial Products. *Journal of Biological Chemistry,* 274**,** 33419-33425.

LIN, P. Y., CLASH, C., PEARCE, E. M., KWEI, T. K. & APONTE, M. A. 1988. Solubility and Miscibility of Poly(Ethyl Oxazoline). *Journal of Polymer Science Part B-Polymer Physics,* 26**,** 603-619.

LIU, J., KUZNETSOVA, L. A., EDWARDS, G. O., XU, J., MA, M., PURCELL, W. M., JACKSON, S. K. & COAKLEY, W. T. 2007. Functional three-dimensional HepG2 aggregate cultures generated from an ultrasound trap: Comparison with HepG2 spheroids. *Journal of Cellular Biochemistry,* 102**,** 1180-1189.

LIU, Y., WANG, Y., ZHANG, Y., MIAO, Y., ZHAO, Y., ZHANG, P.-X., JIANG, G.-Y., ZHANG, J.-Y., HAN, Y., LIN, X.-Y., YANG, L.-H., LI, Q.-C., ZHAO, C. & WANG, E.-H. 2009. Abnormal expression of p120-catenin, E-cadherin, and small GTPases is significantly associated with malignant phenotype of human lung cancer. *Lung Cancer,* 63**,** 375-382.

LÜ, S., LIU, M. & NI, B. 2011. Degradable, injectable poly(N-isopropylacrylamide)-based hydrogels with low gelation concentrations for protein delivery application. *Chemical Engineering Journal,* 173**,** 241-250.

LUXENHOFER, R., SAHAY, G., SCHULZ, A., ALAKHOVA, D., BRONICH, T. K., JORDAN, R. & KABANOV, A. V. 2011. Structure-property relationship in cytotoxicity and cell uptake of poly (2-oxazoline) amphiphiles. *Journal of Controlled Release,* 153**,** 73-82.

LUXENHOFER, R., SCHULZ, A., ROQUES, C., LI, S., BRONICH, T. K., BATRAKOVA, E. V., JORDAN, R. & KABANOV, A. V. 2010. Doubly amphiphilic poly(2-oxazoline)s as high-capacity delivery systems for hydrophobic drugs. *Biomaterials,* 31**,** 4972-4979.

LYONS, B. L. & SCHWARZ, R. I. 1984. Ascorbate stimulation of PAT cells causes an increase in transcription rates and a decrease in degradation rates of procollagen mRNA. *Nucleic Acids Research,* 12**,** 2569-2579.

MALONNE, H., EECKMAN, F., FONTAINE, D., OTTO, A., VOS, L. D., MOËS, A., FONTAINE, J. & AMIGHI, K. 2005. Preparation of poly (< i> N</i>-isopropylacrylamide) copolymers and preliminary assessment of their acute and subacute toxicity in mice. *European journal of pharmaceutics and biopharmaceutics,* 61**,** 188-194.

MATSUURA, K., HARAGUCHI, Y., SHIMIZU, T. & OKANO, T. Cell sheet transplantation for heart tissue repair. *Journal of Controlled Release*.

MATSUURA, K., HARAGUCHI, Y., SHIMIZU, T. & OKANO, T. 2013. Cell sheet transplantation for heart tissue repair. *J Control Release*.

MCFADDEN, E. R. 1988. Corticosteroids and Cromolyn Sodium as Modulators of Airway Inflammation. *Chest,* 94**,** 181-184.

MERO, A., PASUT, G., VIA, L. D., FIJTEN, M. W. M., SCHUBERT, U. S., HOOGENBOOM, R. & VERONESE, F. M. 2008. Synthesis and characterization of poly(2-ethyl 2-oxazoline)-conjugates with proteins and drugs: Suitable alternatives to PEG-conjugates? *Journal of Controlled Release,* 125**,** 87-95.

MEYER, N. & AKDIS, C. 2013. Vascular Endothelial Growth Factor as a Key Inducer of Angiogenesis in the Asthmatic Airways. *Current Allergy and Asthma Reports,* 13**,** 1-9.

MICHAEL, S., SORG, H., PECK, C.-T., KOCH, L., DEIWICK, A., CHICHKOV, B., VOGT, P. M. & REIMERS, K. 2013. Tissue Engineered Skin Substitutes Created by Laser-Assisted Bioprinting Form Skin-Like Structures in the Dorsal Skin Fold Chamber in Mice. *PLoS ONE,* 8**,** e57741.

MILLER, D. C., THAPA, A., HABERSTROH, K. M. & WEBSTER, T. J. 2004. Endothelial and vascular smooth muscle cell function on poly (lactic-co-glycolic acid) with nano-structured surface features. *Biomaterials,* 25**,** 53-61.

MOFFATT, M. F., KABESCH, M., LIANG, L., DIXON, A. L., STRACHAN, D., HEATH, S., DEPNER, M., VON BERG, A., BUFE, A., RIETSCHEL, E., HEINZMANN, A., SIMMA, B., FRISCHER, T., WILLIS-OWEN, S. A. G., WONG, K. C. C., ILLIG, T., VOGELBERG, C., WEILAND, S. K., VON MUTIUS, E., ABECASIS, G. R., FARRALL, M., GUT, I. G., LATHROP, G. M. & COOKSON, W. O. C. 2007. Genetic variants regulating ORMDL3 expression contribute to the risk of childhood asthma. *Nature,* 448**,** 470-473.

MUKHERJEE, A. B. & ZHANG, Z. 2011. Allergic Asthma: Influence of Genetic and Environmental Factors. *Journal of Biological Chemistry,* 286**,** 32883-32889.

MUL, F. P. J., ZUURBIER, A. E. M., JANSSEN, H., CALAFAT, J., VAN WETERING, S., HIEMSTRA, P. S., ROOS, D. & HORDIJK, P. L. 2000. Sequential migration of neutrophils across monolayers of endothelial and epithelial cells. *Journal of Leukocyte Biology,* 68**,** 529-537.

MURPHY, D. M. & O'BYRNE, P. M. 2010. Recent Advances in the Pathophysiology of Asthma. *Chest,* 137**,** 1417-1426.

NAIR, P., PIZZICHINI, M. M. M., KJARSGAARD, M., INMAN, M. D., EFTHIMIADIS, A., PIZZICHINI, E., HARGREAVE, F. E. & O'BYRNE, P. M. 2009. Mepolizumab for Prednisone-Dependent Asthma with Sputum Eosinophilia. *New England Journal of Medicine,* 360**,** 985-993.

NANDKUMAR, M. A., YAMATO, M., KUSHIDA, A., KONNO, C., HIROSE, M., KIKUCHI, A. & OKANO, T. 2002. Two-dimensional cell sheet manipulation of heterotypically co-cultured lung cells utilizing temperature-responsive culture dishes results in long-term maintenance of differentiated epithelial cell functions. *Biomaterials,* 23**,** 1121-1130.

NASH, M. E., CARROLL, W. M., NIKOLOSKYA, N., YANG, R., CONNELL, C. O., GORELOV, A. V., DOCKERY, P., LIPTROT, C., LYNG, F. M., GARCIA, A. & ROCHEV, Y. A. 2011. Straightforward, One-Step Fabrication of Ultrathin Thermoresponsive Films from Commercially Available pNIPAm for Cell Culture and Recovery. *ACS Applied Materials & Interfaces,* 3**,** 1980-1990.

NETWORK, B. T. S. S. I. G. 2008. British guideline on the management of asthma. *Thorax,* 63**,** iv1.

NICOD, L. P. 1999. Pulmonary defence mechanisms. *Respiration,* 66**,** 2-11.

NIESSEN, C. M. & GUMBINER, B. M. 1998. The juxtamembrane region of the cadherin cytoplasmic tail supports lateral clustering, adhesive strengthening, and interaction with p120ctn. *The Journal of cell biology,* 141**,** 779-789.

NILSSON, J., EVANDER, M., HAMMARSTRÖM, B. & LAURELL, T. 2009. Review of cell and particle trapping in microfluidic systems. *Analytica Chimica Acta,* 649**,** 141-157.

NISHIDA, K., YAMATO, M., HAYASHIDA, Y., WATANABE, K., MAEDA, N., WATANABE, H., YAMAMOTO, K., NAGAI, S., KIKUCHI, A. & TANO, Y. 2004. Functional bioengineered corneal epithelial sheet grafts from corneal stem cells expanded ex vivo on a temperature-responsive cell culture surface. *Transplantation,* 77**,** 379-385.

O'CONNOR, C. M. & FITZGERALD, M. X. 1994. Matrix metalloproteases and lung disease. *Thorax,* 49**,** 602-9.

OBER, C. & YAO, T.-C. 2011. The genetics of asthma and allergic disease: a 21st century perspective. *Immunological Reviews,* 242**,** 10-30.

OKANO, T., YAMADA, N., OKUHARA, M., SAKAI, H. & SAKURAI, Y. 1995. Mechanism of cell detachment from temperature-modulated, hydrophilic-hydrophobic polymer surfaces. *Biomaterials,* 16**,** 297-303.

OKANO, T., YAMADA, N., SAKAI, H. & SAKURAI, Y. 1993. A novel recovery system for cultured cells using plasma-treated polystyrene dishes grafted with poly(N-isopropylacrylamide). *J Biomed Mater Res,* 27**,** 1243-51.

ORDOÑEZ, C. L., KHASHAYAR, R., WONG, H. H., FERRANDO, R., WU, R., HYDE, D. M., HOTCHKISS, J. A., ZHANG, Y., NOVIKOV, A., DOLGANOV, G. & FAHY, J. V. 2001. Mild and Moderate Asthma Is Associated with Airway Goblet Cell Hyperplasia and Abnormalities in Mucin Gene Expression. *American Journal of Respiratory and Critical Care Medicine,* 163**,** 517-523.

PACK, R., AL-UGAILY, L. & MORRIS, G. 1981. The cells of the tracheobronchial epithelium of the mouse: a quantitative light and electron microscope study. *Journal of anatomy,* 132**,** 71.

PAGEAU, S. C., SAZONOVA, O. V., WONG, J. Y., SOTO, A. M. & SONNENSCHEIN, C. 2011. The effect of stromal components on the modulation of the phenotype of human bronchial epithelial cells in 3D culture. *Biomaterials,* 32**,** 7169-80.

PATTON, J. S. & BYRON, P. R. 2007. Inhaling medicines: delivering drugs to the body through the lungs. *Nature Reviews Drug Discovery,* 6**,** 67-74.

PELHAM, R. J. & WANG, Y.-L. 1997. Cell locomotion and focal adhesions are regulated by substrate flexibility. *Proceedings of the National Academy of Sciences,* 94**,** 13661-13665.

PERSSON, C. G. 1985. On the medical history of xanthines and other remedies for asthma: a tribute to HH Salter. *Thorax,* 40**,** 881-6.

PETERSON, L. J., RAJFUR, Z., MADDOX, A. S., FREEL, C. D., CHEN, Y., EDLUND, M., OTEY, C. & BURRIDGE, K. 2004. Simultaneous stretching and contraction of stress fibers in vivo. *Molecular biology of the cell,* 15**,** 3497-3508.

PETERSSON, F., ABERG, L., SWARD-NILSSON, A. M. & LAURELL, T. 2007. Free flow acoustophoresis: microfluidic-based mode of particle and cell separation. *Anal Chem,* 79**,** 5117-23.

PIERSCHBACHER, M. D. & RUOSLAHTI, E. 1984. Variants of the cell recognition site of fibronectin that retain attachment-promoting activity. *Proceedings of the National Academy of Sciences,* 81**,** 5985-5988.

PILEWSKI, J. M., LATOCHE, J. D., ARCASOY, S. M. & ALBELDA, S. M. 1997. Expression of integrin cell adhesion receptors during human airway epithelial repair in vivo. *American Journal of Physiology - Lung Cellular and Molecular Physiology,* 273**,** L256-L263.

PLOPPER, C. G. & HYDE, D. M. 2008. The non-human primate as a model for studying COPD and asthma. *Pulmonary pharmacology & therapeutics,* 21**,** 755-766.

POHL, C., HERMANNS, M., UBOLDI, C., BOCK, M., FUCHS, S., DEI-ANANG, J., MAYER, E., KEHE, K., KUMMER, W. & KIRKPATRICK, C. J. 2009. Barrier functions and paracellular integrity in human cell culture models of the proximal respiratory unit. *European Journal of Pharmaceutics and Biopharmaceutics,* 72**,** 339-349.

POLLARD, T. D. 1986. Rate constants for the reactions of ATP-and ADP-actin with the ends of actin filaments. *The Journal of cell biology,* 103**,** 2747-2754.

POLLARD, T. D. & BORISY, G. G. 2003. Cellular Motility Driven by Assembly and Disassembly of Actin Filaments. *Cell,* 112**,** 453-465.

PRESTA, L. G., LAHR, S. J., SHIELDS, R. L., PORTER, J. P., GORMAN, C. M., FENDLY, B. M. & JARDIEU, P. M. 1993. Humanization of an antibody directed against IgE. *The Journal of Immunology,* 151**,** 2623-32.

PUXEDDU, I., PANG, Y. Y., HARVEY, A., HAITCHI, H. M., NICHOLAS, B., YOSHISUE, H., RIBATTI, D., CLOUGH, G., POWELL, R. M., MURPHY, G., HANLEY, N. A., WILSON, D. I., HOWARTH, P. H., HOLGATE, S. T. & DAVIES, D. E. 2008. The soluble form of a disintegrin and metalloprotease 33 promotes angiogenesis: Implications for airway remodeling in asthma. *Journal of Allergy and Clinical Immunology,* 121**,** 1400-1406.e4.

REDMAN, T. K., RUDOLPH, K., BARR, E. B., BOWEN, L. E., MUGGENBURG, B. A. & BICE, D. E. 2001. Pulmonary immunity to ragweed in a Beagle dog model of allergic asthma. *Exp Lung Res,* 27**,** 433-51.

REINHARDT, A., BOTTOMS, S., LAURENT, G. & MCANULTY, R. 2005. Quantification of collagen and proteoglycan deposition in a murine model of airway remodelling. *Respiratory Research,* 6**,** looking at airway remodelling a mouse model specifically at matrix production. They show increased matrix in a similar increase to asthmatics (based on ova model).

RITTER, M., MENNERICH, D., WEITH, A. & SEITHER, P. 2005. Characterization of Toll-like receptors in primary lung epithelial cells: strong impact of the TLR3 ligand poly (I: C) on the regulation of Toll-like receptors, adaptor proteins and inflammatory response. *Journal of Inflammation,* 2**,** 16.

ROBIN J, M. 2011. Models and approaches to understand the role of airway remodelling in disease. *Pulmonary Pharmacology & Therapeutics,* 24**,** 478-486.

ROCK, J. R., ONAITIS, M. W., RAWLINS, E. L., LU, Y., CLARK, C. P., XUE, Y., RANDELL, S. H. & HOGAN, B. L. M. 2009. Basal cells as stem cells of the mouse trachea and human airway epithelium. *Proceedings of the National Academy of Sciences,* 106**,** 12771-12775.

ROSENWASSER, L. J., KLEMM, D. J., DRESBACK, J. K., INAMURA, H., MASCALI, J. J., KLINNERT, M. & BORISH, L. 1995. Promoter polymorphisms in the chromosome 5 gene cluster in asthma and atopy. *Clinical & Experimental Allergy,* 25**,** 74-78.

RUDNICK, D. 1933. Developmental capacities of the chick lung in chorioallantoic grafts. *Journal of Experimental Zoology,* 66**,** 125-153.

SABATINI, F., SILVESTRI, M., SALE, R., SCARSO, L., DEFILIPPI, A.-C., RISSO, F. M. & ROSSI, G. A. 2002. Fibroblast-eosinophil interaction: Modulation of

adhesion molecules expression and chemokine release by human fetal lung fibroblasts in response to IL-4 and TNF-α. *Immunology Letters,* 84**,** 173-178.

SACHIKO, S., SHIMIZU, T., YAMATO, M. & OKANO, T. 2013. Hormone supplying renal cell sheet in vivo produced by tissue engineering technology. *Biores Open Access,* 2**,** 12-9.

SAGLANI, S., PAYNE, D. N., ZHU, J., WANG, Z., NICHOLSON, A. G., BUSH, A. & JEFFERY, P. K. 2007. Early Detection of Airway Wall Remodeling and Eosinophilic Inflammation in Preschool Wheezers. *American Journal of Respiratory and Critical Care Medicine,* 176**,** 858-864.

SAMMONS, R. L., LUMBIKANONDA, N., GROSS, M. & CANTZLER, P. 2005. Comparison of osteoblast spreading on microstructured dental implant surfaces and cell behaviour in an explant model of osseointegration. *Clinical oral implants research,* 16**,** 657-666.

SAMUELSSON, B. 2000. The discovery of the leukotrienes. *American Journal of Respiratory and Critical Care Medicine,* 161**,** S2-S6.

SANDFORD, A. J., CHAGANI, T., ZHU, S., WEIR, T. D., BAI, T. R., SPINELLI, J. J., FITZGERALD, J. M., BEHBEHANI, N. A., TAN, W. C. & PARÉ, P. D. 2000. Polymorphisms in the IL4 , IL4RA , and FCERIB genes and asthma severity. *Journal of Allergy and Clinical Immunology,* 106**,** 135-140.

SARVAZYAN, A. 2010. Diversity of biomedical applications of acoustic radiation force. *Ultrasonics,* 50**,** 230-234.

SASAGAWA, T., SHIMIZU, T., SEKIYA, S., HARAGUCHI, Y., YAMATO, M., SAWA, Y. & OKANO, T. 2010. Design of prevascularized three-dimensional cell-dense tissues using a cell sheet stacking manipulation technology. *Biomaterials,* 31**,** 1646-1654.

SCHNEIDER, E., THIEBLEMONT, N., DE MORAES, M. L. & DY, M. 2010. Basophils: new players in the cytokine network. *Eur Cytokine Netw,* 21**,** 142-53.

SCHRAMM, C. M., PUDDINGTON, L., WU, C., GUERNSEY, L., GHARAEE-KERMANI, M., PHAN, S. H. & THRALL, R. S. 2004. Chronic Inhaled Ovalbumin Exposure Induces Antigen-Dependent but Not Antigen-Specific Inhalational Tolerance in a Murine Model of Allergic Airway Disease. *The American Journal of Pathology,* 164**,** 295-304.

SEDLACEK, O., MONNERY, B. D., FILIPPOV, S. K., HOOGENBOOM, R. & HRUBY, M. 2012. Poly (2-Oxazoline) s–Are They More Advantageous for Biomedical Applications Than Other Polymers? *Macromolecular rapid communications,* 33**,** 1648-1662.

SEELIGER, W., AUFDERHAAR, E., DIEPERS, W., FEINAUER, R., NEHRING, R., THIER, W. & HELLMANN, H. 1966. Recent syntheses and reactions of cyclic imidic esters. *Angew Chem Int Ed Engl,* 5**,** 875-88.

SHAMRI, R., XENAKIS, J. J. & SPENCER, L. A. 2011. Eosinophils in innate immunity: an evolving story. *Cell Tissue Res,* 343**,** 57-83.

SHANNON, J. M., NIELSEN, L. D., GEBB, S. A. & RANDELL, S. H. 1998. Mesenchyme specifies epithelial differentiation in reciprocal recombinants of embryonic lung and trachea. *Developmental dynamics,* 212**,** 482-494.

SHEPPARD, D. 2003. Functions of Pulmonary Epithelial Integrins: From Development to Disease. *Physiological Reviews,* 83**,** 673-686.

SHI, J., AHMED, D., MAO, X., LIN, S.-C. S., LAWIT, A. & HUANG, T. J. 2009. Acoustic tweezers: patterning cells and microparticles using standing surface acoustic waves (SSAW). *Lab on a Chip,* 9**,** 2890.

SHIMIZU, T., YAMATO, M., ISOI, Y., AKUTSU, T., SETOMARU, T., ABE, K., KIKUCHI, A., UMEZU, M. & OKANO, T. 2002. Fabrication of pulsatile cardiac tissue grafts using a novel 3-dimensional cell sheet manipulation technique and temperature-responsive cell culture surfaces. *Circ Res,* 90**,** e40.

SHIRAKAWA, T., LI, A., DUBOWITZ, M., DEKKER, J. W., SHAW, A. E., FAUX, J. A., RA, C., COOKSON, W. O. & HOPKIN, J. M. 1994. Association between atopy and variants of the beta subunit of the high-affinity immunoglobulin E receptor. *Nat Genet,* 7**,** 125-9.

SIMPSON, A., MANIATIS, N., JURY, F., CAKEBREAD, J. A., LOWE, L. A., HOLGATE, S. T., WOODCOCK, A., OLLIER, W. E. R., COLLINS, A., CUSTOVIC, A., HOLLOWAY, J. W. & JOHN, S. L. 2005. Polymorphisms in A Disintegrin and Metalloprotease 33 (ADAM33) Predict Impaired Early-Life Lung Function. *American Journal of Respiratory and Critical Care Medicine,* 172**,** 55-60.

SOROKIN, L., SONNENBERG, A., AUMAILLEY, M., TIMPL, R. & EKBLOM, P. 1990. Recognition of the laminin E8 cell-binding site by an integrin possessing the alpha 6 subunit is essential for epithelial polarization in developing kidney tubules. *The Journal of Cell Biology,* 111**,** 1265-1273.

SPOONER, B. S. & WESSELLS, N. K. 1970. Mammalian lung development: interactions in primordium formation and bronchial morphogenesis. *Journal of Experimental Zoology,* 175**,** 445-454.

SWINDLE, E. J., COLLINS, J. E. & DAVIES, D. E. 2009. Breakdown in epithelial barrier function in patients with asthma: identification of novel therapeutic approaches. *J Allergy Clin Immunol,* 124**,** 23-34; quiz 35-6.

SWINDLE, E. J. & DAVIES, D. E. 2011. Artificial airways for the study of respiratory disease. *Expert Rev Respir Med,* 5**,** 757-65.

TAKAMIZAWA, K., SHODA, K. & MATSUDA, T. 2002. Pull-out mechanical measurement of tissuesubstrate adhesive strength: Endothelial cell monolayer sheet formed on a thermoresponsive gelatin layer. *Journal of Biomaterials Science, Polymer Edition,* 13**,** 81-94.

TAKEZAWA, T., MORI, Y. & YOSHIZATO, K. 1990. Cell culture on a thermo-responsive polymer surface. *Biotechnology (N Y),* 8**,** 854-6.

TAMBE, D. T., HARDIN, C. C., ANGELINI, T. E., RAJENDRAN, K., PARK, C. Y., SERRA-PICAMAL, X., ZHOU, E. H., ZAMAN, M. H., BUTLER, J. P. & WEITZ, D. A. 2011. Collective cell guidance by cooperative intercellular forces. *Nature materials,* 10**,** 469-475.

TAMM, M., ROTH, M., MALOUF, M., CHHAJED, P., JOHNSON, P., BLACK, J. & GLANVILLE, A. 2001. Primary Fibroblast Cell Cultures From Transbronchial Biopsies of Lung Transplant Recipients1. *Transplantation,* 71**,** 337-339.

TANG, M. L. K., WILSON, J. W., STEWART, A. G. & ROYCE, S. G. 2006. Airway remodelling in asthma: Current understanding and implications for future therapies. *Pharmacology & Therapeutics,* 112**,** 474-488.

TANG, Z., AKIYAMA, Y., ITOGA, K., KOBAYASHI, J., YAMATO, M. & OKANO, T. 2012. Shear stress-dependent cell detachment from temperature-responsive cell culture surfaces in a microfluidic device. *Biomaterials,* 33**,** 7405-7411.

TAUB, D. D., LLOYD, A. R., CONLON, K., WANG, J. M., ORTALDO, J., HARADA, A., MATSUSHIMA, K., KELVIN, D. & OPPENHEIM, J. 1993. Recombinant human interferon-inducible protein 10 is a chemoattractant for human monocytes and T lymphocytes and promotes T cell adhesion to endothelial cells. *The Journal of experimental medicine,* 177**,** 1809-1814.

TAYLOR, D. R. 2009. The β-Agonist Saga and Its Clinical Relevance: On and On It Goes. *American Journal of Respiratory and Critical Care Medicine,* 179**,** 976-978.

TEMELKOVSKI, J., HOGAN, S. P., SHEPHERD, D. P., FOSTER, P. S. & KUMAR, R. K. 1998. An improved murine model of asthma: selective airway inflammation, epithelial lesions and increased methacholine responsiveness following chronic exposure to aerosolised allergen. *Thorax,* 53**,** 849-856.

TIMPL, R. 1989. Structure and biological activity of basement membrane proteins. *European Journal of Biochemistry,* 180**,** 487-502.

TONG, J., YI, X., LUXENHOFER, R., BANKS, W. A., JORDAN, R., ZIMMERMAN, M. C. & KABANOV, A. V. 2012. Conjugates of Superoxide Dismutase 1 with Amphiphilic Poly(2-oxazoline) Block Copolymers for Enhanced Brain Delivery: Synthesis, Characterization and Evaluation in Vitro and in Vivo. *Molecular Pharmaceutics,* 10**,** 360-377.

TOURDOT, S., MATHIE, S., HUSSELL, T., EDWARDS, L., WANG, H., OPENSHAW, P. J. M., SCHWARZE, J. & LLOYD, C. M. 2008. Respiratory syncytial virus infection provokes airway remodelling in allergen-exposed mice in absence of prior allergen sensitization. *Clinical & Experimental Allergy,* 38**,** 1016-1024.

TREPAT, X. & FREDBERG, J. J. 2011. Plithotaxis and emergent dynamics in collective cellular migration. *Trends in Cell Biology,* 21**,** 638-646.

TRUMP, B. F. & BEREZESKY, I. K. 1995. Calcium-mediated cell injury and cell death. *The FASEB Journal,* 9**,** 219-28.

TSUDA, Y. 2005. The use of patterned dual thermoresponsive surfaces for the collective recovery as co-cultured cell sheets. *Biomaterials,* 26**,** 1885-1893.

TURNER, S., PATON, J., HIGGINS, B. & DOUGLAS, G. 2011. British guidelines on the management of asthma: what's new for 2011? *Thorax,* 66**,** 1104-1105.

TZANAKAKIS, E. S., HANSEN, L. K. & HU, W.-S. 2001. The role of actin filaments and microtubules in hepatocyte spheroid self-assembly. *Cell motility and the cytoskeleton,* 48**,** 175-189.

UNDERDOWN, B. J. & SCHIFF, J. M. 1986. Immunoglobulin A: Strategic Defense Initiative at the Mucosal Surface. *Annual Review of Immunology,* 4**,** 389-417.

UYAMA, H. & KOBAYASHI, S. 1992. A Novel Thermosensitive Polymer - Poly(2-Iso-Propyl-2-Oxazoline). *Chemistry Letters***,** 1643-1646.

VALAVANIDIS, A., FIOTAKIS, K. & VLACHOGIANNI, T. 2008. Airborne Particulate Matter and Human Health: Toxicological Assessment and Importance of Size and Composition of Particles for Oxidative Damage and Carcinogenic Mechanisms. *Journal of Environmental Science and Health, Part C,* 26**,** 339-362.

VAN DER SCHANS, C. P. 2007. Bronchial mucus transport. *Respir Care,* 52**,** 1150-6; discussion 1156-8.

VAN DER STRATE, B. W. A., BELJAARS, L., MOLEMA, G., HARMSEN, M. C. & MEIJER, D. K. F. 2001. Antiviral activities of lactoferrin. *Antiviral Research,* 52**,** 225-239.

VAN EERDEWEGH, P., LITTLE, R. D., DUPUIS, J., DEL MASTRO, R. G., FALLS, K., SIMON, J., TORREY, D., PANDIT, S., MCKENNY, J., BRAUNSCHWEIGER, K., WALSH, A., LIU, Z., HAYWARD, B., FOLZ, C., MANNING, S. P., BAWA, A., SARACINO, L., THACKSTON, M., BENCHEKROUN, Y., CAPPARELL, N., WANG, M., ADAIR, R., FENG, Y., DUBOIS, J., FITZGERALD, M. G., HUANG, H., GIBSON, R., ALLEN, K. M., PEDAN, A., DANZIG, M. R., UMLAND, S. P., EGAN, R. W., CUSS, F. M., RORKE, S., CLOUGH, J. B., HOLLOWAY, J. W., HOLGATE, S. T. & KEITH, T. P. 2002. Association of the ADAM33 gene with asthma and bronchial hyperresponsiveness. *Nature,* 418**,** 426-430.

VANHERBERGHEN, B., MANNEBERG, O., CHRISTAKOU, A., FRISK, T., OHLIN, M., HERTZ, H. M., ONFELT, B. & WIKLUND, M. 2010. Ultrasound-controlled cell aggregation in a multi-well chip. *Lab Chip,* 10**,** 2727-32.

VARGHESE, V., RAJ, V., SREENIVASAN, K. & KUMARY, T. V. 2010. In vitro cytocompatibility evaluation of a thermoresponsive NIPAAm-MMA copolymeric surface using L929 cells. *Journal of Materials Science: Materials in Medicine,* 21**,** 1631-1639.

VASILE, C., BUMBU, G. G., PETRONELA DUMITRIU, R. & STAIKOS, G. 2004. Comparative study of the behavior of carboxymethyl cellulose-g-poly(N-isopropylacrylamide) copolymers and their equivalent physical blends. *European Polymer Journal,* 40**,** 1209-1215.

VERCELLI, D. 2008. Discovering susceptibility genes for asthma and allergy. *Nat Rev Immunol,* 8**,** 169-182.

VIHOLA, H., LAUKKANEN, A., VALTOLA, L., TENHU, H. & HIRVONEN, J. 2005. Cytotoxicity of thermosensitive polymers poly(N-isopropylacrylamide), poly(N-vinylcaprolactam) and amphiphilically modified poly(N-vinylcaprolactam). *Biomaterials,* 26**,** 3055-64.

VON RECUM, H., KIKUCHI, A., OKUHARA, M., SAKURAI, Y., OKANO, T. & SUNG WAN, K. 1998. Retinal pigmented epithelium cultures on thermally responsive polymer porous substrates. *Journal of Biomaterials Science, Polymer Edition,* 9**,** 1241-1253.

VRUGT, B., WILSON, S., BRON, A., HOLGATE, S., DJUKANOVIC, R. & AALBERS, R. 2000. Bronchial angiogenesis in severe glucocorticoid-dependent asthma. *European Respiratory Journal,* 15**,** 1014-1021.

WALLACE, S. W., DURGAN, J., JIN, D. & HALL, A. 2010. Cdc42 Regulates Apical Junction Formation in Human Bronchial Epithelial Cells through PAK4 and Par6B. *Molecular Biology of the Cell,* 21**,** 2996-3006.

WAN, H., WINTON, H., SOELLER, C., STEWART, G., THOMPSON, P., GRUENERT, D., CANNELL, M., GARROD, D. & ROBINSON, C. 2000. Tight junction properties of the immortalized human bronchial epithelial cell lines Calu-3 and 16HBE14o. *European Respiratory Journal,* 15**,** 1058-1068.

WANG, X., LI, X., LI, Y., ZHOU, Y., FAN, C., LI, W., MA, S., FAN, Y., HUANG, Y., LI, N. & LIU, Y. 2011. Synthesis, characterization and biocompatibility of poly(2-ethyl-2-oxazoline)–poly(d,l-lactide)–poly(2-ethyl-2-oxazoline) hydrogels. *Acta Biomaterialia,* 7**,** 4149-4159.

WARBURTON, D., SCHWARZ, M., TEFFT, D., FLORES-DELGADO, G., ANDERSON, K. D. & CARDOSO, W. V. 2000. The molecular basis of lung morphogenesis. *Mechanisms of Development,* 92**,** 55-81.

WATANABE, H., NUMATA, K., ITO, T., TAKAGI, K. & MATSUKAWA, A. 2004. Innate Immune Response in Th1- and Th2-Dominant Mouse Strains. *Shock,* 22**,** 460-466.

WEDER, G., GUILLAUME-GENTIL, O., MATTHEY, N., MONTAGNE, F., HEINZELMANN, H., VÖRÖS, J. & LILEY, M. 2010. The quantification of single cell adhesion on functionalized surfaces for cell sheet engineering. *Biomaterials,* 31**,** 6436-6443.

WEI, Q., REIDLER, D., SHEN, M. Y. & HUANG, H. 2013. Keratinocyte cytoskeletal roles in cell sheet engineering. *BMC Biotechnology,* 13**,** 17.

WENZEL, S. & HOLGATE, S. T. 2006. The Mouse Trap. *American Journal of Respiratory and Critical Care Medicine,* 174**,** 1173-1176.

WHITCUTT, M., ADLER, K. & WU, R. 1988. A biphasic chamber system for maintaining polarity of differentiation of culture respiratory tract epithelial cells. *In Vitro Cellular & Developmental Biology - Plant,* 24**,** 420-428.

WICKS, J., HAITCHI, H. M., HOLGATE, S. T., DAVIES, D. E. & POWELL, R. M. 2006. Enhanced upregulation of smooth muscle related transcripts by TGFβ2 in asthmatic (myo) fibroblasts. *Thorax,* 61**,** 313-319.

WICKSTROM, C., DAVIES, J. R., ERIKSEN, G. V., VEERMAN, E. C. I. & CARLSTEDT, I. 1998. MUC5B is a major gel-forming, oligomeric mucin from human salivary gland, respiratory tract and endocervix: identification of glycoforms and C-terminal cleavage. *Biochemical Journal,* 334**,** 685-693.

WU, J. R. 1991. Acoustical tweezers. *J Acoust Soc Am,* 89**,** 2140-3.

WU, Y., LI, J., WU, J., MORGAN, P., XU, X., RANCATI, F., VALLESE, S., RAVEGLIA, L., HOTCHANDANI, R., FULLER, N., BARD, J., CUNNINGHAM, K., FISH, S., KRYKBAEV, R., TAM, S., GOLDMAN, S. J., WILLIAMS, C., MANSOUR, T. S., SAIAH, E., SYPEK, J. & LI, W. 2012. Discovery of potent and selective matrix metalloprotease 12 inhibitors for the potential treatment of chronic obstructive pulmonary disease (COPD). *Bioorg Med Chem Lett,* 22**,** 138-43.

XIAO, C., PUDDICOMBE, S. M., FIELD, S., HAYWOOD, J., BROUGHTON-HEAD, V., PUXEDDU, I., HAITCHI, H. M., VERNON-WILSON, E., SAMMUT, D. & BEDKE, N. 2011. Defective epithelial barrier function in asthma. *Journal of Allergy and Clinical Immunology,* 128**,** 549-556. e12.

XU, F. J., ZHENG, Y. Q., ZHEN, W. J. & YANG, W. T. 2010. Thermoresponsive poly(N-isopropyl acrylamide)-grafted polycaprolactone films with surface immobilization of collagen. *Colloids and Surfaces B: Biointerfaces*.

XU, T., JIN, J., GREGORY, C., HICKMAN, J. J. & BOLAND, T. 2005. Inkjet printing of viable mammalian cells. *Biomaterials,* 26**,** 93-99.

YAMAUCHI, K., TOMITA, M., GIEHL, T. & ELLISON, R. R. 1993. Antibacterial activity of lactoferrin and a pepsin-derived lactoferrin peptide fragment. *Infection and Immunity,* 61**,** 719-728.

YANG, J., YAMATO, M., NISHIDA, K., HAYASHIDA, Y., SHIMIZU, T., KIKUCHI, A., TANO, Y. & OKANO, T. 2006. Corneal epithelial stem cell delivery using cell sheet engineering: Not lost in transplantation. *Journal of Drug Targeting,* 14**,** 471-482.

YOSHIOKA, H., MIKAMI, M., MORI, Y. & TSUCHIDA, E. 1994. Preparation of Poly (N-Msopropylacrylamide)-B-Poly (Ethylene Glycol) and Calorimetric Analysis of Its Aqueous Solution. *Journal of Macromolecular Science—Pure and Applied Chemistry,* 31**,** 109-112.

ZANI, B. G., KOJIMA, K., VACANTI, C. A. & EDELMAN, E. R. 2008. Tissue-engineered endothelial and epithelial implants differentially and synergistically regulate airway repair. *Proceedings of the National Academy of Sciences,* 105**,** 7046-7051.

ZARKA, M. T., NUYKEN, O. & WEBERSKIRCH, R. 2003. Amphiphilic Polymer Supports for the Asymmetric Hydrogenation of Amino Acid Precursors in Water. *Chemistry – A European Journal,* 9**,** 3228-3234.

ZHANG, M., DESAI, T. & FERRARI, M. 1998. Proteins and cells on PEG immobilized silicon surfaces. *Biomaterials,* 19**,** 953-960.

ZHANG, N., POMPE, T., AMIN, I., LUXENHOFER, R., WERNER, C. & JORDAN, R. 2012. Tailored Poly(2-oxazoline) Polymer Brushes to Control Protein Adsorption and Cell Adhesion. *Macromolecular Bioscience,* 12**,** 926-936.

ZHOU, W., HAN, C., SONG, Y., YAN, X., LI, D., CHAI, Z., FENG, Z., DONG, Y., LI, L. & XIE, X. 2010. The performance of bone marrow mesenchymal stem cell – Implant complexes prepared by cell sheet engineering techniques. *Biomaterials,* 31**,** 3212-3221.

ZOSKY, G. R. & SLY, P. D. 2007. Animal models of asthma. *Clinical & Experimental Allergy,* 37**,** 973-988.

9. Appendix

9.1 Oxazoline Polymer characterisation

Chain length and LCST data for the *i*PrOx coating polymers

Polymer code	Repeating units	End groups	Estimated mass (kDa)	LCST (°C)
pIPOX-1	34	CH3, OH	3.8[†]	44.6
pIPOX-2	50	CH3, OH	5.7	43.4
pIPOX-3	80	CH3, OH	9.1	41.2
pIPOX-4	100	CH3, OH	11.3	39.3
pIPOX-5	130	CH3, OH	14.7	38.9
pIPOX-6	150	CH3, OH	17.0	38.2
pIPOX-7	200	CH3, OH	22.6	37
pIPOX-8	250	CH3, OH	28.3	36.5
pIPOX-9	300	CH3, OH	33.9	35.8
pIPOX-10	300	CH3, OH	33.9	36.5
pIPOX-11	400	CH3, OH	45.3	34.2
pIPOX-12	500	CH3, OH	56.6	34.8

[†] Calculated using Maldi-TOF

Maldi-TOF spectrum of iPrOx

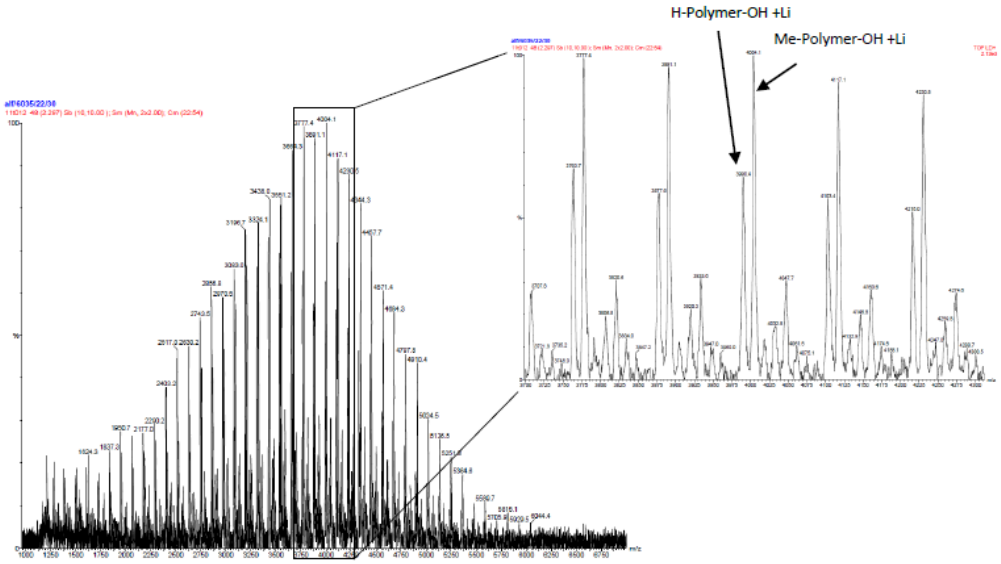

From the Maldi-TOF the PDI can be calculated. The number average molecular weight (M_n) and the weight average molecular weight (M_w) can be calculated. From these the PDI

can be calculated. For IPROX this equals 1.06. The lower the PDI the more uniform the chain lengths are, for IPROX this was very low as expected.

$$M_n = \frac{{}_i N_i M_i}{{}_i N_i}$$

Number average molecular weight

$$M_w = \frac{{}_i N_i M_i^2}{{}_i N_i M_i}$$

Weight average molecular weight

$$PDI = \frac{M_w}{M_n} = \frac{3772.71}{4013.81} = 1.06$$

Polydispersity index

NMR analysis of Bis*i*PrOx showing that the Bis*i*PrOx element is present in the polymer

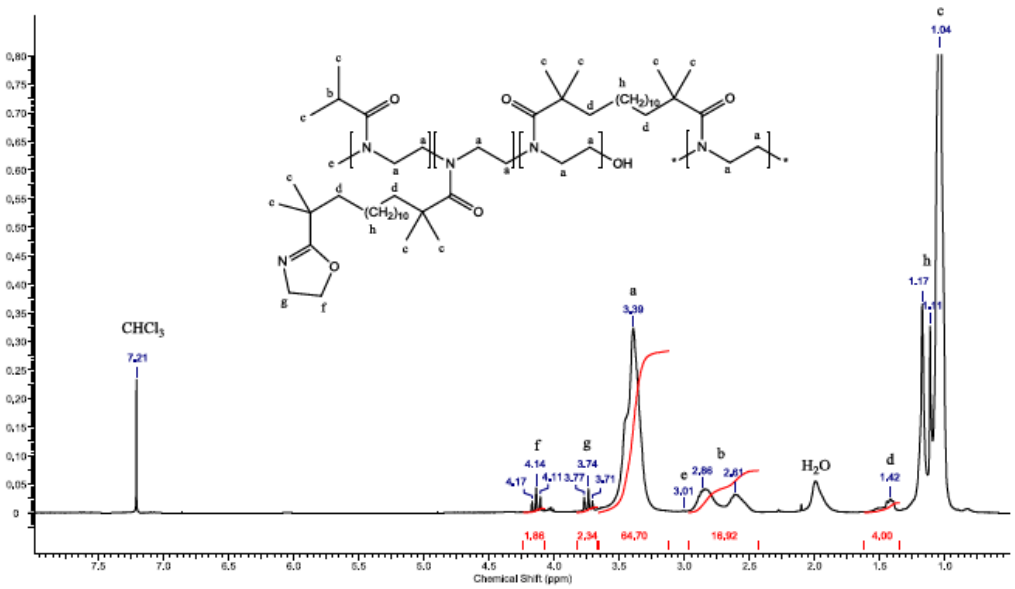

LCST analysis of the Bis*i*PrOx co-polymers

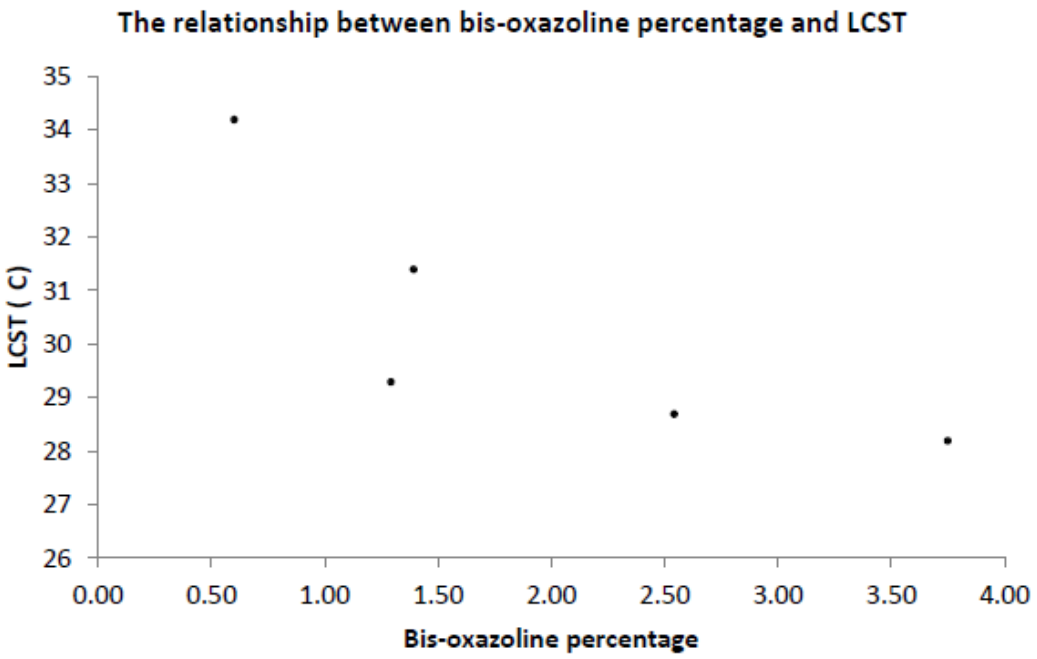

Characteristics of the Co-polymer Bis*i*PrOx

Polymer code	Repeating units	End groups	Estimated mass (kDa)	Percentage of bis-oxazoline	LCST (°C)	Tg (°C)	Thermal stability (°C)
pIPOX-BisOx 1	1334	CH3, OH	174.1	6.18	Insoluble	45	422
pIPOX-BisOx 2	102	CH3, OH	11.8	0.60	34.2		
pIPOX-BisOx 3	102	CH3, OH	11.9	1.39	31.4		
pIPOX-BisOx 4	102	CH3, OH	12.0	1.29	29.3		
pIPOX-BisOx 5	102	CH3, OH	12.3	2.54	28.7		
pIPOX-BisOx 6	102	CH3, OH	12.8	3.75	28.2		

Contact angles for *i*PrOx 'grown on' functionalised glass slides

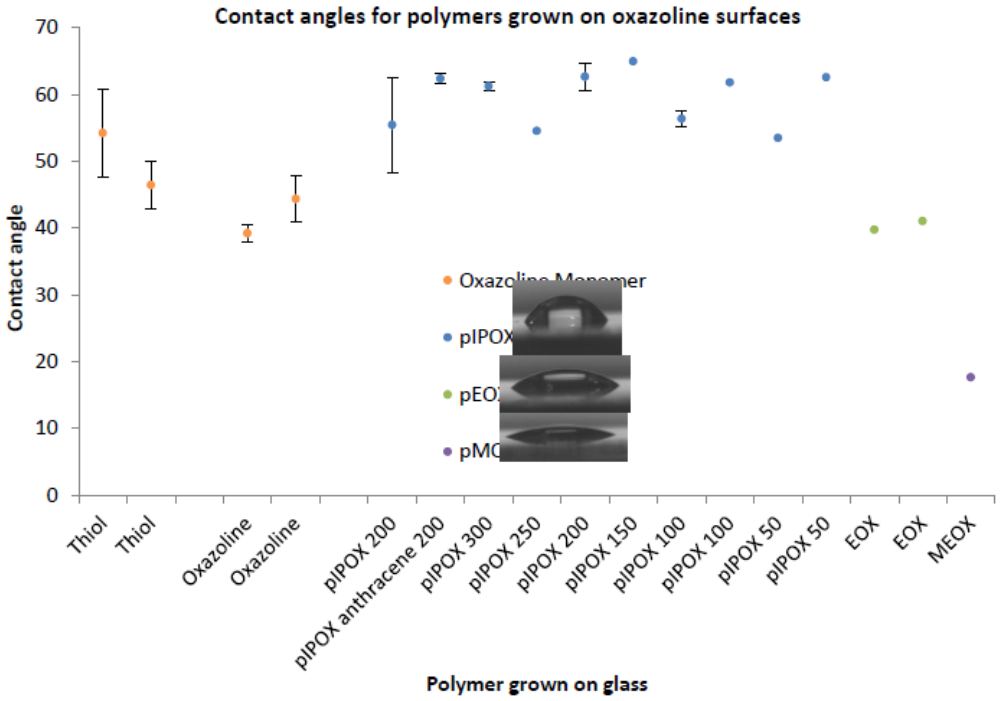

16HBE cell adhesion assay on a clear 96 well plate. Standard curve analysed by the fluorescent plate reader.

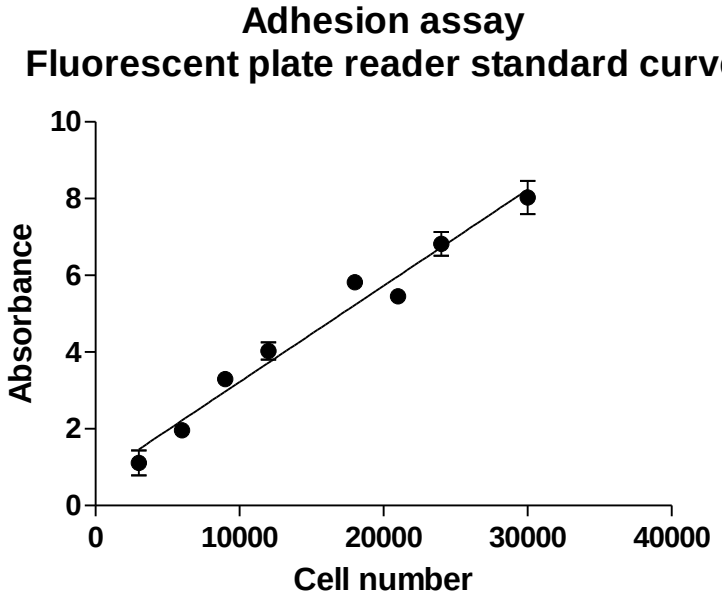

Clear 96 well plate adhesion assay microscopic analysis corrected for area and image J

Time	Collagen				corrected for image area				corrected for image J		
5	1110	977	1051		4017.736	3536.332	3804.181		6135.083	5399.978	5808.984
15	1605	1222	1397		5809.429	4423.129	5056.556		8870.998	6754.118	7721.361
30	1487	1708	1532		5382.318	6182.246	5545.2		8218.8	9440.29	8467.52
45	1947	1757	1799		7047.326	6359.605	6511.628		10761.27	9711.118	9943.256
60	1595	1701	1592		5773.233	6156.909	5762.374		8815.727	9401.6	8799.146
	Gelatine										
5	660	601	763		2388.924	2175.369	2761.741		3647.887	3321.788	4217.179
15	981	887	805		3550.81	3210.569	2913.763		5422.087	4902.539	4449.317
30	1690	1730	1493		6117.093	6261.877	5404.036		9340.802	9561.886	8251.963
45	1551	1785	1722		5613.972	6460.954	6232.92		8572.535	9865.876	9517.669
60	1316	1057	1105		4763.37	3825.898	3999.638		7273.666	5842.146	6107.447
	BSA										
5	314	701	404		1136.549	2537.327	1462.311		1735.51	3874.498	2232.949
15	371	174	110		1342.865	629.8073	398.154		2050.555	961.7157	607.9812
30	197	362	145		713.0576	1310.289	524.8394		1088.839	2000.811	801.4297
45	412	303	147		1491.268	1096.733	532.0785		2277.166	1674.712	812.4839
60	32	68	62		115.8266	246.1316	224.4141		176.8673	375.8429	342.6803
	Tissue culture plastic										
5	388	243	393		1404.398	879.5584	1422.496		2144.515	1343.086	2172.151
15	585	490	900		2117.455	1773.595	3257.624		3233.354	2708.28	4974.391
30	227	436	352		821.6451	1578.138	1274.093		1254.652	2409.816	1945.54
45	121	162	290		437.9694	586.3723	1049.679		668.7793	895.3905	1602.859
60	488	487	333		1766.356	1762.736	1205.321		2697.226	2691.698	1840.525

16HBE 2nd adhesion assay analysed by microscopy, before the data was corrected for image J

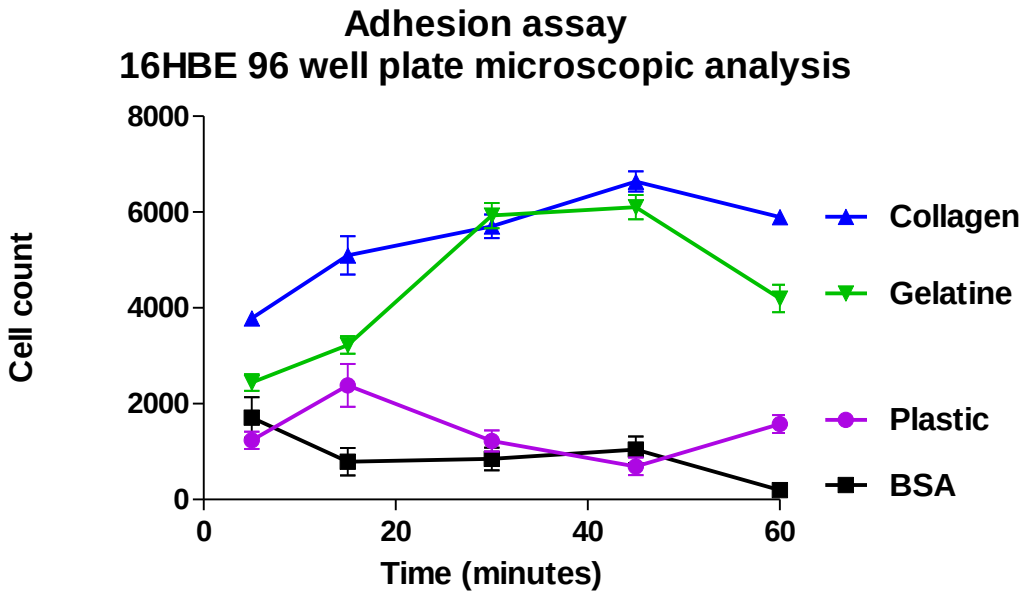

.

Example of the data for the 16HBE western blot densitometry

		Pan p38	phospho p38			
	area	percentage	area	percentage	relative intensity	% change
control	5570.305	20.659	5436.77	16.728	0.976027345	100
TNF1ng	4111.477	15.248	6440.276	19.816	1.566414211	160.4888
TNF 10ng	5273.012	19.556	5322.012	16.375	1.009292602	103.4082
TNF 100ng	4201.941	15.584	4759.912	14.646	1.132788871	116.0612
IL-1b 1ng	3975.648	14.745	4446.841	13.682	1.118519799	114.5992
IL-1b 10ng	3830.941	14.208	6094.426	18.752	1.590843085	162.9917

Thermoresponsive amine-terminated poly(2-alkyl-2-oxazoline)s synthesized

Polymer	Butyl[a] (% Mol)	Mw[b] (kDa)	Mn[b] (kDa)	PDI	LCST[c] (°C)
P*i*Pr	0	44.56	39.85	1.11	38.5
P*i*Pr-Bu	33	35.21	42.24	1.19	14.17

[a]NMR, [b]GPC (Chloroform:Methanol, 3:1, 2mM LiBr), [c]Determined usingfluorescent spectroscopy

Visual confirmation of thermogelling behavior of P*i*Pr-Bu-CMC (4% by weight in PBS), below the gelating temperature 29°C (left) and above 37°C (right)

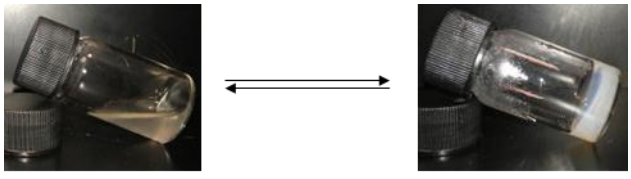

Thermo-gelling polymers synthesized

Thermogel	Gelation temperature[a] (°C)
P*i*Pr-CMC-1	49
P*i*Pr-CMC-2	58
P*i*Pr-CMC-3	No gelation
P*i*Pr-Bu-CMC	29

[a]Determined using 4% by weight solutions in PBS.